

1032 107108

~~CONFIDENTIAL~~

NASA TECHNICAL
MEMORANDUM

NASA TM X-2633



NASA TM X-2633

CASE
COPY

CONFIDENTIAL	CLASSIFIED
by Henry A. Fedzick	
SUBJECT TO GENERAL DECLASSIFICATION SCHEDULE OF EXECUTIVE ORDER 11652 AUTOMATICALLY DOWNGRADED AT TWO YEAR INTERVALS AND DECLASSIFIED ON DEC 31 1978	

DOWNGRADED TO UNCLASSIFIED
 BY AUTHORITY OF EXECUTIVE ORDER 11652
 CHANGE NOTICES NO. 240 DATE 30 SEP 76
 ITEM NO. 39

AERODYNAMIC CHARACTERISTICS OF
AN NASA SUPERCRITICAL-WING RESEARCH
AIRPLANE MODEL WITH AND WITHOUT
FUSELAGE AREA-RULE ADDITIONS
AT MACH 0.25 TO 1.00

by Dennis W. Bartlett and Charles D. Harris

Langley Research Center
Hampton, Va. 23365

PUBLIC RELEASE JUNE 13, 1978

~~CONFIDENTIAL~~

**AERODYNAMIC CHARACTERISTICS OF AN NASA SUPERCRITICAL-WING
RESEARCH AIRPLANE MODEL WITH AND WITHOUT FUSELAGE
AREA-RULE ADDITIONS AT MACH 0.25 TO 1.00***

By Dennis W. Bartlett and Charles D. Harris
Langley Research Center

SUMMARY

An investigation has been conducted in the Langley 8-foot transonic pressure tunnel at Mach numbers from 0.25 to 1.00 to determine the effects of area-rule additions to the sides of the fuselage on the aerodynamic characteristics of a 0.087-scale model of an NASA supercritical-wing research airplane.

The results of this investigation indicated that, compared with the basic configuration, a significant reduction in drag occurred at Mach numbers of 0.99 and 1.00 near the design cruise lift coefficient with the area-rule additions on the model, whereas only a small drag penalty was incurred at the lower subsonic Mach numbers.

The results also indicated that the fuselage area-rule additions have only small effects on the longitudinal stability characteristics and the horizontal-tail effectiveness over the Mach number and angle-of-attack range of the investigation.

Near the cruise lift coefficient, the fuselage area-rule additions did alter the spanload distribution unfavorably; however, based upon earlier results, this disadvantage could be alleviated by a reduction in the wing inboard trailing-edge camber.

INTRODUCTION

Several "proof of concept" flight-test investigations (refs. 1, 2, and 3) have been initiated on supercritical-wing research airplane configurations. One of these programs, currently being conducted at the Flight Research Center (ref. 1), utilizes a U.S. Navy airplane (TF-8A) as a flying test bed to evaluate the potential gains in cruise speed of a sweptback supercritical wing designed for possible future application to an advanced, near-sonic-cruise, transport-type airplane. This wing incorporates the NASA supercritical airfoil which was developed at the Langley Research Center. (See refs. 4 to 6.) Preliminary full-scale results on the TF-8A supercritical-wing research airplane contained in reference 1 substantiate the significant increase, as indicated by wind-tunnel

*Title, Unclassified.

~~CONFIDENTIAL~~

tests (refs. 7 and 8), in drag-divergence Mach number over that exhibited by present-day transports having wings with conventional airfoil sections.

The drag results presented in reference 8 indicate a drag-divergence Mach number of about 0.97 for the complete airplane; however, wing pressure data and oil-flow studies of the boundary layer indicated relatively clean flow to a Mach number of 0.99 with no appreciable separation evident. It was felt, therefore, that the drag break was primarily associated with the nonoptimum cross-sectional area distribution for the complete configuration rather than a break down of flow over the wing. Consequently, in an attempt to improve the performance of the airplane at near-sonic speeds, fore and aft side fuselage area-rule additions were developed for the model on the basis of an experimentally refined Mach number 1.00, area-rule concept that compensates for the equivalent area due to lift. This follow-on configuration, which will have an area distribution more representative of an advanced near-sonic-cruise transport airplane, is now under development and will be flown in the later phases of the flight-test program.

The purpose of this paper is to present the effects on the longitudinal aerodynamic force and moment characteristics and on selected wing and fuselage pressures of the fuselage area-rule additions as measured in the Langley 8-foot transonic pressure tunnel at Mach numbers from 0.25 to 1.00. Complete wing and fuselage pressure data for the present investigation are tabulated in reference 9; however, some of these data near the design cruise lift coefficient are presented herein to aid in the discussion of results.

SYMBOLS

Values are given in both SI and U.S. Customary Units. Measurements and calculations were made in U.S. Customary Units. The longitudinal aerodynamic characteristics presented herein are referred to the stability axis system. All coefficients are based on the geometry of the basic wing panel which does not include the leading-edge glove or the trailing-edge extension. (See fig. 1(a).) Moments are referenced to the quarter-chord point of the mean geometric chord of the basic wing panel. This point is located at model station 99.45 centimeters (39.155 inches) as shown in figure 1(a).

A_e	individual duct exit area
A_i	total model inlet area
b	wing span, 114.30 centimeters (45.00 inches)
C_D	drag coefficient, $\frac{\text{Drag}}{qS}$, where drag is total measured drag minus base drag

- ~~XXXXXXXXXXXXXXXXXXXXXXXXXXXX~~
- $C_{D,i}$ internal drag coefficient, $\frac{\text{Internal drag}}{qS}$
- C_L lift coefficient, $\frac{\text{Lift}}{qS}$
- $C_{L,0}$ lift coefficient at zero angle of attack
- C_m pitching-moment coefficient, $\frac{\text{Pitching moment}}{qS\bar{c}}$
- $C_{m,0}$ pitching-moment coefficient at zero lift
- C_p pressure coefficient, $\frac{p_l - p}{q}$
- c local streamwise chord of basic wing panel
- \bar{c} mean geometric chord of basic wing panel, 18.087 centimeters (7.121 inches),

$$\frac{2}{S} \int_0^{1.0} c^2 d \frac{y}{b/2}$$
- c' local streamwise chord of total wing planform which includes leading-edge glove and trailing-edge extension
- c_{av} average chord of basic wing panel, S/b , 16.87 centimeters (6.64 inches)
- c_n wing-section normal-force coefficient, $\int_{l.e.}^{t.e.} (C_{p,L} - C_{p,U}) d \frac{x}{c}$ where $C_{p,L}$ is lower-surface pressure coefficient and $C_{p,U}$ is upper-surface pressure coefficient
- M free-stream Mach number
- p free-stream static pressure
- p_l local static pressure
- q free-stream dynamic pressure
- S area of basic wing panels including fuselage intercept, 0.193 meter² (2.075 feet²)
- ~~XXXXXXXXXXXXXXXXXXXXXXXXXXXX~~

V_e	velocity of flow in duct at duct exit
V_∞	free-stream velocity
w/w_∞	mass-flow ratio of individual duct referenced to one-half inlet area, $\frac{\rho_e V_e A_e}{\rho_\infty V_\infty A_i / 2}$
$(w/w_\infty)_{av}$	average mass-flow ratio of ducts, $\frac{[(w/w_\infty)_{duct\ 1} + (w/w_\infty)_{duct\ 2}]}{2}$
x	streamwise distance measured from leading edge of basic wing panel, positive toward wing trailing edge
x'	streamwise distance measured from leading edge of total wing planform, positive toward wing trailing edge
y	spanwise distance measured normal to model plane of symmetry, 0 at fuselage center line
z'	vertical distance measured from model reference water line, 26.205 centimeters (10.317 inches)
α	angle of attack, referred to model water line, degrees
β	angle of sideslip, referred to model center line (positive when nose is left), degrees
δ_h	horizontal-tail deflection angle, referred to model water line (positive when trailing edge is down), degrees
θ	circumferential location of pressure orifice on rear of fuselage, degrees
ρ_e	mass density of flow in duct at duct exit
ρ_∞	mass density of free stream

Abbreviations:

l.e. leading edge

t.e. trailing edge

APPARATUS AND PROCEDURES

Model

Model description. - Geometric characteristics of the model are presented in figure 1, and photographs of the model are presented as figure 2.

The model was a sting-supported, 0.087-scale model of the TF-8A supercritical-wing research airplane. The sweptback supercritical wing was mounted in a high-wing position with 1.5° of incidence at the root chord. The supercritical wing, constructed of a steel core with plastic fill on the upper right and lower left wing panels in which steel pressure tubing was embedded, incorporates approximately 5° of twist between the root and tip chords (washout) in the unloaded condition and has maximum thickness-chord (c') ratios that vary from approximately 0.12 at the root to 0.07 at the tip. The basic wing panel, which excludes the leading-edge glove and the trailing-edge extension (fig. 1(a)), has an aspect ratio of 6.8, a taper ratio of 0.36, and 42.24° of sweepback at the quarter-chord line. The area of the basic wing panels including the fuselage intercept is 0.193 m^2 (2.075 ft^2), and the mean geometric chord of the basic wing panel is 18.087 cm (7.121 in.). Nondimensional wing coordinates referenced to the total streamwise chord (c') for each semispan station are presented in table I.

For the present investigation, the model was tested with and without the side fuselage area-rule additions shown in figure 1(a). However, the vortex generators (shown in fig. 1(c) and discussed in ref. 10), the aileron-hinge fairings (figs. 1(d) and 1(e)), and simulated major full-scale airplane protuberances (fig. 1(f)) were included on the model for the entire investigation. It might be noted that the drogue-parachute fairing at the base of the model shown in the first photograph of figure 2 was not included on the model for this investigation nor is it on the full-scale airplane.

The longitudinal progression of cross-sectional area taken normal to the fuselage center line for the model with and without the area-rule additions is presented in figure 3(a), and typical cross sections for the model with the fuselage area-rule additions on are shown in figure 1(b). The area distribution for the model with the fuselage area-

~~TOP SECRET~~

rule additions is also shown in figure 3(b) with the design envelope. The difference between these two curves is the experimentally determined equivalent area due to lift. It should be pointed out, however, that because of the existing tail arrangement on the TF-8A airplane, it was not possible to design the aft-fuselage area-rule additions large enough to match completely the design envelope for the rear of the model. This limitation resulted in some relatively higher slopes in the area distribution beyond fuselage station 127.0 cm (50.0 in.). (See fig. 3(a).) The desirable shape for this region is shown as the dashed line in figure 3(b).

The basic fuselage and tails are scaled versions of those on the TF-8A airplane. The rear upper-surface fuselage fairing (fig. 2) was added to the model during the early part of the wind-tunnel development program (ref. 8) and was included initially on the full-scale airplane. This fairing serves the dual purpose of smoothing the abrupt corner in the area distribution associated with the buildup of the horizontal- and vertical-tail-surface areas and of covering the wing rear attachment fittings. As emphasized in reference 1, the rear upper-surface fuselage fairing does not result in either a "Coke-bottle" fuselage shape or an ideal area distribution but rather provides a fuselage area progression closer to that which would exist on a transport configuration with a cylindrical fuselage.

The model fuselage was provided with flow-through ducts which are split toward the rear of the fuselage to allow room for the model support sting. The model has a total inlet capture area of 28.387 cm^2 (4.40 in^2) and a combined duct exit area of 31.935 cm^2 (4.95 in^2). The internal-drag and mass-flow characteristics are presented in figure 4 for the model with and without the fuselage area-rule additions.

Comparison with earlier configurations. - Reference 8 listed several dissimilarities between the model configurations of that paper and the full-scale airplane; however, before initiation of the present investigation, these contour differences were corrected on the model. In summary, the model wing was lowered to match the wing position on the full-scale airplane, and the contour lines of the rear upper-surface fuselage fairing were also made to conform to those of the full-scale airplane. In addition, the model wing has been closely refined to match the coordinates of the full-scale supercritical wing. These coordinates are presented in references 7 and 8 and also in table I.

The wing coordinates published in reference 10 reflect an inboard trailing-edge slope modification that was made in conjunction with the addition of the fore and aft fuselage area-rule additions. Since it was not possible to incorporate this inboard trailing-edge slope change into the full-scale airplane without major modification, it was therefore not included on the model wing for the present investigation. Except for the inboard region, the wing coordinates presented in reference 10 are the same as those presented in table I.



Other configuration details varied throughout the wind-tunnel development program, and these features are outlined in the following table:

Model component	Model configuration of present report and reference 9	Model configuration of reference 10	Model configuration of references 7 and 8	Full-scale airplane configuration of reference 1
Rear upper-surface fuselage fairing	On (fig. 2)	On	On	On
Vortex generators	On (figs. 1(c) and 2)	On and off	Off	On
Aileron-hinge fairings	On (figs. 1(d) and 1(e))	On	Off	On
Side-fuselage area-rule additions	On and off (figs. 1(a) and 2)	On	Off	Off
Drogue-parachute fairing	Off (fig. 2)	On	Off	Off
Major protuberances	On (figs. 1(f) and 2)	Off	Off	On

As a result of the continued refinement to the model, as discussed in the previous paragraphs, the configuration of the present report without the fuselage area-rule additions is considered to be a very close geometric simulation of the full-scale airplane.

Test Facility

The investigation was conducted in the Langley 8-foot transonic pressure tunnel (ref. 11). This facility is a continuous-flow, single-return, rectangular slotted-throat tunnel having controls that allow for the independent variation of Mach number, density, temperature, and dewpoint. The test section is square in cross section with the upper and lower walls axially slotted (each wall having an open ratio of approximately 0.06) to permit changing the test-section Mach number continuously through the transonic speed range. The stagnation pressure in the tunnel can be varied from a minimum value of about 0.25 atmosphere at all test Mach numbers to a maximum value of approximately 1.5 atmospheres at transonic Mach numbers and approximately 2.0 atmospheres at Mach numbers of 0.40 or less.

Due to the relatively large size of the present model, special test-section sidewall inserts were employed for this investigation (fig. 1(g)) to help reduce subsonic blockage



[REDACTED]

effects (refs. 10 and 12). These sidewall inserts were indented to account for 40 percent of the longitudinal development of model cross-sectional area. This effectively resulted in a "scalloping" of the sidewalls of the tunnel test section adjacent to the model. Fore and aft of the model, these inserts reduced the tunnel test-section, cross-sectional area by approximately 0.24 percent.

Boundary-Layer Transition

Boundary-layer transition was fixed on the model for the entire investigation. The boundary-layer trip locations and carborundum grain sizes used on the wing are shown in figure 5. The more rearward boundary-layer trip positions (figs. 5(a) and 5(b)) were located on the wing by using the techniques described in references 13 and 14 to simulate the full-scale Reynolds number boundary-layer characteristics at the trailing edge and the full-scale Reynolds number wing-shock location.

For all test Mach numbers, boundary-layer trips of No. 120 carborundum grains were located on the horizontal and vertical tails at 5 percent of the local streamwise chords. Trips of No. 120 carborundum grains were also applied around the fuselage 2.54 cm (1.00 in.) aft of the model nose and 1.27 cm (0.50 in.) rearward of the inlet lip on both the inner and outer surfaces. All transition strips were 0.127 cm (0.05 in.) wide and were located by measurements taken in the streamwise direction.

Measurements and Test Conditions

Six-component force and moment data were obtained with an electrical strain-gage balance housed within the fuselage cavity, and in addition, the wing and fuselage were instrumented with flush-surface static-pressure orifices. The orifices on the wing were distributed in streamwise rows over the upper right and lower left wing panels, and orifices were distributed on the fuselage over the left pair of fore and aft area-rule additions and on the right side of the fuselage boattail. The orifice locations for the wing and fuselage are given in table II. All surface pressures were recorded with the use of differential-pressure, scanning-valve units mounted in the nose section of the model.

For determination of the base drag, the static pressures in the balance chamber and in the plane of the model base were recorded with differential-pressure transducers referenced to the free-stream static pressure.

The internal-drag coefficients and mass-flow ratios (fig. 4) were determined from measurements of the total-pressure distribution and the static pressure in the duct exit planes by use of a rake consisting of 10 pitot-pressure tubes and 1 static-pressure tube per duct. These measurements were made during an earlier test at Reynolds numbers slightly higher than those of the present investigation. The Reynolds numbers for the earlier investigation are the same as the higher Reynolds numbers in reference 8 for the

████████████████████

Langley 8-foot transonic pressure tunnel, whereas the Reynolds numbers for the present investigation are presented in table III. Other tests have shown, however, that this small difference in Reynolds number would have a negligible effect on these parameters.

Measurements were taken over a Mach number range varying from 0.25 to 1.00 for angles of attack that varied from approximately -5° to 12° at a sideslip angle of 0° . The entire investigation was conducted at a stagnation temperature of 322 K (120° F) and at a dewpoint low enough to avoid significant condensation effects. (See ref. 15.)

The tunnel test conditions for the present investigation are summarized in table III.

Corrections

Drag results presented herein have been adjusted to correspond to free-stream static pressure acting in the balance chamber and at the model base, but no adjustments have been made to the drag for the internal flow through the ducts or for the Reynolds number difference between the tunnel and full-scale conditions. However, the internal-drag coefficients and mass-flow ratios for the model with and without fuselage area-rule additions are presented in figure 4.

No corrections have been applied to the data for sting interference effects other than the exclusion of the base drag from the total measured drag; however, the model support sting was designed on the basis of the results in reference 16 to minimize sting interference at near-sonic Mach numbers. Furthermore, no corrections have been applied to the data for the effects of either solid or wake blockage or boundary-induced lift interference.

Corrections have been made to the measured angle of attack for model support sting and balance deflections occurring as a result of aerodynamic loads on the model and for tunnel airflow angularity.

Based on wind-tunnel tests in the Langley 8-foot transonic pressure tunnel and free-drop tests of a supercritical body of revolution (ref. 17), it appears that the wind-tunnel drag results presented herein for Mach numbers beyond the drag rise are low. The preliminary comparison presented in reference 1 between the wind-tunnel and flight data on the TF-8A supercritical-wing research airplane also indicates the same trend. Although these discrepancies in the data at these Mach numbers have not been completely explained, they are generally felt to be associated with the pronounced, wind-tunnel-wall interference effects encountered near Mach 1.00. However, the drag increments measured between the present configurations at Mach numbers 0.99 and 1.00 are felt to be indicative of the beneficial effect of the fuselage area-rule additions on the drag characteristics at these Mach numbers.

████████████████████

Accuracy

Based on static calibrations, the model balance is capable of measuring normal force within ± 55.6 N (± 12.5 lb), axial force within ± 4.4 N (1.0 lb), and pitching moment within ± 2.0 m-N (± 1.5 ft-lb).

The accuracy with which angle of attack can be determined generally decreases with increasing aerodynamic loads and model support system dynamics. At the maximum lift coefficients of this investigation, the angles of attack are estimated to be within $\pm 0.1^\circ$. Near cruise conditions, the angles of attack are estimated to be accurate within $\pm 0.05^\circ$.

The transducers of the differential-pressure, scanning-valve units used to measure the wing upper surface, the wing lower surface, and the fuselage pressures had maximum ranges of 103.4 kN/m² (15.0 psi), 82.7 kN/m² (12.0 psi), and 17.2 kN/m² (2.5 psi), respectively. The estimated accuracies of these transducers are 1 percent of the maximum ranges.

The Mach numbers of this investigation are estimated to be accurate within ± 0.003 .

PRESENTATION OF RESULTS

The results of this investigation are presented in the following figures:

	Figure
Longitudinal aerodynamic characteristics:	
Effect of fuselage area-rule additions on longitudinal aerodynamic characteristics. $\beta = 0^\circ$; $\delta_h = -2.5^\circ$	6
Effect of fuselage area-rule additions on horizontal-tail effectiveness. $\beta = 0^\circ$	7
Variation of drag characteristics with Mach number. $\beta = 0^\circ$	8
Wing and fuselage pressure distributions:	
Effect of fuselage area-rule additions on wing streamwise pressure distributions near cruise lift coefficient. $\beta = 0^\circ$; $\delta_h = -2.5^\circ$	9
Effect of fuselage area-rule additions on span-load distributions near cruise lift coefficient. $\beta = 0^\circ$; $\delta_h = -2.5^\circ$	10
Effect of fuselage area-rule additions on wing upper-surface pressure coefficients near trailing edge. $\beta = 0^\circ$; $x/c = 0.98$; $\delta_h = -2.5^\circ$	11
Effect of fuselage area-rule additions on pressure distributions over rear of fuselage near cruise lift coefficient. $\beta = 0^\circ$; $\delta_h = -2.5^\circ$	12
Effect of fuselage area-rule additions on pressure distributions along top of fuselage near cruise lift coefficient. $\beta = 0^\circ$; $\delta_h = -2.5^\circ$	13
Typical pressure distributions along side of fuselage near cruise lift coefficient with area-rule additions on model. $\beta = 0^\circ$; $\delta_h = -2.5^\circ$; data from reference 10	14

DISCUSSION OF RESULTS

Area-Rule Considerations

In optimizing the area distribution of a configuration so as to reduce shock strengths and consequently the drag at Mach numbers near 1.00, the axial development of cross-sectional area normal to the free stream is of primary importance. (See ref. 18.) At Mach numbers near 1.00, the second-order effect caused by the expansion of the supersonic stream tubes above the wing upper surface at positive lift coefficients becomes significant and should be taken into account along with the basic geometric areas to provide an overall smooth area distribution. This conclusion is supported by earlier experimental work at transonic Mach numbers (ref. 19) which indicated that the typical fuselage indentations associated with the zero-lift area distribution for a wing-body combination could be modified to produce significant additional drag reductions at lifting conditions. Theoretical methods exist for calculating the equivalent-body area due to lift at supersonic speeds (ref. 20); however, the linear theory on which these methods are based is not applicable near a Mach number of 1.00. Consequently, the side fuselage area-rule additions incorporated on the present model were developed on the basis of an experimentally refined Mach number 1.00, area-rule concept that compensates for the equivalent area due to lift.

For the present investigation, a design envelope area distribution (fig. 3(b)) was derived from wind-tunnel tests of a supercritical body of revolution having a drag-divergence Mach number very close to 1.00 and a fineness ratio the same as the F-8 supercritical-wing research airplane. The fore and aft fuselage area-rule additions were designed, therefore, to provide the model with the same area distribution as the supercritical body of revolution except in the region of the wing where area was omitted to allow for the equivalent area due to lift. However, as previously discussed, the existing empennage arrangement of the basic airplane made it impossible to design the aft fuselage area-rule additions large enough to completely match the design envelope for the rear of the model.

The amount of lift-compensation area was arrived at experimentally and is approximately the same as that determined in a similar fashion in reference 21 for a model of a low-wing, advanced transport configuration. This was not unexpected since that configuration incorporated a similar supercritical wing and had approximately the same design envelope area distribution. It should be noted, however, that ideally the additional physical indentation required to compensate for the lift should be concentrated on top of the fuselage rather than on the sides as was done on the present configuration because of the high-wing location provided by the basic F-8 fuselage. Furthermore, the constraints imposed on the design of the present area-rule additions by the existing fuselage lines and the horizontal tail, made it impractical to match the design envelope completely. For

~~CONFIDENTIAL~~

these reasons, the present configuration with the area-rule additions should not be considered to be a thoroughly optimized configuration.

Basic Longitudinal Aerodynamic Characteristics

The basic longitudinal aerodynamic characteristics for the model with and without the fuselage area-rule additions is presented in figure 6 for a horizontal-tail deflection angle of -2.5° . Significant drag reductions associated with the area-rule additions are noted in the data at a Mach number of 1.00 (fig. 6(i)) with only a small drag penalty evident at the lower subsonic Mach numbers. With regard to the lift and pitching-moment characteristics, the fuselage area-rule additions have generally only small effects. Positive $C_{m,0}$ shifts are evident at Mach numbers 0.25 to 0.98, and a positive $C_{L,0}$ shift is noted for all the Mach numbers with the area-rule additions on the model. Slight variations in the pitching-moment and lift-curve slopes also result with the inclusion of the area-rule additions on the model, but again, these are generally small.

As shown in figure 7, the fuselage area-rule additions have no significant effect on the horizontal-tail effectiveness. It is interesting to note, however, that the differences in $C_{m,0}$ which are shown for $\delta_h = -2.5^\circ$ are not evident for $\delta_h = -5^\circ$, and overall, the pitching-moment curves for the two configurations are much closer in shape for the more negative tail angle.

Drag-Rise Characteristics

The variation of the drag coefficient at lift coefficients from 0.20 to 0.50 for the model with and without the area-rule additions is presented in figure 8(a) for a horizontal-tail deflection angle of -2.5° . A slight improvement in drag-divergence Mach number (drag-divergence Mach number is defined as the Mach number where $\frac{\partial C_D}{\partial M} = 0.1$) is obtained for the configuration with the area-rule additions at lift coefficients of 0.30 and 0.40. Beyond the drag-divergence Mach number, however, a significant reduction in the severity of the drag rise is noted for the configuration incorporating the area-rule additions for all the lift coefficients at which data are presented in figure 8(a). It would be expected, therefore, that the problem of wind-tunnel—flight correlation at the design wing Mach number of 0.99 would be alleviated somewhat as a result of the decreased sensitivity of drag with Mach number.

A comparison of the incremental drag-rise characteristics of the present model configurations with the configurations of references 10 and 21 is presented in figure 8(b). The F-8 supercritical-wing model configuration of reference 10 employed the same fore and aft fuselage area-rule additions used in the present investigation. The lower drag increments above Mach number 0.95 for the configuration of reference 10 can be attributed, in part, to a better area distribution for the rear of the model as a result of the



drogue-parachute fairing (fig. 2) and to a modification on the inboard section of the wing discussed in a subsequent section. The simulated drogue-parachute fairing used in the investigation reported in reference 10 brought the area distribution for the aft section of the model closer to the design envelope. (See fig. 3(b).)

Of the four configurations for which data are presented in figure 8(b), the low-wing, advanced transport model of reference 21 has the lowest drag increments between Mach numbers 0.95 and 0.99. (No results are presented in ref. 21 for $M = 1.00$.) These lower drag increments for the model of reference 21 result because it has a more thoroughly refined area distribution and a higher fineness ratio than the F-8 supercritical-wing model configurations.

Pressure Distributions Near Cruise Lift Coefficient

Wing-pressure distributions. - With the fuselage area-rule additions on, there is a general reduction in the induced velocities over the inboard region of the wing for all Mach numbers at which data are presented in figure 9. Although the induced velocities are decreased, the relative pressure difference between the upper and lower surfaces is seen to increase. As shown in figure 10, this increase results in a higher loading on the wing inboard semispan stations ($\frac{y}{b/2} = 0.133$ and 0.307) for the configuration with the area-rule additions.

For the midsemispan stations ($\frac{y}{b/2} = 0.480, 0.653, \text{ and } 0.804$), the fuselage area-rule additions tend to move the wing upper-surface shock wave forward and produce a higher second peak in the pressure distributions, particularly at the 0.804 station. These changes in the wing upper-surface pressure distributions are characteristic of changes that occur with a reduction of free-stream Mach number for the two-dimensional supercritical airfoil results. (See ref. 5.) Thus, the area-rule additions apparently reduce the local Mach numbers on this region of the wing as well as the inboard section by decreasing the slopes of the area distribution fore and aft of the maximum cross-sectional area of the model. (See fig. 3(a).)

At the station near the tip, $\frac{y}{b/2} = 0.933$, the single aft shock wave on the wing upper surface is moved closer to the trailing edge with the inclusion of the fuselage area-rule additions on the model for all Mach numbers at which pressure distributions are presented in figure 9. The extent to which the shock wave moves rearward is greater for Mach numbers 0.99 and 1.00, and this results in the higher section normal-force coefficients for this region of the wing at these Mach numbers with the area-rule additions on the model. (See fig. 10.) Generally, rearward movements of shock waves can be attributed to increased angle of attack or Mach number. In this particular case, the more aft-located shock probably results from an increase in local Mach number since, usually, an increase in angle of attack also results in more negative leading-edge pressure coefficients. This increase



████████████████████

in local Mach number near the wing tip with the area-rule additions on the model would be expected to result from the influence of the high velocity field associated with the negative peak in the fuselage pressure distributions near fuselage station 135 cm (53.2 in.). (See figs. 13 and 14.) These negative pressure peaks are, in turn, associated with the relatively abrupt change in slope of the area distribution near fuselage station 127 cm (50 in.). (See fig. 3(a).)

Span-load distributions. - Since the wing was optimized without the area-rule additions, it is felt that the span-load distribution (fig. 10) of the present configuration with the area-rule additions is not optimum. A comparison of the span-load distributions of figure 10 indicates that the modification of reference 10, which decreased the inboard trailing-edge slopes (reduced trailing-edge camber), practically eliminated the effect of the fuselage area-rule additions on the span-load distribution, especially on the inboard region of the wing. This modification, although not practical to incorporate on the full-scale airplane, produced a similar elliptically shaped span-load distribution near the design cruise lift coefficient as existed before the fuselage area-rule additions were included on the model. The improvement in the drag characteristics for the configuration of reference 10 (fig. 8(b)) over the present configuration with the area-rule additions is a probable result of the more optimum span-load distribution (associated with a reduction in induced drag) and, as noted previously, a better area distribution for the rear of the model which is attributable to the drogue-parachute fairing.

Trailing-edge pressure recovery. - The fuselage area-rule additions also appear to be detrimental to the wing upper-surface, trailing-edge pressure recovery at all Mach numbers of figure 9 except Mach number 1.00. It should be pointed out, however, that the wing trailing-edge pressures are influenced by disturbances emanating from the fuselage, and as shown in figures 13 and 14, the aft fuselage area-rule additions produce a relatively low pressure field in the vicinity of the wing trailing edge. For this reason, the reduced trailing-edge pressures associated with the area-rule additions may not be necessarily indicative of more trailing-edge separation. Instead, the wing pressures near the trailing edge are probably recovering to a locally lower pressure as a result of the area-rule additions. This conclusion is supported somewhat by figure 11 which shows that the wing pressure coefficients near the trailing edge with the area-rule additions on the model are generally more negative throughout the angle-of-attack range, even in the "bucket" of the curve where very little separation should exist, and, in general, the point of trailing-edge pressure divergence is approximately the same for both configurations.

Fuselage pressure distributions. - The fuselage pressure distributions of figures 12 and 13 indicate improved pressure recovery over the fuselage boattail with the area-rule additions on the model. Although the difference in the pressure coefficients for the two configurations is small at a Mach number of 0.97, the difference is significantly larger at



Mach number 1.00. (See fig. 12.) A typical pressure profile (from ref. 10) along the crest of the fore and aft fuselage area-rule additions is presented in figure 14 at Mach numbers 0.98, 0.99, and 1.00; however, no pressure data are available along the side of the fuselage for the model without the area-rule additions. More extensive pressure data over the area-rule additions and the right side of the fuselage boattail are contained in reference 9.

Schlieren Observations

When the area-rule additions were utilized, schlieren observations at a Mach number near 1.00 indicated a significant reduction in the strength of the shock-wave pattern propagating from the model. The weaker shock waves, resulting from the better area distribution provided by the area-rule additions, decrease the overall wave drag of the airplane and produce the favorable effect on the pressure recovery over the fuselage boattail as noted above. It is felt, therefore, that the reduction in drag at Mach numbers 0.99 and 1.00 with the area-rule additions on the model (fig. 8(a)) primarily results from a decrease in model shock strengths.

CONCLUSIONS

The present wind-tunnel investigation of effects of side fuselage area-rule additions on the aerodynamic characteristics of an NASA supercritical-wing research airplane has shown the following results:

1. Near the design cruise lift coefficient ($C_L = 0.40$), a significant reduction in drag, associated with the fuselage area-rule additions, is obtained at Mach numbers 0.99 and 1.00, whereas only a small drag penalty was incurred at the lower subsonic Mach numbers.

2. The fuselage area-rule additions have only small effects on the longitudinal stability characteristics and the horizontal-tail effectiveness over the Mach number and angle-of-attack range of the investigation.

3. Near the cruise lift coefficient, the fuselage area-rule additions alter the wing span-load distribution unfavorably; however, based upon earlier results (NASA TM X-2471), this disadvantage could be alleviated by a reduction in the wing, inboard trailing-edge camber.

Langley Research Center,
National Aeronautics and Space Administration,
Hampton, Va., October 5, 1972.



REFERENCES

1. Anon.: Supercritical Wing Technology – A Progress Report on Flight Evaluations. NASA SP-301, 1972.
2. Palmer, W. E.; Elliott, D. W.; and White, J. E.: Flight and Wind Tunnel Evaluation of a 17% Thick Supercritical Airfoil on a T-2C Airplane. NR71H-150 (Contract N00019-70-C-0474), North American Rockwell Corp., July 31, 1971.
Vol. I – Basic Report. (Available from DDC as AD 517 436L.)
Vol. II – Flight Measured Wing Wake Profiles and Surface Pressures. (Available from DDC as AD 517 437L.)
3. Ferris, James C.: Aerodynamic Characteristics of a Model With a 17-Percent-Thick Supercritical Wing. NASA TM X-2551, 1972.
4. Harris, Charles D.: Wind-Tunnel Investigation of Effects of Trailing-Edge Geometry on a NASA Supercritical Airfoil Section. NASA TM X-2336, 1971.
5. Harris, Charles D.; and Blackwell, James A., Jr.: Wind-Tunnel Investigation of Effects of Rear Upper Surface Modification on an NASA Supercritical Airfoil. NASA TM X-2454, 1972.
6. Harris, Charles D.: Aerodynamic Characteristics of Two NASA Supercritical Airfoils With Different Maximum Thicknesses. NASA TM X-2532, 1972.
7. Harris, Charles D.: Wind-Tunnel Measurements of Aerodynamic Load Distribution on an NASA Supercritical-Wing Research Airplane Configuration. NASA TM X-2469, 1972.
8. Bartlett, Dennis W.; and Re, Richard J.: Wind-Tunnel Investigation of Basic Aerodynamic Characteristics of a Supercritical-Wing Research Airplane Configuration. NASA TM X-2470, 1972.
9. Harris, Charles D.; and Bartlett, Dennis W.: Tabulated Pressure Measurements on an NASA Supercritical-Wing Research Airplane Model With and Without Fuselage Area-Rule Additions at Mach 0.25 to 1.00. NASA TM X-2634, 1972.
10. Harris, Charles D.; and Bartlett, Dennis W.: Wind-Tunnel Investigation of Effects of Underwing Leading-Edge Vortex Generators on a Supercritical-Wing Research Airplane Configuration. NASA TM X-2471, 1972.
11. Schaefer, William T., Jr.: Characteristics of Major Active Wind Tunnels at the Langley Research Center. NASA TM X-1130, 1965.
12. Goethert, Bernhard H.: Transonic Wind Tunnel Testing. AGARDograph No. 49, Pergamon Press, 1961, pp. 41-56.


- 
13. Loving, Donald L.: Wind-Tunnel—Flight Correlation of Shock-Induced Separated Flow. NASA TN D-3580, 1966.
 14. Blackwell, James A., Jr.: Preliminary Study of Effects of Reynolds Number and Boundary-Layer Transition Location on Shock-Induced Separation. NASA TN D-5003, 1969.
 15. Jordan, Frank L., Jr.: Investigation at Near-Sonic Speed of Some Effects of Humidity on the Longitudinal Aerodynamic Characteristics of an NASA Supercritical Wing Research Airplane Model. NASA TM X-2618, 1972.
 16. Lee, George; and Summers, James L.: Effects of Sting-Support Interference on the Drag of an Ogive-Cylinder Body With and Without a Boattail at 0.6 to 1.4 Mach Number. NACA RM A57I09, 1957.
 17. Usry, J. W.; and Wallace, John W.: Drag of a Supercritical Body of Revolution in Free Flight at Transonic Speeds and Comparison With Wind-Tunnel Data. NASA TN D-6580, 1971.
 18. Whitcomb, Richard T.: A Study of the Zero-Lift Drag-Rise Characteristics of Wing-Body Combinations Near the Speed of Sound. NACA Rep. 1273, 1956. (Supersedes NACA RM L52H08, 1952.)
 19. Loving, Donald L.: A Transonic Wind-Tunnel Investigation of the Effect of Modifications to an Indented Body in Combination With a 45° Sweptback Wing. NACA RM L53F02, 1953.
 20. Harris, Roy V., Jr.: A Numerical Technique for Analysis of Wave Drag at Lifting Conditions. NASA TN D-3586, 1966.
 21. Langhans, Richard A.; and Flechner, Stuart G.: Wind-Tunnel Investigation at Mach Numbers From 0.25 to 1.01 of a Transport Configuration Designed To Cruise at Near-Sonic Speeds. NASA TM X-2622, 1972.

TABLE I. - WING COORDINATES ALONG STREAMWISE CHORDS

(a) Wing planform coordinate layout

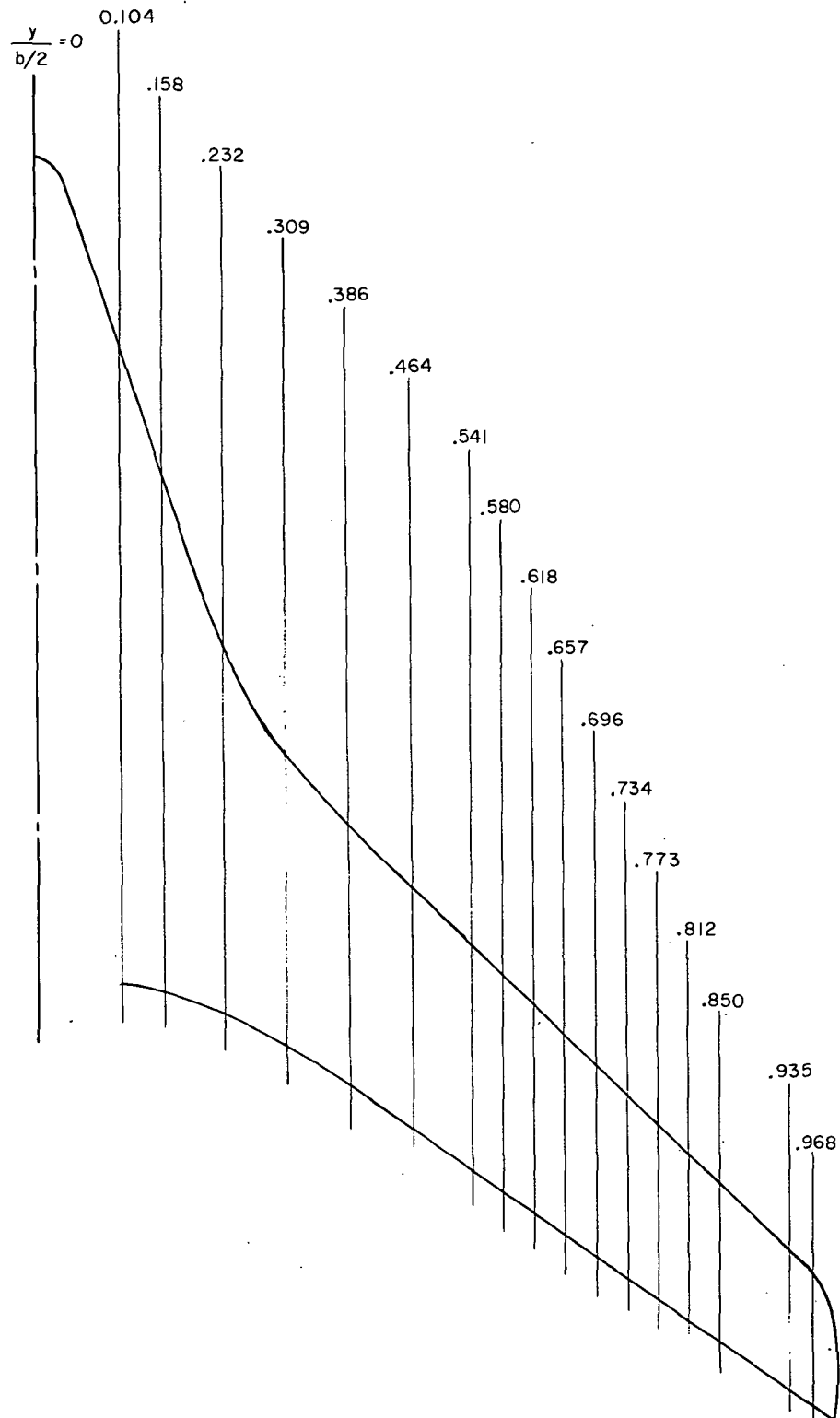


TABLE I. - WING COORDINATES ALONG STREAMWISE CHORDS - Continued

(b) $\frac{y}{b/2} = 0.104$; $c' = 45.839$ cm (18.047 in.)

x'/c'	z'/c'		x'/c'	z'/c'		x'/c'	z'/c'	
	Upper surface	Lower surface		Upper surface	Lower surface		Upper surface	Lower surface
0	0.0379	0.0379	0.0240	0.0608	0.0133	0.0958	0.0777	-0.0057
.00001	.0384	.0373	.0250	.0613	.0128	.0979	.0781	-.0061
.00004	.0389	.0368	.0261	.0617	.0123	.1000	.0784	-.0064
.00010	.0395	.0362	.0272	.0621	.0118	.1022	.0787	-.0068
.0002	.0400	.0357	.0283	.0625	.0114	.1043	.0790	-.0071
.0003	.0406	.0351	.0294	.0629	.0109	.1065	.0793	-.0075
.0004	.0411	.0345	.0306	.0633	.0104	.1087	.0797	-.0078
.0006	.0417	.0340	.0318	.0637	.0100	.1110	.0800	-.0081
.0007	.0422	.0334	.0330	.0641	.0095	.1132	.0803	-.0085
.0009	.0428	.0329	.0342	.0645	.0091	.1155	.0806	-.0088
.0011	.0433	.0323	.0355	.0649	.0086	.1178	.0809	-.0091
.0014	.0438	.0318	.0368	.0653	.0082	.1201	.0812	-.0094
.0016	.0444	.0312	.0381	.0657	.0078	.1224	.0815	-.0097
.0019	.0449	.0307	.0394	.0661	.0073	.1248	.0818	-.0100
.0022	.0454	.0301	.0408	.0665	.0069	.1272	.0821	-.0103
.0025	.0460	.0296	.0421	.0669	.0065	.1296	.0824	-.0107
.0029	.0465	.0290	.0435	.0673	.0061	.1321	.0827	-.0110
.0033	.0470	.0285	.0449	.0677	.0056	.1345	.0829	-.0113
.0037	.0475	.0279	.0464	.0681	.0052	.1370	.0832	-.0116
.0041	.0481	.0274	.0478	.0685	.0048	.1395	.0835	-.0119
.0045	.0486	.0268	.0493	.0688	.0044	.1420	.0838	-.0122
.0050	.0491	.0263	.0508	.0692	.0040	.1446	.0840	-.0125
.0055	.0496	.0257	.0523	.0696	.0036	.1471	.0843	-.0128
.0060	.0501	.0252	.0539	.0700	.0032	.1497	.0845	-.0131
.0065	.0506	.0246	.0555	.0703	.0027	.1523	.0848	-.0134
.0071	.0511	.0241	.0571	.0707	.0024	.1550	.0851	-.0136
.0077	.0516	.0236	.0587	.0710	.0020	.1576	.0853	-.0139
.0083	.0521	.0230	.0603	.0713	.0016	.1603	.0855	-.0142
.0089	.0526	.0225	.0620	.0717	.0012	.1630	.0858	-.0145
.0095	.0531	.0220	.0637	.0720	.0008	.1658	.0860	-.0148
.0102	.0536	.0214	.0654	.0723	.0004	.1685	.0863	-.0150
.0109	.0541	.0209	.0671	.0727	0	.1713	.0865	-.0153
.0116	.0546	.0204	.0689	.0730	-.0004	.1741	.0868	-.0156
.0123	.0550	.0198	.0707	.0733	-.0007	.1769	.0870	-.0158
.0131	.0555	.0193	.0725	.0736	-.0011	.1797	.0872	-.0161
.0139	.0560	.0188	.0743	.0740	-.0015	.1826	.0874	-.0163
.0147	.0565	.0183	.0761	.0743	-.0019	.1855	.0877	-.0166
.0155	.0569	.0178	.0780	.0747	-.0023	.1884	.0879	-.0168
.0163	.0574	.0172	.0799	.0750	-.0026	.1913	.0881	-.0171
.0172	.0578	.0167	.0818	.0754	-.0030	.1943	.0883	-.0173
.0181	.0583	.0162	.0837	.0757	-.0034	.1973	.0885	-.0175
.0190	.0587	.0157	.0857	.0760	-.0038	.2003	.0887	-.0178
.0200	.0591	.0152	.0877	.0764	-.0042	.2033	.0889	-.0180
.0209	.0596	.0147	.0897	.0767	-.0046	.2063	.0891	-.0182
.0219	.0600	.0142	.0917	.0771	-.0050	.2094	.0892	-.0184
.0229	.0604	.0137	.0938	.0779	-.0053	.2125	.0894	-.0187

TABLE I. - WING COORDINATES ALONG STREAMWISE CHORDS - Continued

(b) $\frac{y}{b/2} = 0.104$; $c' = 45.839$ cm (18.047 in.) - Concluded

x'/c'	z'/c'		x'/c'	z'/c'	
	Upper surface	Lower surface		Upper surface	Lower surface
0.2156	0.0896	-0.0189	0.3833	0.0876	-0.0238
.2187	.0897	-.0191	.3875	.0873	-.0238
.2219	.0899	-.0193	.3917	.0871	-.0238
.2251	.0900	-.0195	.3959	.0868	-.0237
.2283	.0902	-.0197	.4001	.0865	-.0237
.2315	.0903	-.0200	.4044	.0861	-.0236
.2348	.0905	-.0201	.4087	.0858	-.0235
.2380	.0906	-.0203	.4130	.0855	-.0234
.2413	.0907	-.0205	.4173	.0851	-.0233
.2446	.0908	-.0206	.4217	.0848	-.0232
.2480	.0909	-.0208	.4261	.0844	-.0230
.2513	.0910	-.0210	.4305	.0841	-.0230
.2547	.0911	-.0212	.4817	.0793	-.0209
.2581	.0911	-.0213	.5515	.0726	-.0155
.2616	.0912	-.0215	.6095	.0669	-.0095
.2650	.0912	-.0216	.6591	.0617	-.0035
.2685	.0913	-.0218	.7023	.0571	.0018
.2720	.0913	-.0219	.7406	.0530	.0065
.2755	.0913	-.0220	.7748	.0493	.0105
.2791	.0913	-.0222	.8057	.0454	.0135
.2826	.0913	-.0223	.8341	.0414	.0157
.2862	.0913	-.0224	.8602	.0374	.0168
.2898	.0913	-.0225	.8843	.0336	.0170
.2935	.0912	-.0226	.9068	.0299	.0163
.2971	.0912	-.0227	.9277	.0265	.0153
.3008	.0912	-.0228	.9474	.0232	.0140
.3045	.0911	-.0229	.9659	.0196	.0124
.3082	.0910	-.0230	.9747	.0178	.0115
.3120	.0909	-.0231	.9833	.0159	.0103
.3157	.0908	-.0232	.9943	.0132	.0088
.3195	.0907	-.0232	.9966	.0126	.0085
.3233	.0906		1.0000		.0080
.3272	.0904				
.3310	.0903				
.3349	.0901				
.3388	.0900				
.3428	.0898				
.3467	.0897				
.3507	.0895				
.3547	.0893	-.0238			
.3587	.0891	-.0238			
.3627	.0888	-.0239			
.3668	.0886	-.0239			
.3709	.0884	-.0239			
.3750	.0881	-.0239			
.3791	.0879	-.0239			

TABLE I. - WING COORDINATES ALONG STREAMWISE CHORDS - Continued

(c) $\frac{y}{b/2} = 0.158$; $c' = 36.873$ cm (14.517 in.)

x'/c'	z'/c'		x'/c'	z'/c'		x'/c'	z'/c'	
	Upper surface	Lower surface		Upper surface	Lower surface		Upper surface	Lower surface
0	0.0384	0.0384	0.1373	0.0834	-0.0104	0.2747	0.0881	-0.0191
.0030	.0472	.0294	.1403	.0837	-.0107	.2776	.0881	-.0191
.0060	.0507	.0257	.1433	.0839	-.0110	.2806	.0880	-.0192
.0090	.0533	.0229	.1463	.0842	-.0113	.2836	.0880	-.0193
.0119	.0554	.0206	.1493	.0844	-.0116	.2866	.0879	-.0194
.0149	.0572	.0186	.1523	.0846	-.0118	.2896	.0879	-.0194
.0179	.0588	.0168	.1552	.0848	-.0121	.2926	.0878	-.0195
.0209	.0602	.0152	.1582	.0851	-.0124	.2956	.0878	-.0196
.0239	.0615	.0137	.1612	.0853	-.0127	.2985	.0877	-.0196
.0269	.0626	.0124	.1642	.0855	-.0129	.3015	.0876	-.0197
.0299	.0636	.0112	.1672	.0857	-.0132	.3045	.0876	-.0197
.0328	.0646	.0100	.1702	.0859	-.0135	.3075	.0875	-.0198
.0358	.0656	.0090	.1732	.0860	-.0137	.3105	.0874	-.0198
.0388	.0665	.0079	.1761	.0862	-.0139	.3828	.0845	-.0192
.0418	.0674	.0070	.1791	.0864	-.0142	.4600	.0802	-.0158
.0448	.0683	.0061	.1821	.0865	-.0144	.5245	.0761	-.0115
.0478	.0691	.0053	.1851	.0867	-.0146	.5797	.0721	-.0068
.0508	.0698	.0045	.1881	.0868	-.0148	.6279	.0681	-.0021
.0537	.0706	.0037	.1911	.0869	-.0151	.6707	.0642	.0027
.0567	.0713	.0029	.1941	.0871	-.0153	.7095	.0605	.0071
.0597	.0719	.0022	.1970	.0872	-.0155	.7447	.0568	.0114
.0627	.0726	.0015	.2000	.0873	-.0157	.7769	.0533	.0153
.0657	.0732	.0008	.2030	.0874	-.0159	.8066	.0501	.0183
.0687	.0738	.0002	.2060	.0874	-.0161	.8341	.0470	.0205
.0717	.0744	-.0005	.2090	.0875	-.0162	.8596	.0438	.0219
.0746	.0750	-.0011	.2120	.0876	-.0164	.8836	.0402	.0225
.0776	.0756	-.0017	.2149	.0877	-.0166	.9075	.0368	.0225
.0806	.0761	-.0022	.2179	.0877	-.0167	.9313	.0333	.0220
.0836	.0766	-.0028	.2209	.0878	-.0169	.9548	.0295	.0207
.0866	.0771	-.0033	.2239	.0878	-.0170	.9663	.0276	.0199
.0896	.0775	-.0038	.2269	.0879	-.0172	.9776	.0255	.0190
.0925	.0780	-.0043	.2299	.0879	-.0174	.9924	.0226	.0174
.0955	.0784	-.0048	.2329	.0880	-.0175	.9956	.0220	.0170
.0985	.0789	-.0052	.2358	.0880	-.0176	1.0000		.0164
.1015	.0793	-.0057	.2388	.0881	-.0178			
.1045	.0797	-.0061	.2418	.0881	-.0179			
.1075	.0801	-.0066	.2448	.0882	-.0180			
.1105	.0804	-.0070	.2478	.0882	-.0182			
.1134	.0808	-.0074	.2508	.0882	-.0183			
.1164	.0811	-.0078	.2538	.0882	-.0184			
.1194	.0815	-.0082	.2567	.0882	-.0185			
.1224	.0818	-.0086	.2597	.0882	-.0186			
.1254	.0821	-.0090	.2627	.0882	-.0187			
.1284	.0825	-.0093	.2657	.0882	-.0188			
.1314	.0828	-.0097	.2687	.0882	-.0189			
.1343	.0831	-.0101	.2717	.0881	-.0190			

TABLE I. - WING COORDINATES ALONG STREAMWISE CHORDS - Continued

(d) $\frac{y}{b/2} = 0.232;$

$c' = 26.355 \text{ cm (10.376 in.)}$

(e) $\frac{y}{b/2} = 0.309;$

$c' = 20.808 \text{ cm (8.192 in.)}$

(f) $\frac{y}{b/2} = 0.386;$

$c' = 18.654 \text{ cm (7.344 in.)}$

x'/c'	z'/c'	
	Upper surface	Lower surface
0	0.0378	0.0378
.0006	.0420	.0336
.0028	.0471	.0284
.0055	.0507	.0246
.0096	.0545	.0206
.0150	.0581	.0167
.0204	.0607	.0136
.0335	.0654	.0080
.0648	.0723	0
.0942	.0764	-.0045
.1218	.0792	-.0073
.1727	.0826	-.0109
.2184	.0843	-.0130
.2987	.0860	-.0140
.3683	.0859	-.0128
.4293	.0847	-.0105
.4835	.0827	-.0077
.5322	.0805	-.0044
.5764	.0780	-.0007
.6174	.0751	.0033
.6575	.0725	.0081
.6962	.0699	.0129
.7335	.0669	.0178
.7694	.0641	.0228
.8043	.0611	.0273
.8382	.0579	.0310
.8713	.0544	.0334
.9038	.0506	.0347
.9361	.0461	.0346
.9522	.0438	.0339
.9683	.0414	.0329
.9893	.0381	.0308
.9937	.0374	.0302
1.0000		.0293

x'/c'	z'/c'	
	Upper surface	Lower surface
0	0.0318	0.0318
.0004	.0349	.0288
.0018	.0385	.0251
.0035	.0411	.0224
.0062	.0439	.0196
.0097	.0465	.0169
.0131	.0486	.0147
.0217	.0529	.0107
.0426	.0597	.0046
.0626	.0642	.0007
.0819	.0677	-.0020
.1186	.0725	-.0063
.1530	.0758	-.0091
.2174	.0804	-.0117
.2770	.0828	-.0122
.3329	.0837	-.0117
.3857	.0838	-.0102
.4362	.0833	-.0081
.4846	.0822	-.0054
.5318	.0807	-.0020
.5781	.0794	.0023
.6236	.0780	.0076
.6682	.0763	.0139
.7120	.0745	.0209
.7549	.0722	.0283
.7972	.0696	.0353
.8388	.0665	.0408
.8799	.0628	.0441
.9204	.0582	.0449
.9404	.0554	.0441
.9604	.0523	.0424
.9866	.0475	.0385
.9921	.0464	.0374
1.0000		.0358

x'/c'	z'/c'	
	Upper surface	Lower surface
0	0.0255	0.0255
.0002	.0282	.0229
.0013	.0314	.0196
.0025	.0337	.0173
.0044	.0361	.0148
.0069	.0384	.0124
.0094	.0402	.0106
.0156	.0435	.0074
.0310	.0492	.0024
.0462	.0532	-.0010
.0613	.0563	-.0037
.0911	.0610	-.0076
.1204	.0646	-.0103
.1777	.0697	-.0129
.2334	.0728	-.0141
.2876	.0750	-.0139
.3405	.0765	-.0129
.3922	.0773	-.0111
.4430	.0775	-.0088
.4927	.0775	-.0057
.5417	.0773	-.0017
.5898	.0768	.0034
.6373	.0760	.0099
.6842	.0749	.0179
.7306	.0733	.0266
.7765	.0712	.0355
.8220	.0688	.0427
.8671	.0655	.0471
.9118	.0610	.0481
.9341	.0582	.0471
.9562	.0549	.0448
.9852	.0495	.0397
.9913	.0482	.0383
1.0000		.0364

TABLE I. - WING COORDINATES ALONG STREAMWISE CHORDS - Continued

(g) $\frac{y}{b/2} = 0.464;$

$c' = 12.537$ cm (4.936 in.)

(h) $\frac{y}{b/2} = 0.541;$

$c' = 16.231$ cm (6.390 in.)

(i) $\frac{y}{b/2} = 0.580;$

$c' = 15.624$ cm (6.151 in.)

x'/c'	z'/c'	
	Upper surface	Lower surface
0	0.0193	0.0193
.0002	.0218	.0168
.0012	.0248	.0137
.0023	.0270	.0115
.0041	.0294	.0091
.0064	.0316	.0068
.0088	.0332	.0051
.0146	.0367	.0020
.0291	.0420	-.0029
.0435	.0459	-.0062
.0578	.0488	-.0087
.0862	.0530	-.0122
.1143	.0561	-.0145
.1697	.0610	-.0170
.2241	.0646	-.0177
.2776	.0673	-.0173
.3304	.0694	-.0161
.3824	.0707	-.0144
.4338	.0720	-.0119
.4846	.0729	-.0085
.5347	.0734	-.0045
.5841	.0735	.0008
.6329	.0732	.0075
.6810	.0725	.0156
.7284	.0714	.0250
.7752	.0700	.0341
.8213	.0677	.0416
.8669	.0646	.0464
.9118	.0603	.0476
.9341	.0576	.0464
.9562	.0542	.0438
.9852	.0487	.0388
.9913	.0474	.0374
1.0000		.0352

x'/c'	z'/c'	
	Upper surface	Lower surface
0	0.0122	0.0122
.0002	.0146	.0097
.0011	.0175	.0068
.0023	.0197	.0046
.0040	.0219	.0023
.0063	.0240	.0001
.0086	.0257	-.0015
.0143	.0289	-.0046
.0286	.0343	-.0093
.0429	.0380	-.0123
.0570	.0410	-.0145
.0852	.0454	-.0177
.1132	.0488	-.0198
.1686	.0540	-.0215
.2232	.0578	-.0218
.2770	.0608	-.0211
.3300	.0633	-.0195
.3823	.0654	-.0173
.4338	.0672	-.0147
.4846	.0686	-.0112
.5347	.0694	-.0069
.5841	.0700	-.0013
.6329	.0704	.0055
.6810	.0702	.0141
.7284	.0696	.0235
.7752	.0683	.0326
.8213	.0663	.0402
.8669	.0635	.0452
.9118	.0592	.0463
.9341	.0565	.0452
.9562	.0531	.0427
.9852	.0475	.0376
.9913	.0462	.0362
1.0000		.0339

x'/c'	z'/c'	
	Upper surface	Lower surface
0	0.0082	0.0082
.0002	.0106	.0058
.0011	.0135	.0029
.0023	.0156	.0008
.0040	.0178	-.0015
.0063	.0199	-.0037
.0086	.0216	-.0053
.0143	.0248	-.0082
.0286	.0301	-.0127
.0429	.0340	-.0157
.0570	.0369	-.0178
.0852	.0414	-.0207
.1132	.0450	-.0226
.1686	.0504	-.0241
.2232	.0545	-.0241
.2770	.0577	-.0230
.3300	.0603	-.0214
.3823	.0626	-.0191
.4338	.0646	-.0163
.4846	.0662	-.0126
.5347	.0673	-.0082
.5841	.0681	-.0025
.6329	.0687	.0045
.6810	.0688	.0129
.7284	.0686	.0225
.7752	.0676	.0318
.8213	.0656	.0395
.8669	.0628	.0444
.9118	.0586	.0455
.9341	.0559	.0445
.9562	.0525	.0421
.9852	.0484	.0385
.9913	.0454	.0354
1.0000		.0331

TABLE I. - WING COORDINATES ALONG STREAMWISE CHORDS - Continued

(j) $\frac{y}{b/2} = 0.618;$

$c' = 15.019 \text{ cm (5.913 in.)}$

(k) $\frac{y}{b/2} = 0.657;$

$c' = 14.412 \text{ cm (5.674 in.)}$

(l) $\frac{y}{b/2} = 0.696;$

$c' = 13.807 \text{ cm (5.436 in.)}$

x'/c'	z'/c'	
	Upper surface	Lower surface
0	0.0043	0.0043
.0002	.0066	.0019
.0012	.0095	-.0010
.0023	.0116	-.0031
.0040	.0138	-.0053
.0063	.0158	-.0075
.0086	.0174	-.0091
.0143	.0205	-.0119
.0286	.0259	-.0164
.0429	.0298	-.0194
.0570	.0328	-.0213
.0852	.0374	-.0239
.1132	.0411	-.0255
.1686	.0467	-.0268
.2232	.0509	-.0265
.2770	.0543	-.0251
.3300	.0571	-.0233
.3823	.0597	-.0209
.4338	.0618	-.0180
.4846	.0637	-.0142
.5347	.0650	-.0097
.5841	.0661	-.0039
.6329	.0669	.0033
.6810	.0673	.0117
.7284	.0672	.0216
.7752	.0664	.0308
.8213	.0647	.0385
.8669	.0620	.0437
.9118	.0579	.0446
.9341	.0551	.0436
.9562	.0518	.0414
.9782	.0476	.0376
.9913	.0445	.0346
1.0000		.0322

x'/c'	z'/c'	
	Upper surface	Lower surface
0	0.0002	0.0002
.0002	.0025	-.0022
.0011	.0054	-.0050
.0023	.0074	-.0071
.0040	.0096	-.0093
.0063	.0116	-.0114
.0086	.0131	-.0129
.0143	.0162	-.0160
.0286	.0218	-.0201
.0429	.0256	-.0230
.0570	.0287	-.0250
.0852	.0333	-.0273
.1132	.0370	-.0286
.1686	.0428	-.0294
.2232	.0472	-.0289
.2770	.0507	-.0274
.3300	.0538	-.0253
.3823	.0564	-.0229
.4338	.0588	-.0199
.4846	.0608	-.0159
.5347	.0626	-.0112
.5841	.0639	-.0053
.6329	.0650	.0018
.6810	.0656	.0106
.7284	.0657	.0205
.7752	.0650	.0297
.8213	.0636	.0374
.8669	.0610	.0425
.9118	.0570	.0436
.9341	.0543	.0426
.9562	.0509	.0404
.9782	.0467	.0367
.9913	.0436	.0336
1.0000		.0312

x'/c'	z'/c'	
	Upper surface	Lower surface
0	-0.0041	-0.0041
.0002	-.0018	-.0064
.0011	.0010	-.0092
.0023	.0031	-.0112
.0040	.0052	-.0134
.0063	.0072	-.0155
.0086	.0087	-.0170
.0143	.0119	-.0201
.0286	.0175	-.0241
.0429	.0214	-.0266
.0570	.0244	-.0285
.0852	.0291	-.0306
.1132	.0328	-.0318
.1686	.0388	-.0325
.2232	.0434	-.0317
.2770	.0469	-.0299
.3300	.0503	-.0277
.3823	.0530	-.0251
.4338	.0557	-.0219
.4846	.0579	-.0178
.5347	.0600	-.0129
.5841	.0616	-.0069
.6329	.0627	.0004
.6810	.0636	.0093
.7284	.0640	.0191
.7752	.0636	.0284
.8213	.0623	.0360
.8669	.0599	.0411
.9118	.0559	.0424
.9341	.0532	.0414
.9562	.0498	.0393
.9782	.0457	.0357
.9913	.0426	.0326
1.0000		.0302

TABLE I. - WING COORDINATES ALONG STREAMWISE CHORDS - Continued

(m) $\frac{y}{b/2} = 0.734;$

$c' = 13.200$ cm (5.197 in.)

(n) $\frac{y}{b/2} = 0.773;$

$c' = 12.596$ cm (4.959 in.)

(o) $\frac{y}{b/2} = 0.812;$

$c' = 11.989$ cm (4.720 in.)

x'/c'	z'/c'	
	Upper surface	Lower surface
0	-0.0085	-0.0085
.0002	-.0063	-.0108
.0011	-.0035	-.0136
.0023	-.0015	-.0156
.0040	.0006	-.0177
.0063	.0025	-.0197
.0086	.0041	-.0212
.0143	.0074	-.0239
.0286	.0130	-.0282
.0429	.0170	-.0305
.0570	.0199	-.0321
.0852	.0246	-.0340
.1132	.0285	-.0352
.1686	.0347	-.0357
.2232	.0394	-.0347
.2770	.0432	-.0327
.3300	.0467	-.0304
.3823	.0497	-.0274
.4338	.0525	-.0240
.4846	.0550	-.0198
.5347	.0572	-.0148
.5841	.0590	-.0086
.6329	.0603	-.0012
.6810	.0614	.0077
.7284	.0620	.0174
.7752	.0619	.0268
.8213	.0608	.0345
.8669	.0587	.0396
.9118	.0546	.0409
.9341	.0520	.0400
.9562	.0485	.0379
.9782	.0445	.0344
.9913	.0414	.0314
1.0000		.0290

x'/c'	z'/c'	
	Upper surface	Lower surface
0	-0.0128	-0.0128
.0002	-.0106	-.0151
.0011	-.0078	-.0178
.0023	-.0059	-.0198
.0040	-.0038	-.0219
.0063	-.0019	-.0239
.0086	-.0002	-.0253
.0143	.0029	-.0282
.0286	.0083	-.0322
.0429	.0121	-.0344
.0570	.0151	-.0361
.0852	.0199	-.0377
.1132	.0241	-.0387
.1686	.0305	-.0389
.2232	.0353	-.0377
.2770	.0393	-.0356
.3306	.0430	-.0332
.3823	.0461	-.0300
.4338	.0491	-.0263
.4846	.0518	-.0220
.5347	.0541	-.0169
.5841	.0561	-.0105
.6329	.0578	-.0031
.6810	.0590	.0058
.7284	.0596	.0154
.7752	.0598	.0249
.8213	.0590	.0328
.8669	.0569	.0378
.9118	.0531	.0393
.9341	.0505	.0384
.9562	.0471	.0364
.9782	.0431	.0330
.9913	.0398	.0301
1.0000		.0276

x'/c'	z'/c'	
	Upper surface	Lower surface
0	-0.0173	-0.0173
.0002	-.0151	-.0196
.0011	-.0124	-.0223
.0023	-.0105	-.0242
.0040	-.0085	-.0263
.0063	-.0066	-.0282
.0086	-.0049	-.0296
.0143	-.0018	-.0325
.0286	.0035	-.0363
.0429	.0073	-.0384
.0570	.0104	-.0400
.0852	.0153	-.0416
.1132	.0194	-.0425
.1686	.0258	-.0425
.2232	.0309	-.0411
.2770	.0352	-.0388
.3300	.0389	-.0362
.3823	.0422	-.0329
.4338	.0454	-.0288
.4846	.0482	-.0244
.5347	.0506	-.0191
.5841	.0528	-.0127
.6329	.0548	-.0052
.6810	.0561	.0037
.7284	.0570	.0133
.7752	.0574	.0227
.8213	.0568	.0306
.8669	.0548	.0357
.9118	.0514	.0374
.9341	.0489	.0366
.9562	.0455	.0347
.9782	.0414	.0314
.9913	.0382	.0286
1.0000		.0261

TABLE I. - WING COORDINATES ALONG STREAMWISE CHORDS - Concluded

(p) $\frac{y}{b/2} = 0.850;$

$c' = 11.382$ cm (4.481 in.)

(q) $\frac{y}{b/2} = 0.935;$

$c' = 10.051$ cm (3.957 in.)

(r) $\frac{y}{b/2} = 0.968;$

$c' = 9.467$ cm (3.727 in.)

x'/c'	z'/c'	
	Upper surface	Lower surface
0	-0.0221	-0.0221
.0002	-.0199	-.0243
.0011	-.0172	-.0270
.0023	-.0153	-.0289
.0040	-.0133	-.0309
.0063	-.0115	-.0328
.0086	-.0099	-.0342
.0143	-.0068	-.0368
.0286	-.0014	-.0405
.0429	.0025	-.0425
.0570	.0057	-.0440
.0852	.0105	-.0458
.1132	.0144	-.0467
.1686	.0208	-.0465
.2232	.0261	-.0448
.2770	.0304	-.0424
.3300	.0344	-.0394
.3823	.0379	-.0361
.4338	.0411	-.0318
.4846	.0440	-.0271
.5347	.0466	-.0217
.5841	.0493	-.0153
.6329	.0513	-.0077
.6810	.0529	.0014
.7284	.0541	.0109
.7752	.0547	.0202
.8213	.0542	.0282
.8669	.0526	.0334
.9118	.0494	.0353
.9341	.0469	.0347
.9562	.0438	.0329
.9782	.0397	.0296
.9913	.0367	.0269
1.0000		.0246

x'/c'	z'/c'	
	Upper surface	Lower surface
0	-0.0330	-0.0330
.0002	-.0309	-.0352
.0011	-.0283	-.0378
.0023	-.0264	-.0397
.0040	-.0245	-.0416
.0063	-.0227	-.0434
.0086	-.0213	-.0448
.0143	-.0185	-.0473
.0286	-.0133	-.0509
.0429	-.0094	-.0532
.0570	-.0064	-.0549
.0852	-.0014	-.0568
.1132	.0026	-.0574
.1686	.0090	-.0568
.2232	.0143	-.0546
.2770	.0189	-.0519
.3300	.0231	-.0481
.3823	.0271	-.0441
.4338	.0307	-.0395
.4846	.0340	-.0343
.5347	.0371	-.0287
.5841	.0401	-.0221
.6329	.0426	-.0141
.6810	.0447	-.0050
.7284	.0465	.0043
.7752	.0477	.0135
.8213	.0477	.0215
.8669	.0468	.0274
.9118	.0441	.0299
.9341	.0419	.0295
.9562	.0393	.0277
.9852	.0342	.0233
.9913	.0330	.0221
1.0000		.0202

x'/c'	z'/c'	
	Upper surface	Lower surface
0	-0.0382	-0.0382
.0002	-.0362	-.0405
.0011	-.0339	-.0432
.0023	-.0321	-.0450
.0040	-.0301	-.0467
.0063	-.0282	-.0484
.0086	-.0266	-.0497
.0143	-.0235	-.0522
.0286	-.0180	-.0558
.0429	-.0410	-.0580
.0570	-.0108	-.0598
.0852	-.0057	-.0618
.1132	-.0014	-.0622
.1686	.0052	-.0611
.2232	.0102	-.0590
.2770	.0147	-.0560
.3300	.0188	-.0521
.3823	.0230	-.0478
.4338	.0268	-.0428
.4846	.0303	-.0373
.5347	.0338	-.0314
.5841	.0368	-.0247
.6329	.0395	-.0166
.6810	.0417	-.0075
.7284	.0434	.0015
.7752	.0446	.0101
.8213	.0453	.0185
.8669	.0448	.0248
.9118	.0425	.0278
.9341	.0403	.0274
.9562	.0374	.0258
.9852	.0322	.0215
.9913	.0310	.0203
1.0000		.0184

TABLE II. - LOCATION OF PRESSURE ORIFICES ON MODEL

(a) Orifices on wing

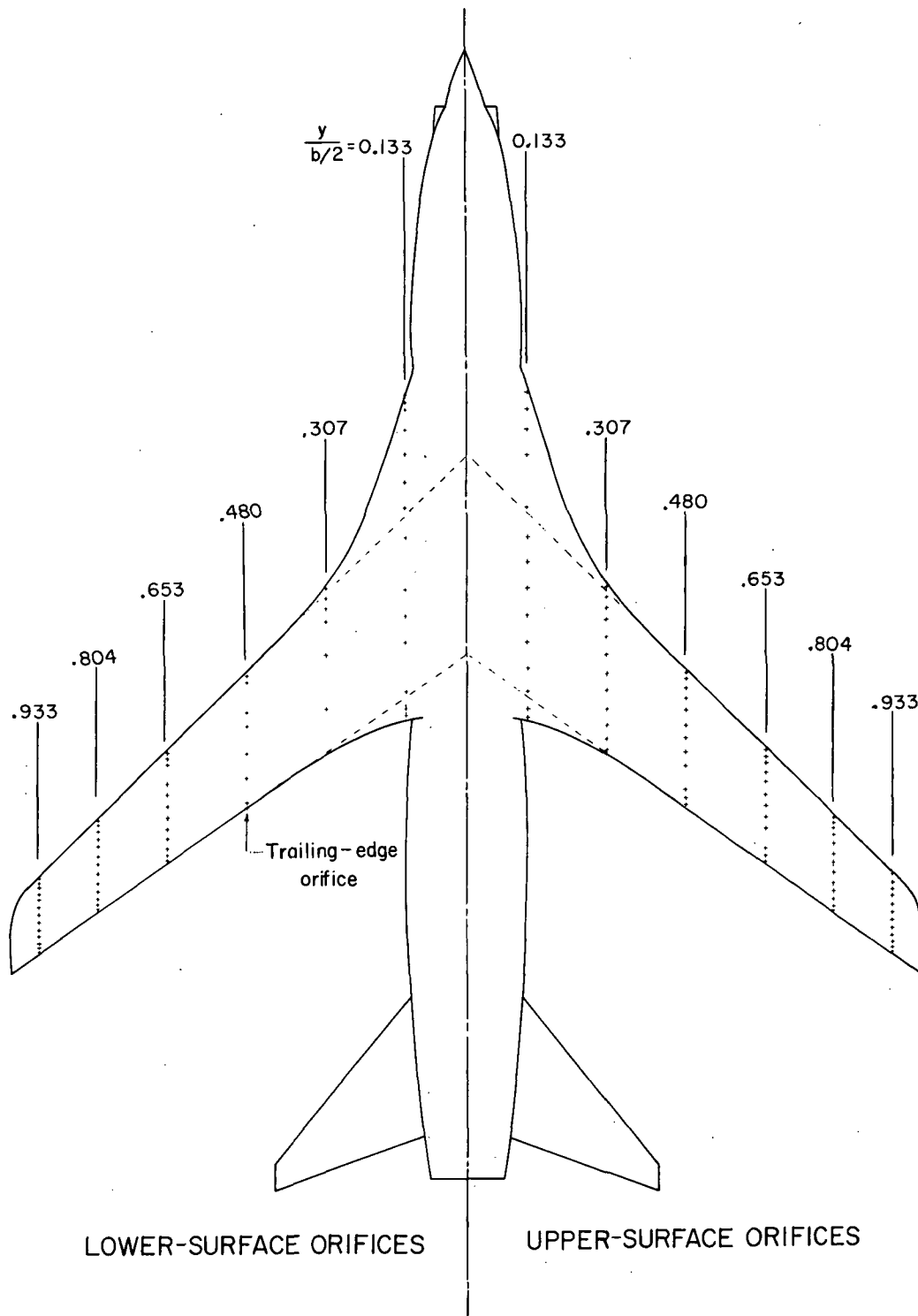


TABLE II. - LOCATION OF PRESSURE ORIFICES ON MODEL - Continued

(a) Orifices on wing - Concluded

[c in cm (in.)]

Wing orifice location, $\frac{x}{c}$, at semispan station, $\frac{y}{b/2}$, of -					
0.133 (c = 22.614) (8.903)	0.307 (c = 19.883) (7.828)	0.480 (c = 17.160) (6.756)	0.653 (c = 14.442) (5.686)	0.804 (c = 12.070) (4.752)	0.933 (c = 10.043) (3.954)
Right wing upper surface					
-0.660	-0.021	0.023	0.025	0.022	0.018
-.567	.035	.068	.079	.075	.077
-.452	.105	.134	.133	.129	.129
-.311	.178	.209	.214	.201	.209
-.023	.286	.294	.295	.294	.293
.133	.396	.404	.407	.397	.494
.272	.514	.497	.502	.495	.590
.416	.618	.599	.601	.594	.693
.565	.733	.700	.698	.693	.777
.713	.835	.864	.863	.784	.861
.854	.919	.926	.923	.856	.918
.980	.987	.975	.977	.926	.972
1.074				.977	
1.122					
Left wing lower surface					
-0.660	-0.022	0.024	0.025	0.019	0.020
-.616	.038	.075	.074	.066	.076
-.572	.101	.297	.130	.136	.136
-.462	.185	.400	.298	.214	.221
-.329	.398	.604	.397	.292	.295
-.172	.737	.785	.501	.403	.396
-.030		.967	.603	.489	.497
.128		1.000	.703	.594	.597
.418			.784	.700	.702
.564			.868	.786	.786
.710			.923	.858	.864
.976			.972	.919	.912
1.072				.967	.985
1.110					

TABLE II. - LOCATION OF PRESSURE ORIFICES ON MODEL - Continued

(b) Orifices on rear of fuselage

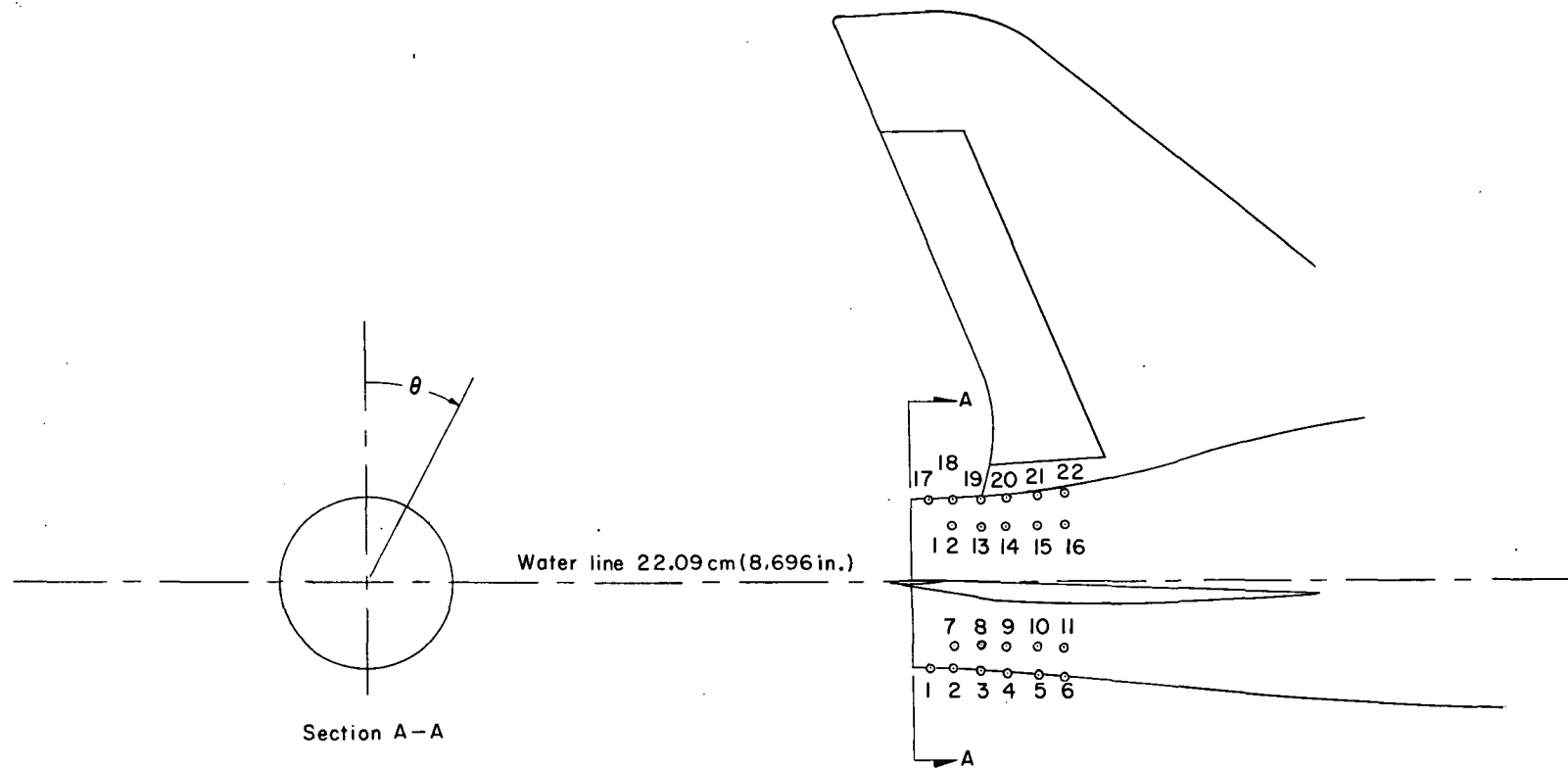


TABLE II. - LOCATION OF PRESSURE ORIFICES ON MODEL - Concluded

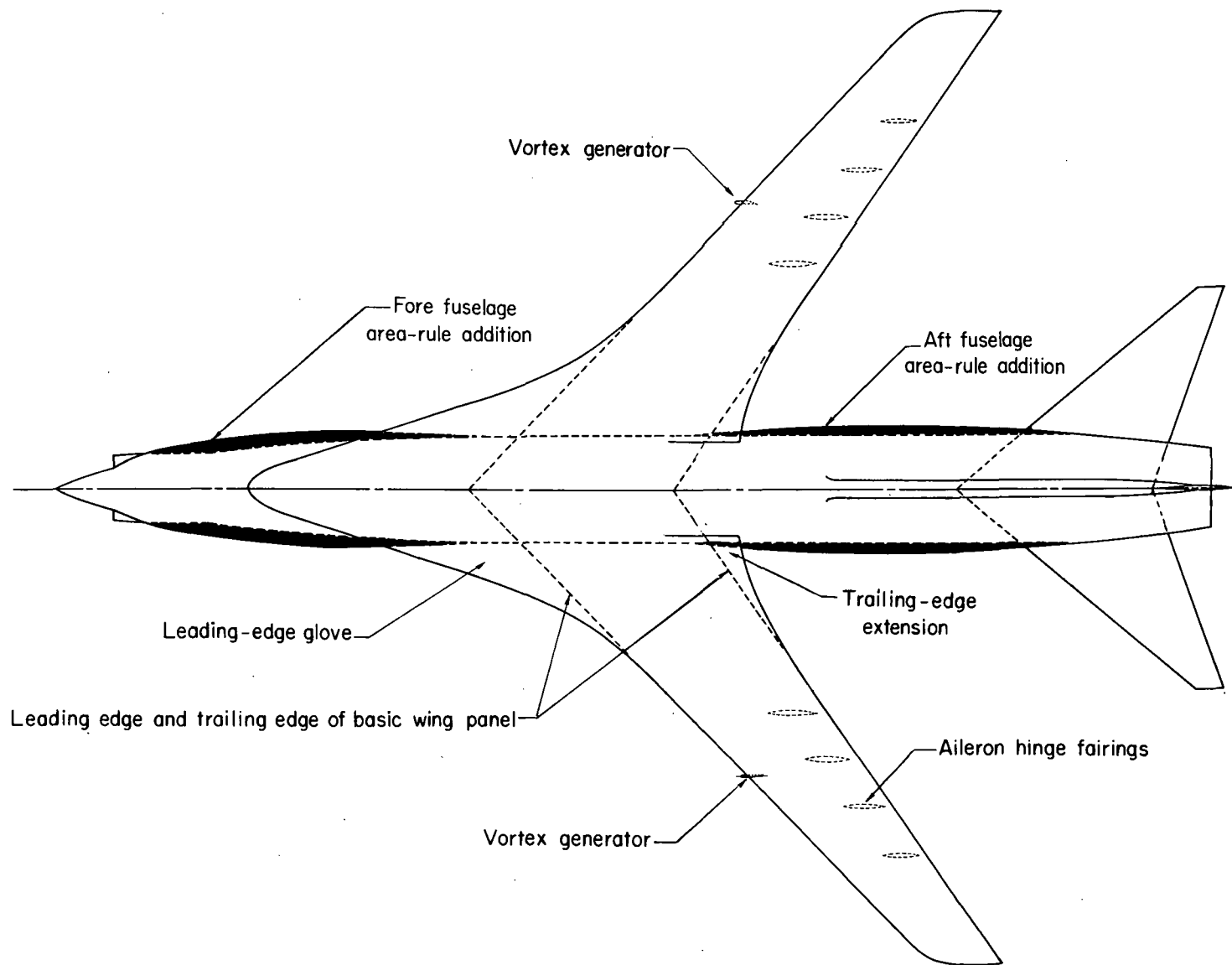
(b) Orifices on rear of fuselage - Concluded

Orifice	θ , deg	Model fuselage station	
		cm	in.
1	179.7	160.45	63.17
2	179.7	159.08	62.63
3	179.7	157.56	62.03
4	181.0	156.13	61.47
5	180.6	154.25	60.73
6	179.8	152.88	60.19
7	137.1	159.16	62.66
8	137.3	157.84	62.14
9	136.6	156.21	61.50
10	135.5	154.61	60.87
11	135.2	152.96	60.22
12	45.1	159.16	62.66
13	45.7	157.63	62.06
14	45.5	156.06	61.44
15	45.2	154.36	60.77
16	45.1	152.88	60.19
17	8.1	160.78	63.30
18	8.2	159.03	62.61
19	8.6	157.56	62.03
20	9.2	156.01	61.42
21	8.6	154.28	60.74
22	9.6	153.01	60.24

TABLE III. - TUNNEL TEST CONDITIONS

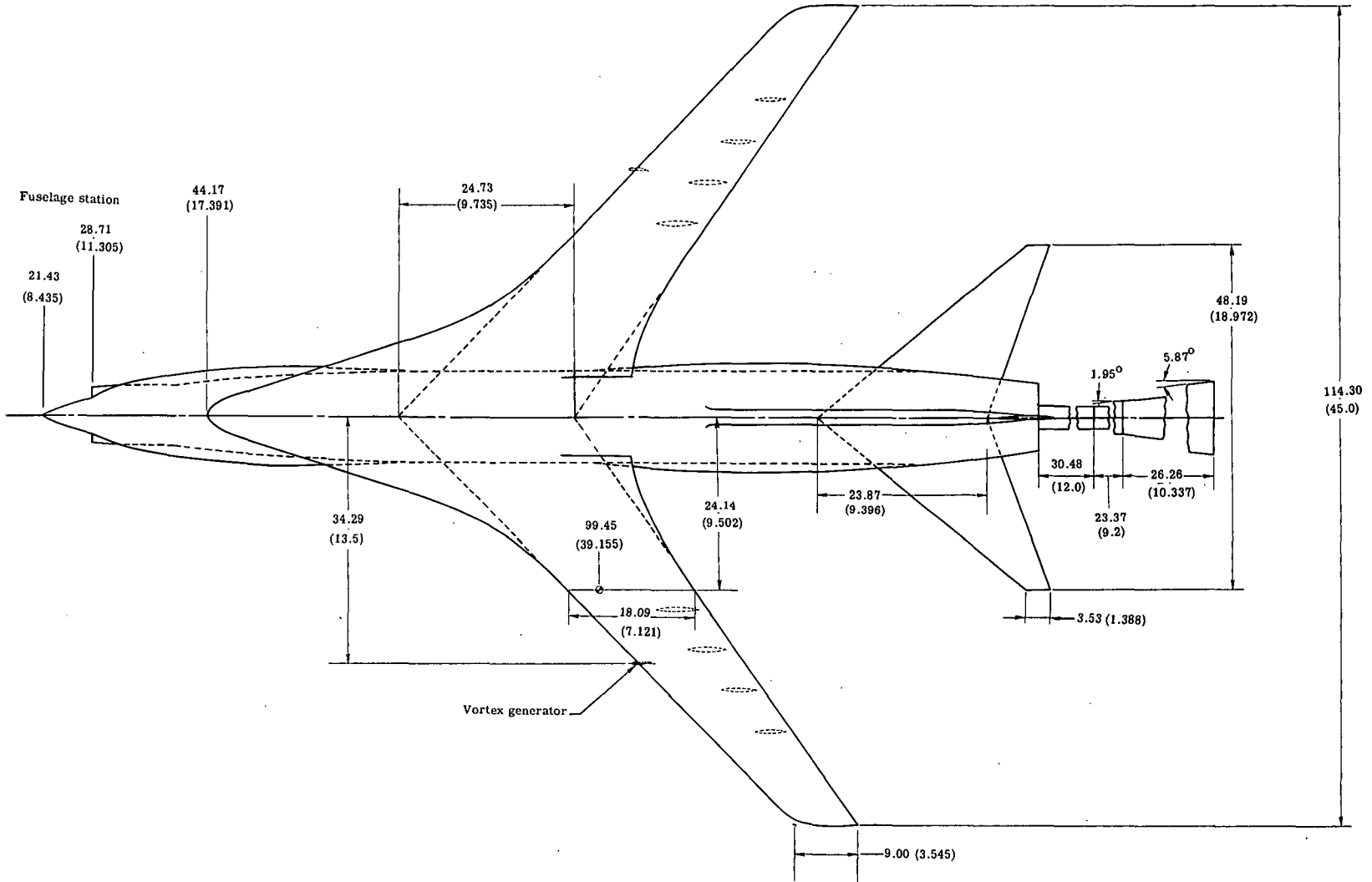
Mach number	Temperature		Reynolds number		Dynamic pressure	
	K	°F	per m	per ft	N/m ²	lb/ft ²
1.00	322	120	14.8	4.5	40 698	850
.99	322	120	14.8	4.5	40 698	850
.98	322	120	14.8	4.5	40 698	850
.97	322	120	14.8	4.5	40 698	850
.95	322	120	15.1	4.6	40 698	850
.90	322	120	15.7	4.8	40 698	850
.80	322	120	17.1	5.2	40 698	850
.50	322	120	13.1	4.0	21 546	450
.25	322	120	10.2	3.1	8 571	179





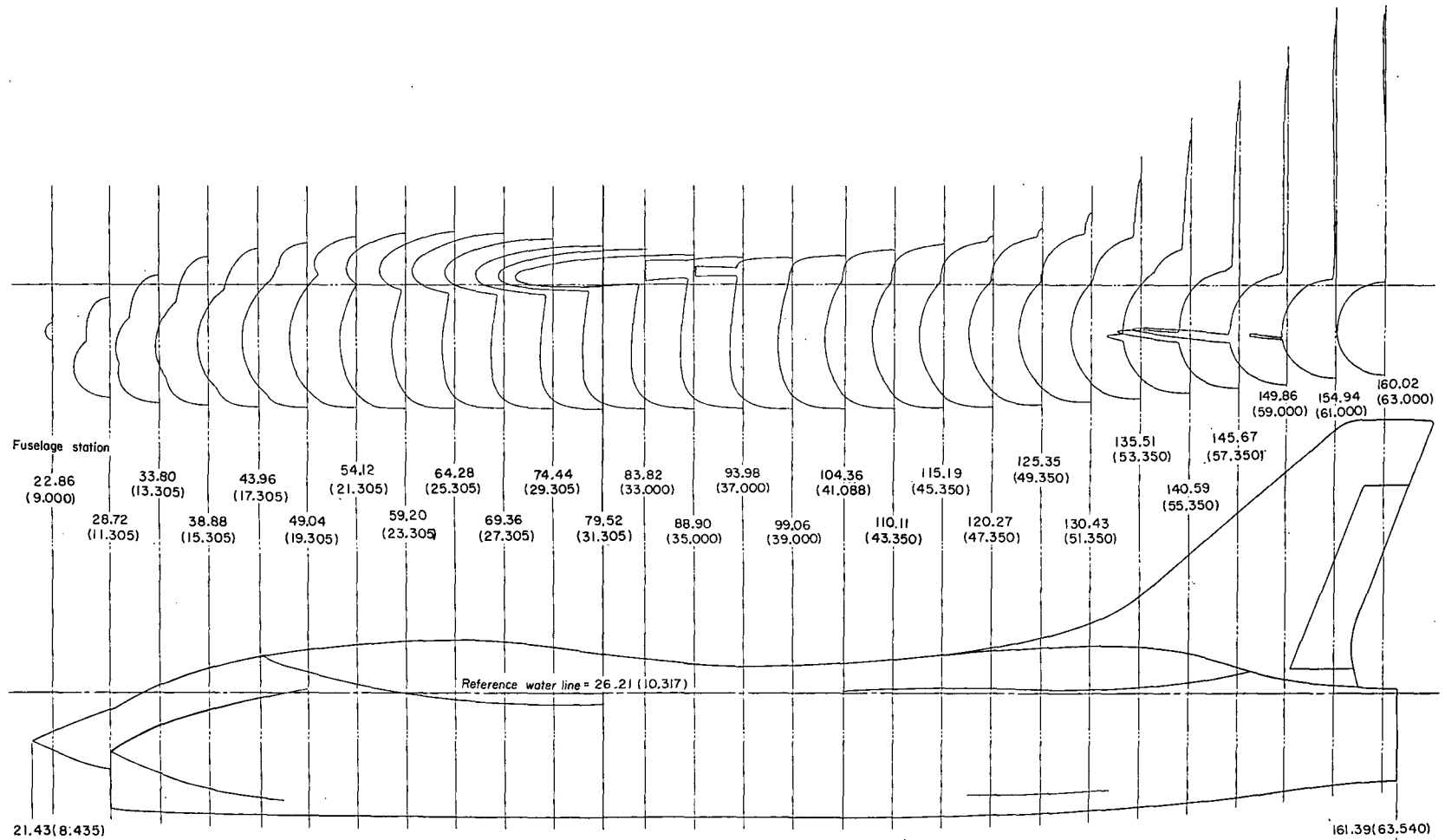
(a) General planform arrangement of 0.087-scale model.

Figure 1.- Model details. Linear dimensions are in cm (in.).



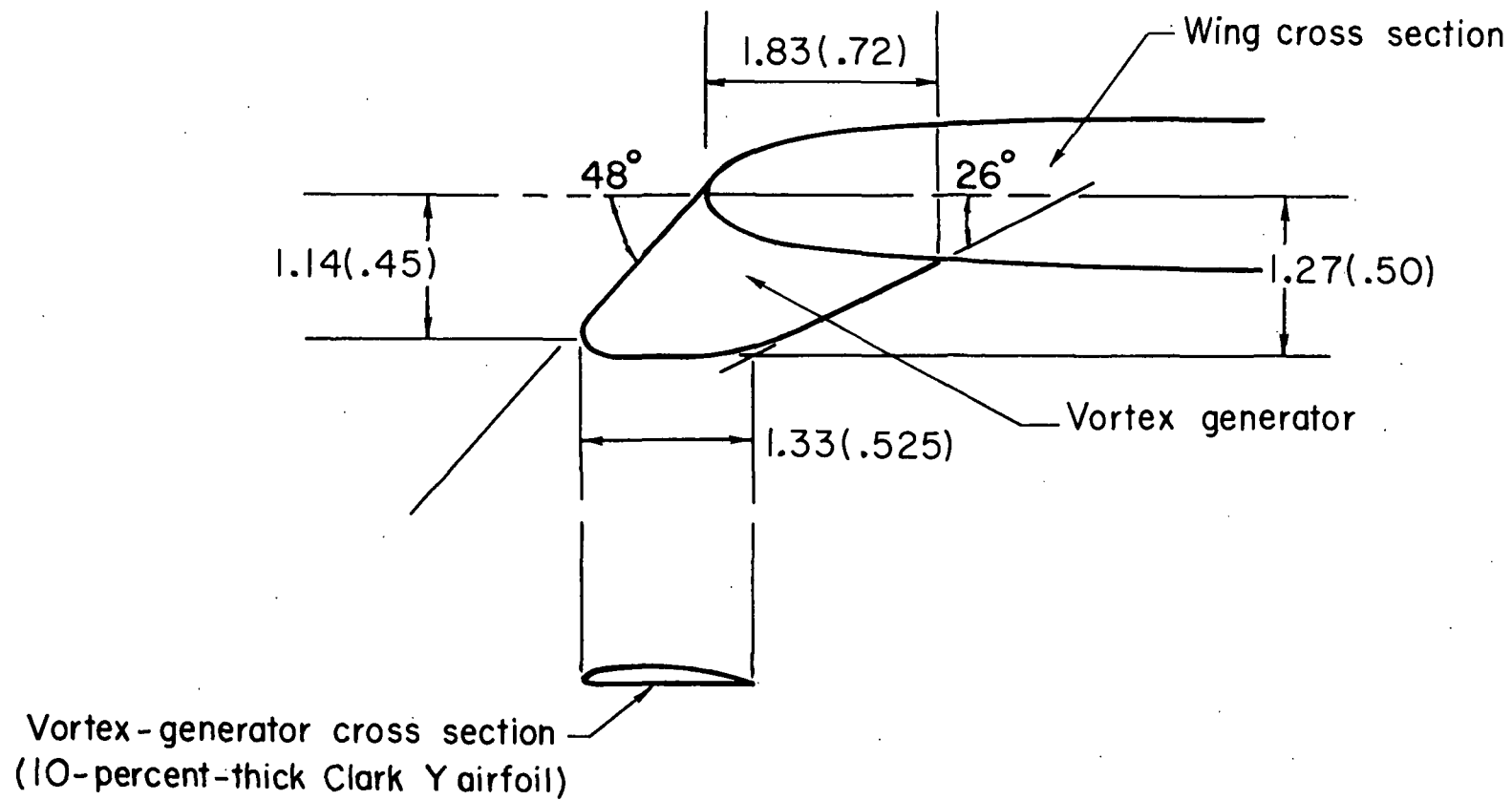
(a) Concluded.

Figure 1. - Continued.



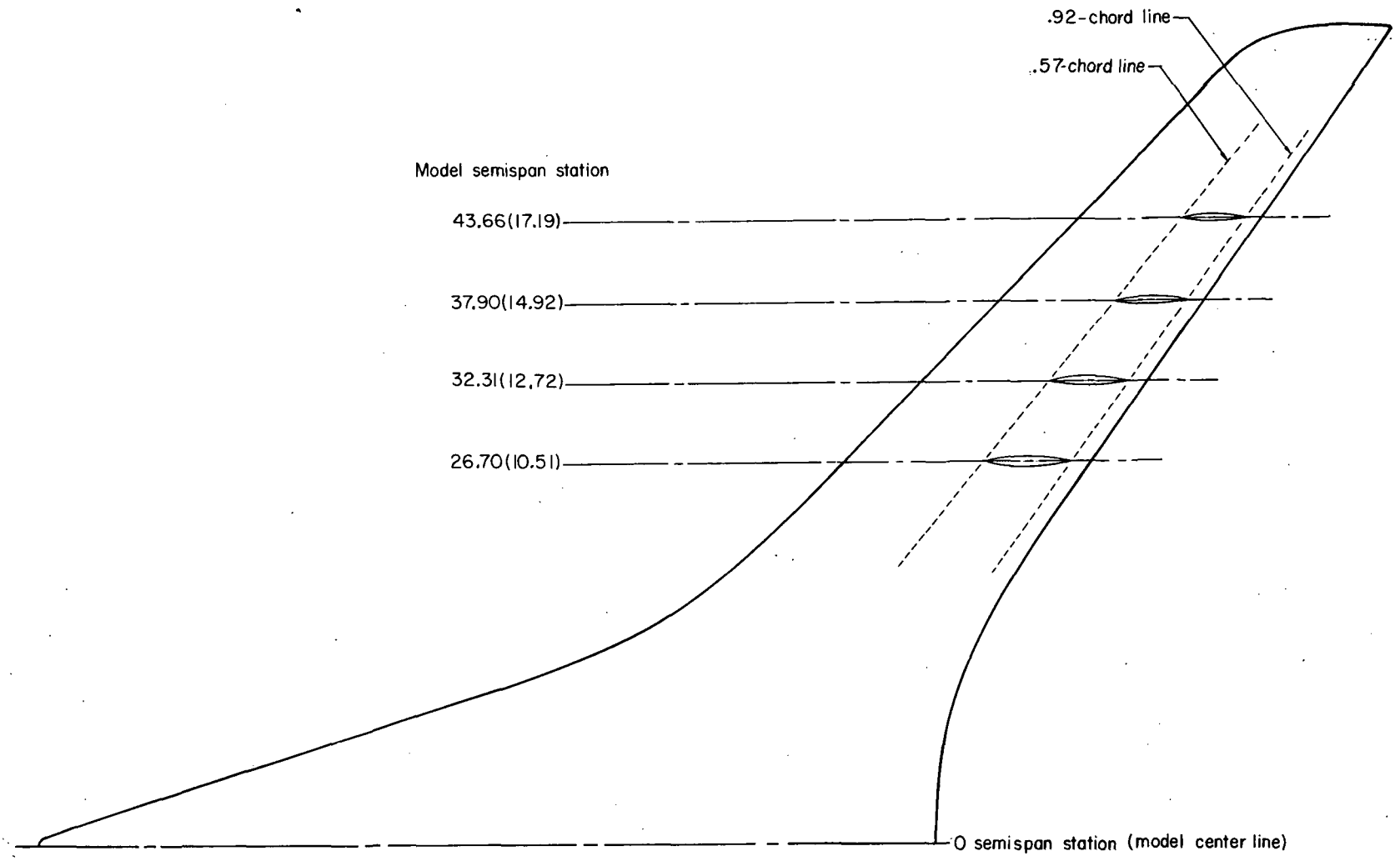
(b) Cross-section layout of 0.087-scale model with fuselage area-rule additions.

Figure 1. - Continued.



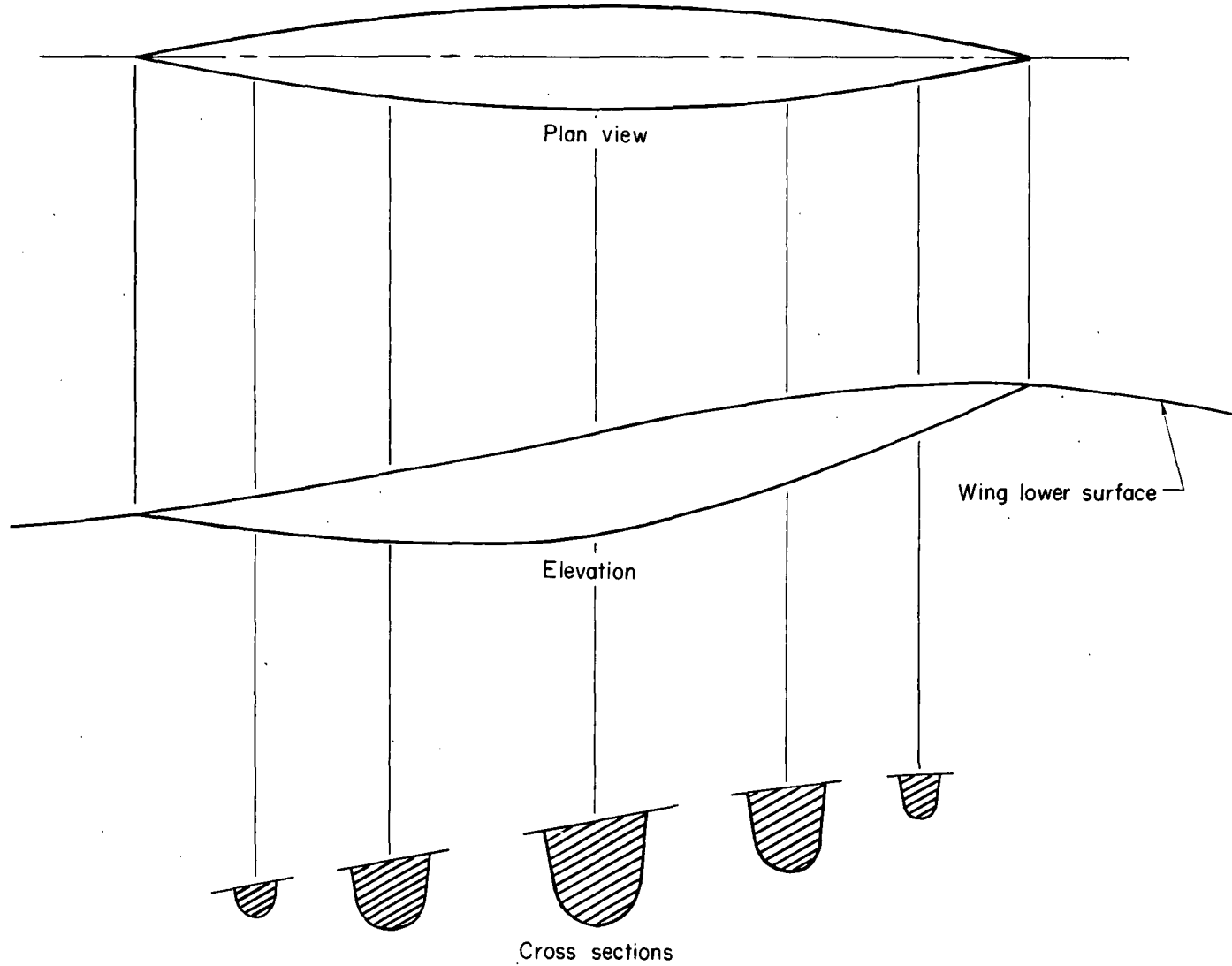
(c) Sketch of underwing leading-edge vortex generator.

Figure 1. - Continued.



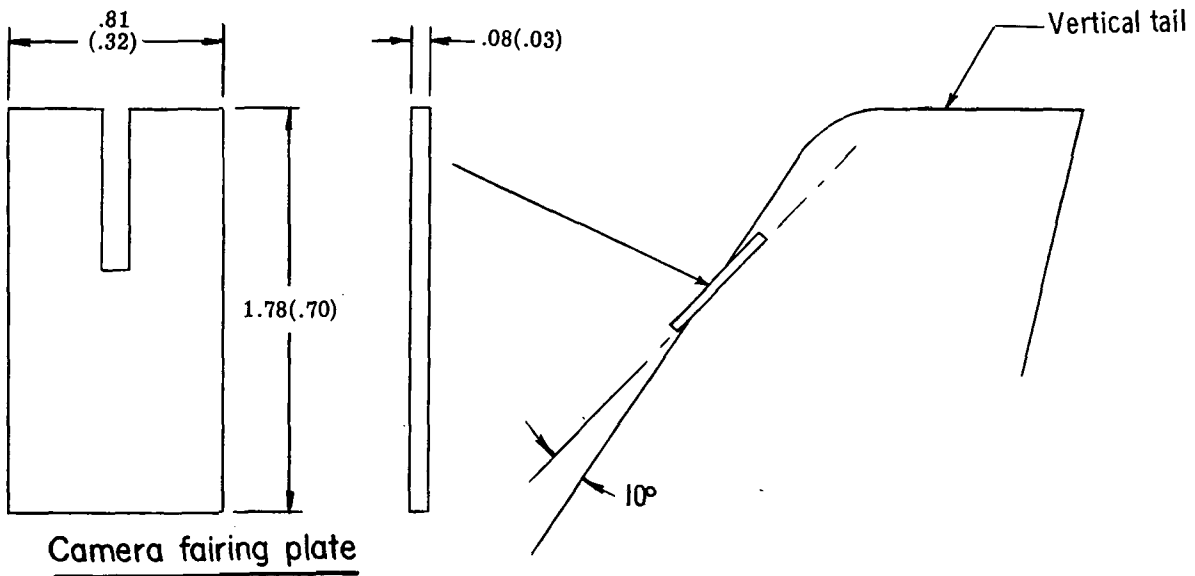
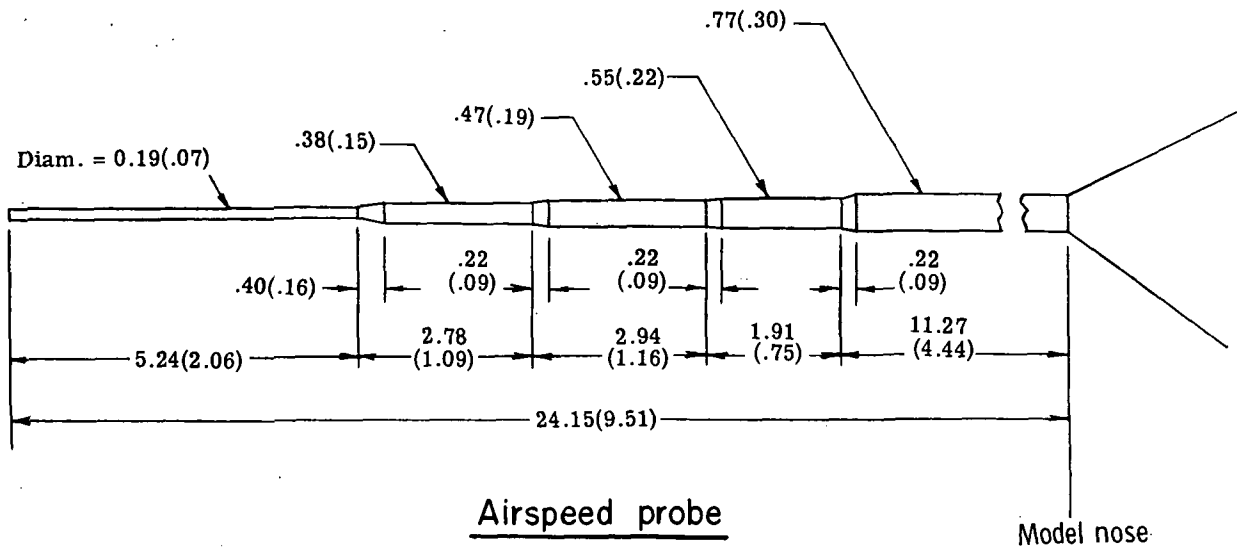
(d) Location of aileron hinge fairings.

Figure 1. - Continued.



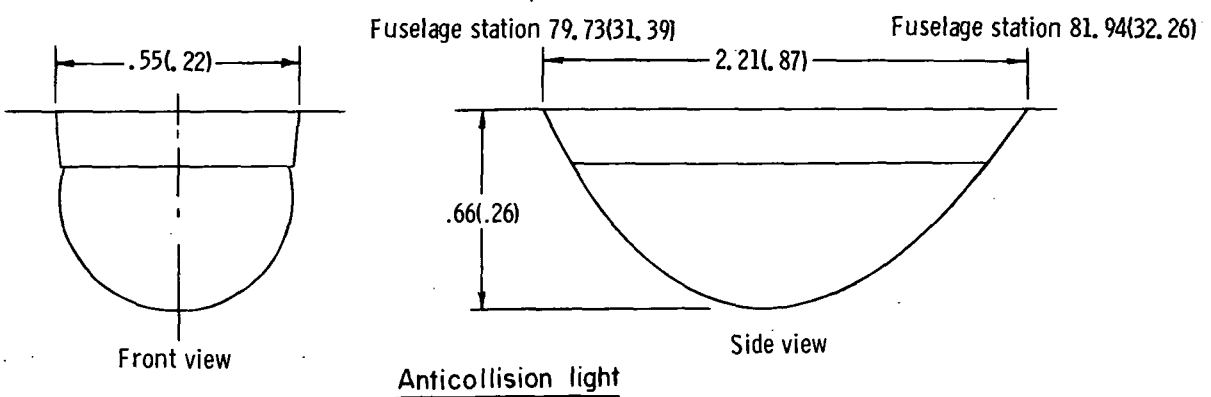
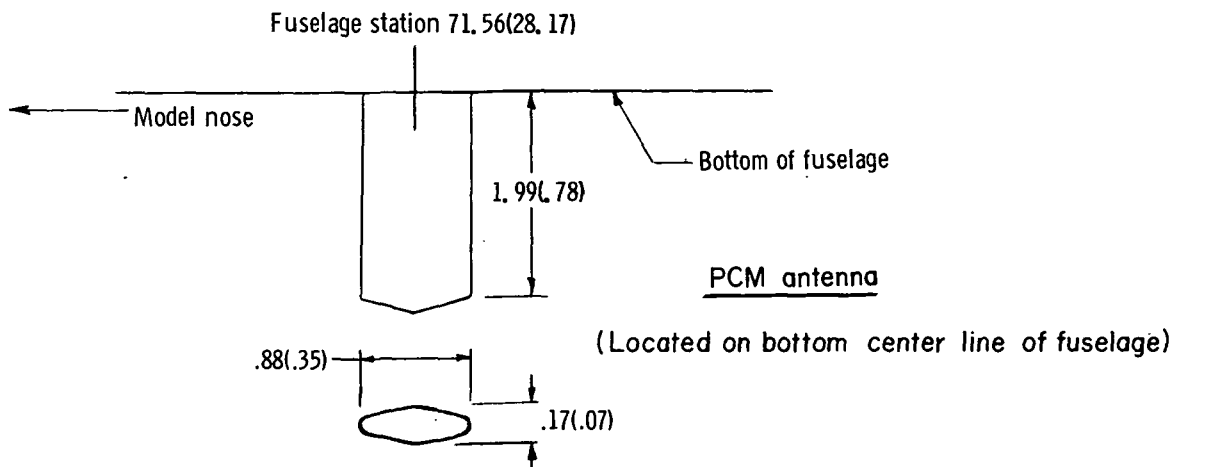
(e) Sketch of typical aileron hinge fairing.

Figure 1.- Continued.

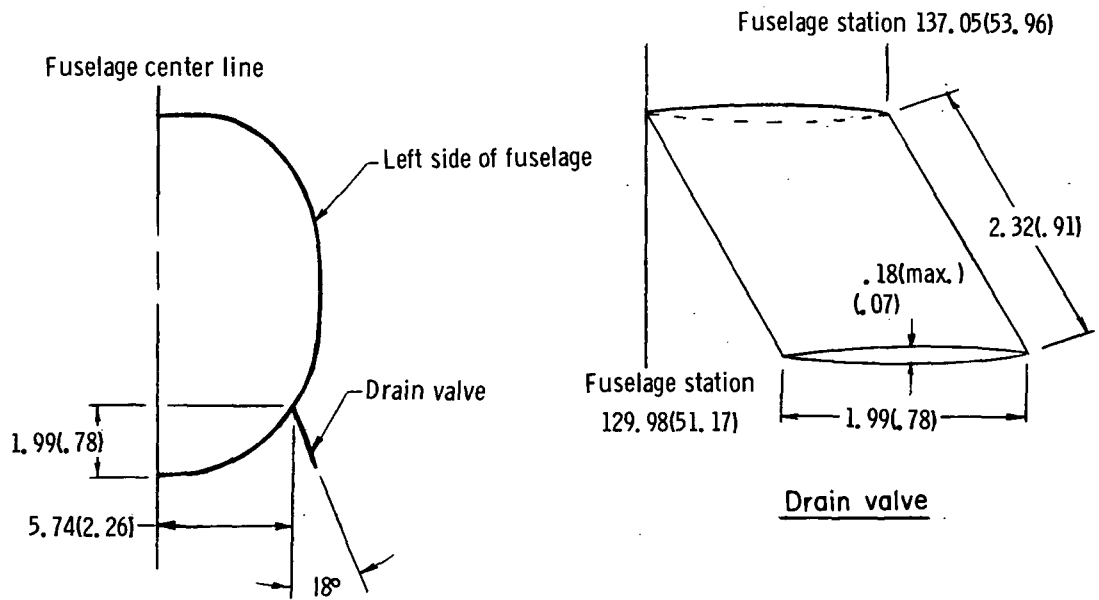


(f) Simulated full-scale airplane protuberances.

Figure 1.- Continued.

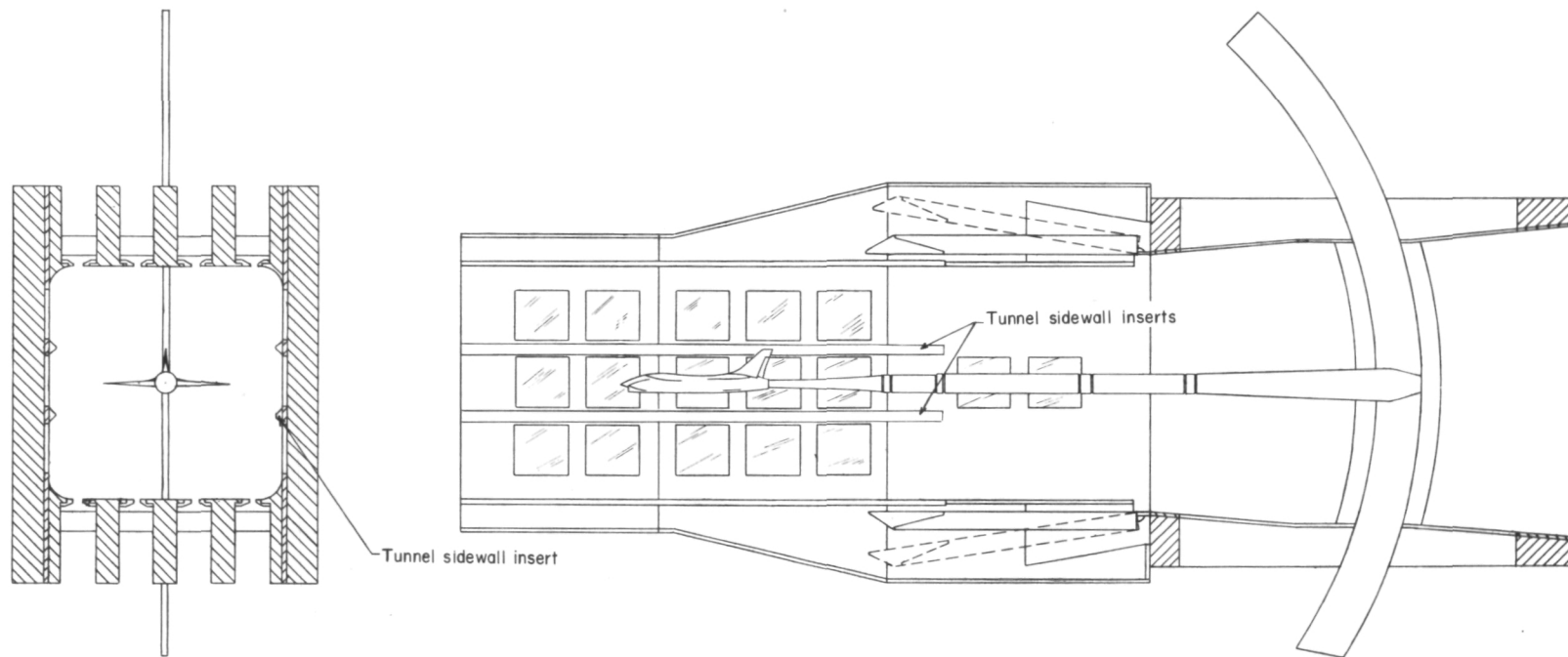


(Located 15.24 cm [6 in.] left of bottom center line of fuselage)



(f) Concluded.

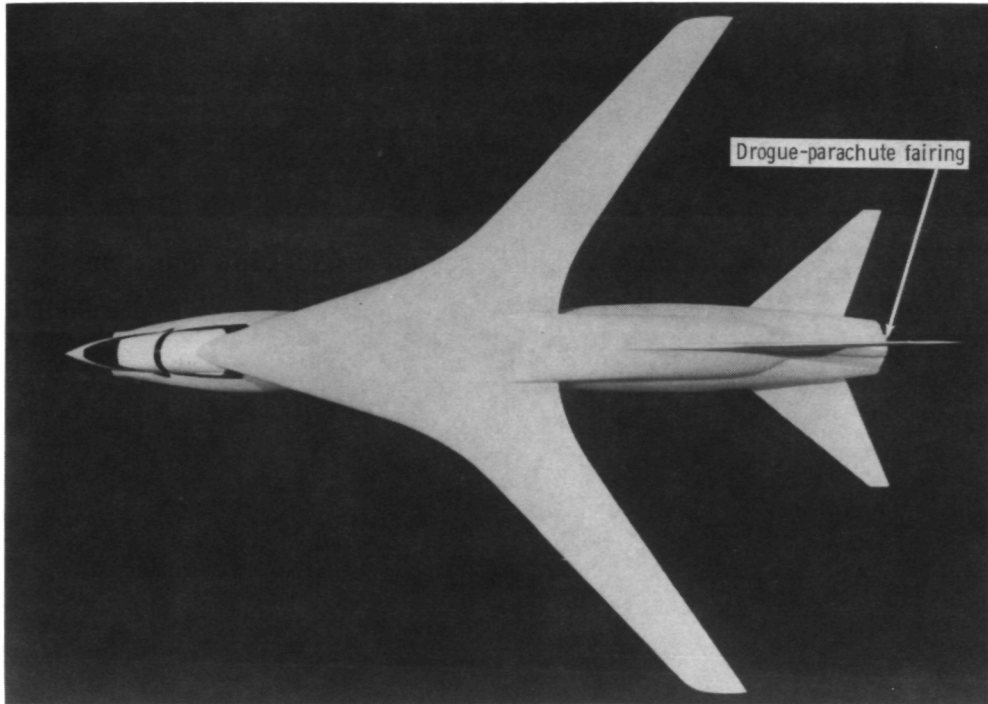
Figure 1.- Continued.



(g) Tunnel test section with sidewall inserts.

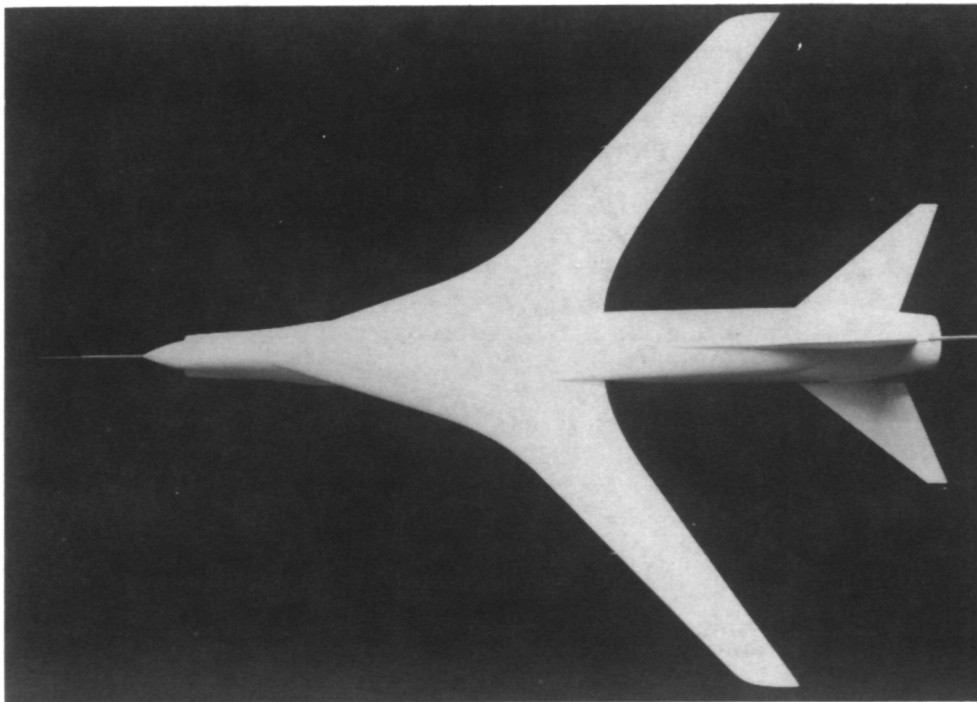
Figure 1. - Concluded.

~~CONFIDENTIAL~~



L-70-3988.1

Top view of model with fuselage area-rule additions



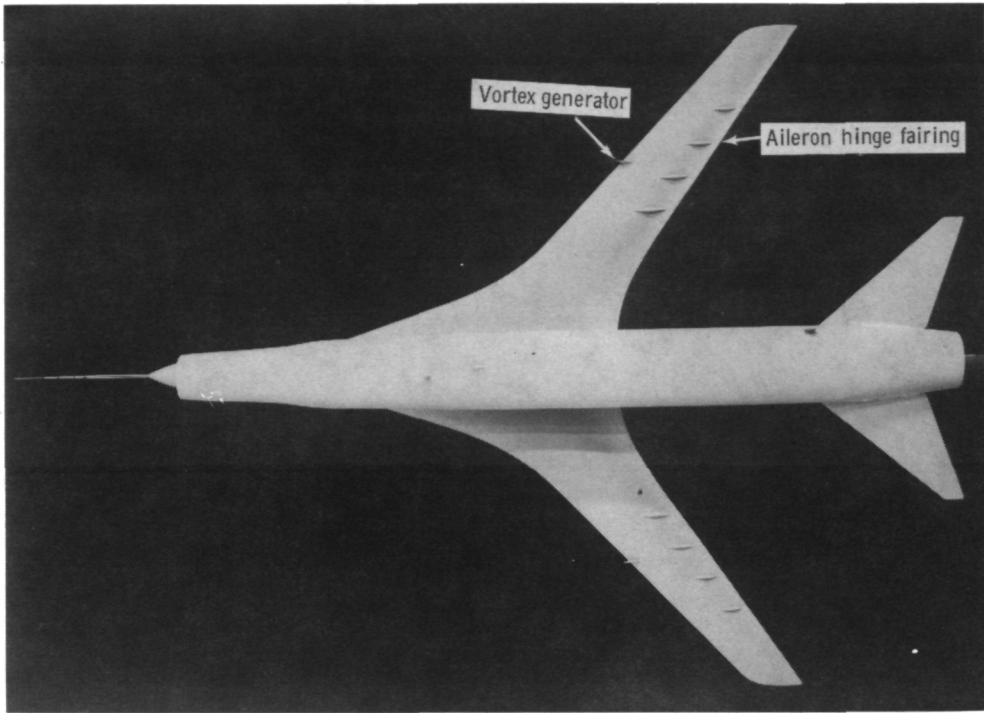
L-71-6987

Top view of model without fuselage area-rule additions

Figure 2.- Photographs of 0.087-scale wind-tunnel model.

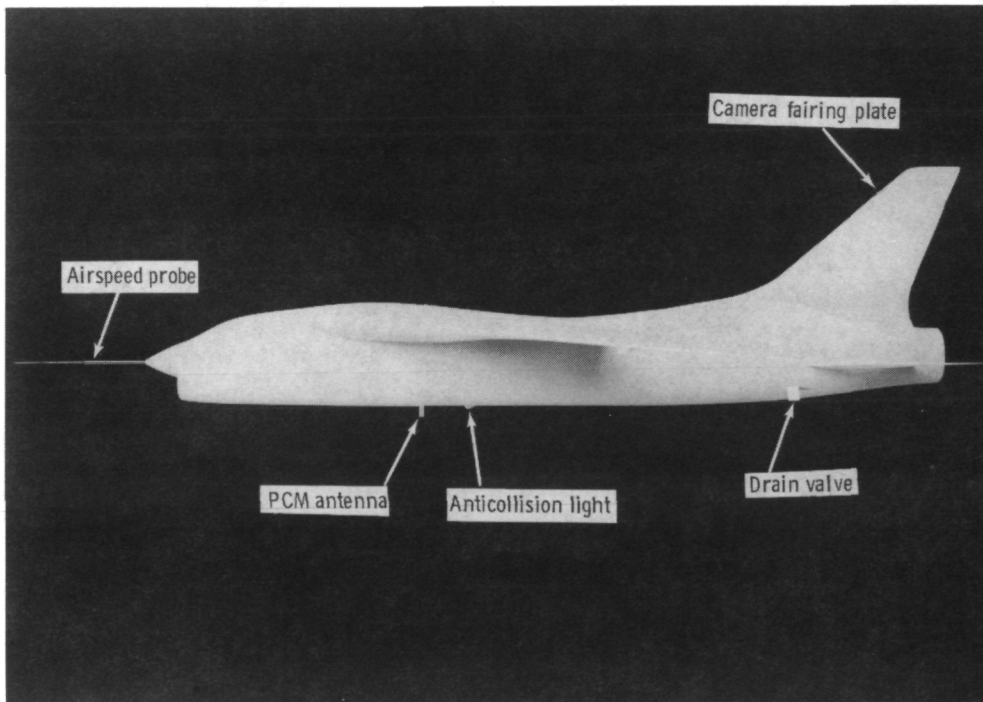
~~CONFIDENTIAL~~

~~CONFIDENTIAL~~



L-71-6992.1

Bottom view of model without fuselage area-rule additions

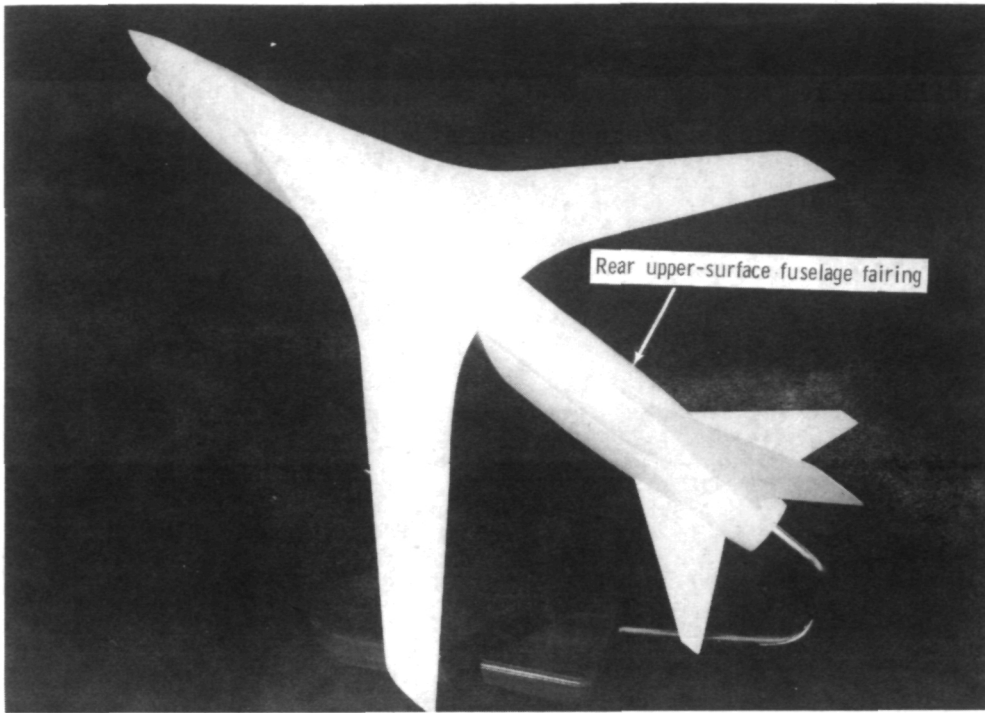


L-71-6991.1

Side view of model without fuselage area-rule additions

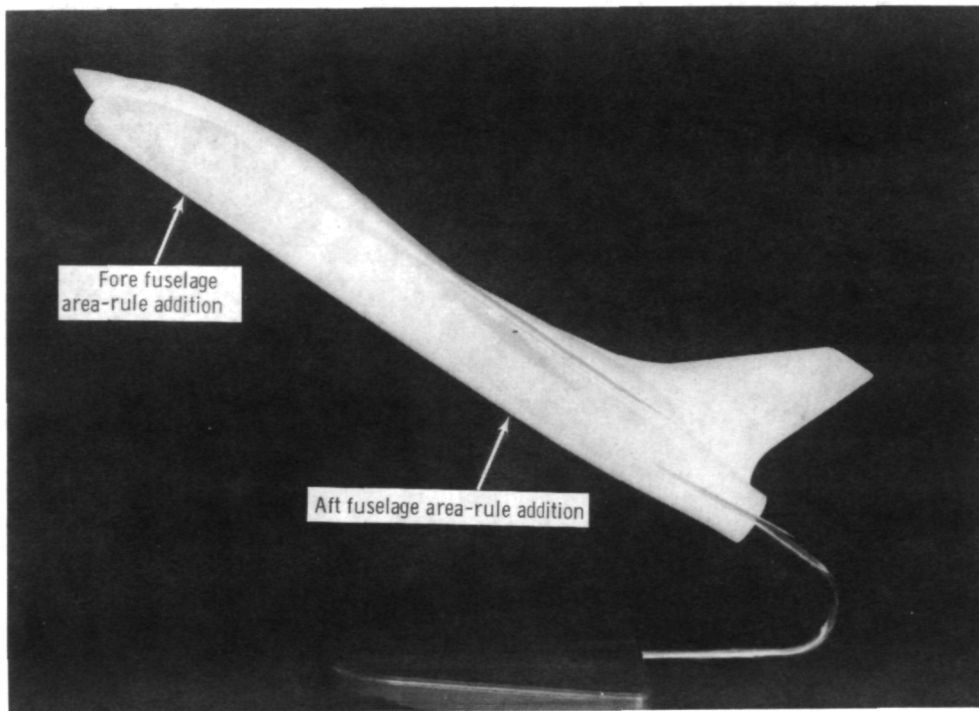
Figure 2.- Continued.

~~CONFIDENTIAL~~



L-72-1117.1

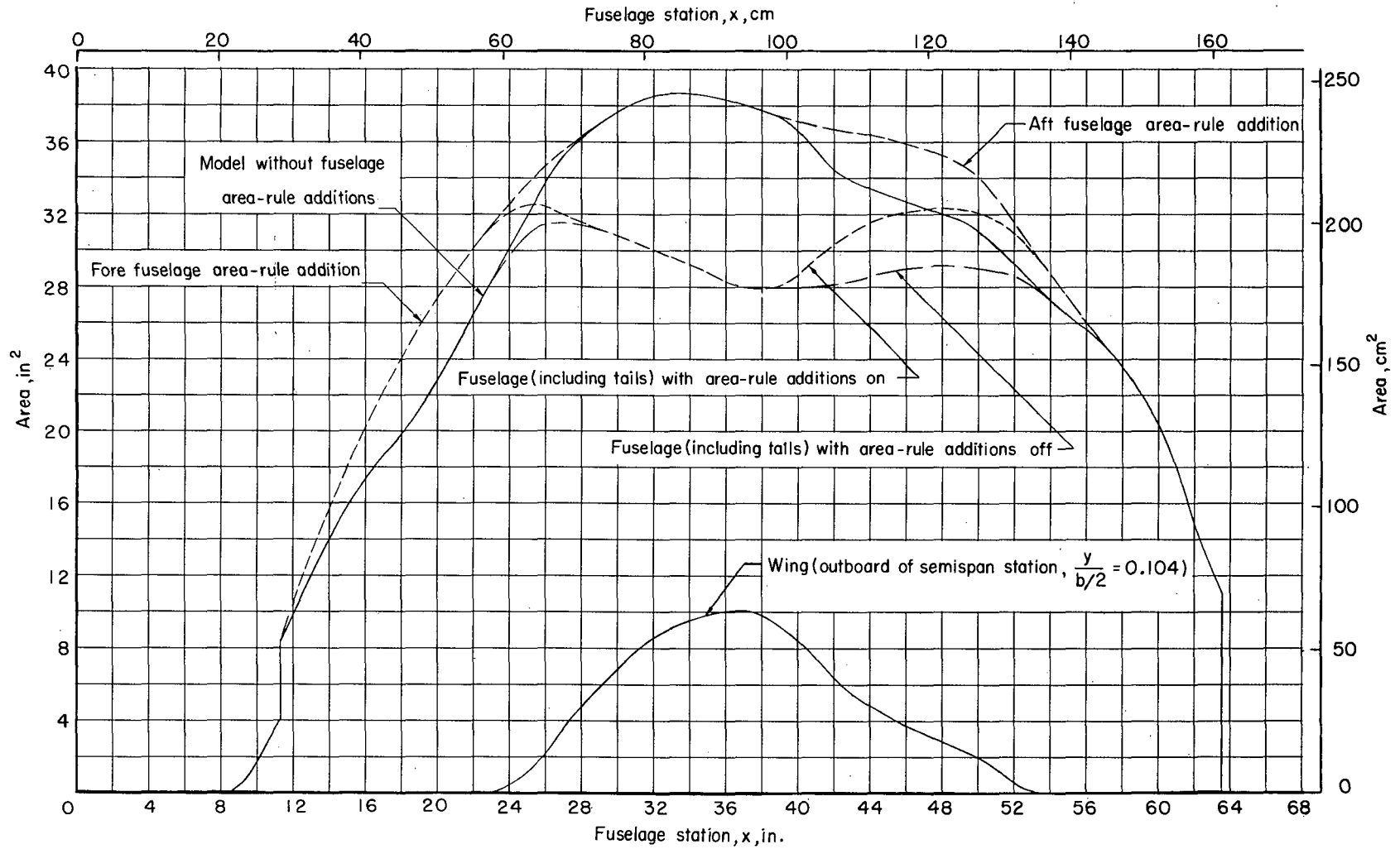
Three-quarter top view of model with fuselage area-rule additions



L-72-1119.1

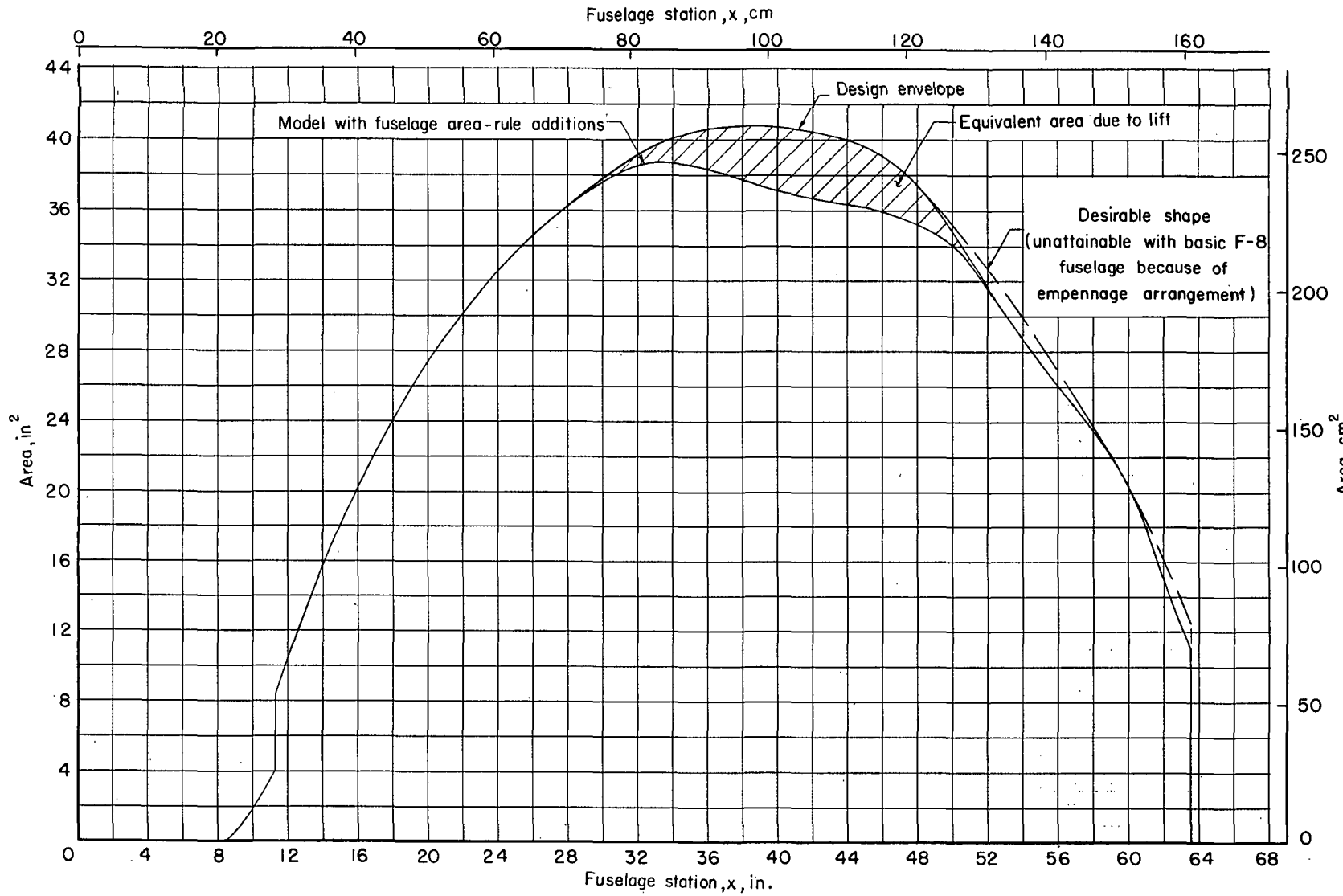
Side view of model with fuselage area-rule additions

Figure 2.- Concluded.



(a) Geometric areas.

Figure 3.- Longitudinal progression of cross-sectional area taken normal to fuselage center line.
 Model and fuselage areas include 28.39 cm² (4.40 in²) of inlet area.

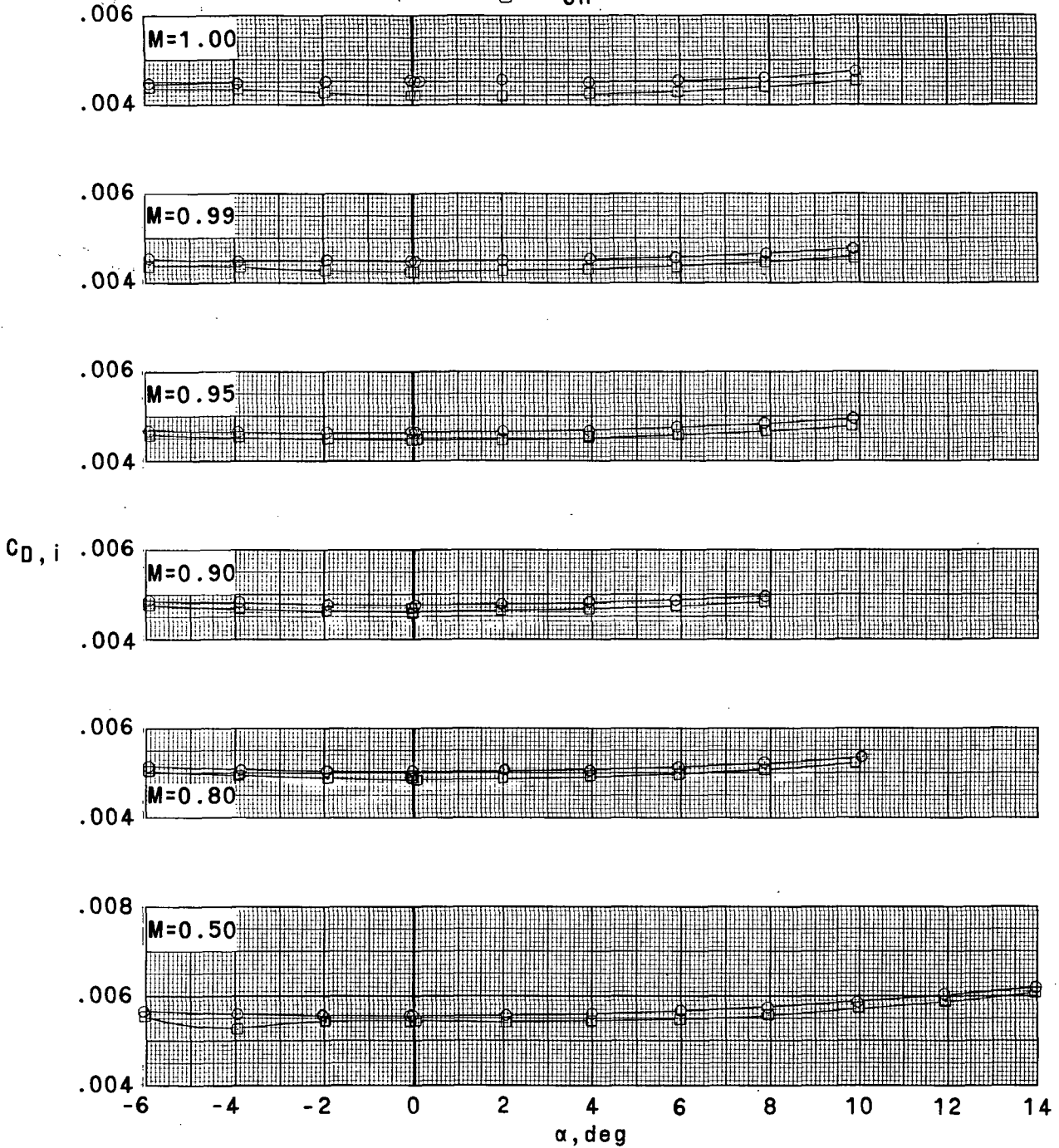


(b) Design envelope, including equivalent area due to lift.

Figure 3. - Concluded.

Area-rule additions

○ Off
□ On

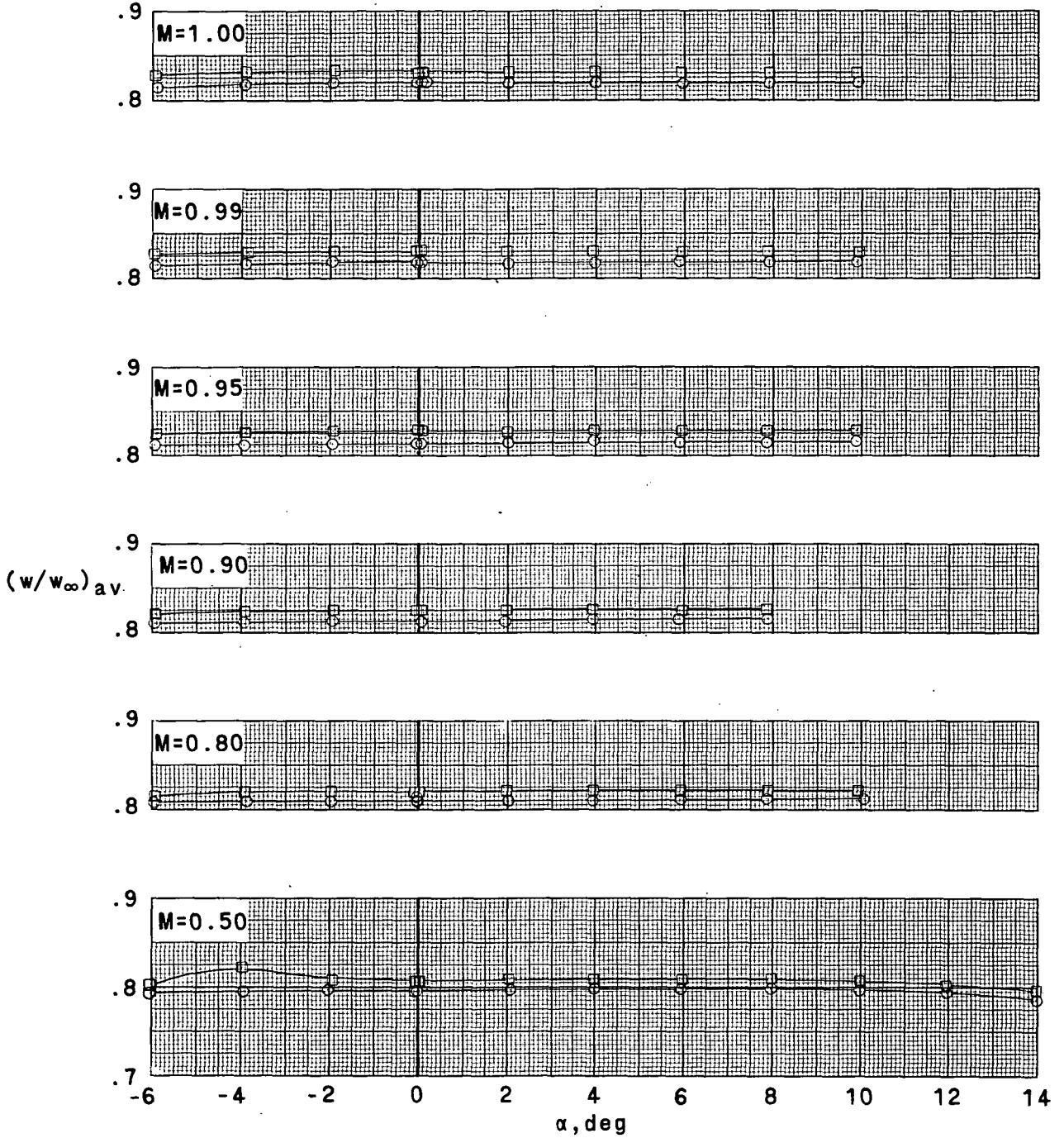


(a) Variation with angle of attack of internal-drag coefficient.

Figure 4.- Effect of fuselage area-rule additions on the internal drag and mass-flow characteristics. $\beta = 0^\circ$; $\delta_h = -2.5^\circ$.

Area-rule additions

○ Off
□ On



(b) Variation with angle of attack of average mass-flow ratio of ducts.

Figure 4.- Concluded.

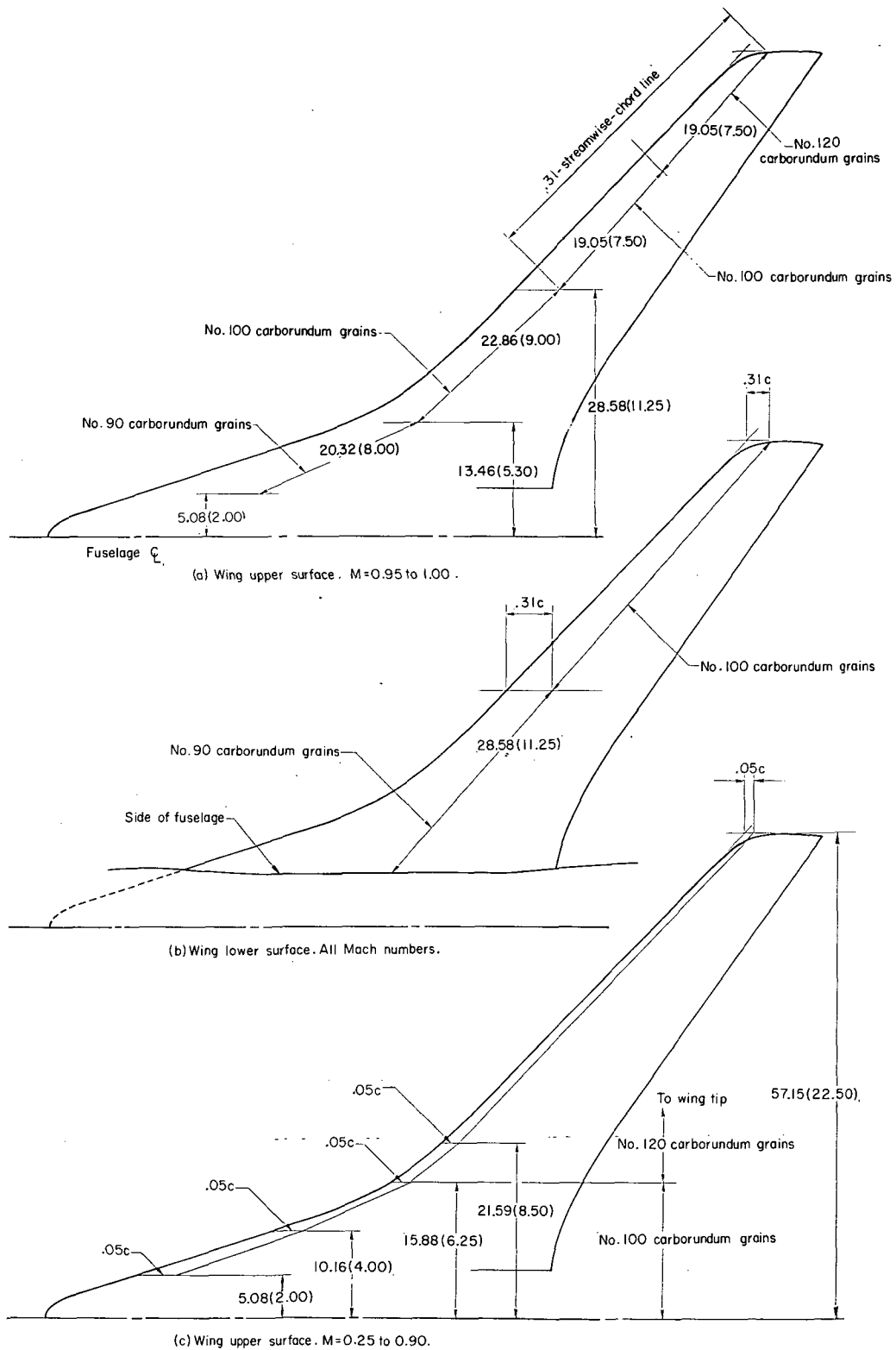
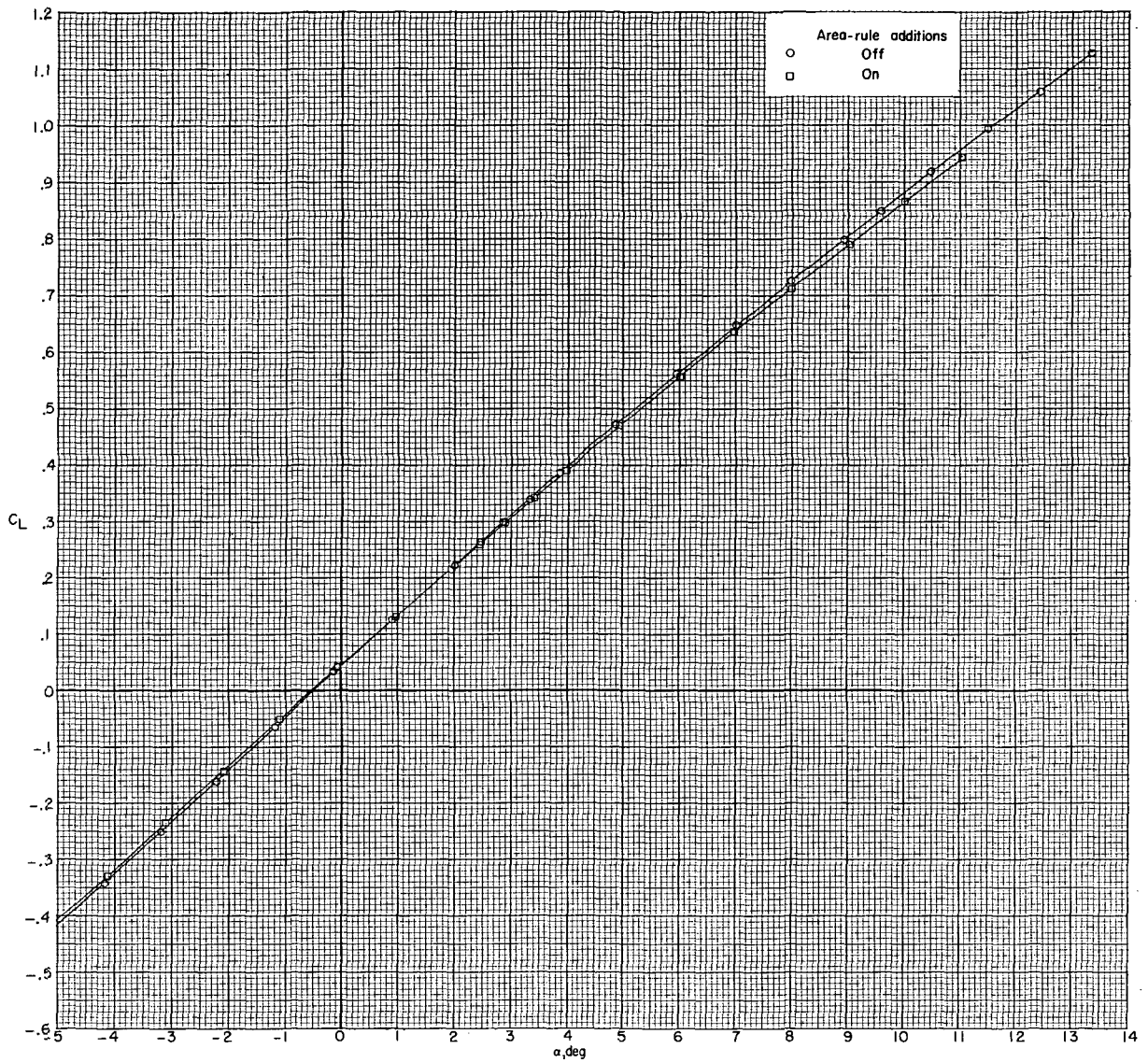
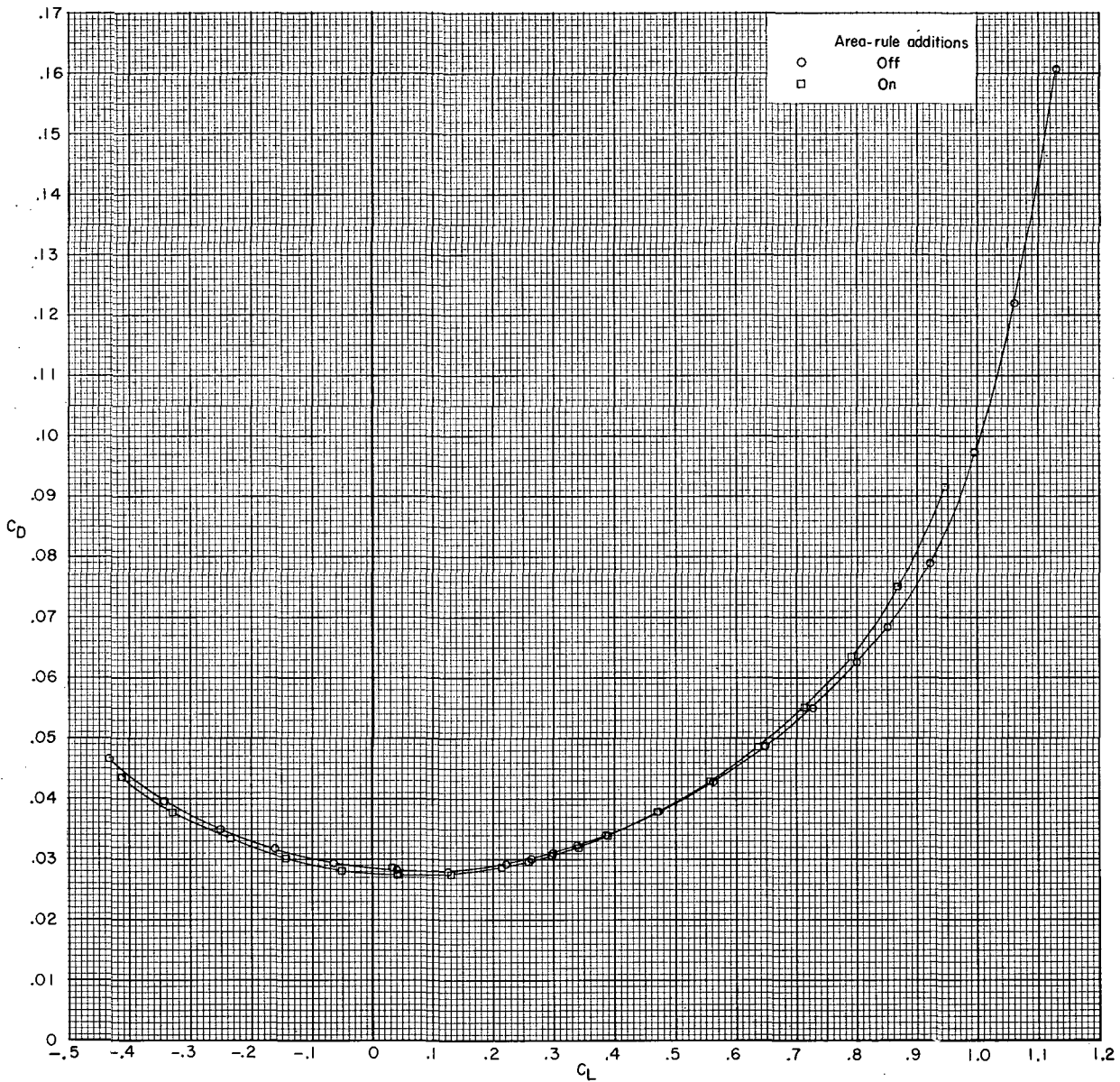


Figure 5.- Boundary-layer trip arrangements. Dimensions are in cm (in.).



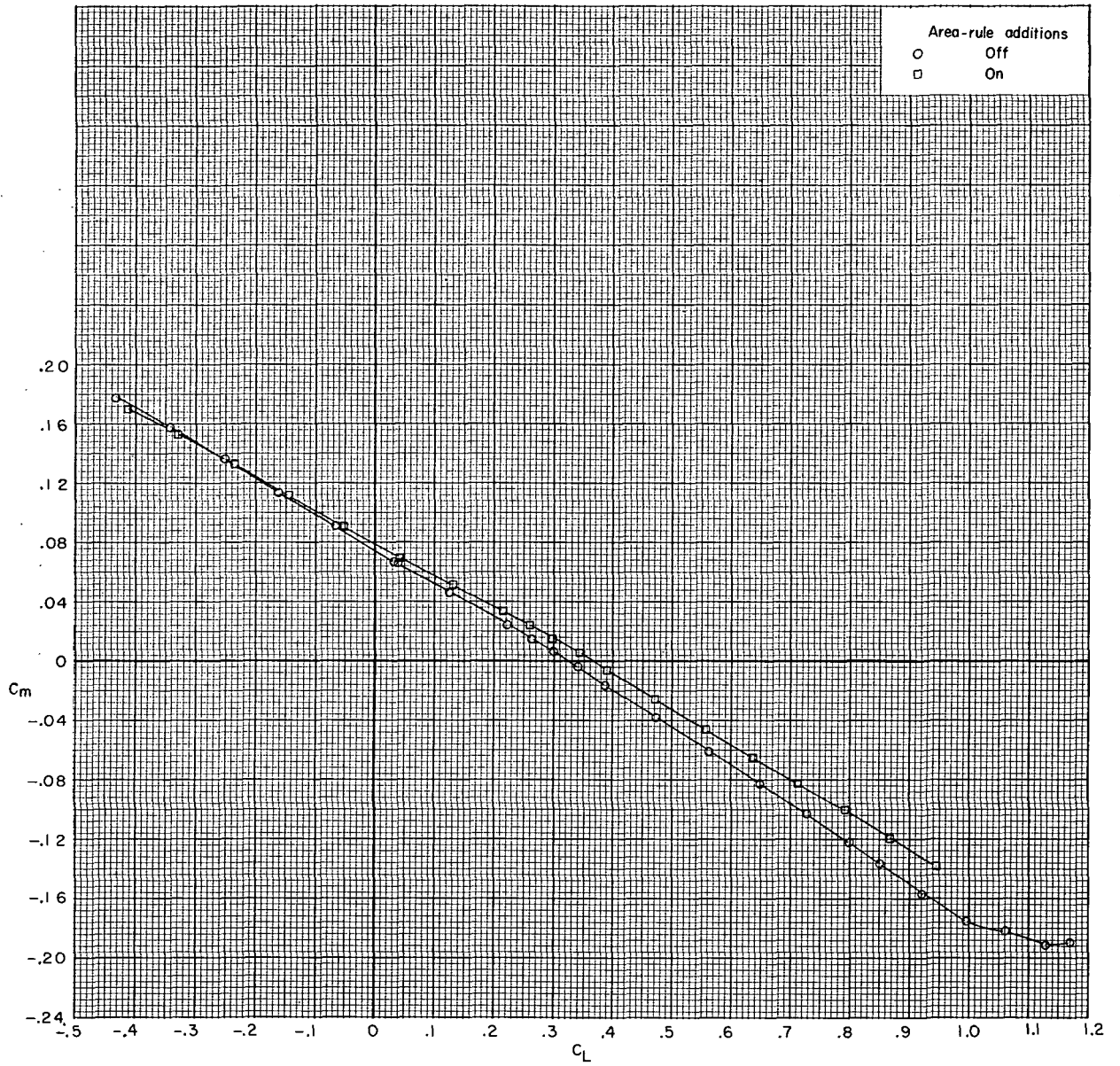
(a) $M = 0.25$.

Figure 6.- Effect of fuselage area-rule additions on longitudinal aerodynamic characteristics. $\beta = 0^\circ$; $\delta_h = -2.5^\circ$.



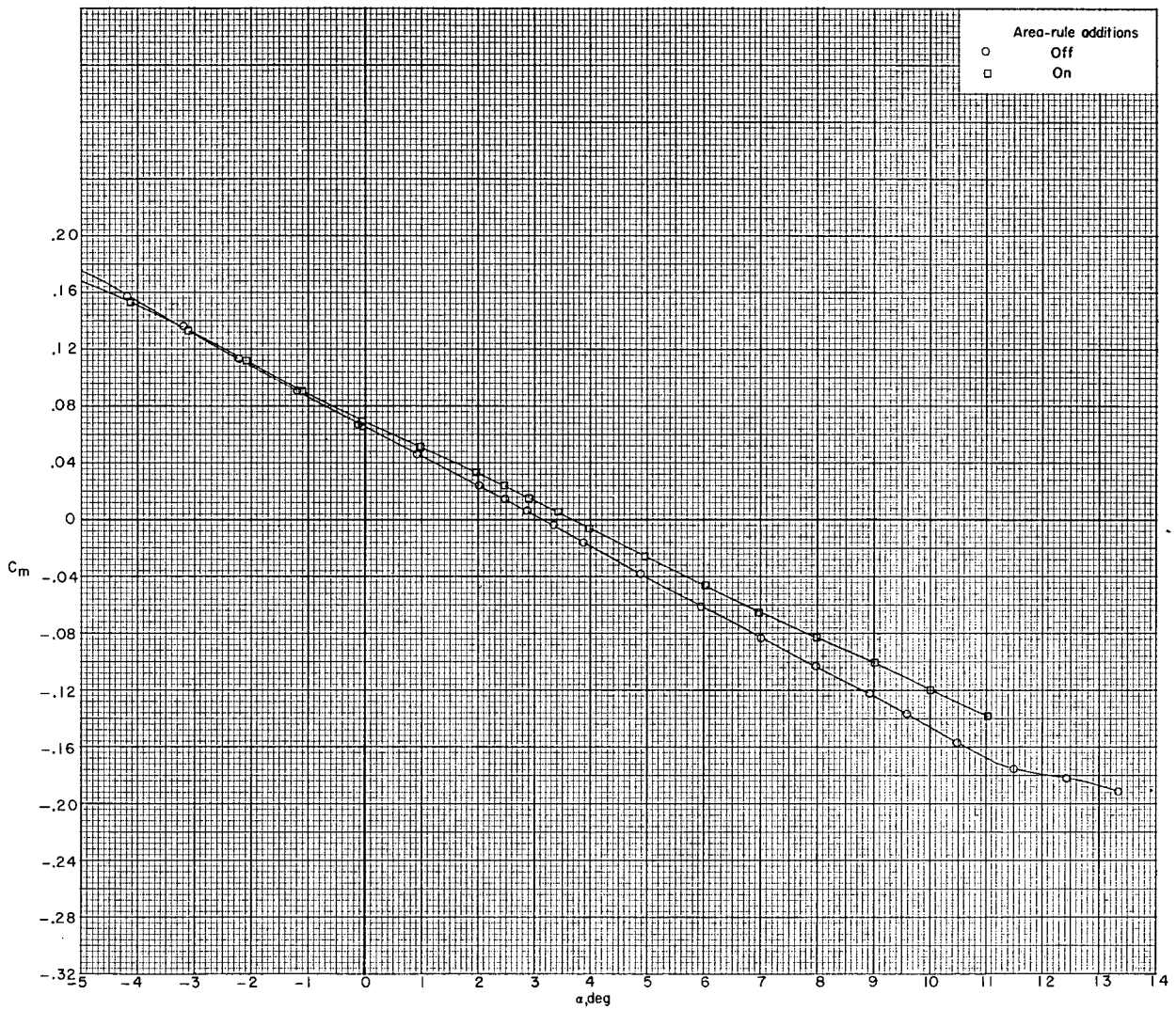
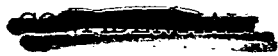
(a) $M = 0.25$. Continued.

Figure 6.- Continued.



(a) $M = 0.25$. Continued.

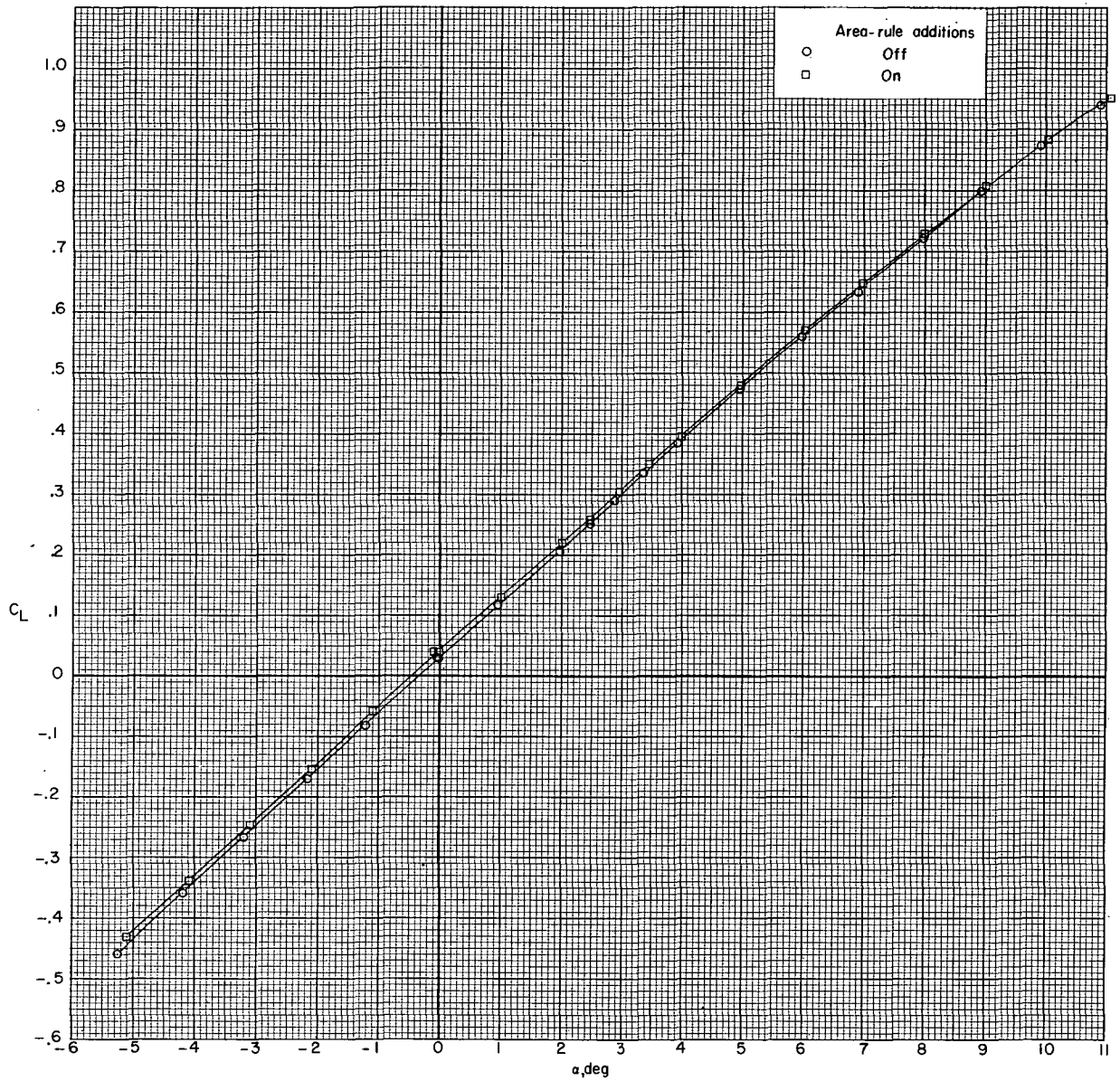
Figure 6.- Continued.



(a) $M = 0.25$. Concluded.

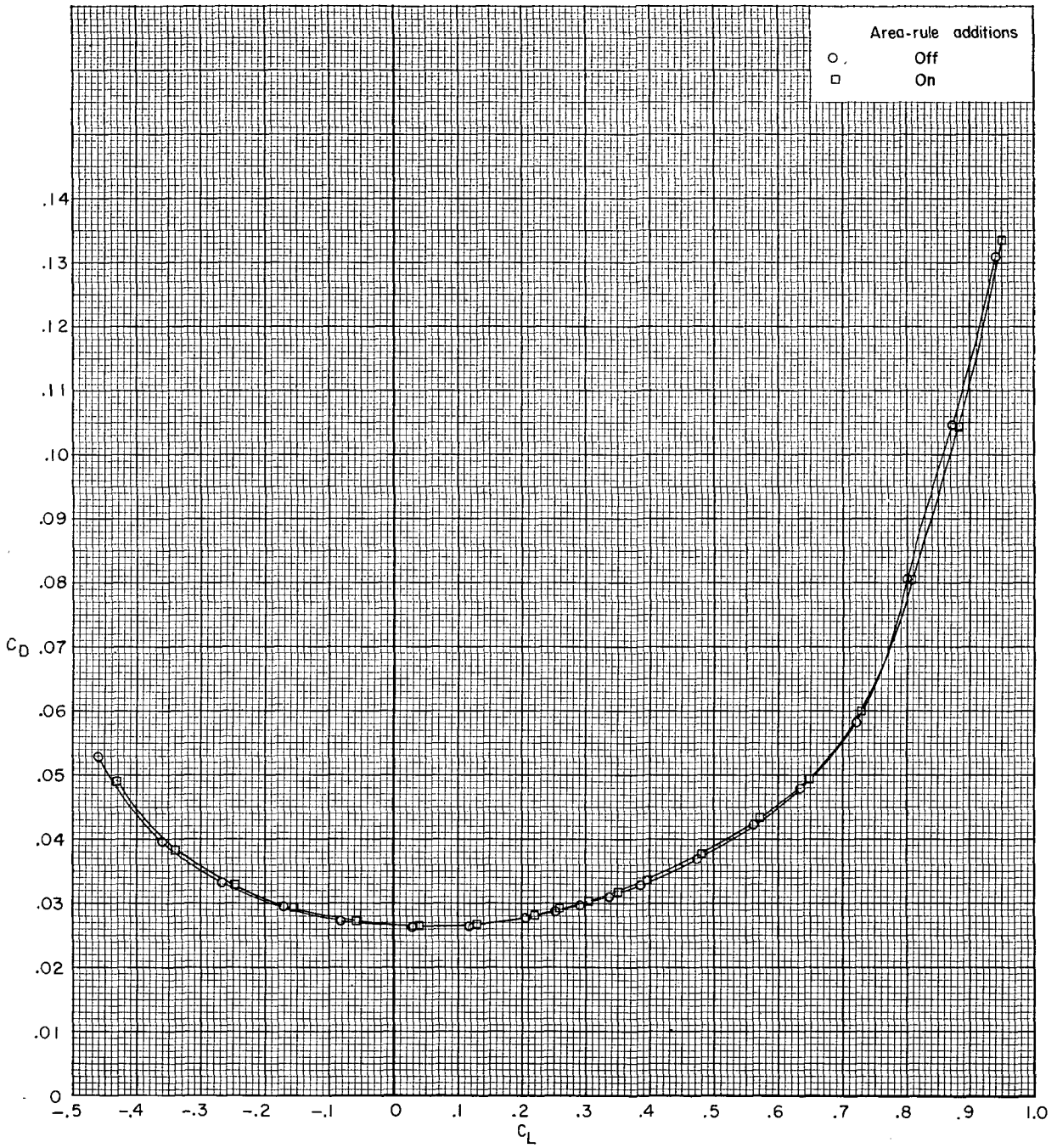
Figure 6.- Continued.





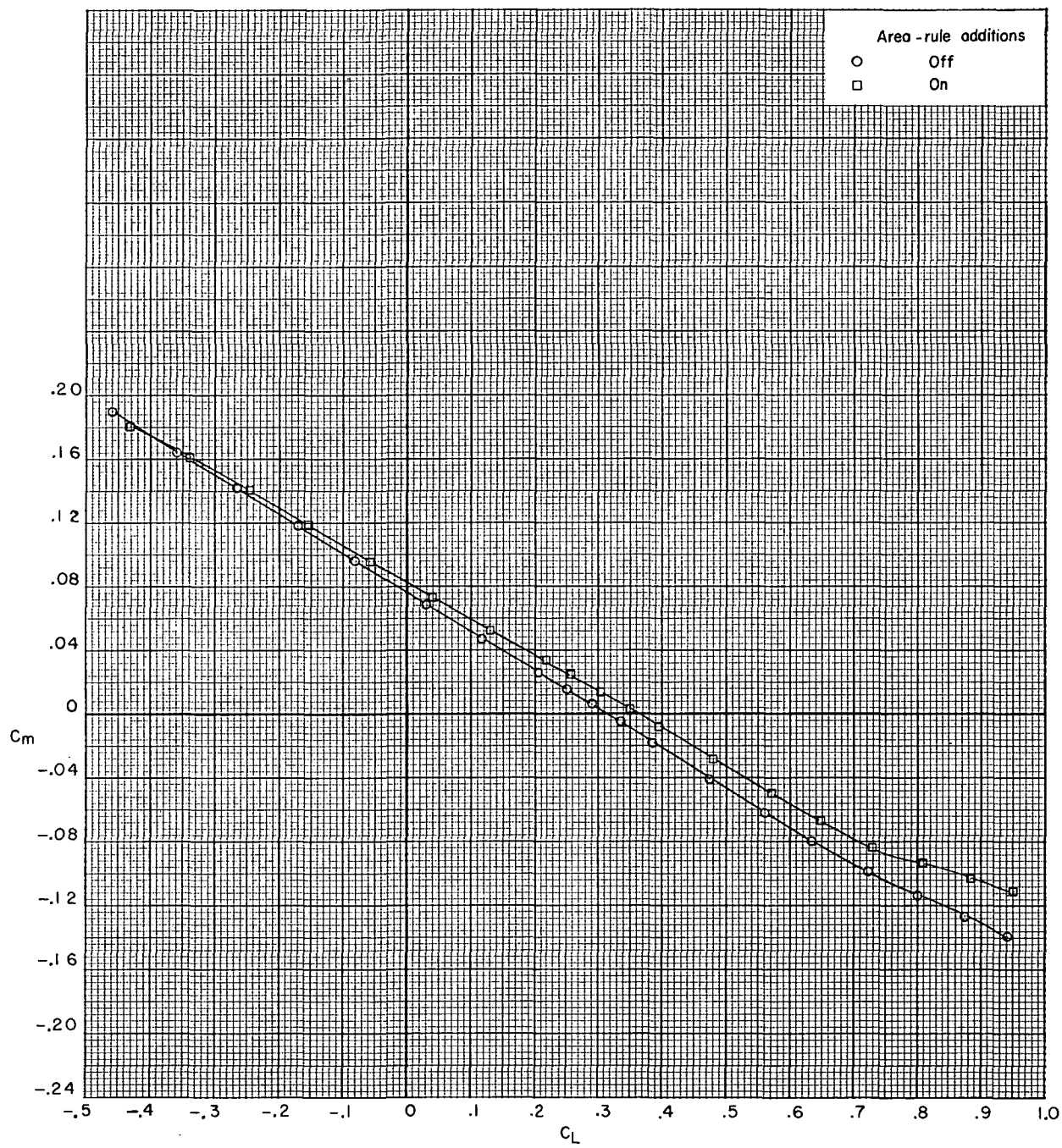
(b) $M = 0.50$.

Figure 6.- Continued.



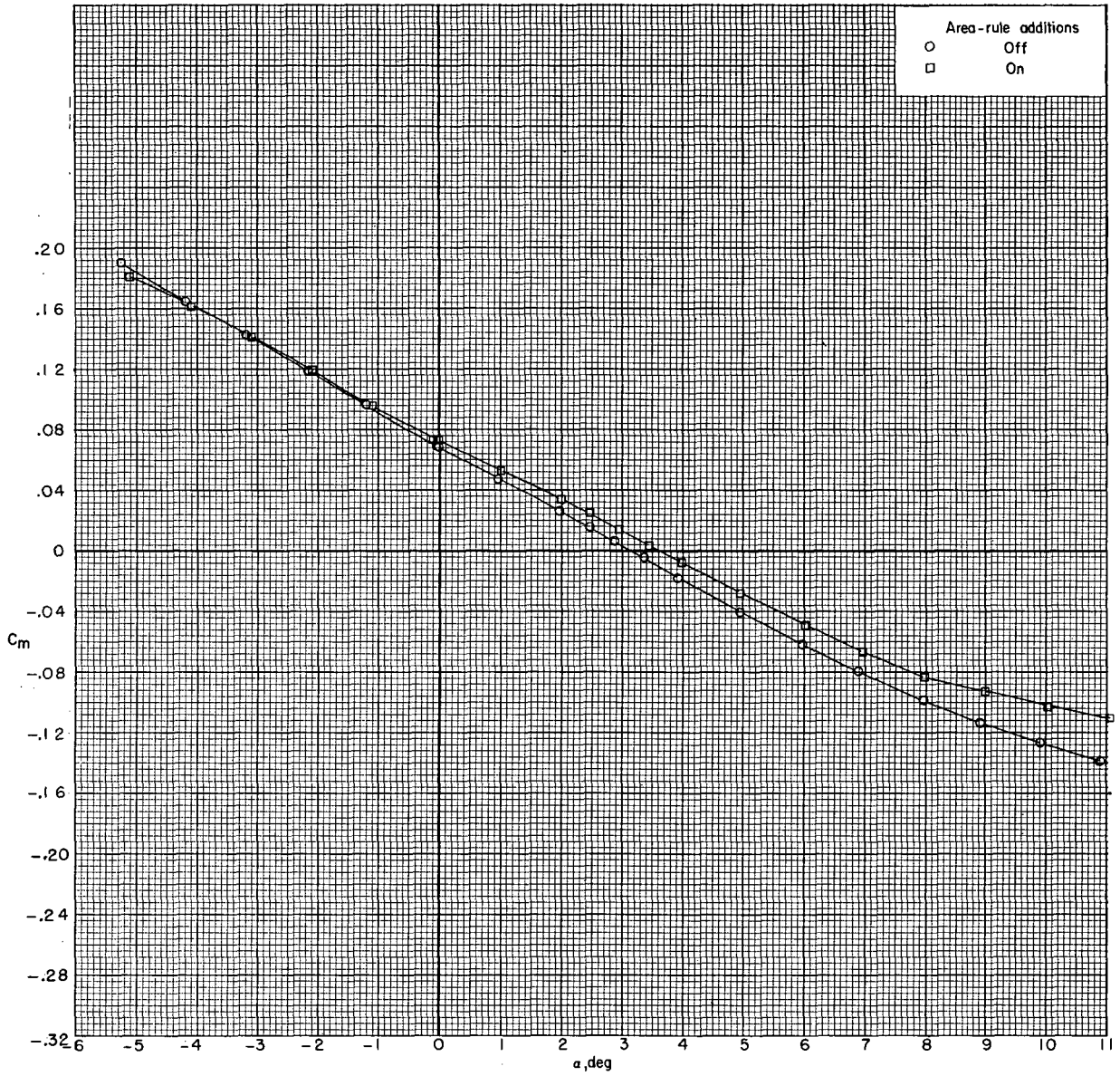
(b) $M = 0.50$. Continued.

Figure 6.- Continued.



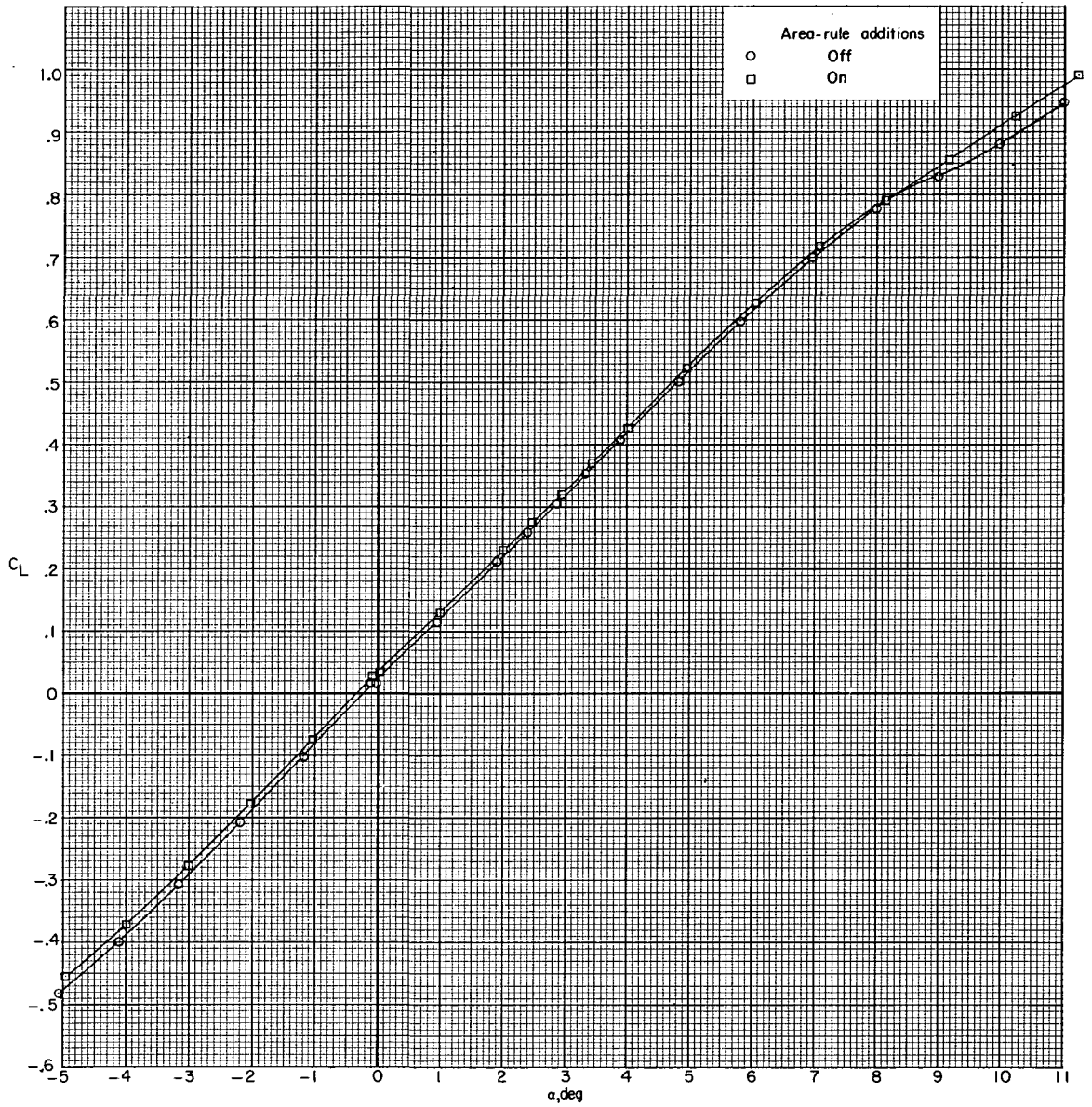
(b) $M = 0.50$. Continued.

Figure 6.- Continued.



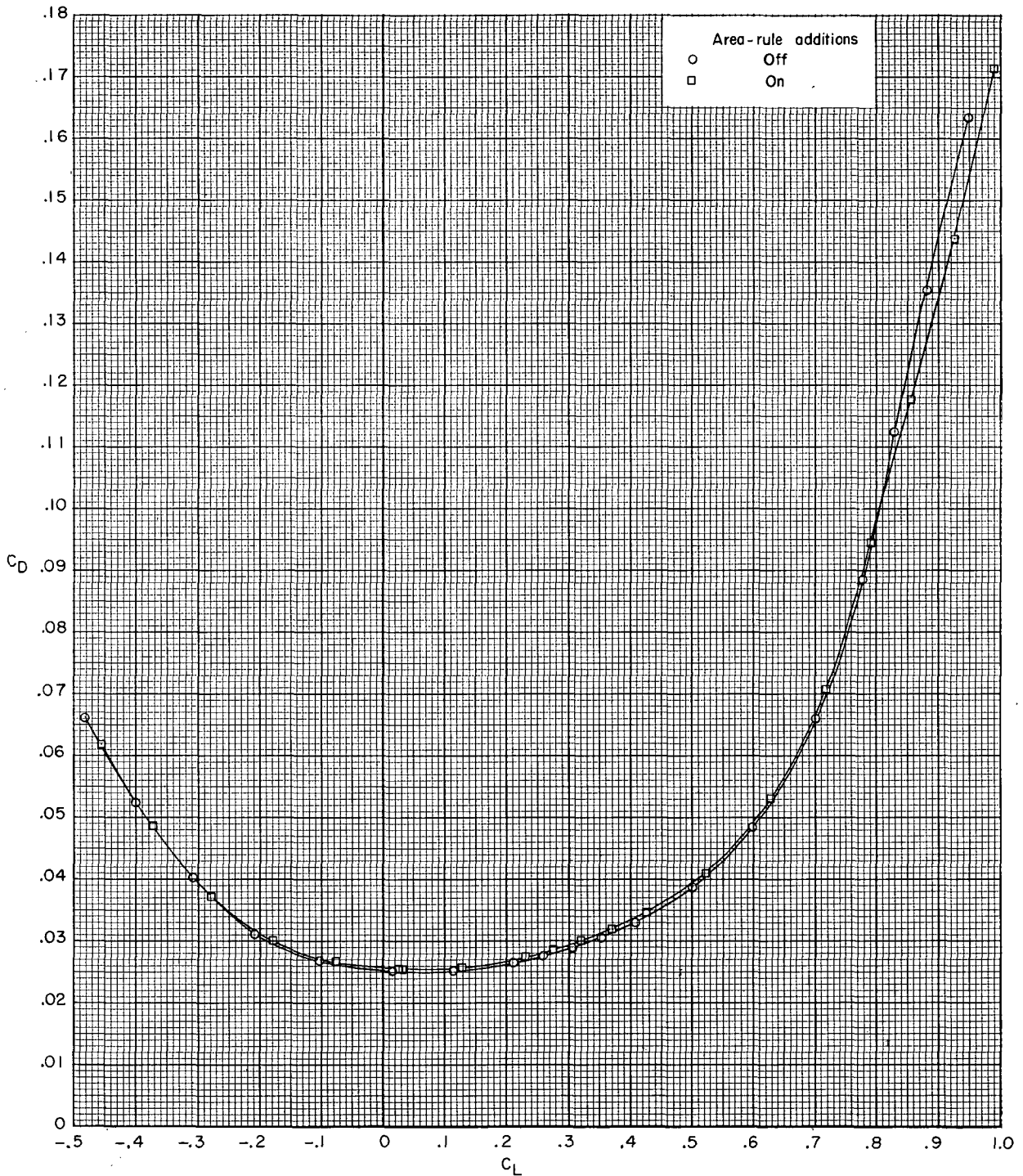
(b) $M = 0.50$. Concluded.

Figure 6.- Continued.



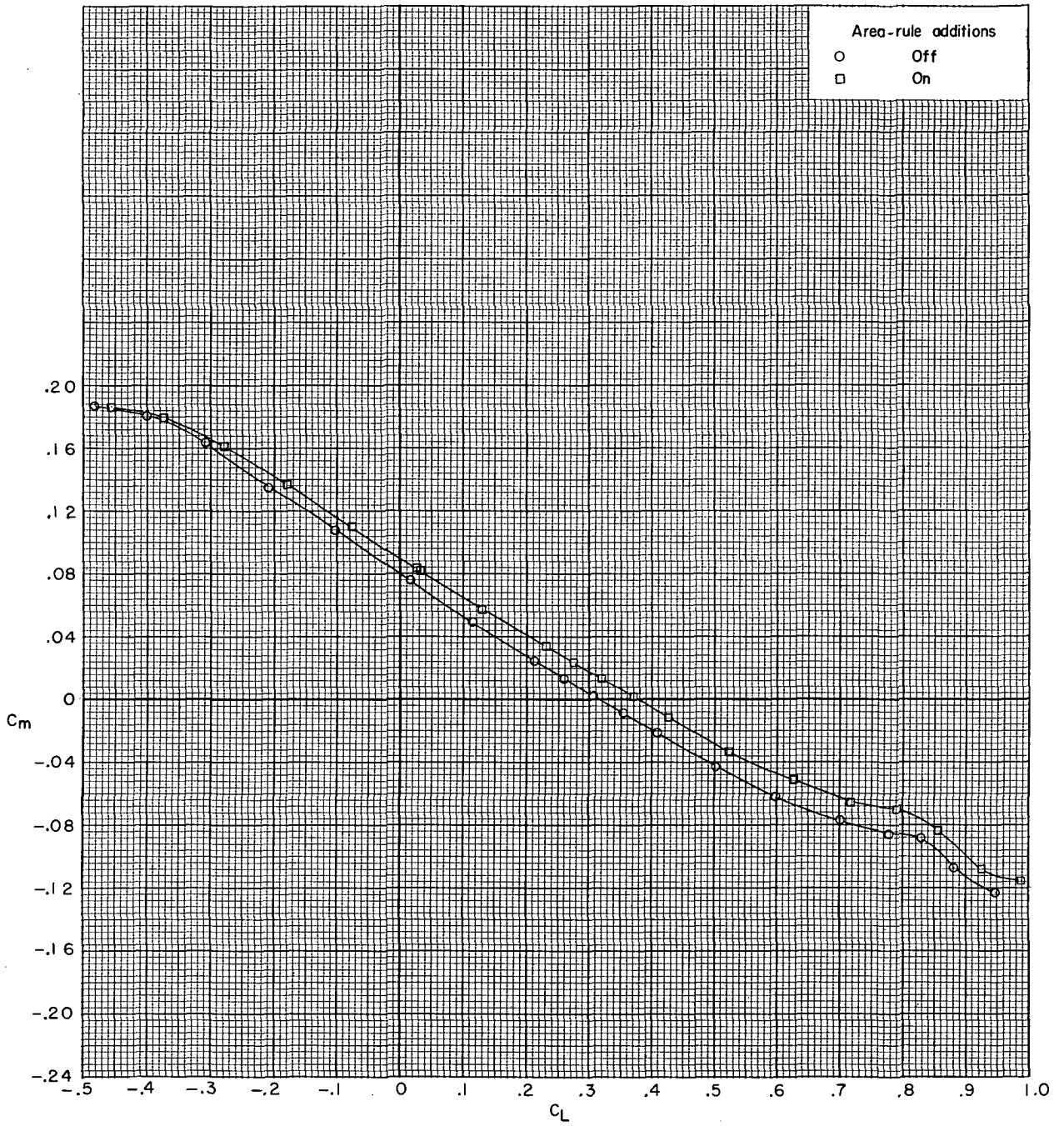
(c) $M = 0.80$.

Figure 6.- Continued.



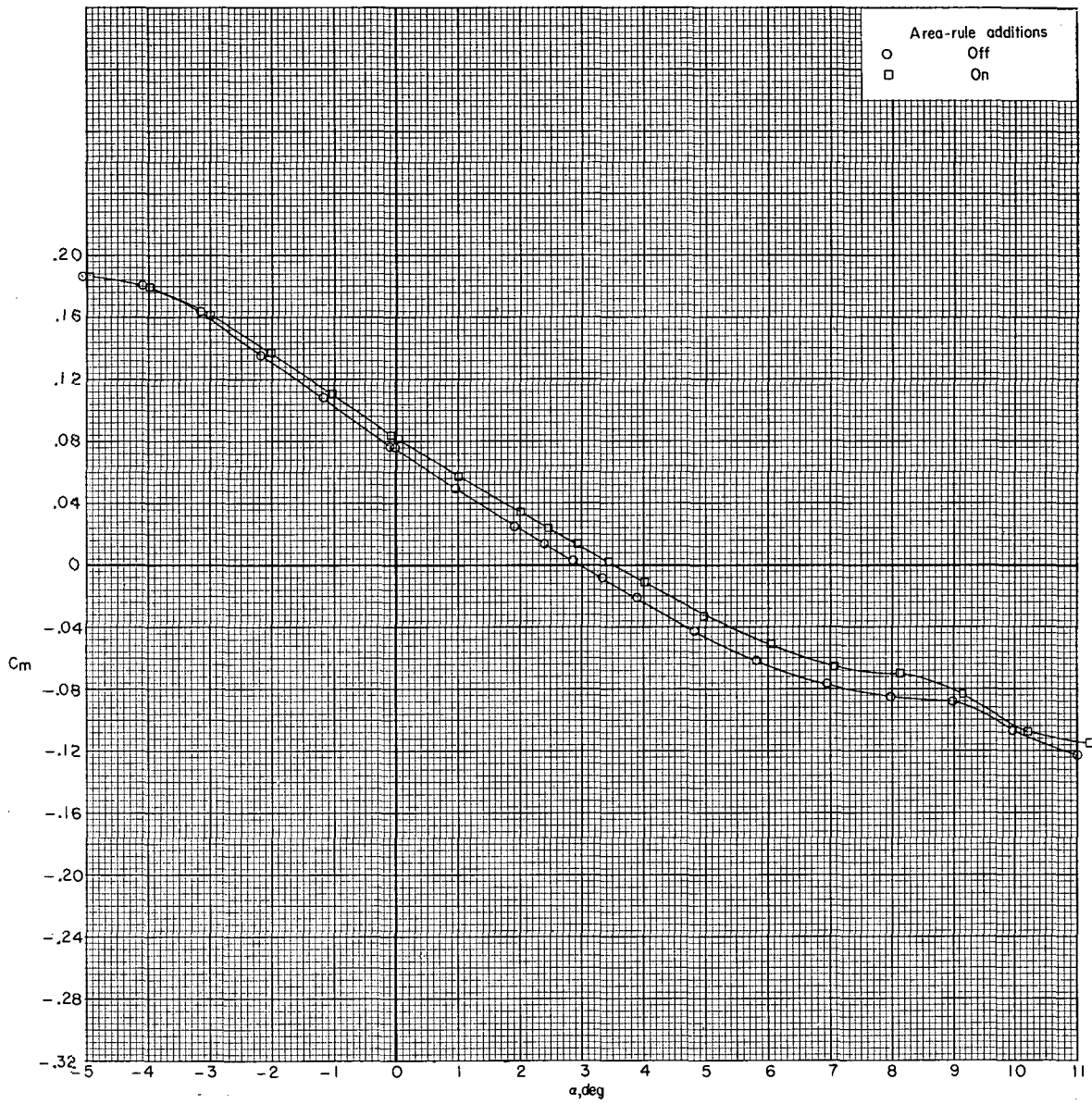
(c) $M = 0.80$. Continued.

Figure 6.- Continued.



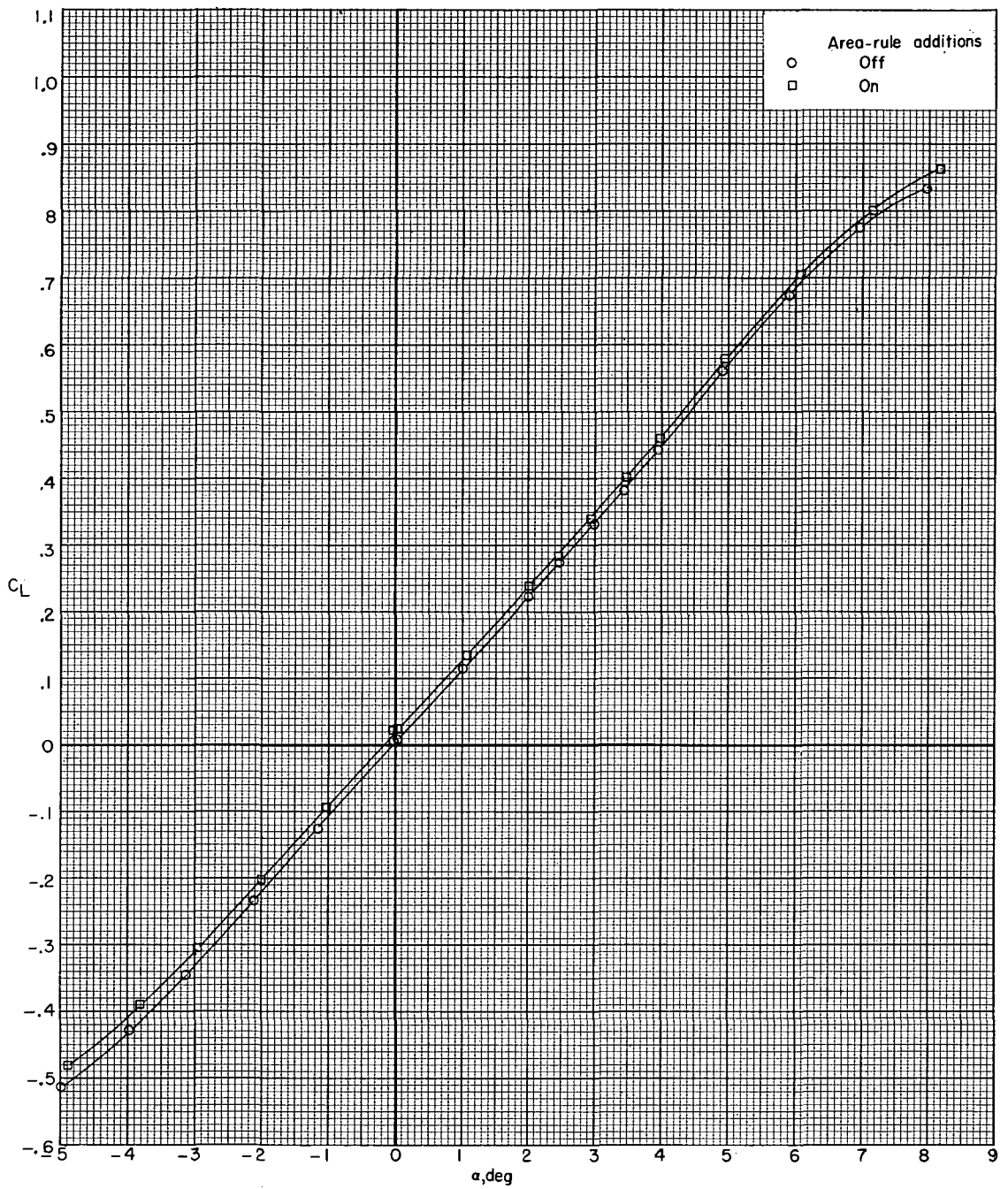
(c) $M = 0.80$. Continued.

Figure 6.- Continued.



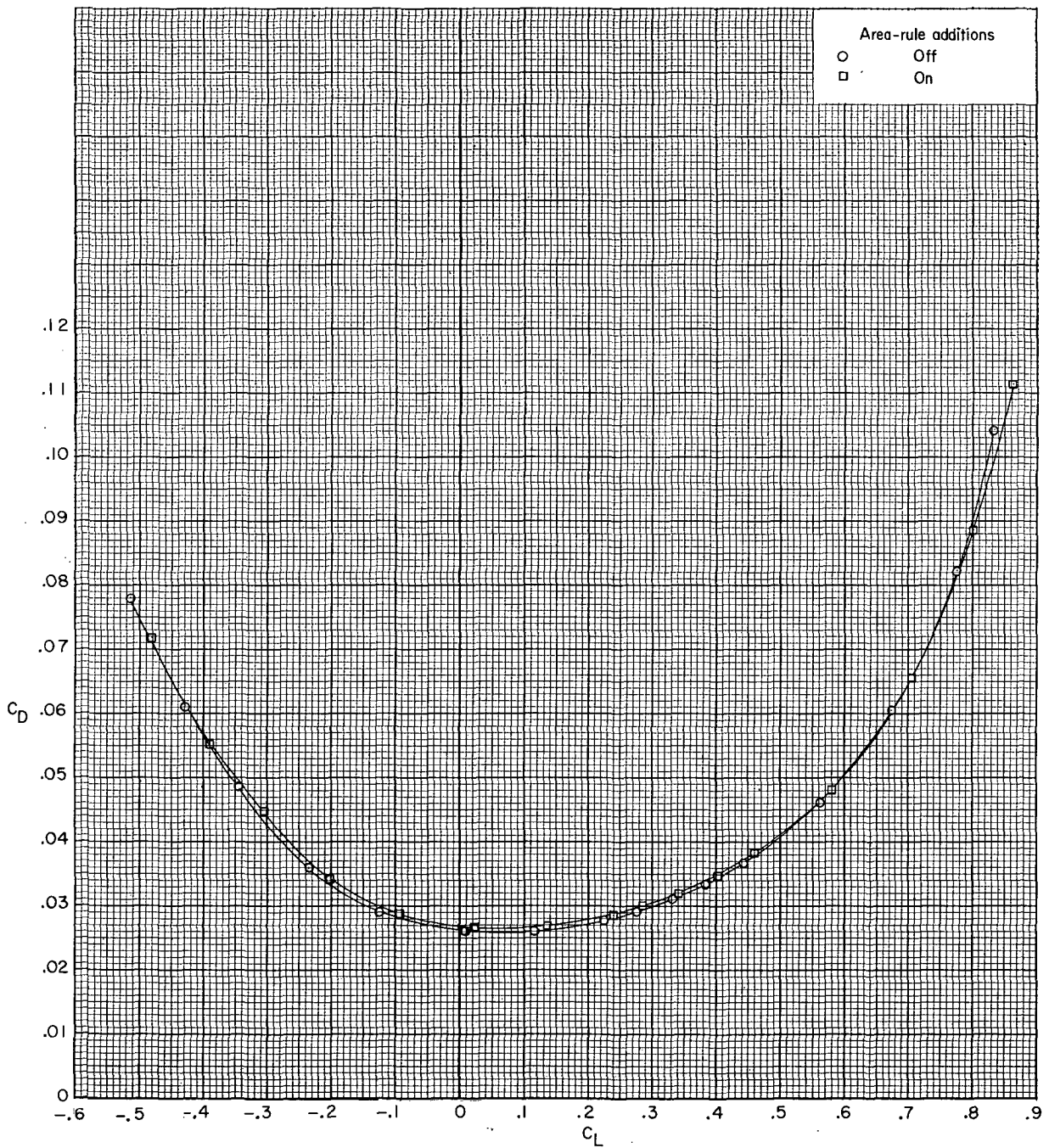
(c) $M = 0.80$. Concluded.

Figure 6.- Continued.



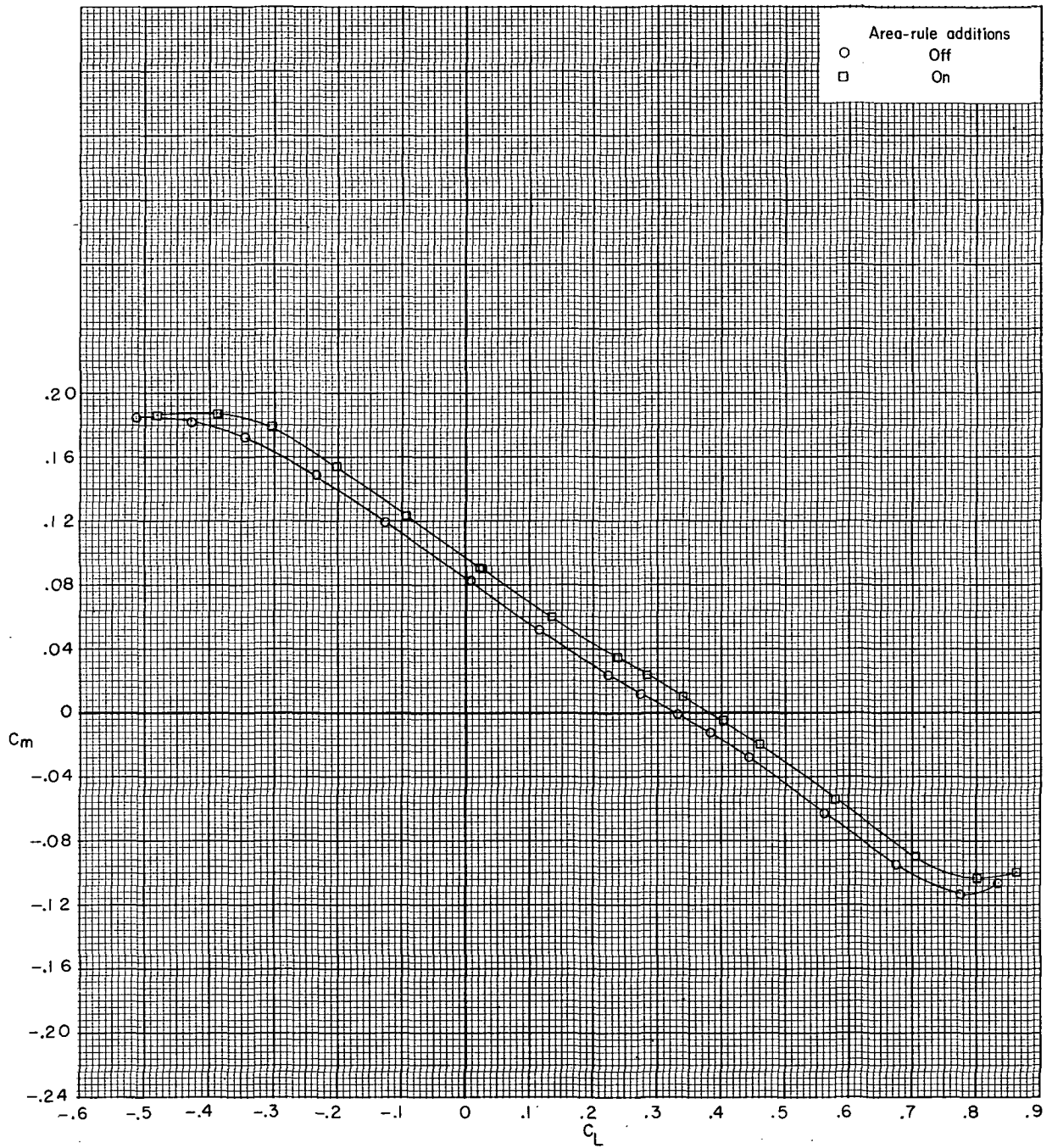
(d) $M = 0.90$.

Figure 6.- Continued.



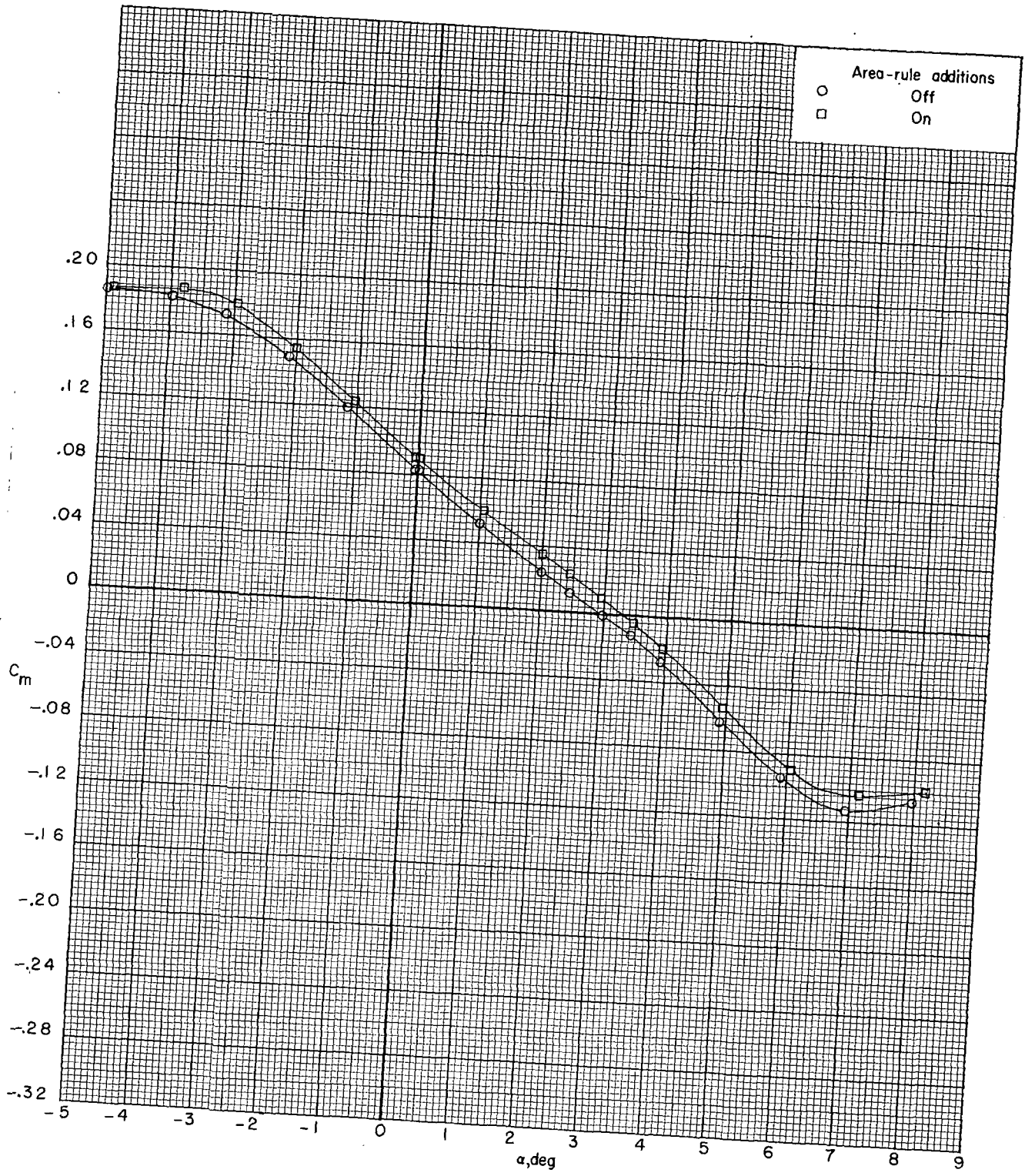
(d) $M = 0.90$. Continued.

Figure 6.- Continued.



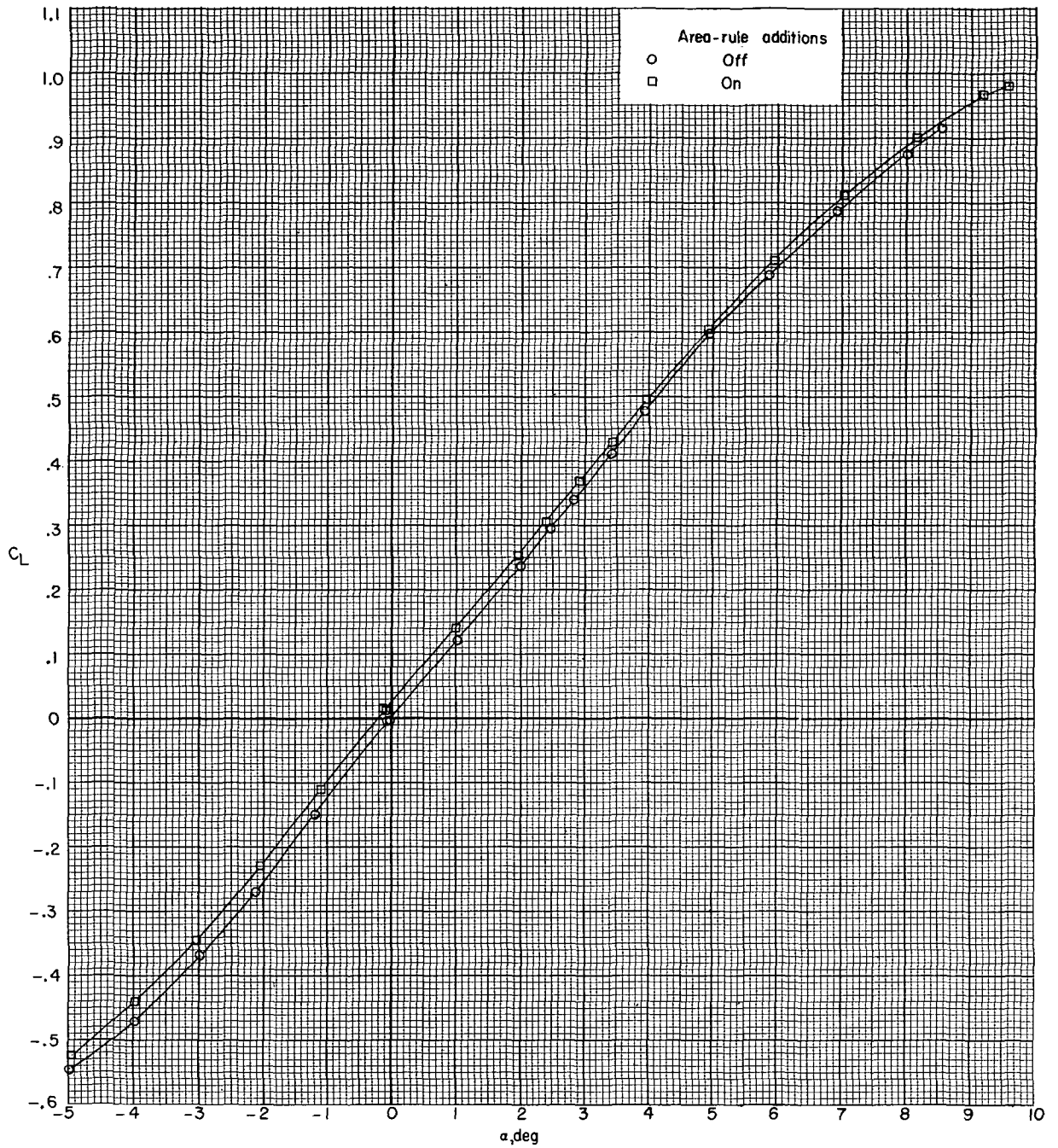
(d) $M = 0.90$. Continued.

Figure 6.- Continued.



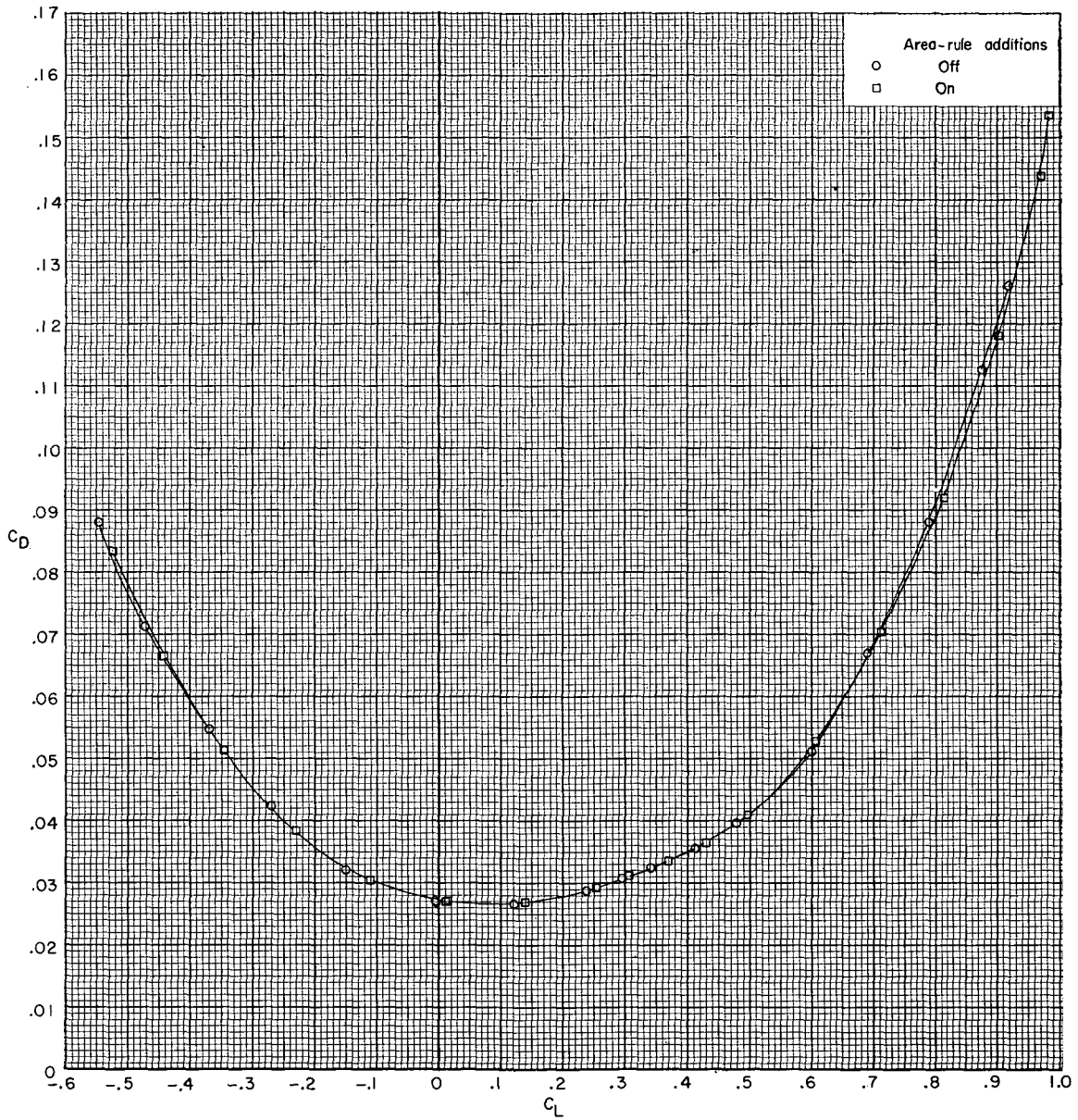
(d) $M = 0.90$. Concluded.

Figure 6. - Continued.



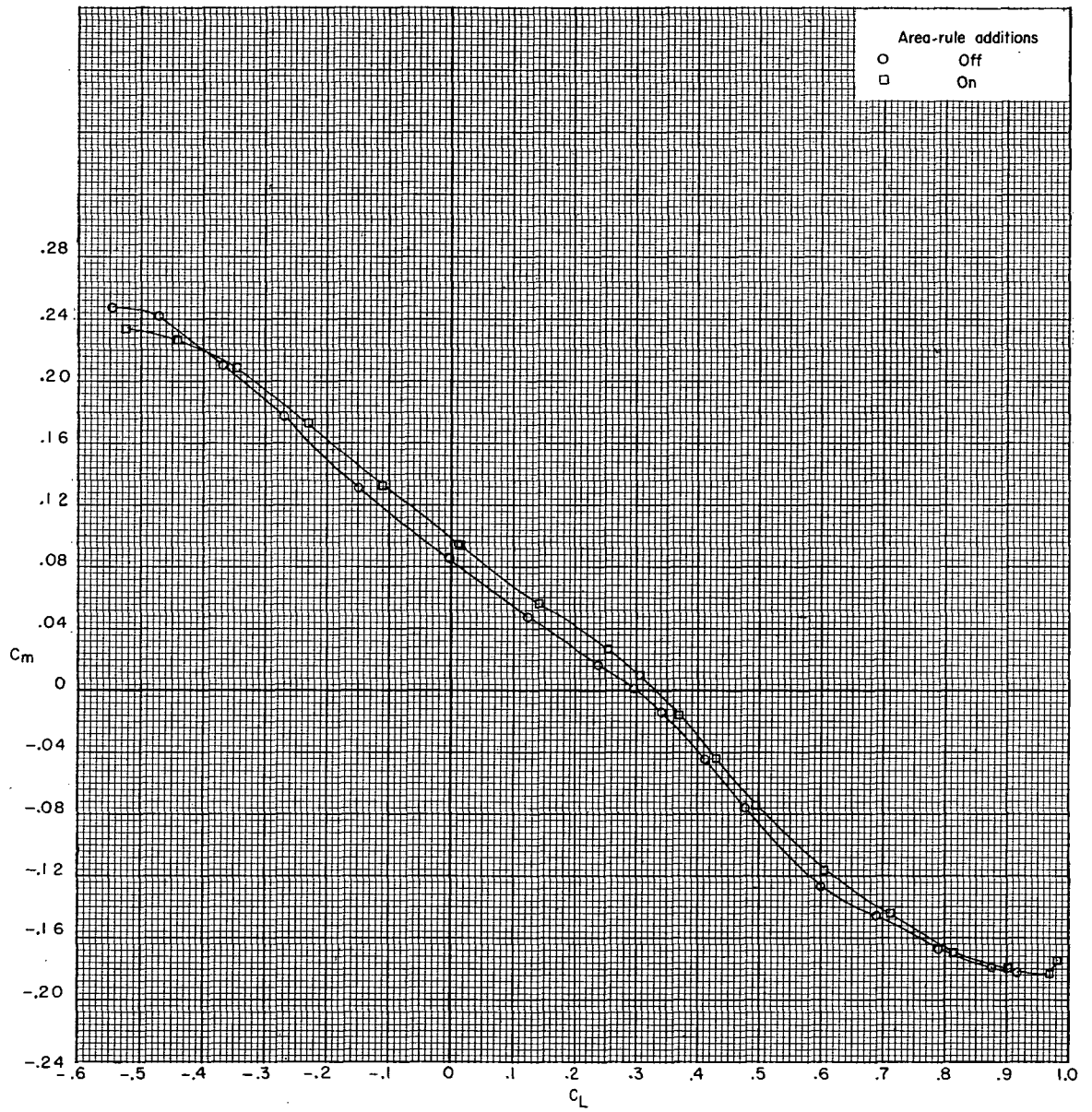
(e) $M = 0.95$.

Figure 6.- Continued.



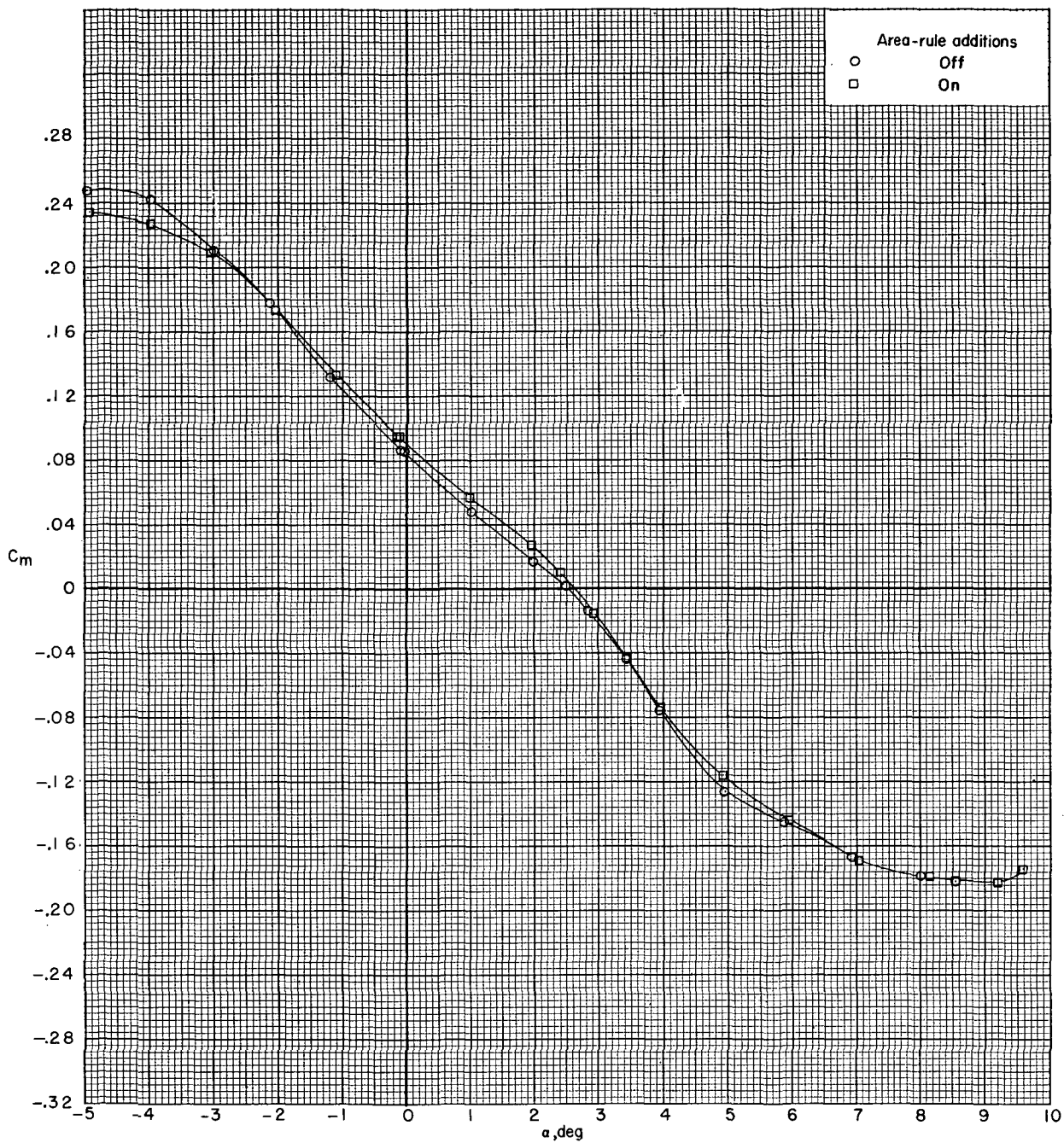
(e) $M = 0.95$. Continued.

Figure 6.- Continued.



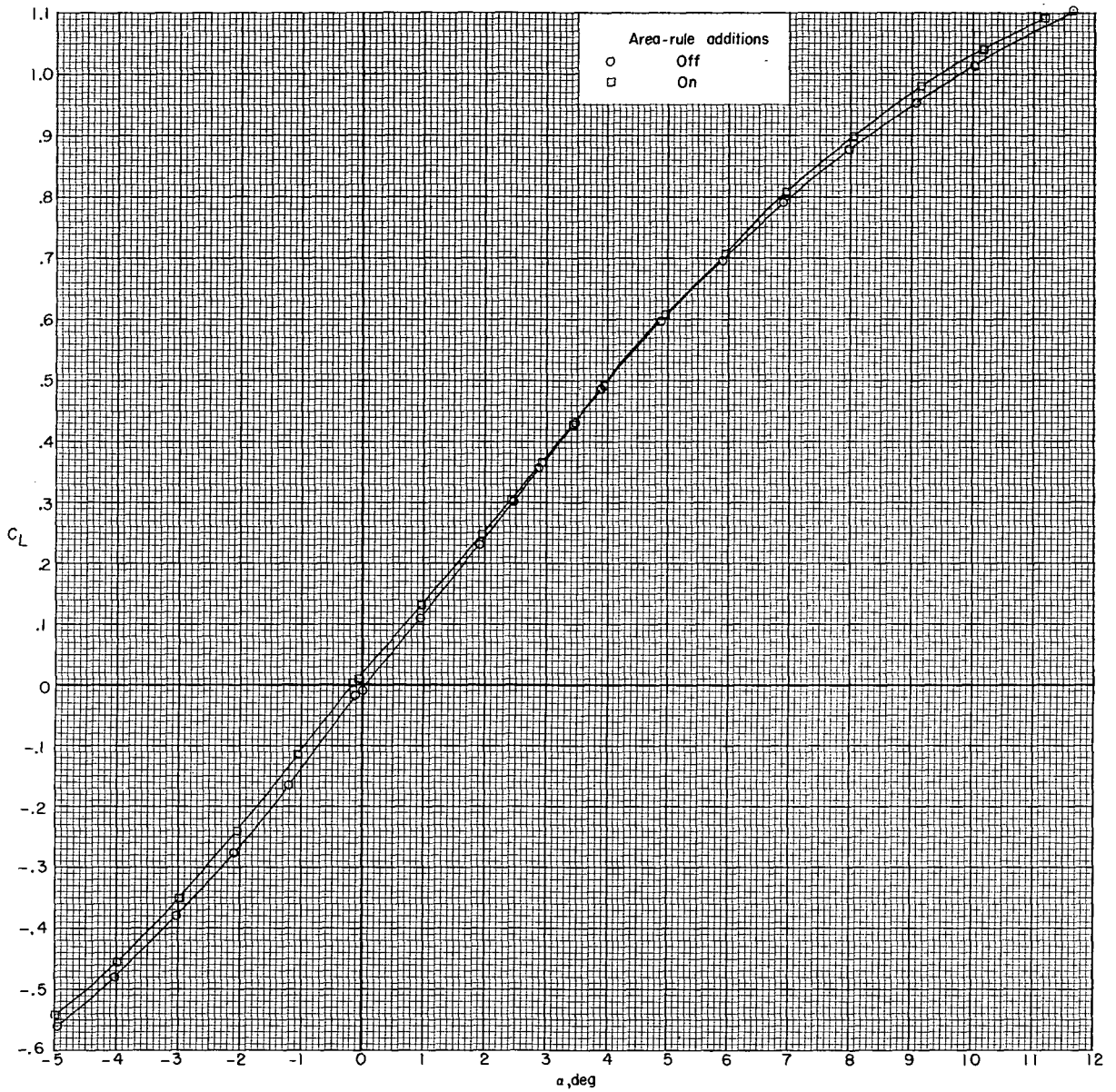
(e) $M = 0.95$. Continued.

Figure 6. - Continued.



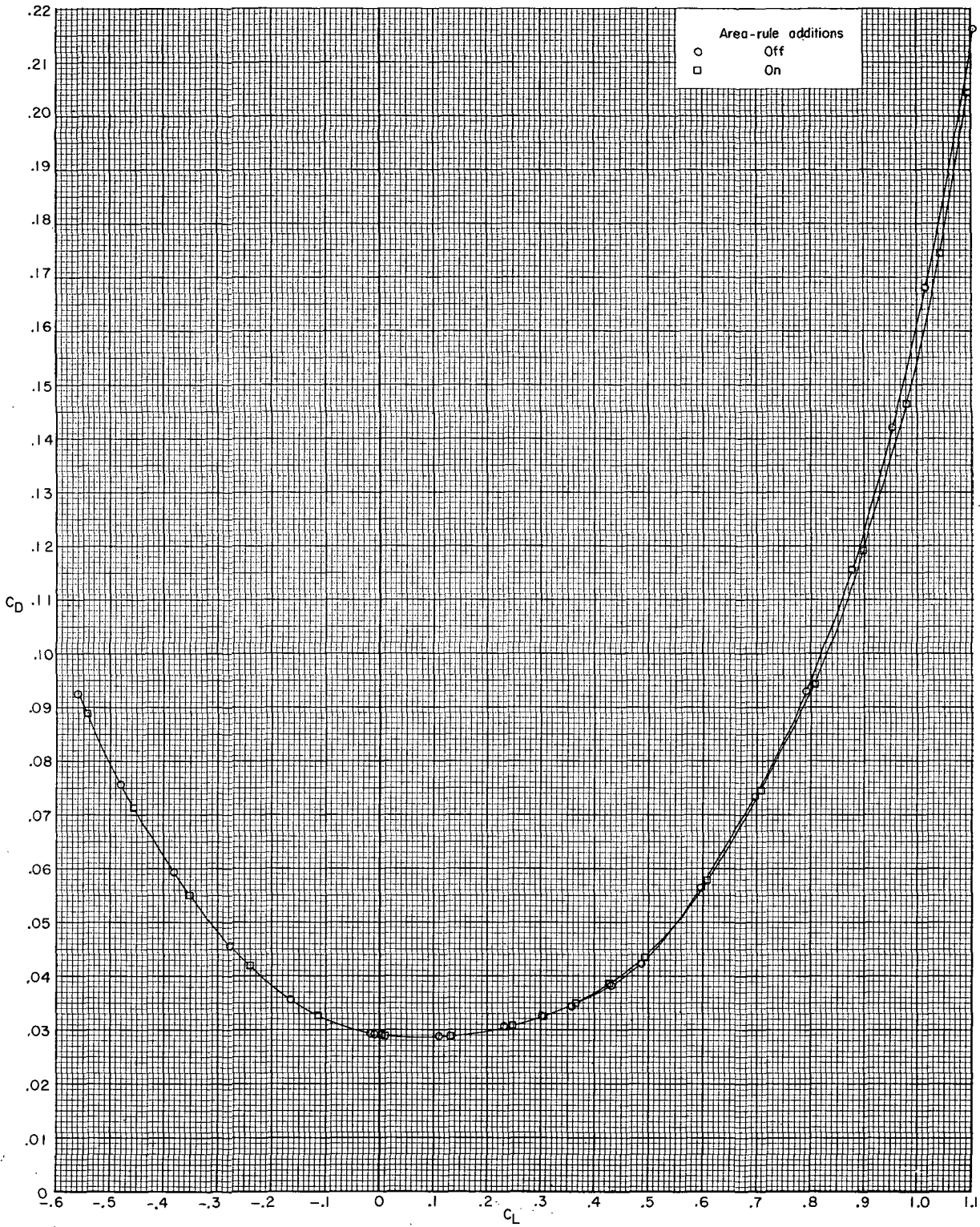
(e) $M = 0.95$. Concluded.

Figure 6.- Continued.



(f) $M = 0.97$.

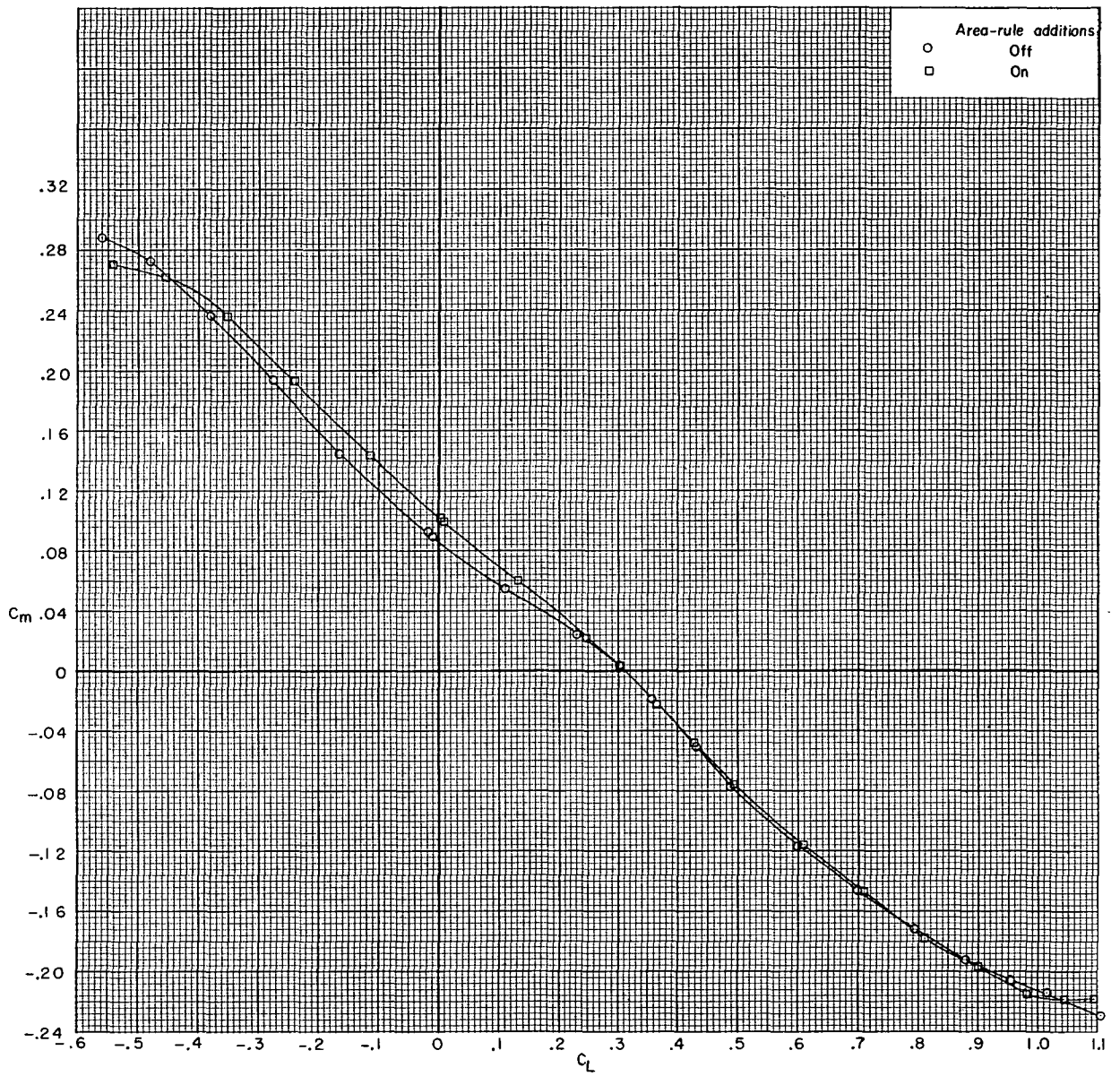
Figure 6. - Continued.



(f) $M = 0.97$. Continued.

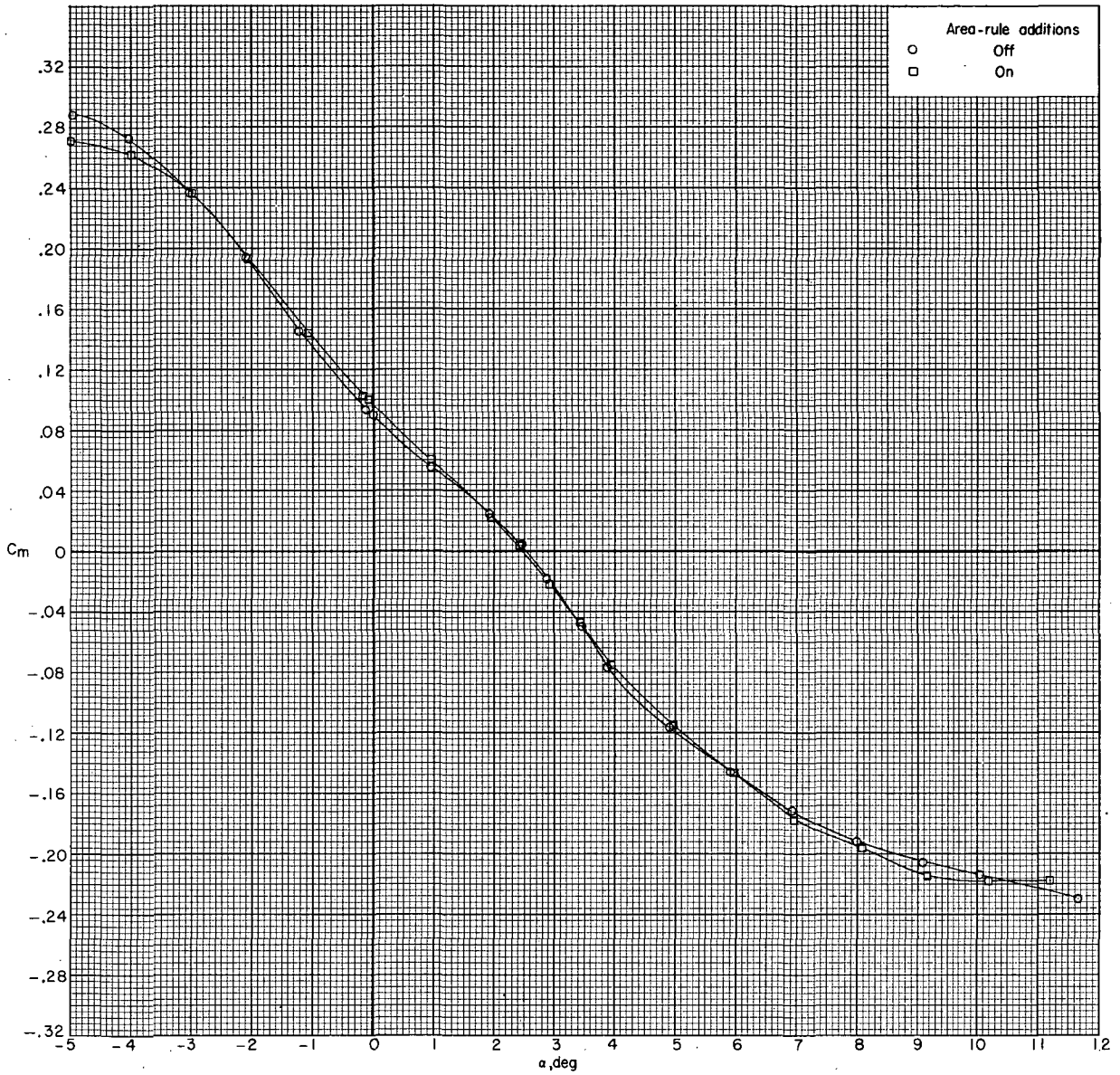
Figure 6. - Continued.





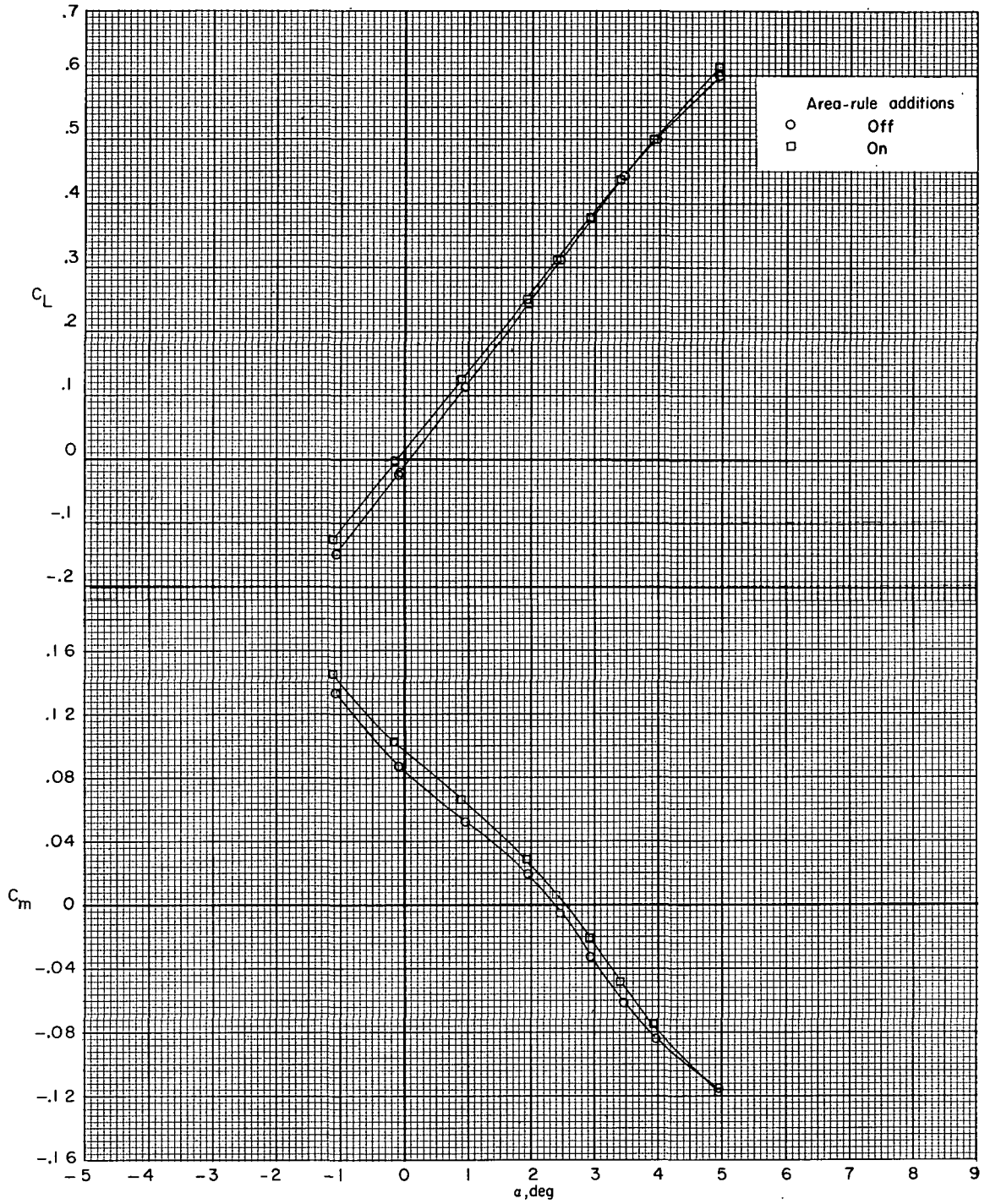
(f) $M = 0.97$. Continued.

Figure 6.- Continued.



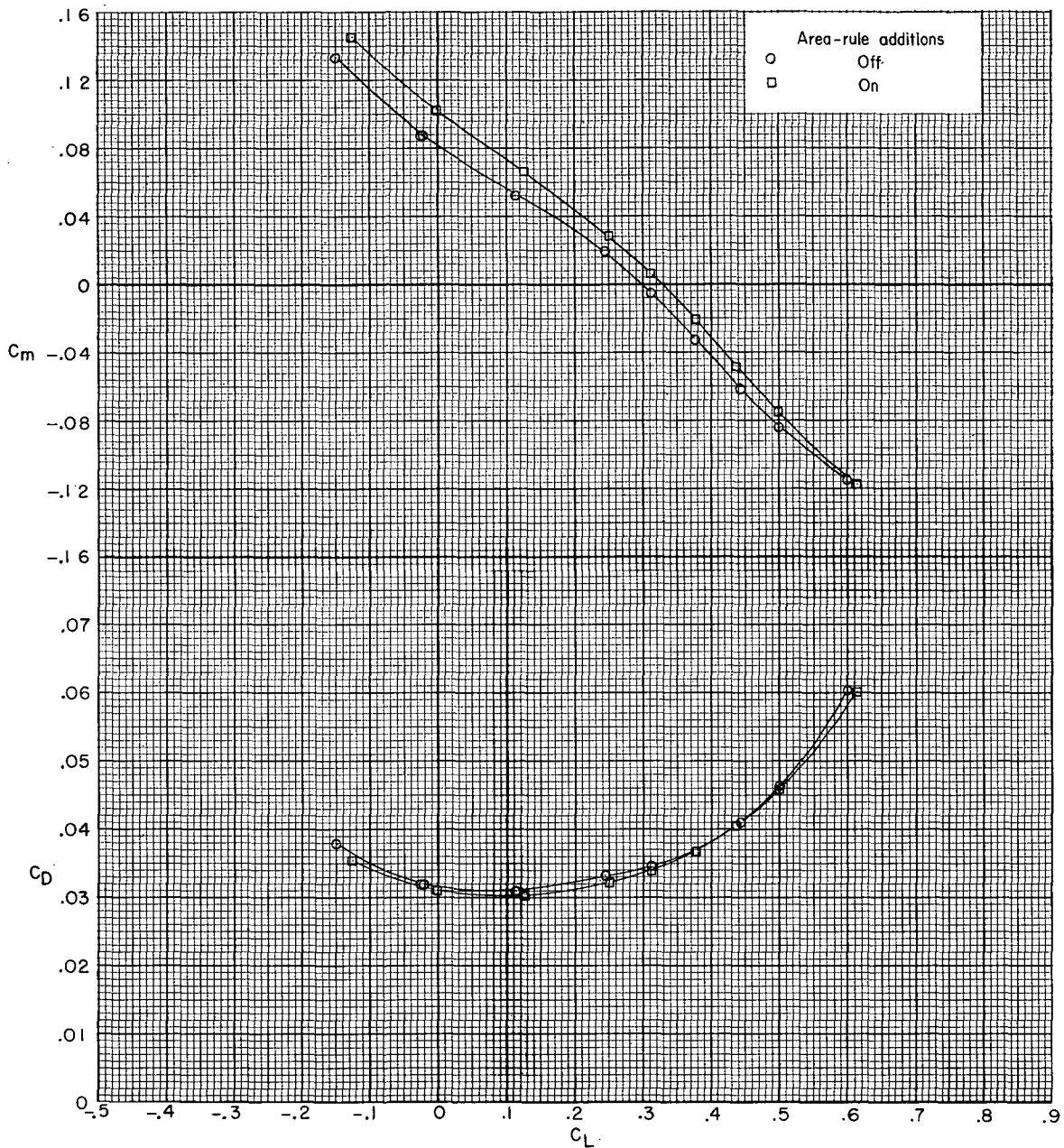
(f) $M = 0.97$. Concluded.

Figure 6.- Continued.



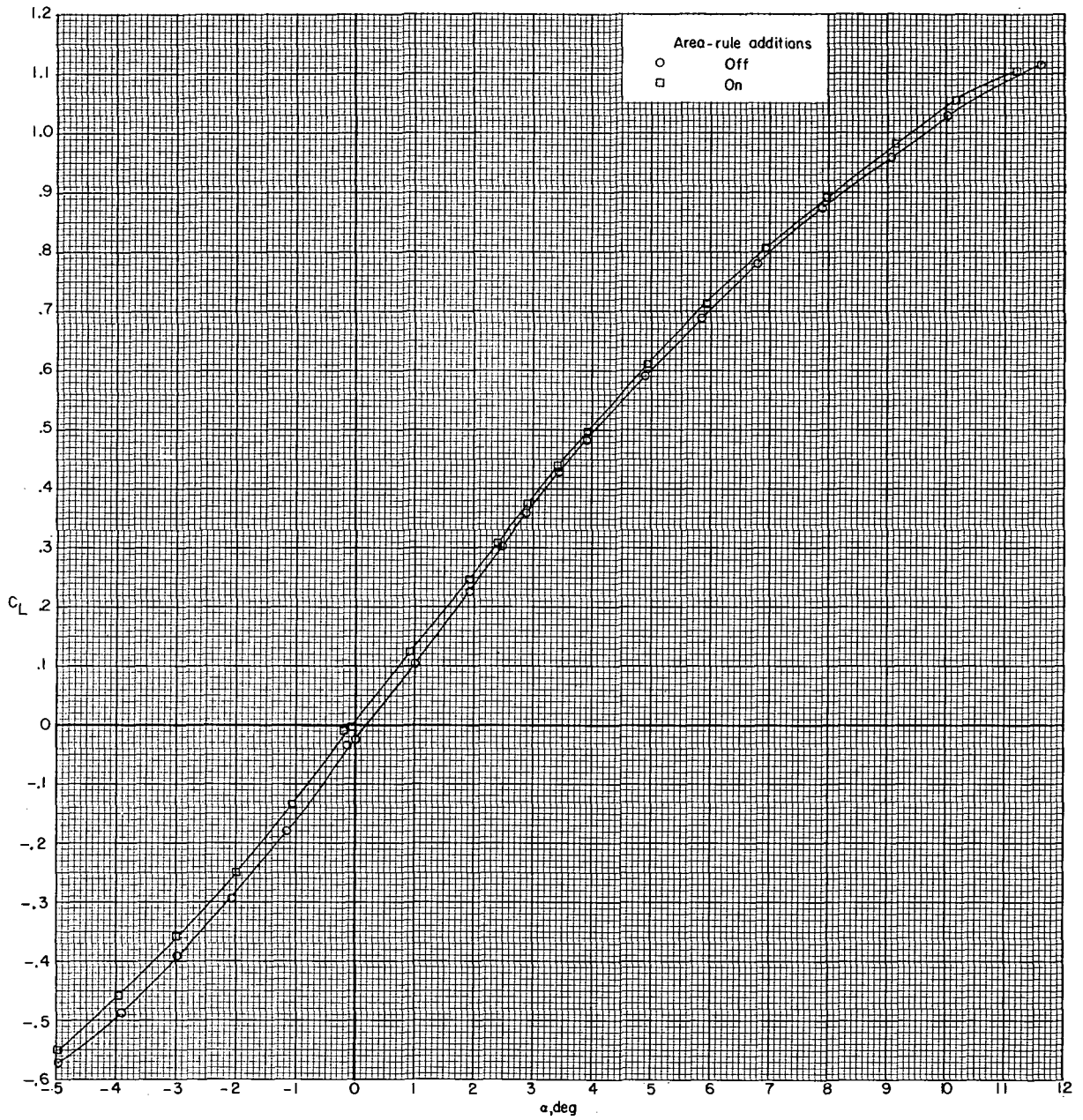
(g) $M = 0.98$.

Figure 6. - Continued.



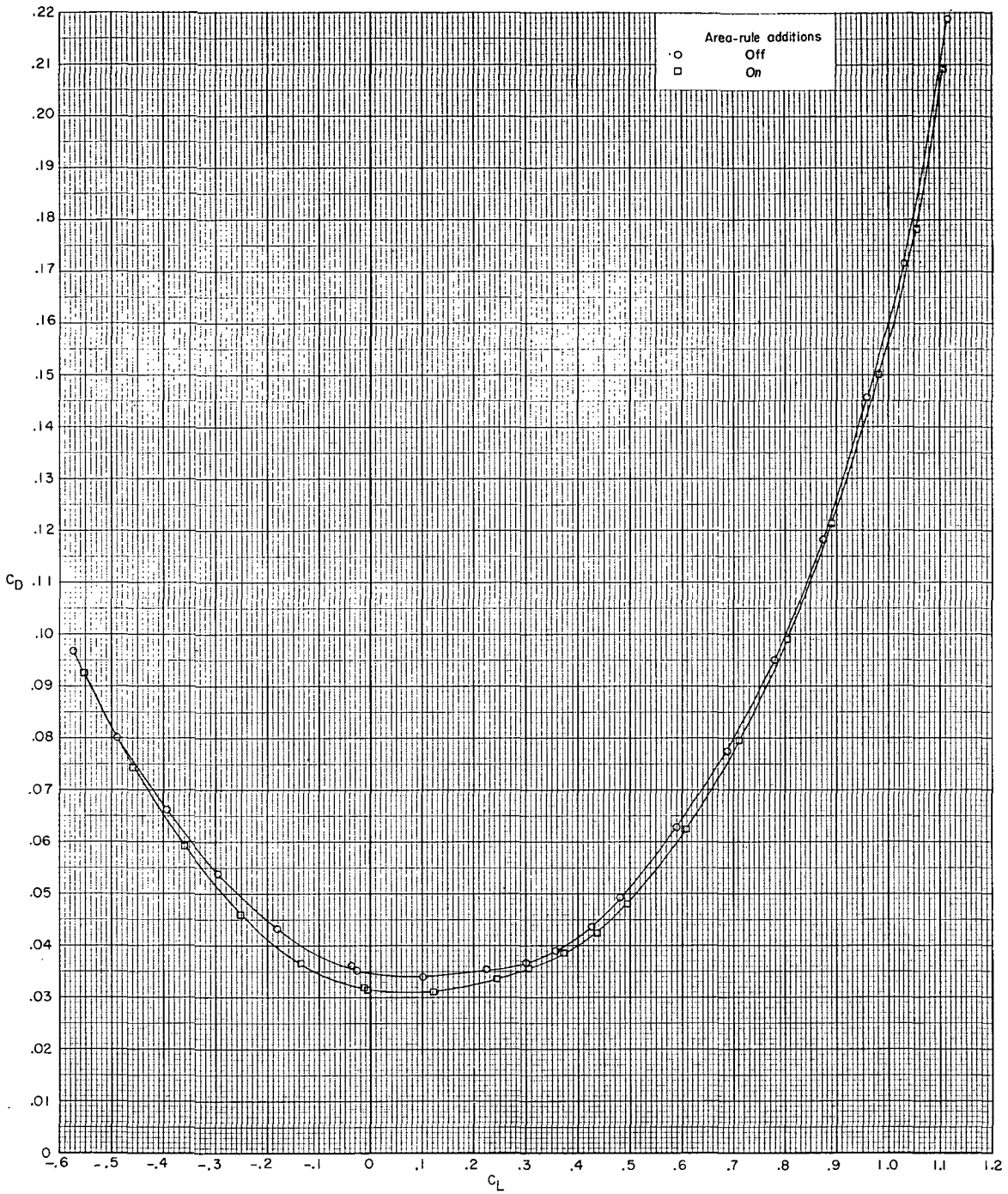
(g) $M = 0.98$. Concluded.

Figure 6.- Continued.



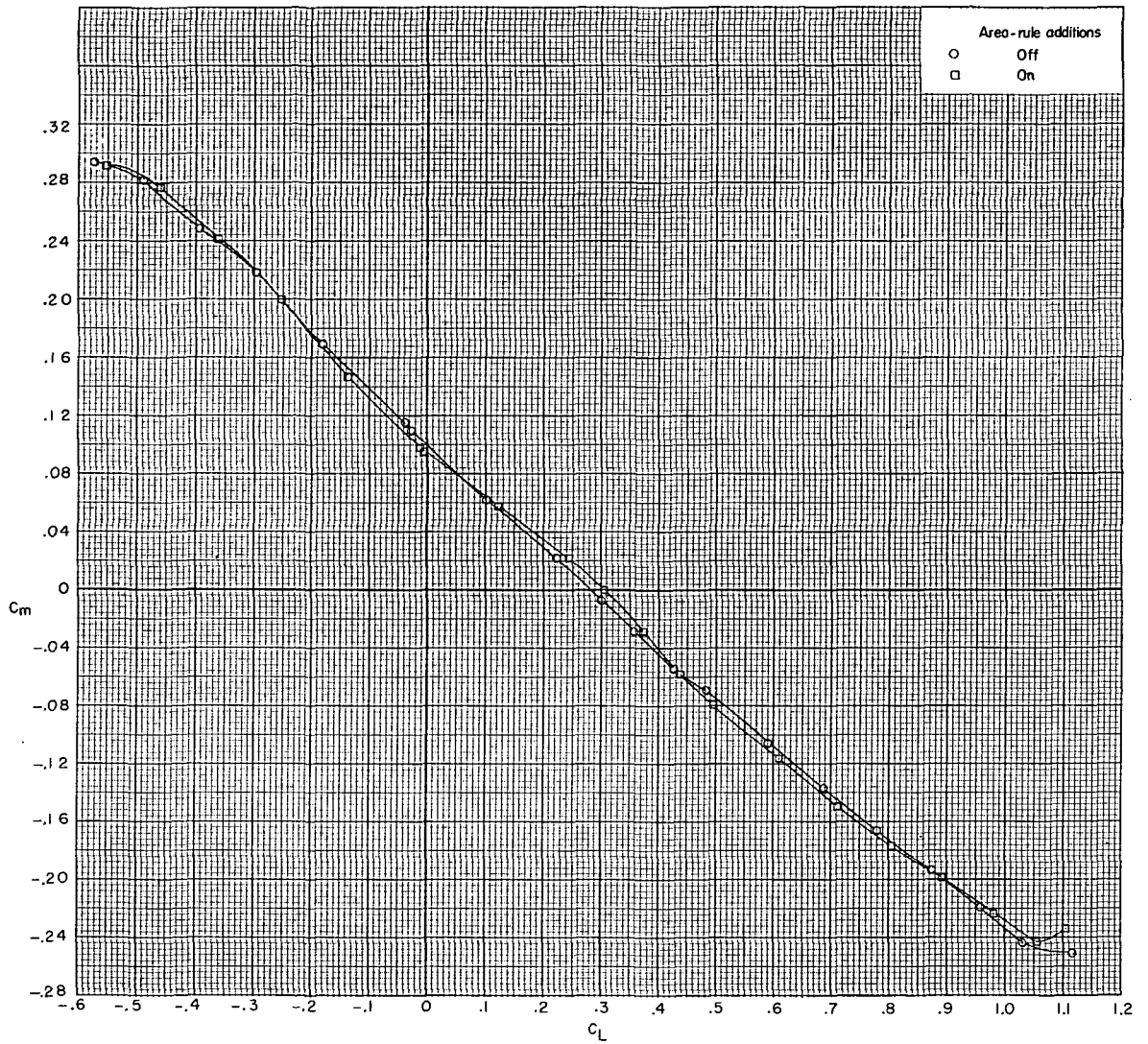
(h) $M = 0.99$.

Figure 6.- Continued.



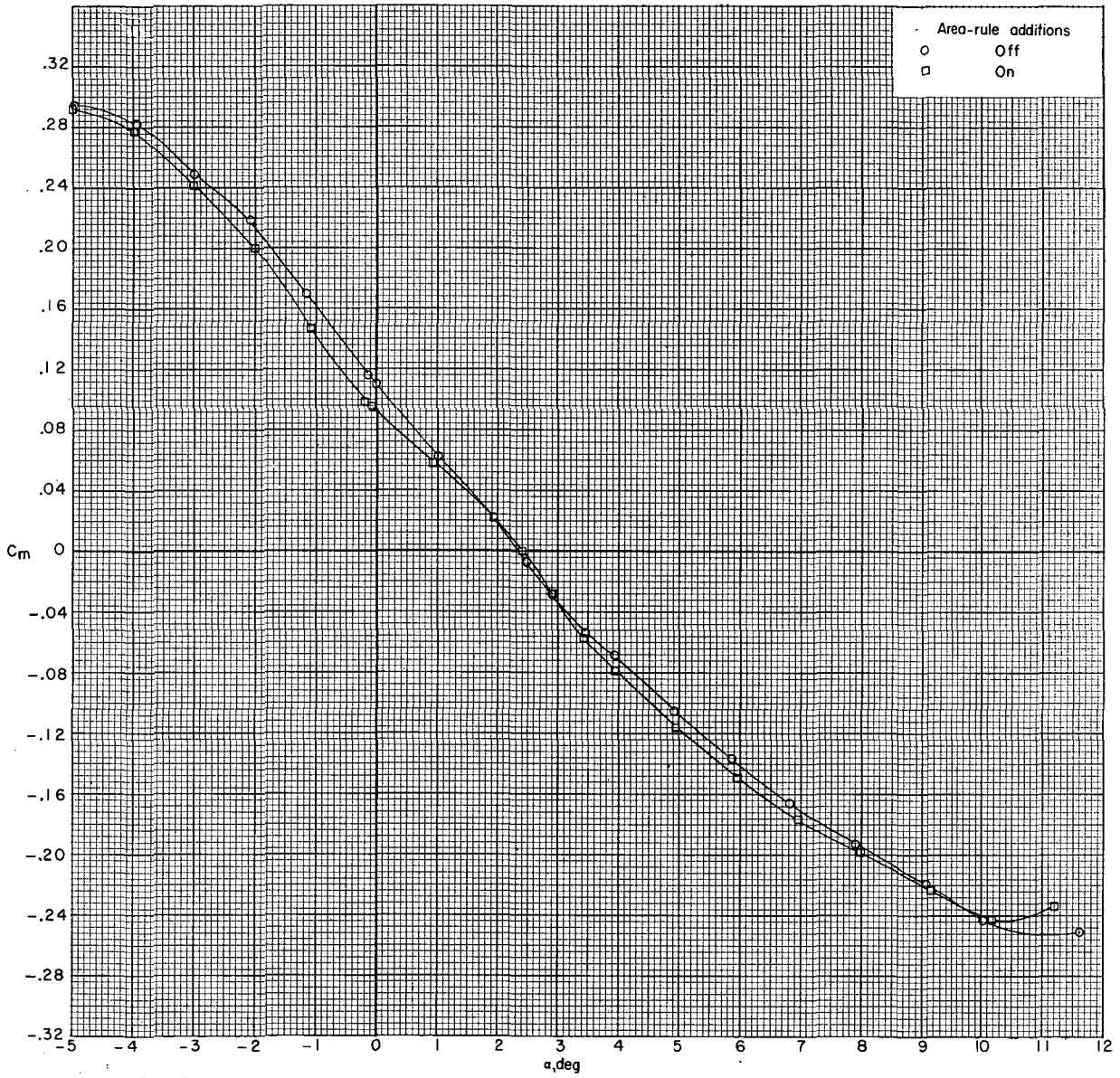
(h) $M = 0.99$. Continued.

Figure 6.- Continued.



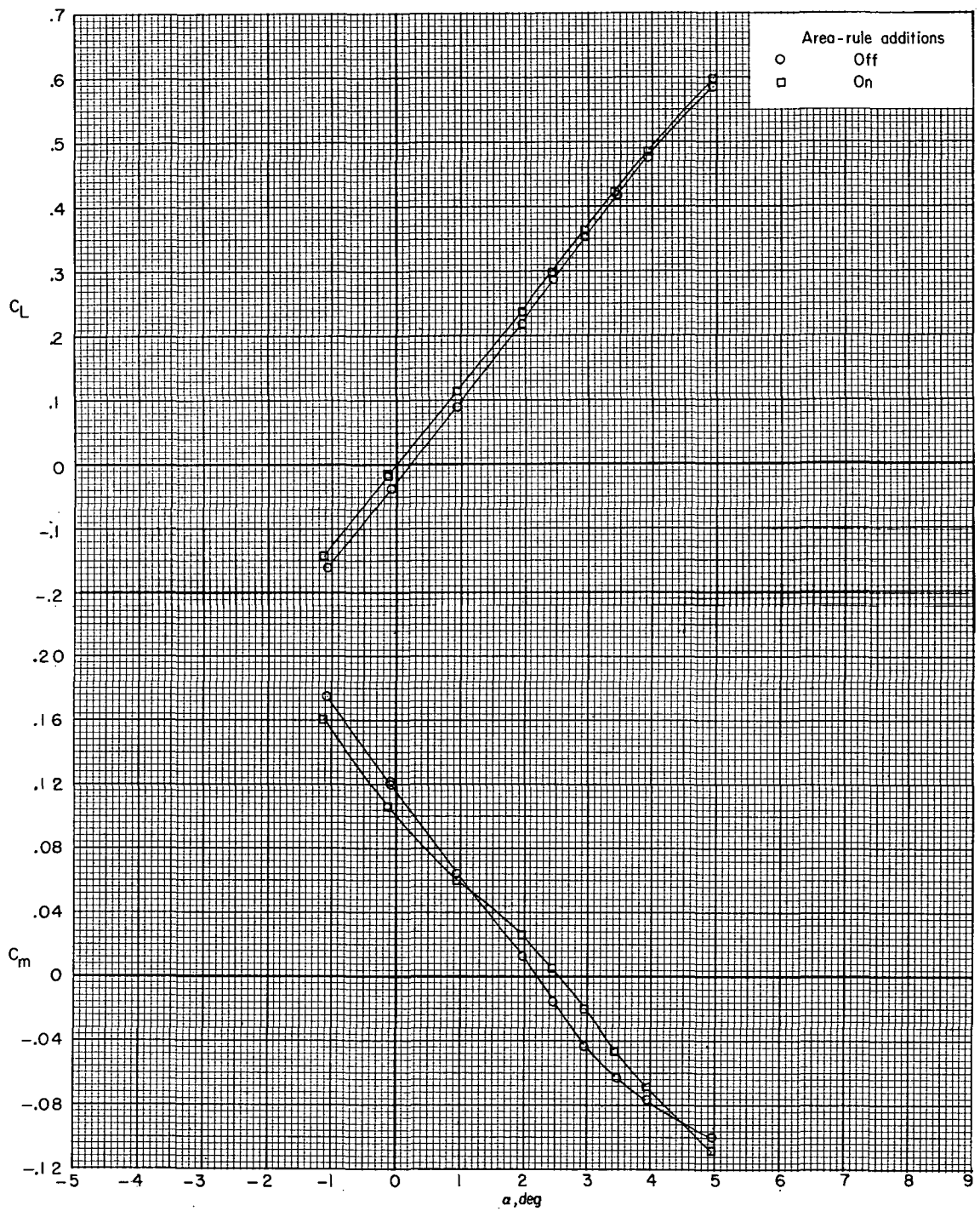
(h) $M = 0.99$. Continued.

Figure 6.- Continued.



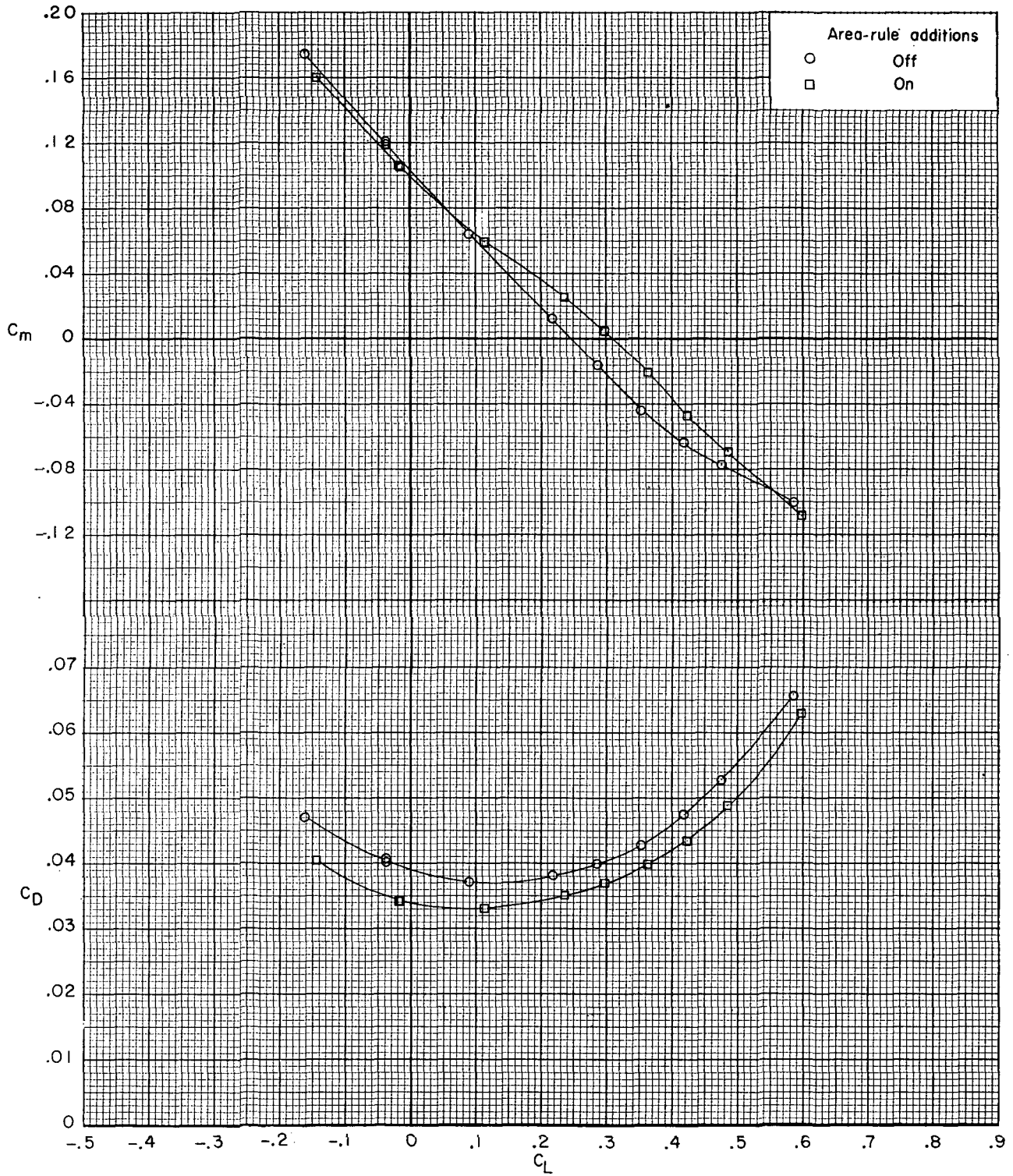
(h) $M = 0.99$. Concluded.

Figure 6.- Continued.



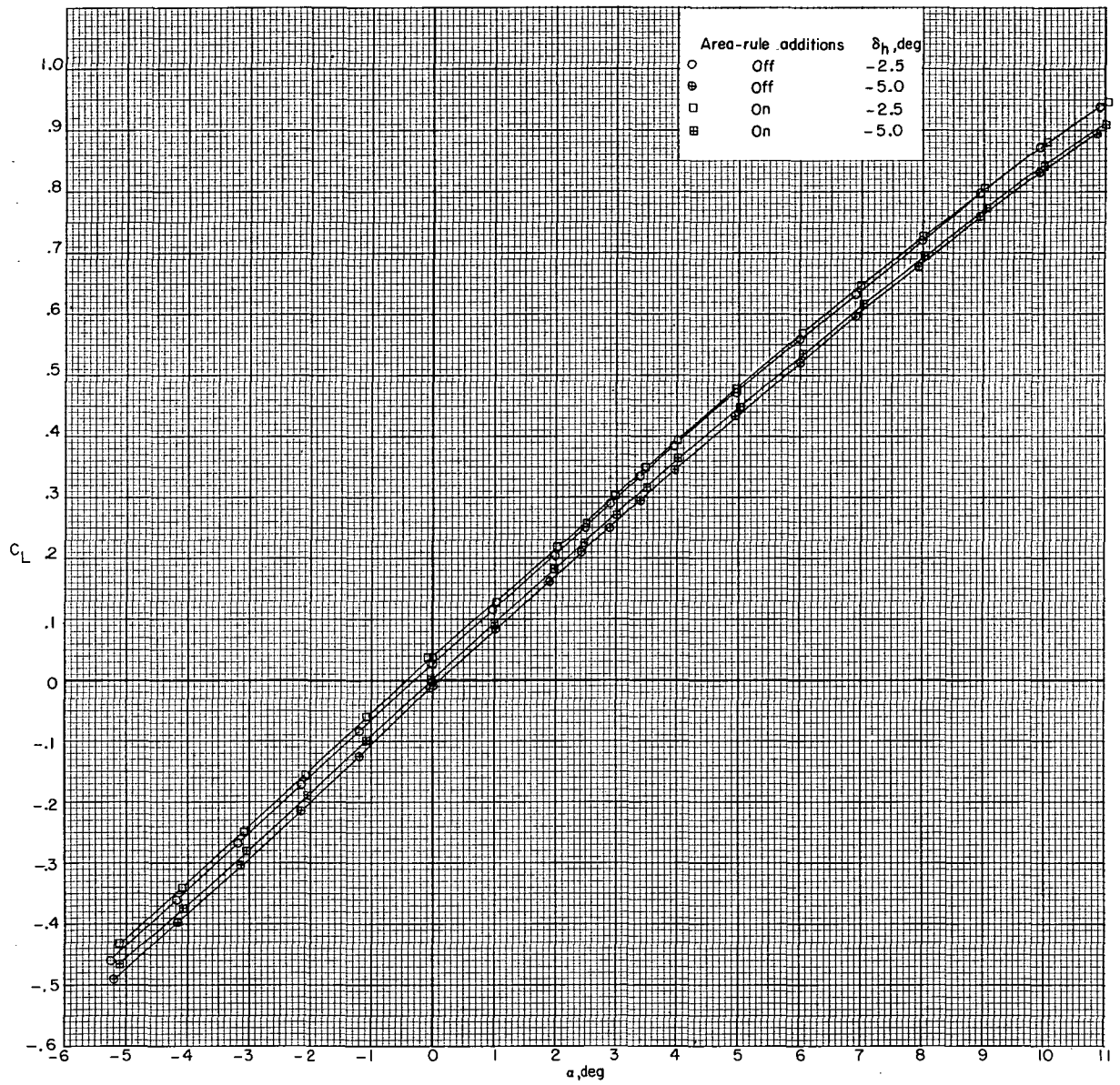
(i) $M = 1.00$.

Figure 6. - Continued.



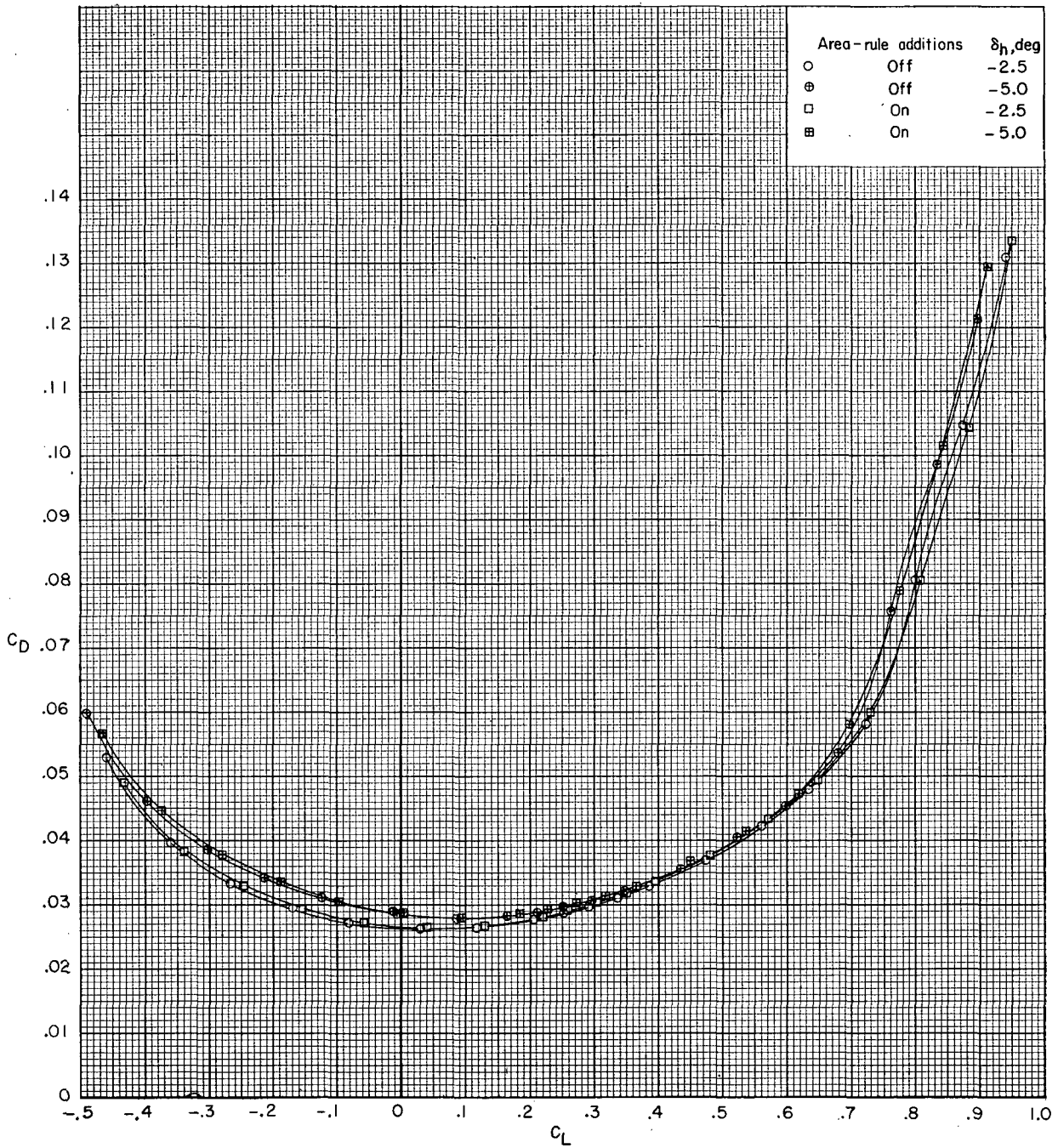
(i) $M = 1.00$. Concluded.

Figure 6.- Concluded.



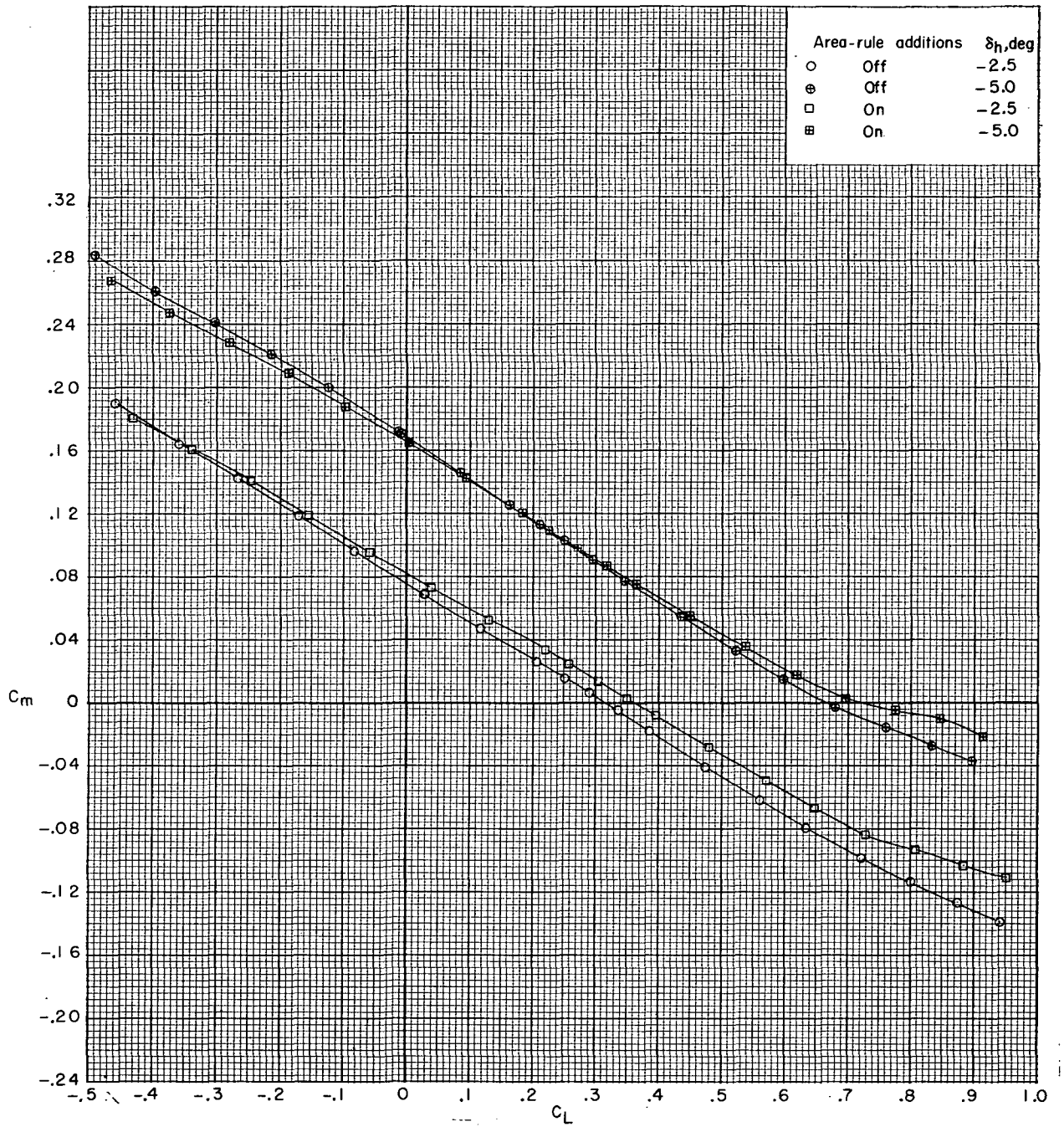
(a) $M = 0.50$.

Figure 7.- Effect of fuselage area-rule additions on horizontal-tail effectiveness. $\beta = 0^\circ$.



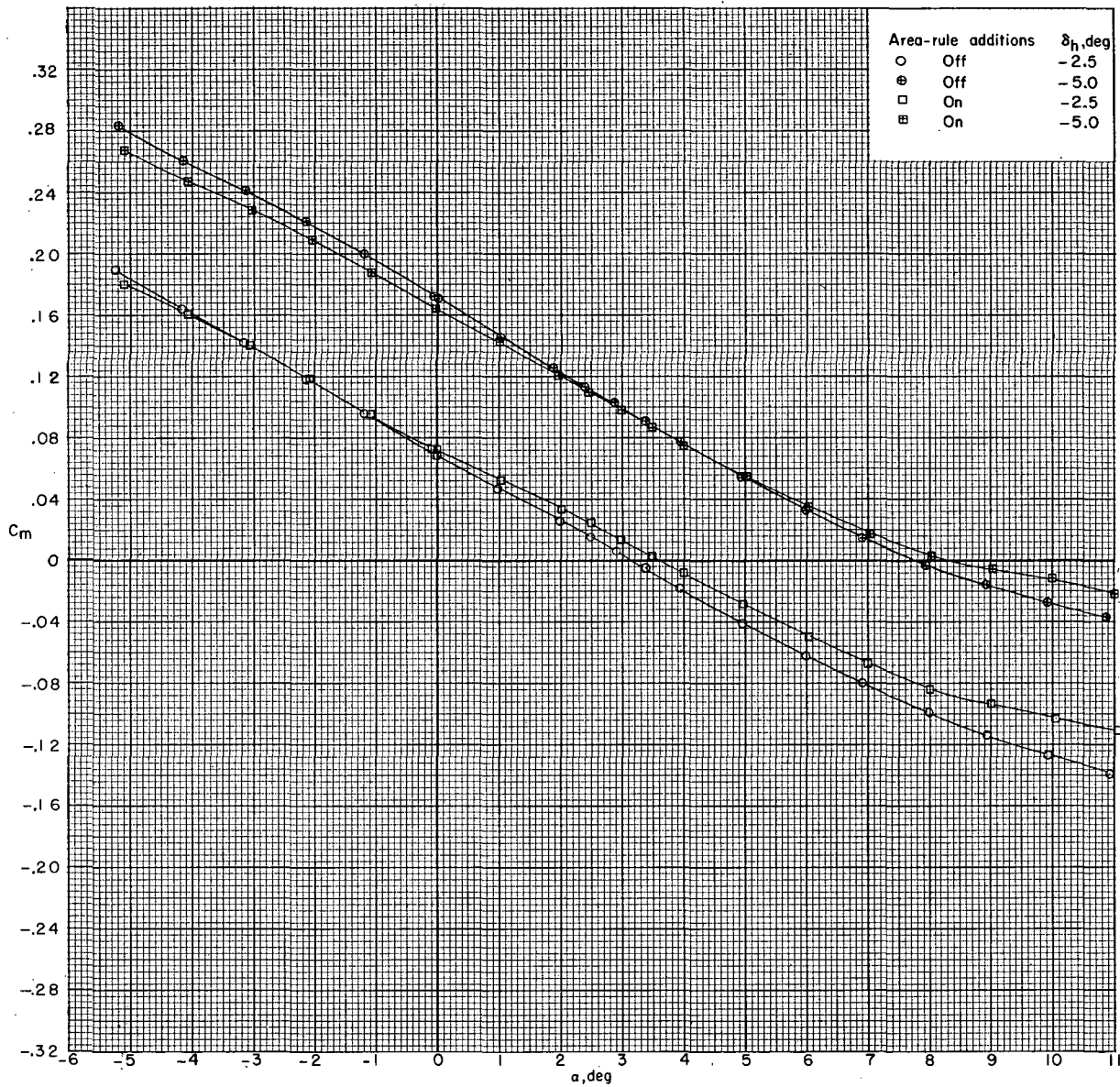
(a) $M = 0.50$. Continued.

Figure 7.- Continued.



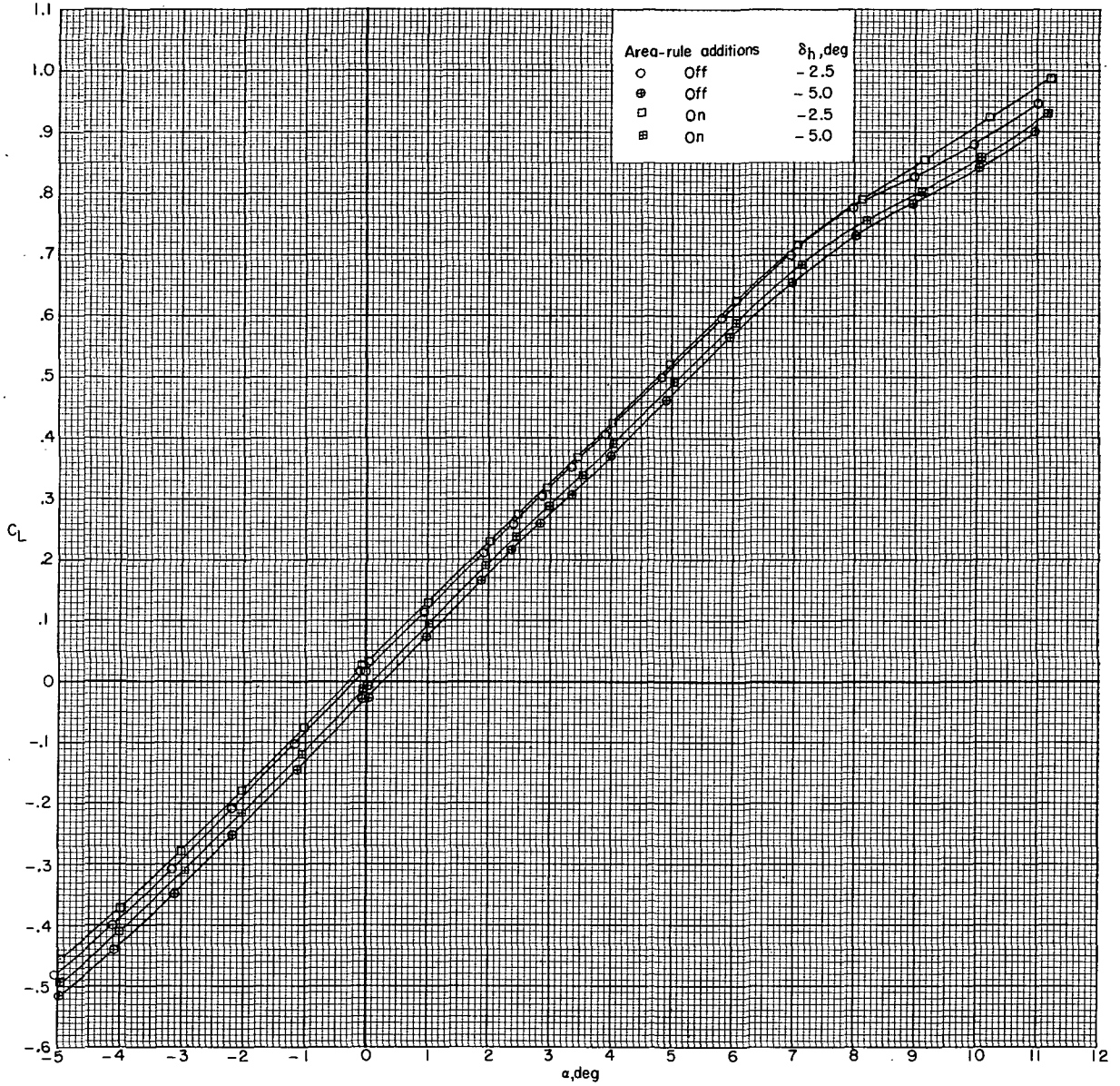
(a) $M = 0.50$. Continued.

Figure 7.- Continued.



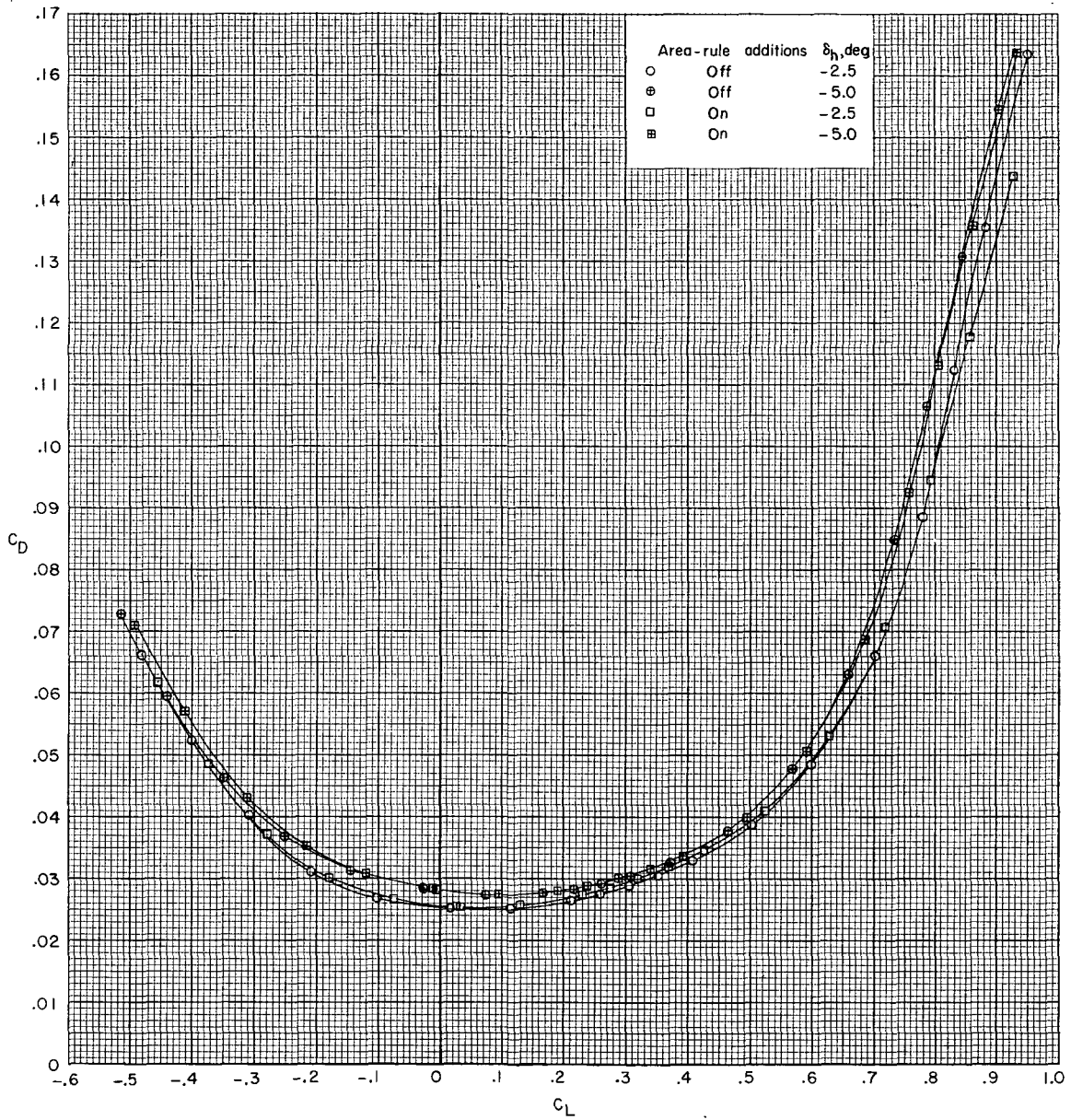
(a) $M = 0.50$. Concluded.

Figure 7. - Continued.



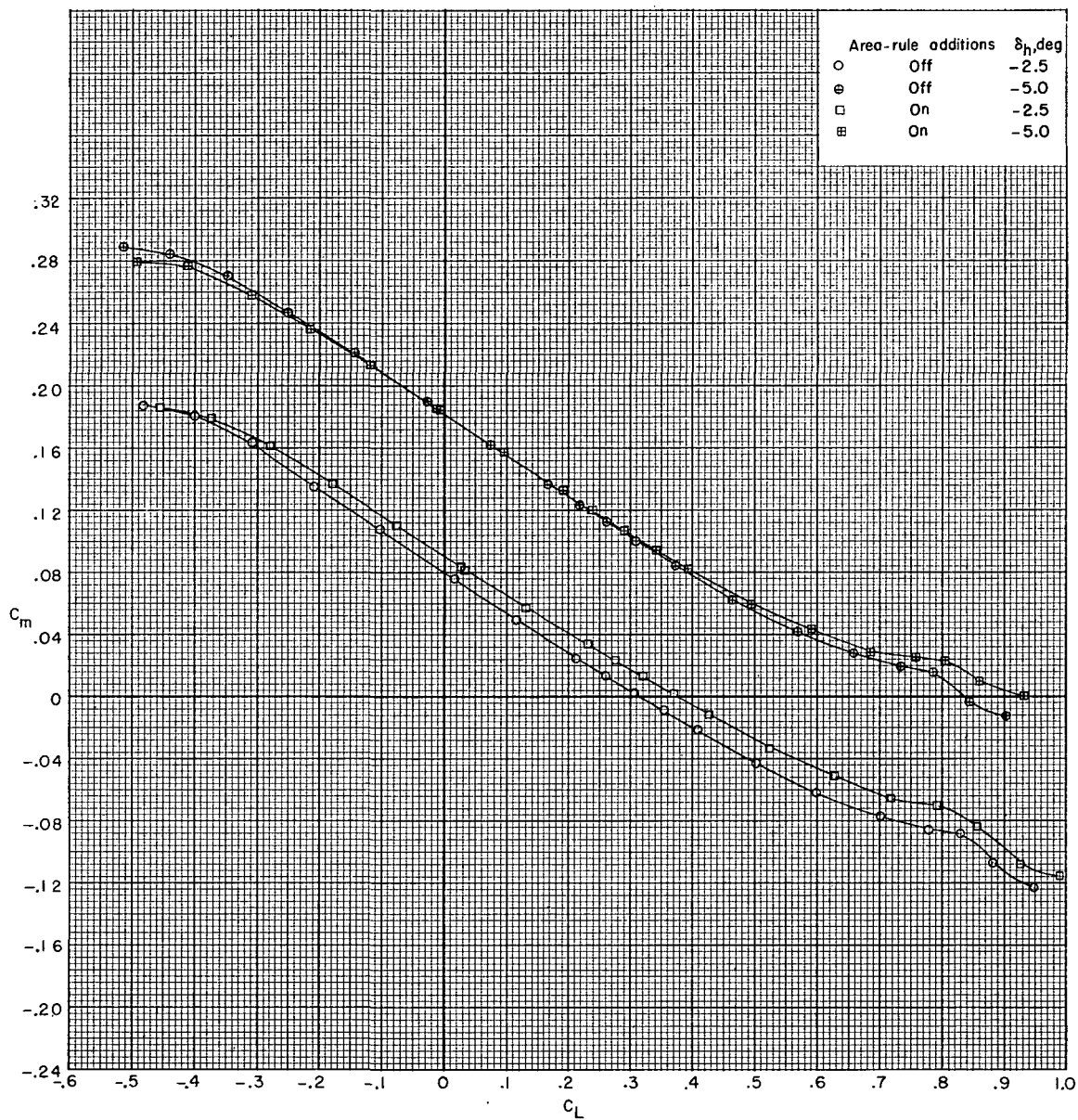
(b) $M = 0.80$.

Figure 7. Continued.



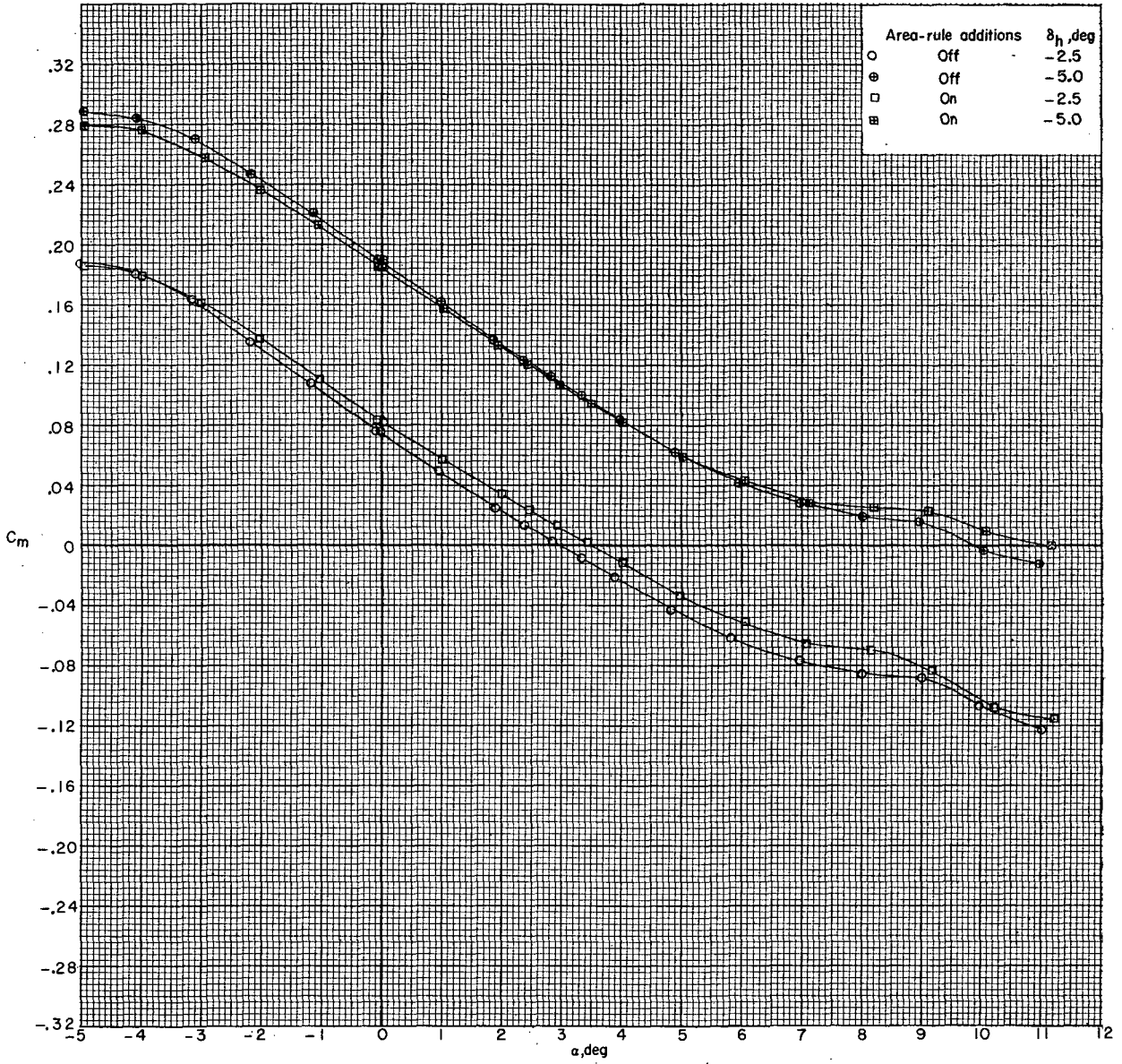
(b) $M = 0.80$. Continued.

Figure 7.- Continued.



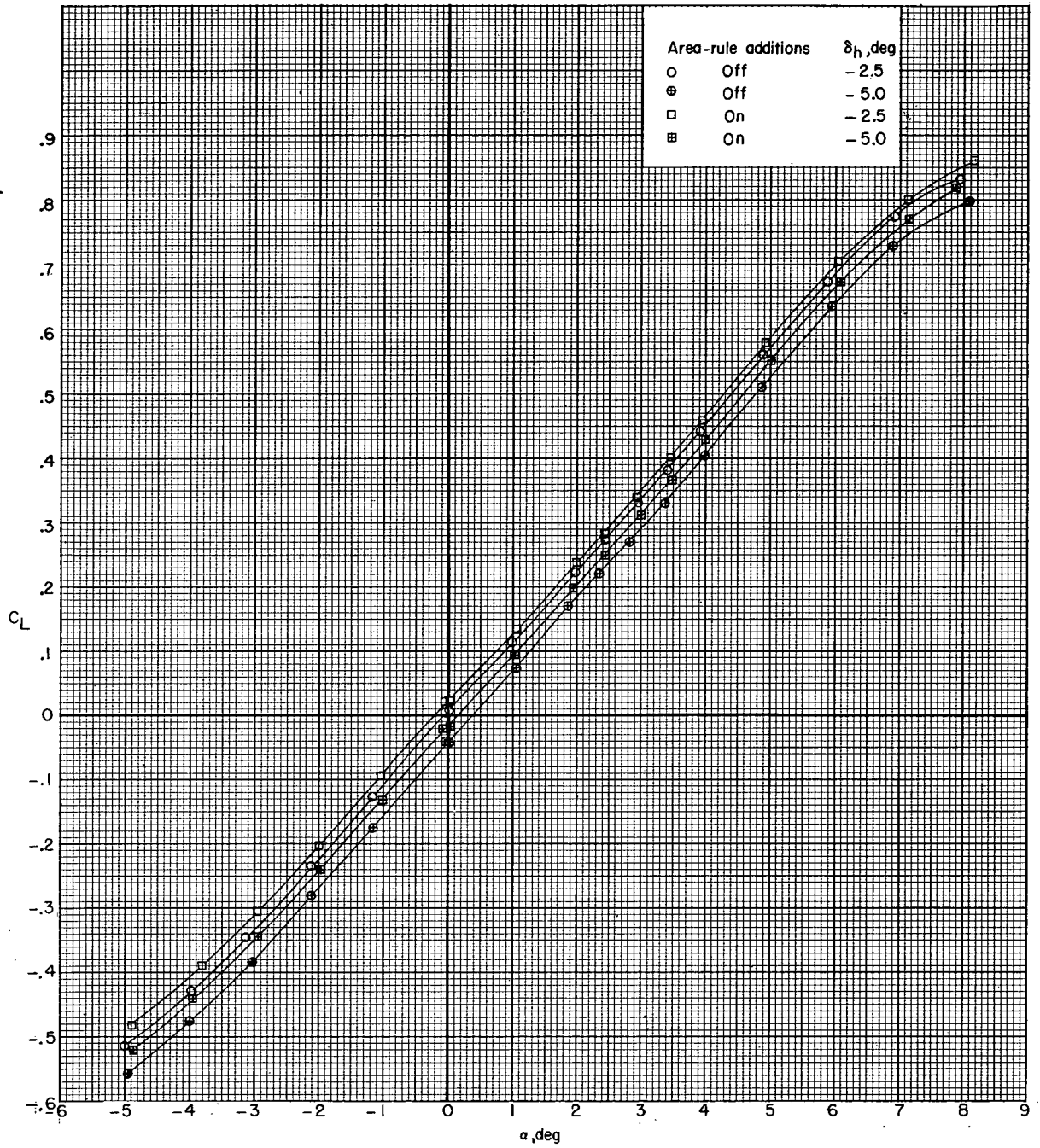
(b) $M = 0.80$. Continued.

Figure 7. - Continued.



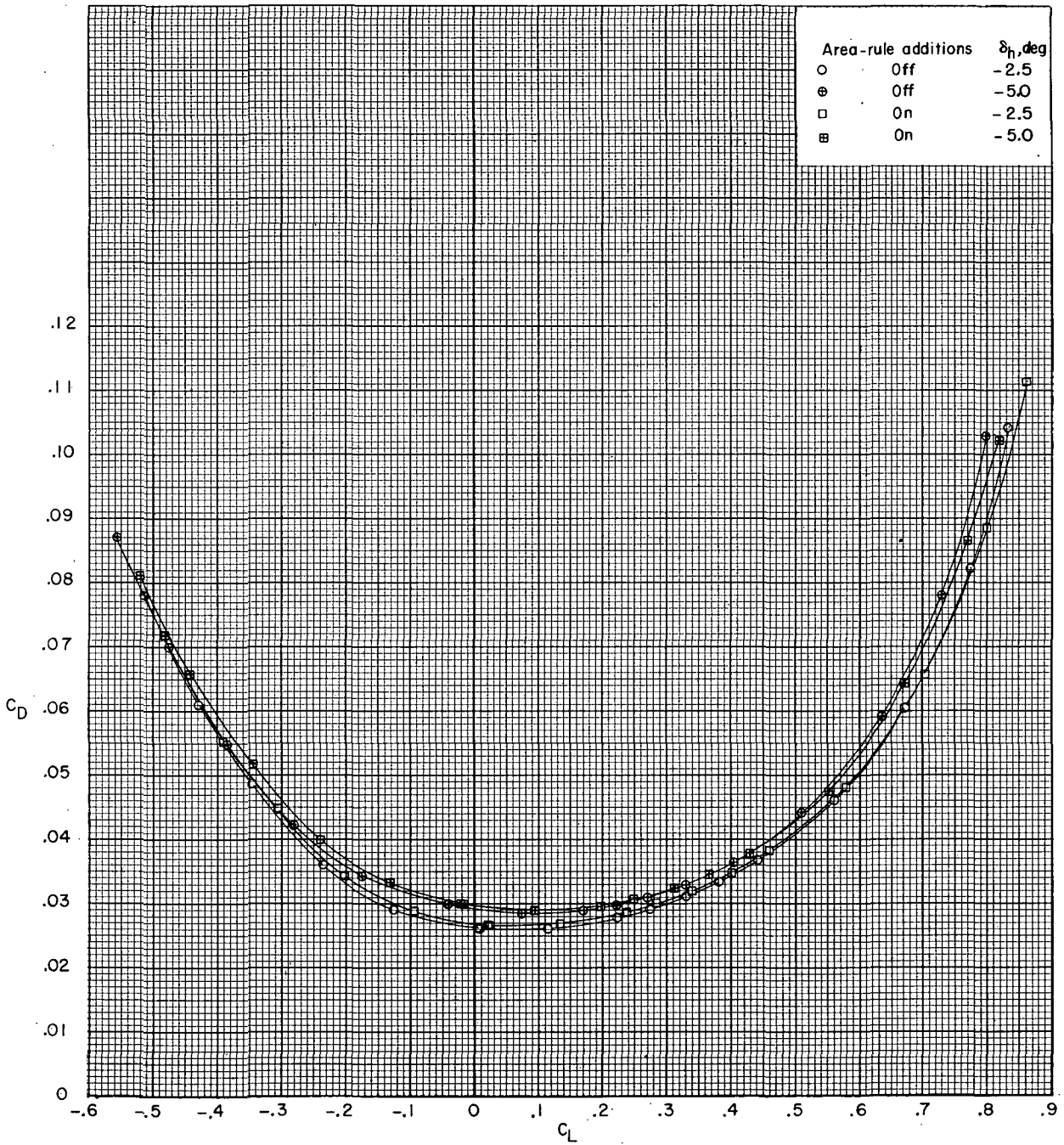
(b) $M = 0.80$. Concluded.

Figure 7.- Continued.



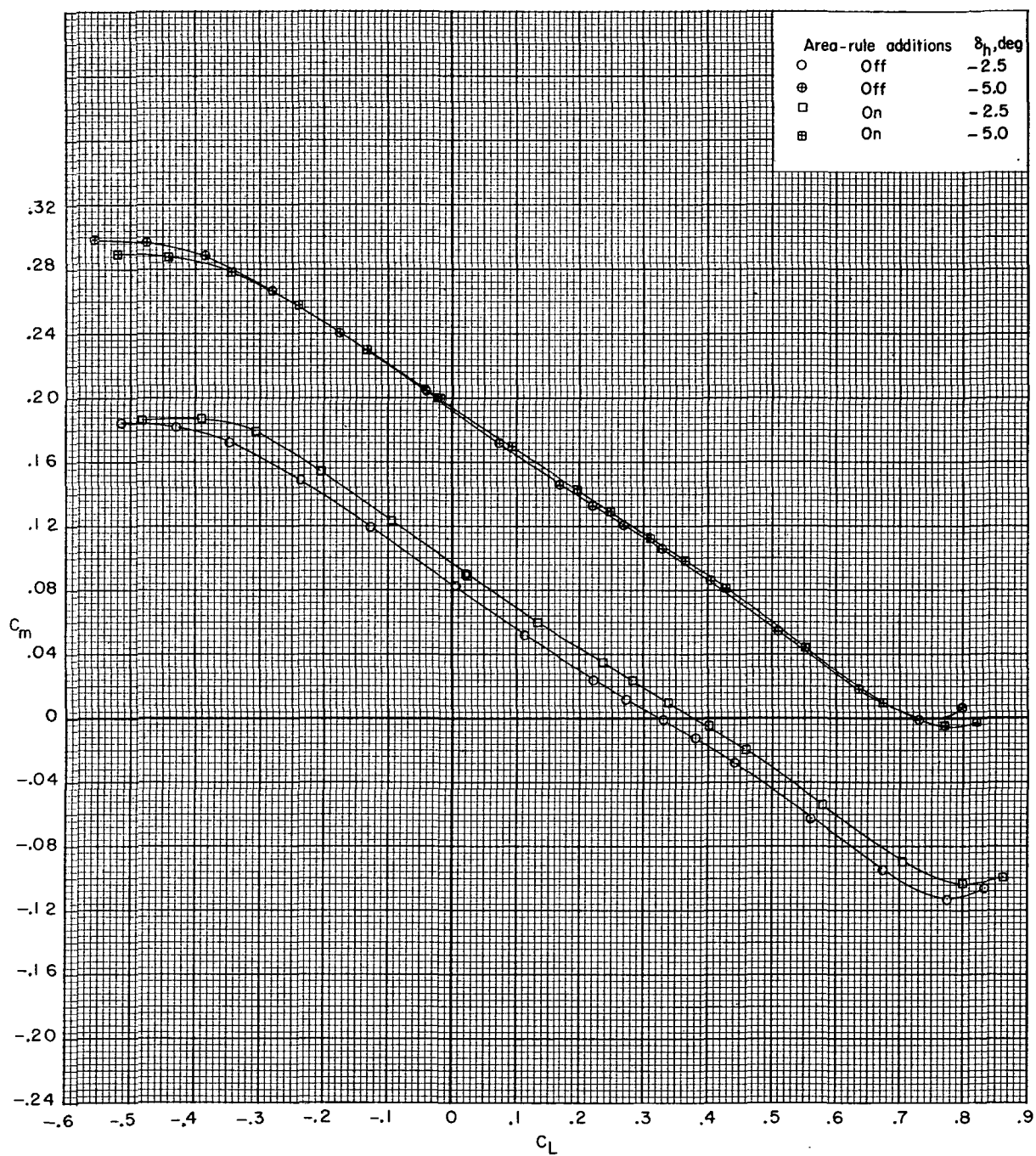
(c) $M = 0.90$.

Figure 7.- Continued.



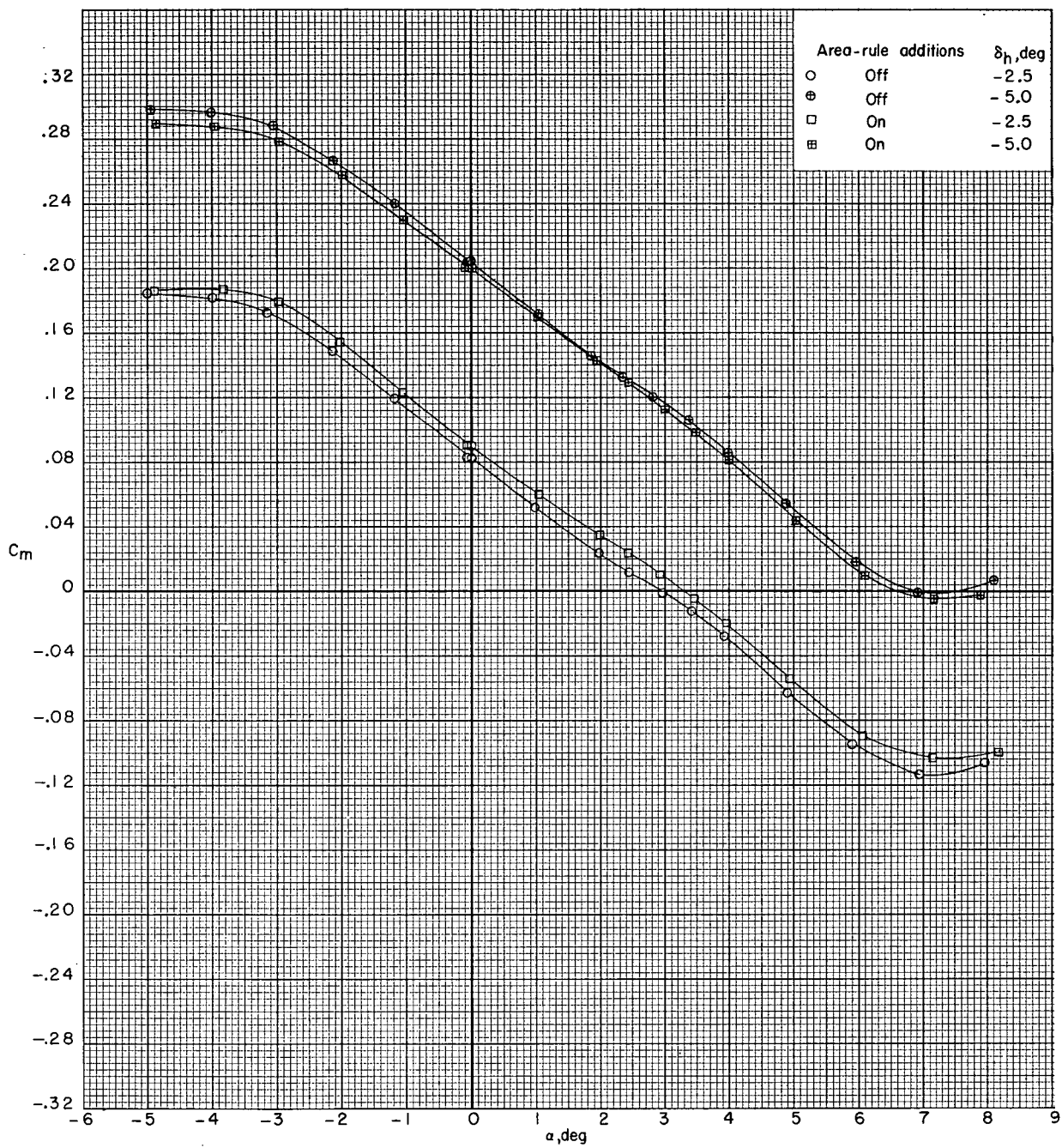
(c) $M = 0.90$. Continued.

Figure 7.- Continued.



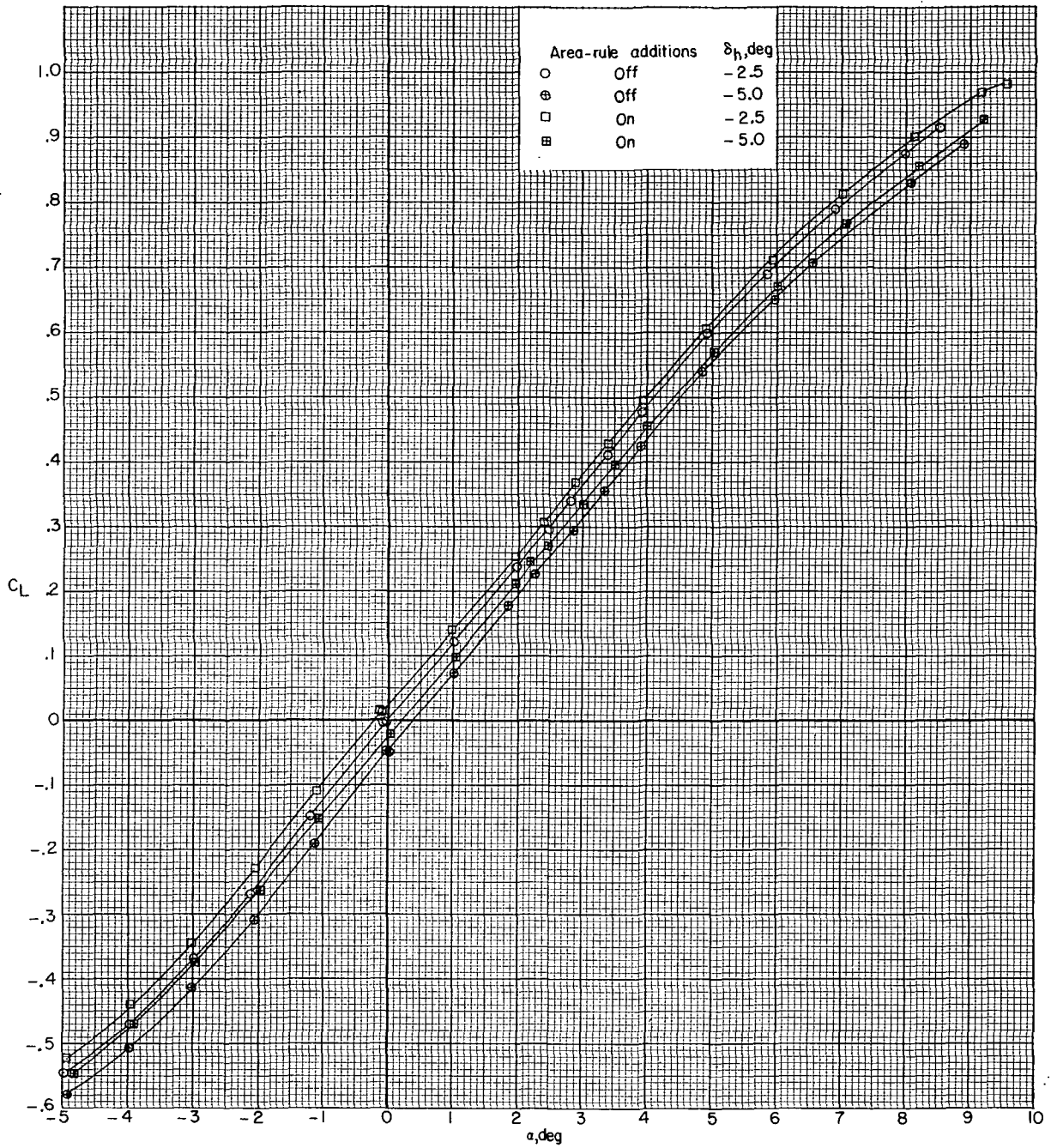
(c) $M = 0.90$, Continued.

Figure 7.- Continued.



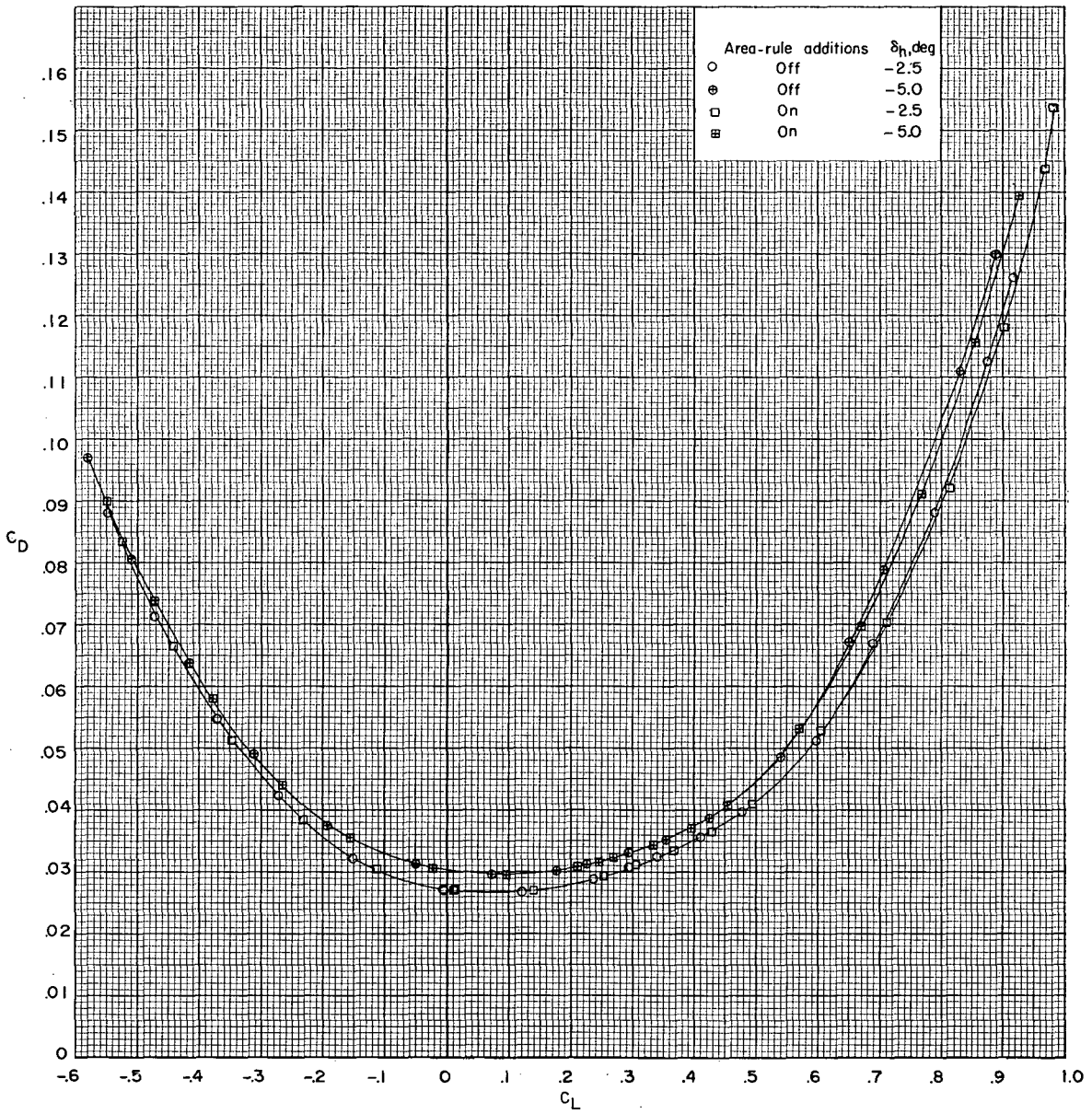
(c) $M = 0.90$. Concluded.

Figure 7.- Continued.



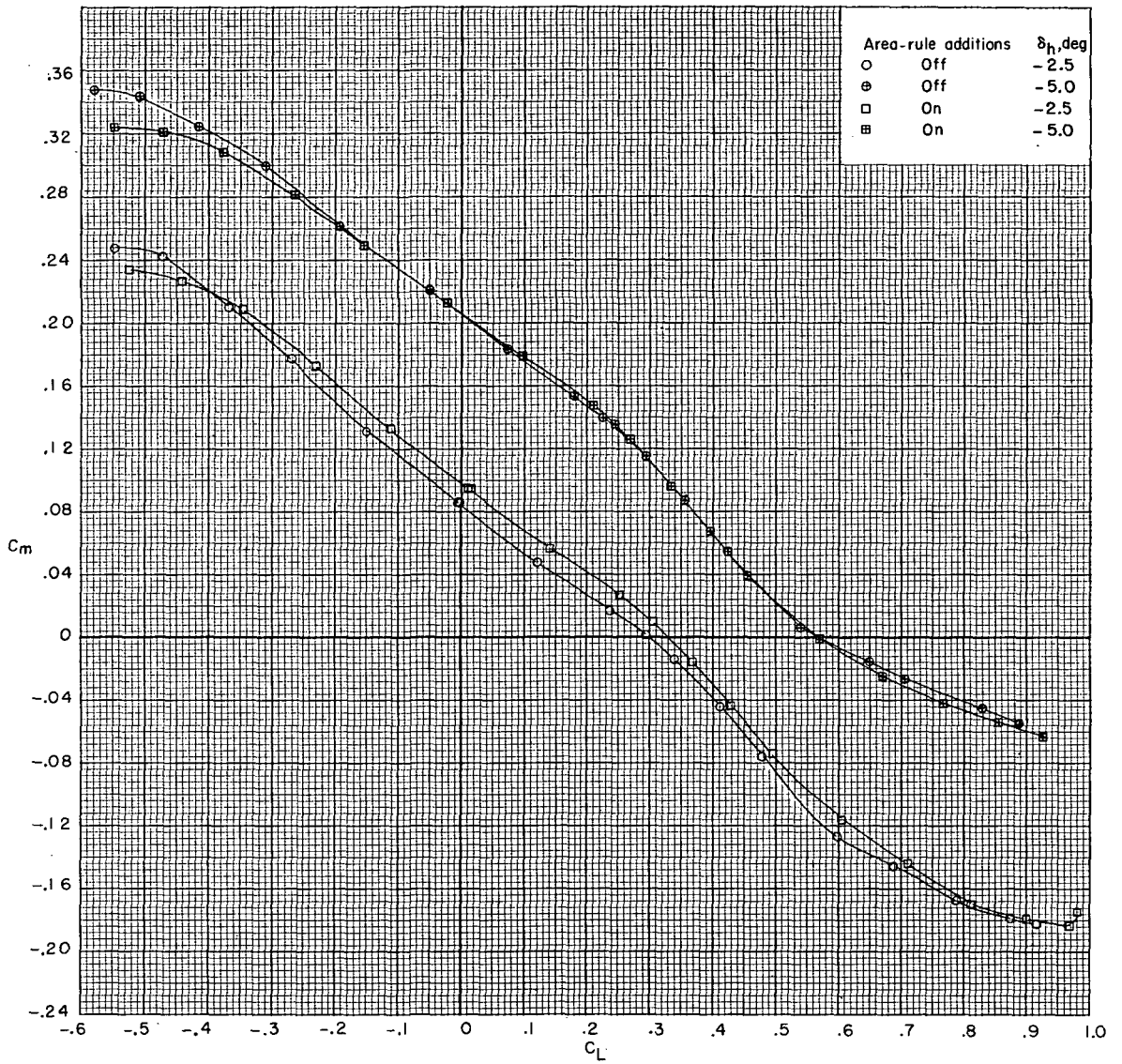
(d) $M = 0.95$.

Figure 7.- Continued.



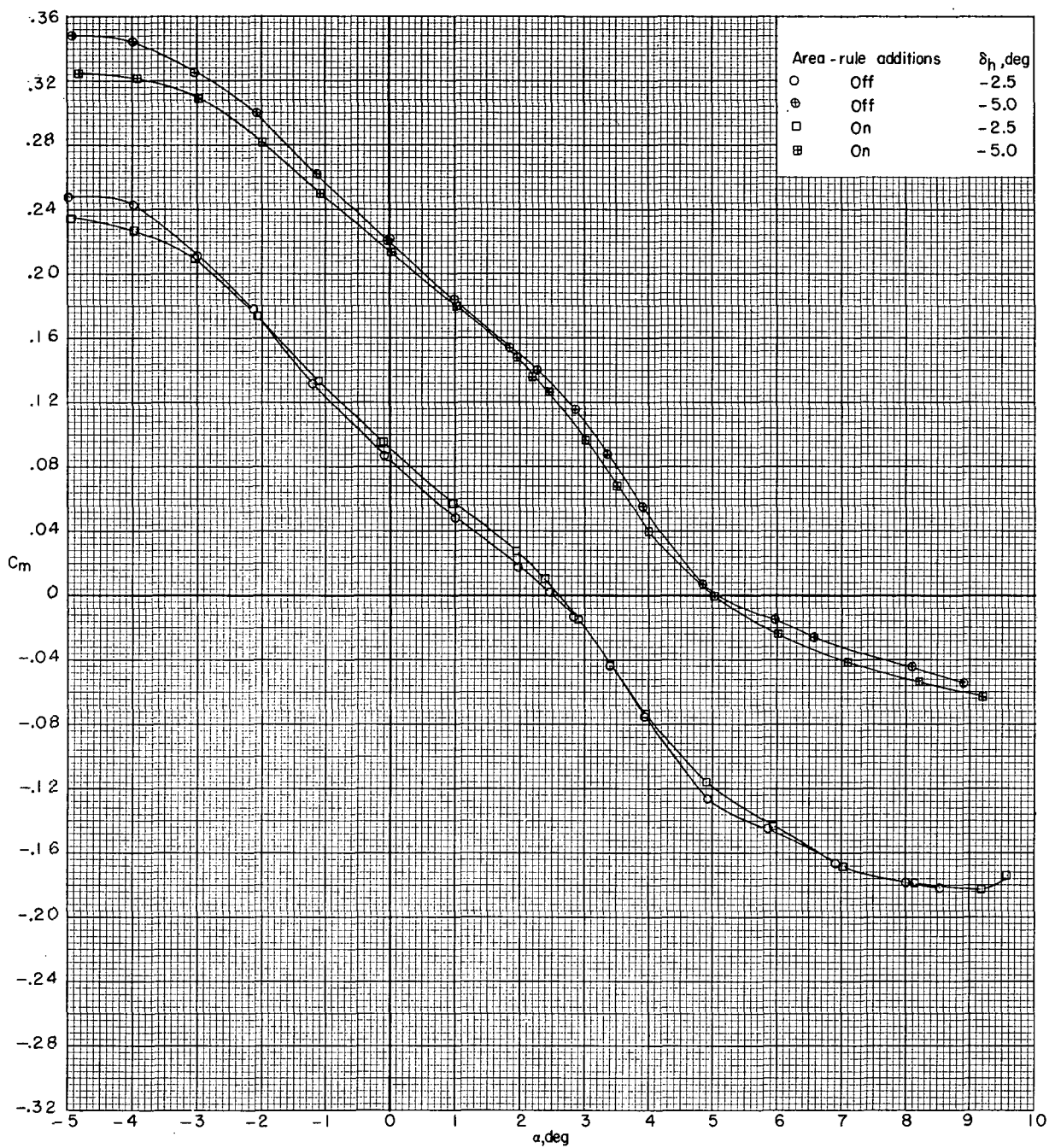
(d) $M = 0.95$. Continued.

Figure 7.- Continued.



(d) $M = 0.95$. Continued.

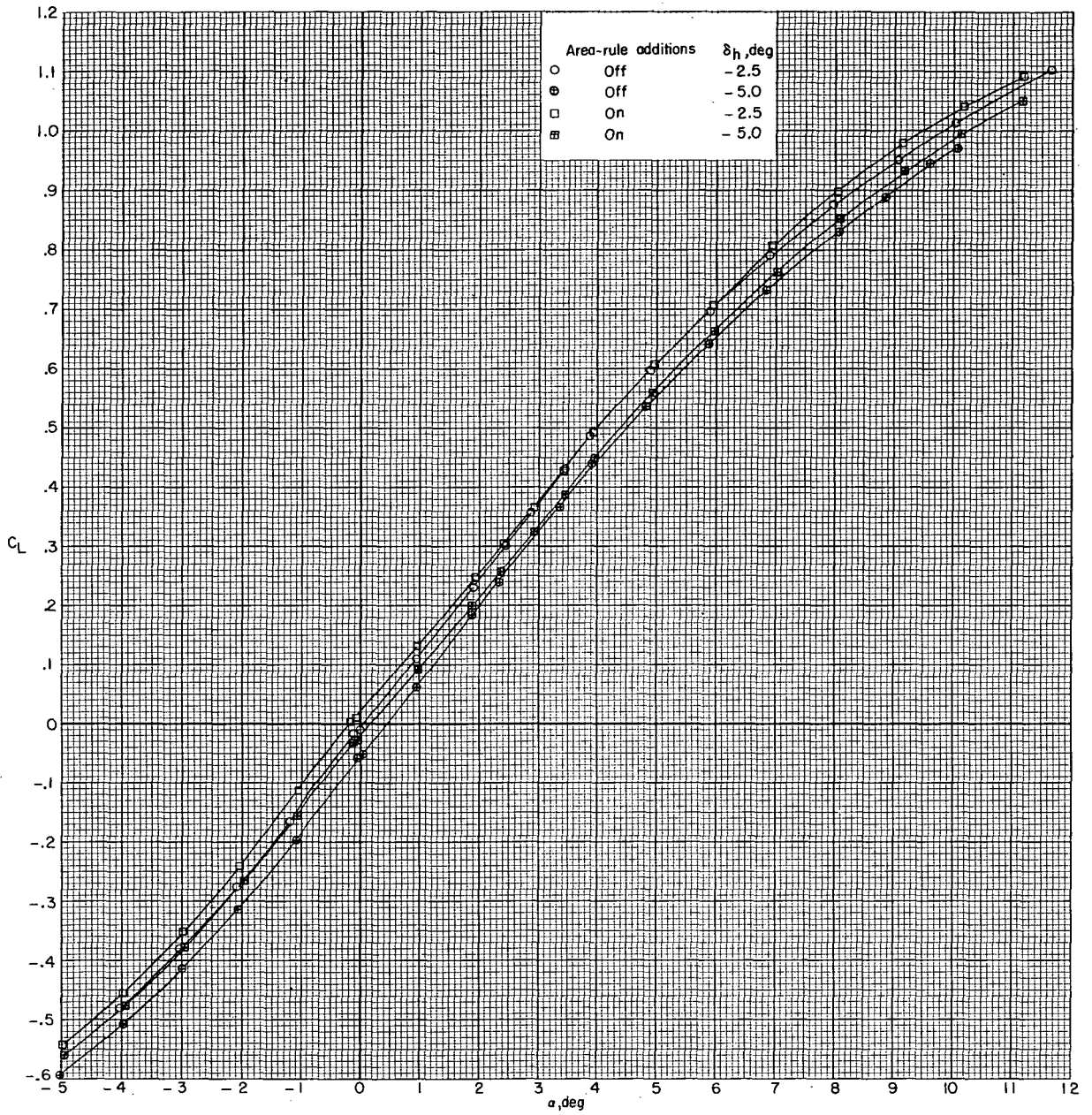
Figure 7.- Continued.



(d) $M = 0.95$. Concluded.

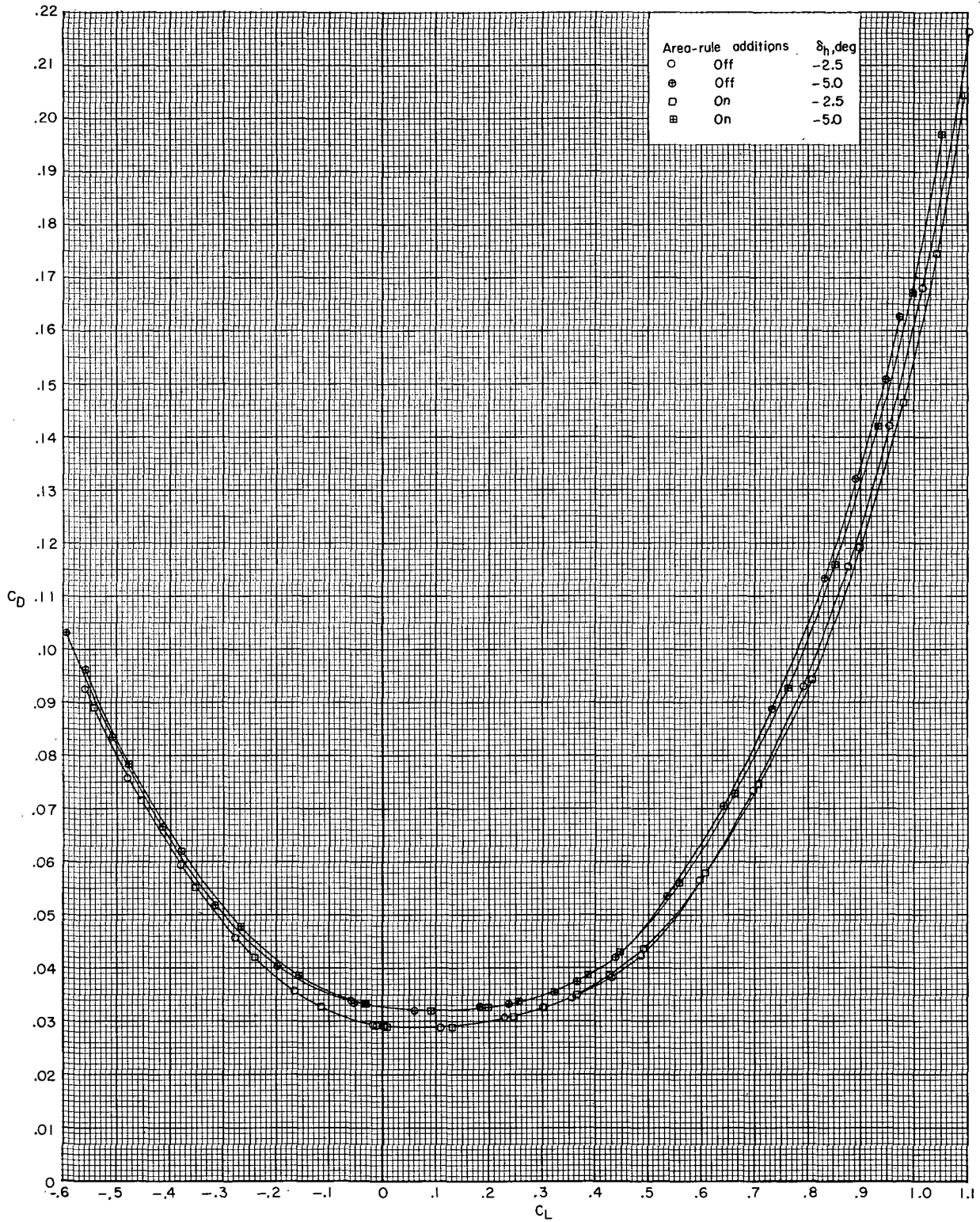
Figure 7.- Continued.





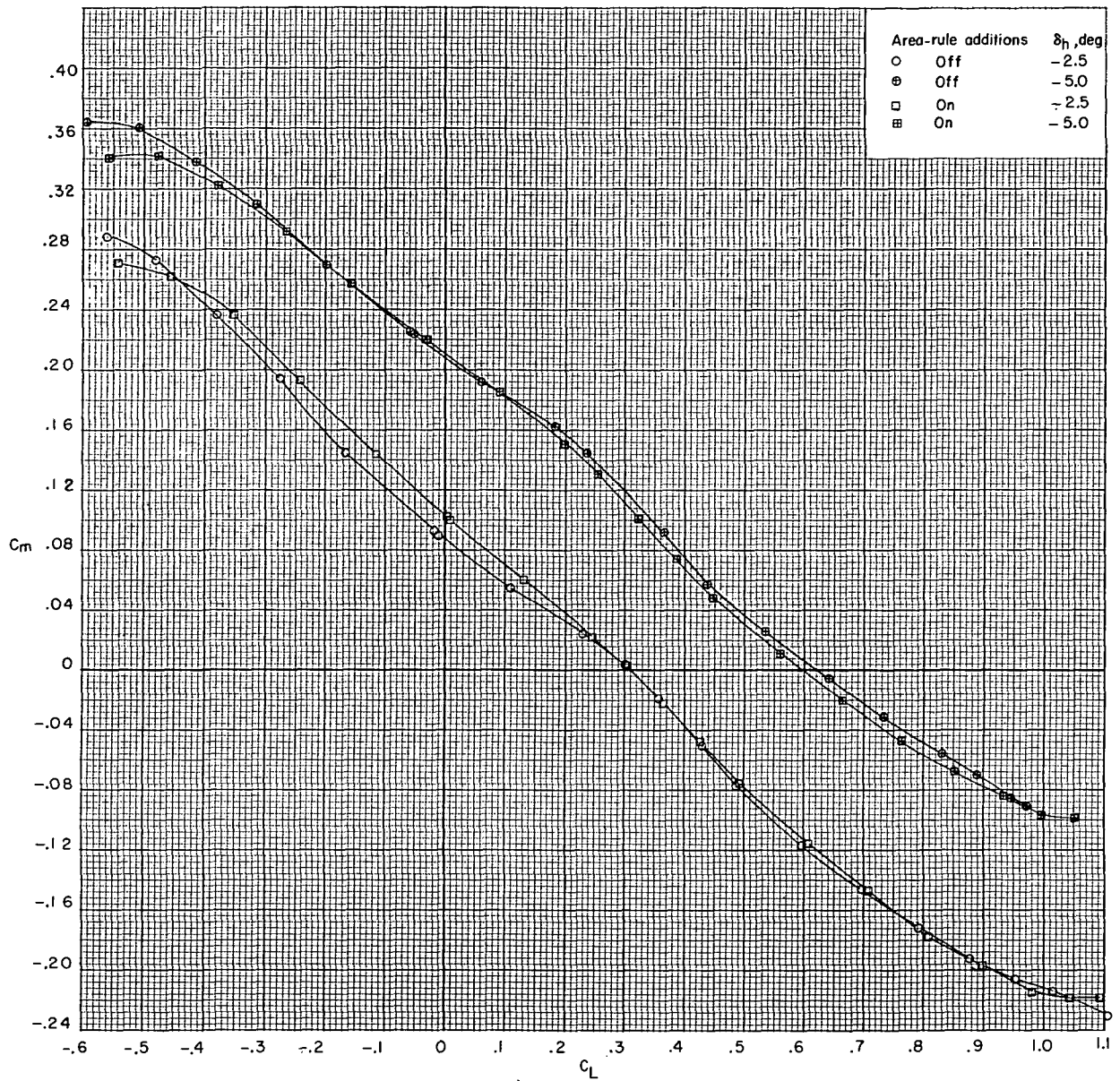
(e) $M = 0.97$.

Figure 7.- Continued.



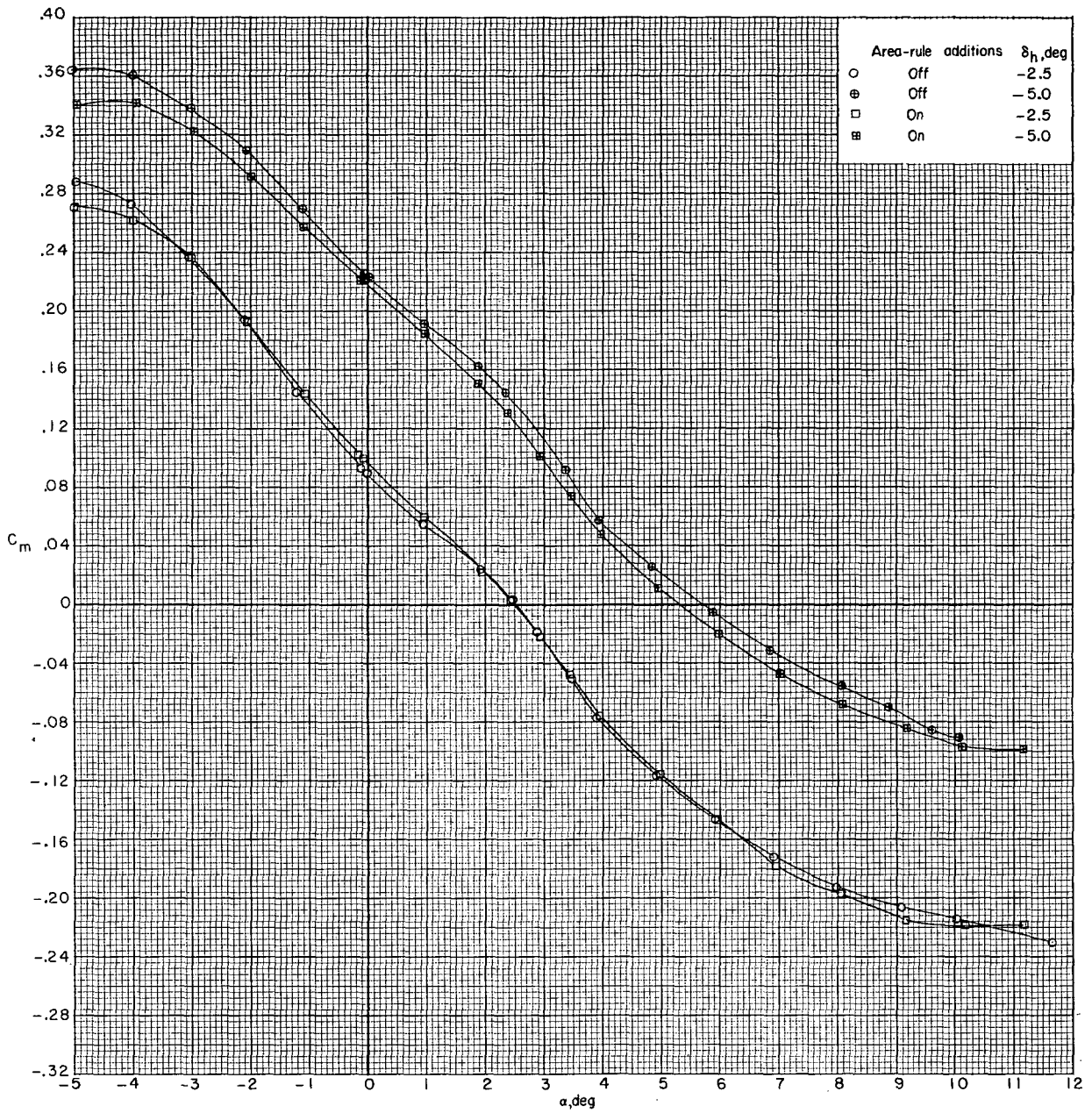
(e) $M = 0.97$. Continued.

Figure 7.- Continued.



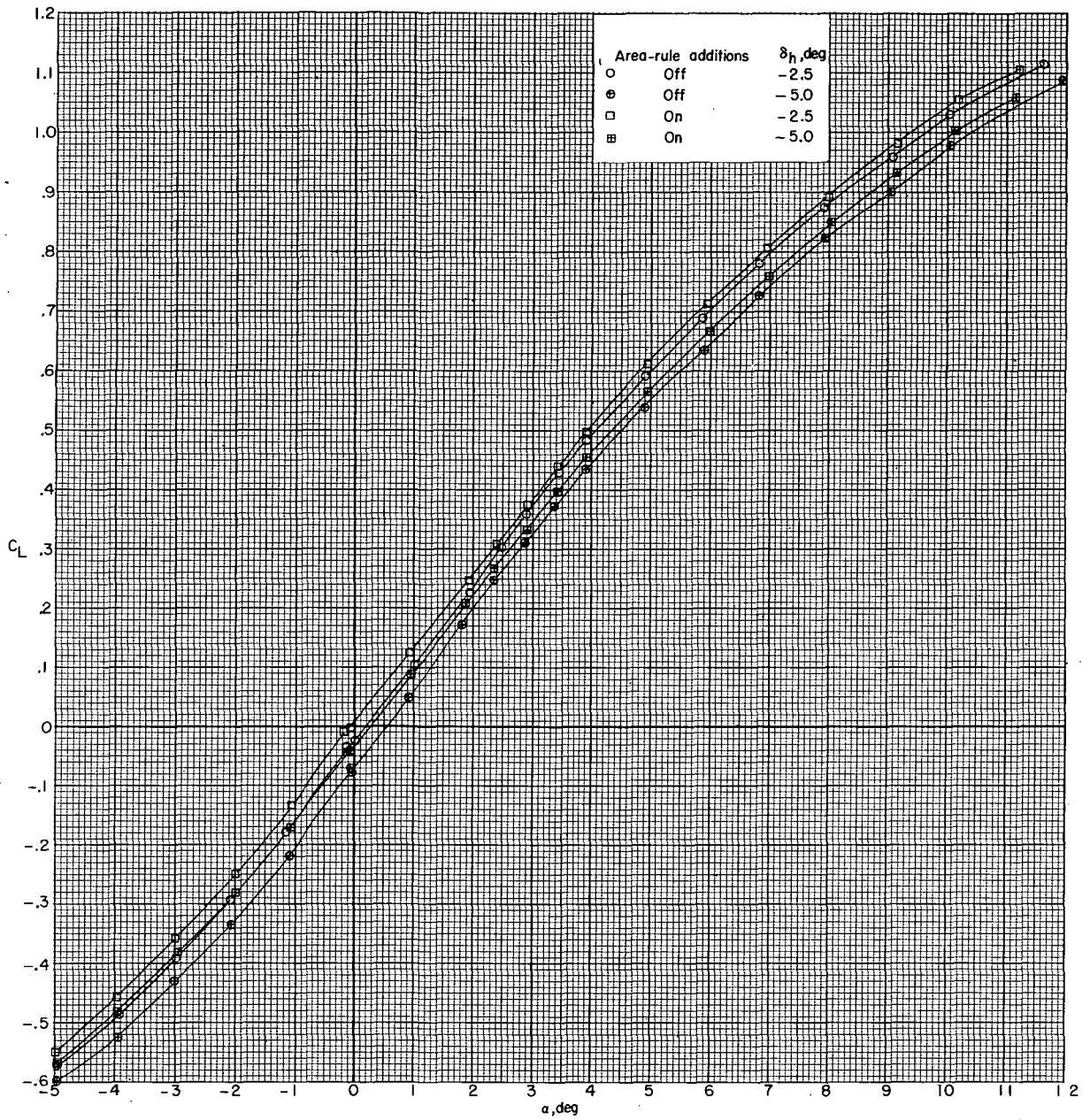
(e) $M = 0.97$. Continued.

Figure 7. - Continued.



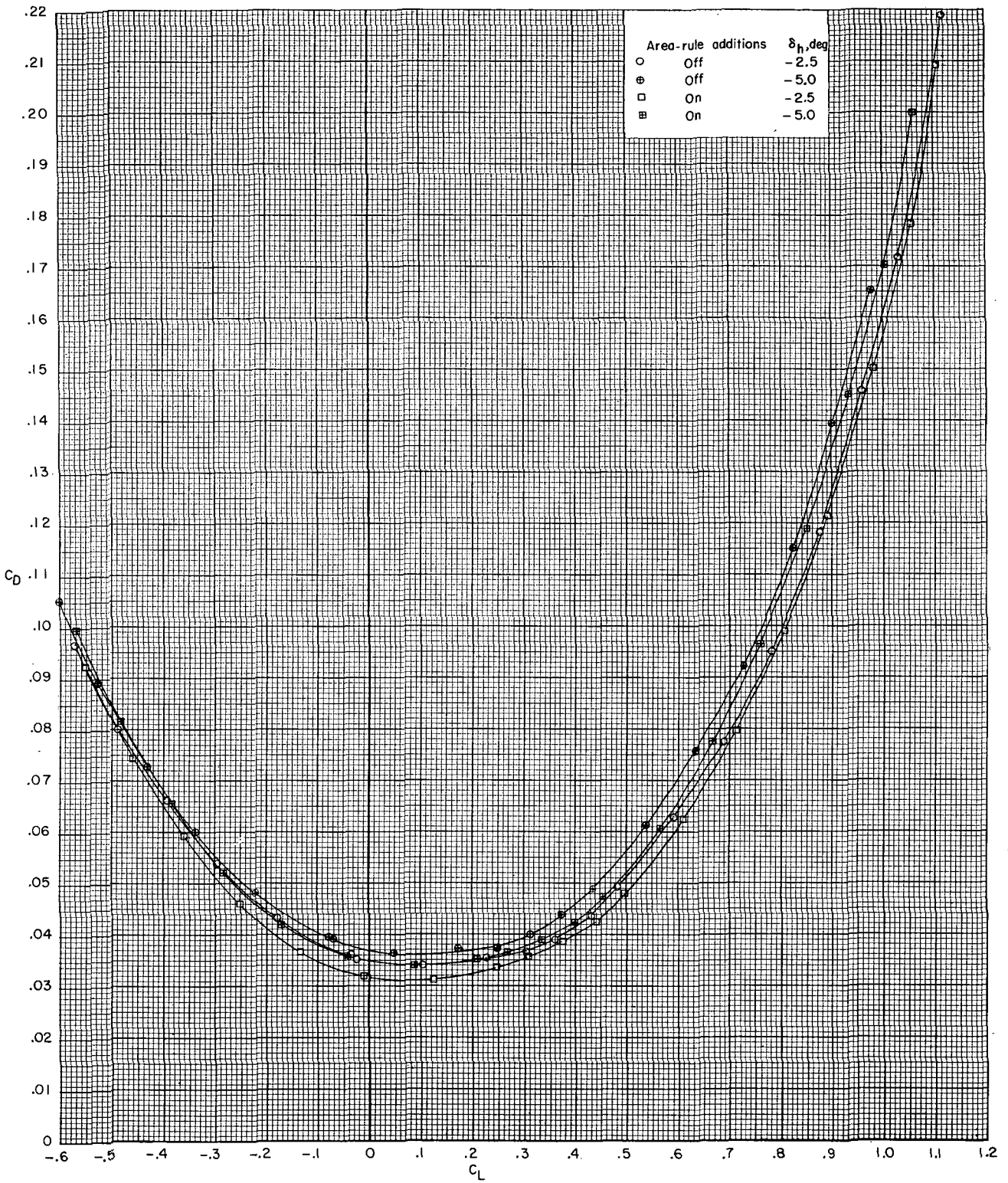
(e) $M = 0.97$. Concluded.

Figure 7.- Continued.



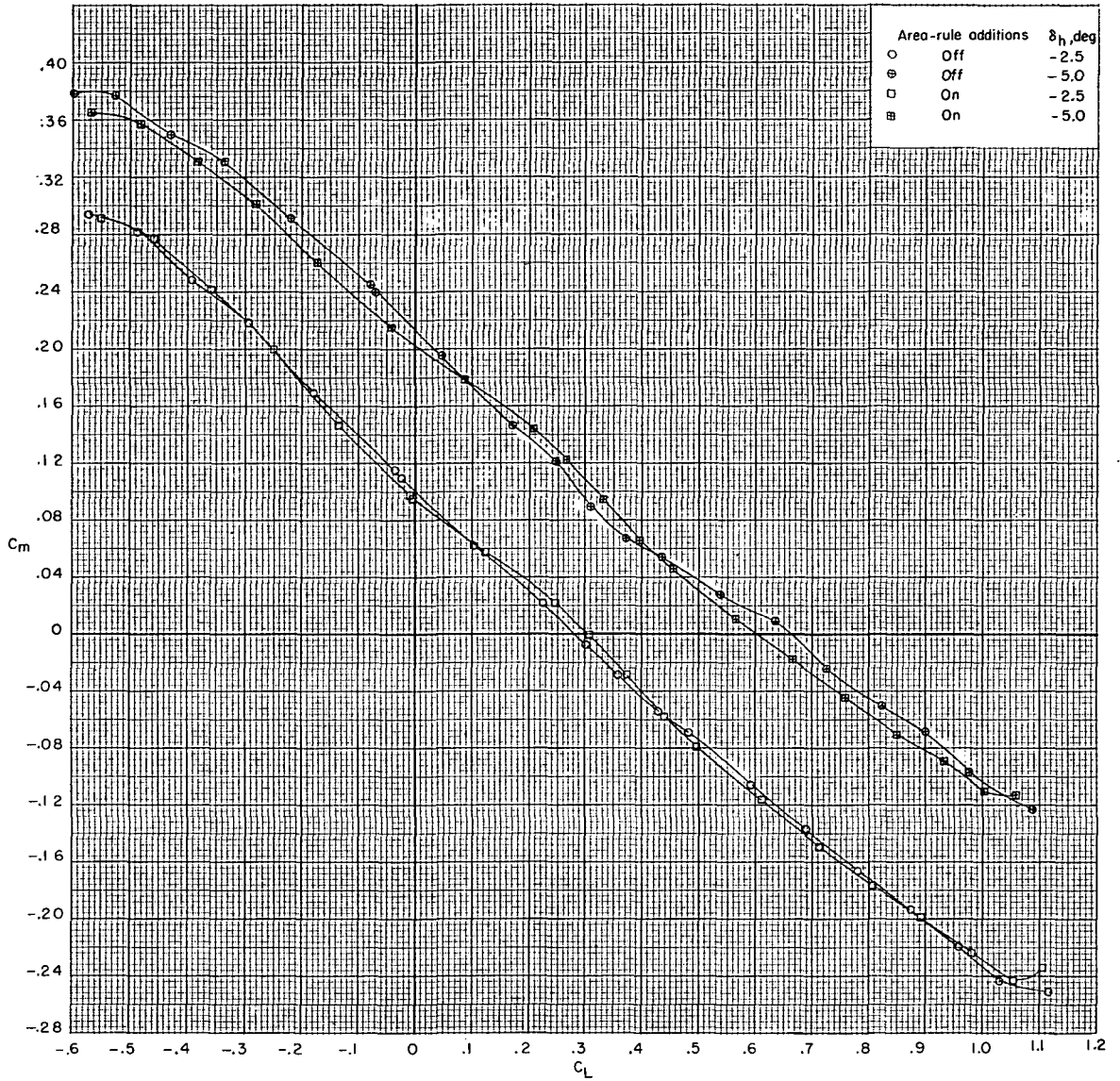
(f) $M = 0.99$.

Figure 7. - Continued.



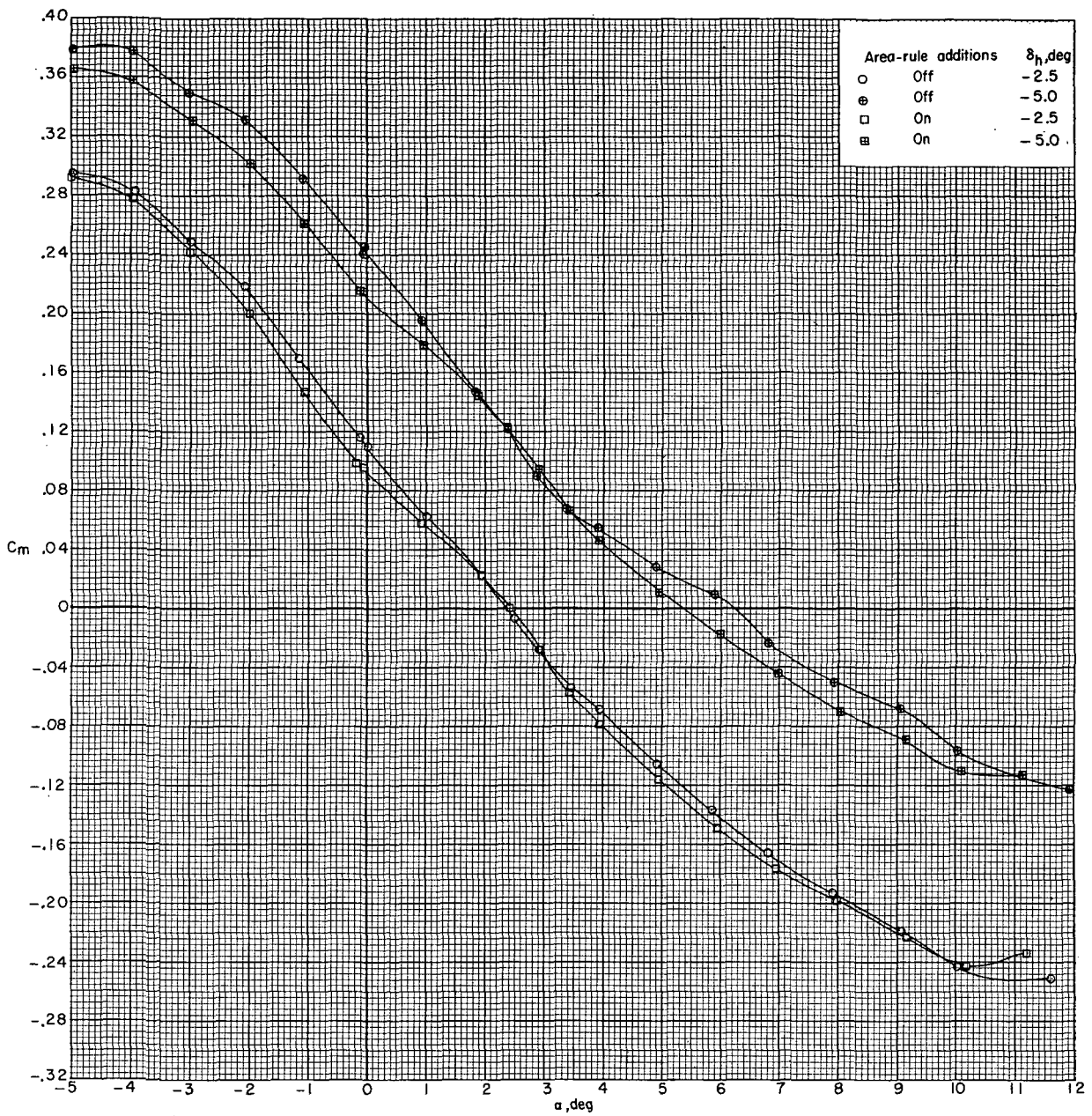
(f) $M = 0.99$. Continued.

Figure 7. - Continued.



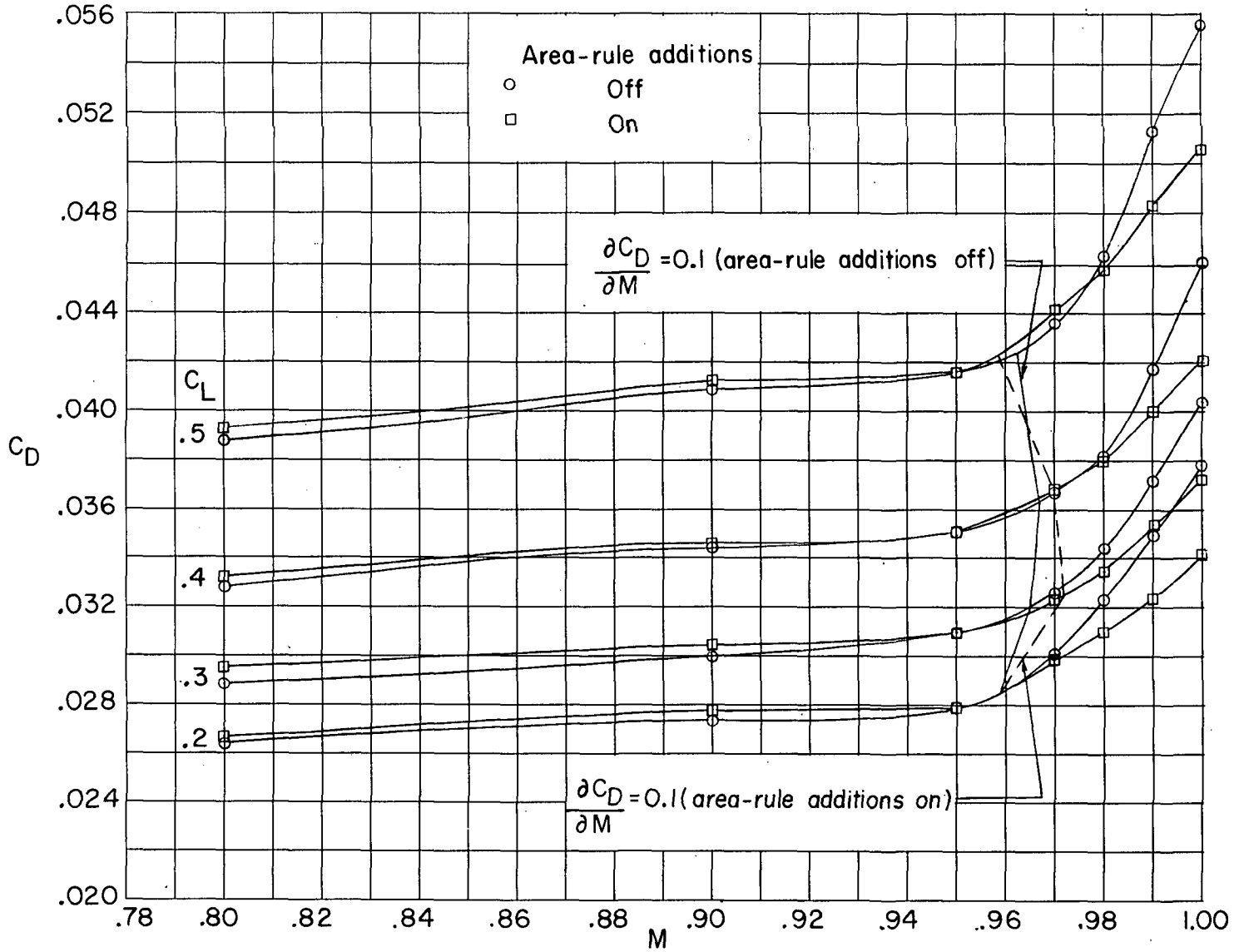
(f) $M = 0.99$. Continued.

Figure 7.- Continued.



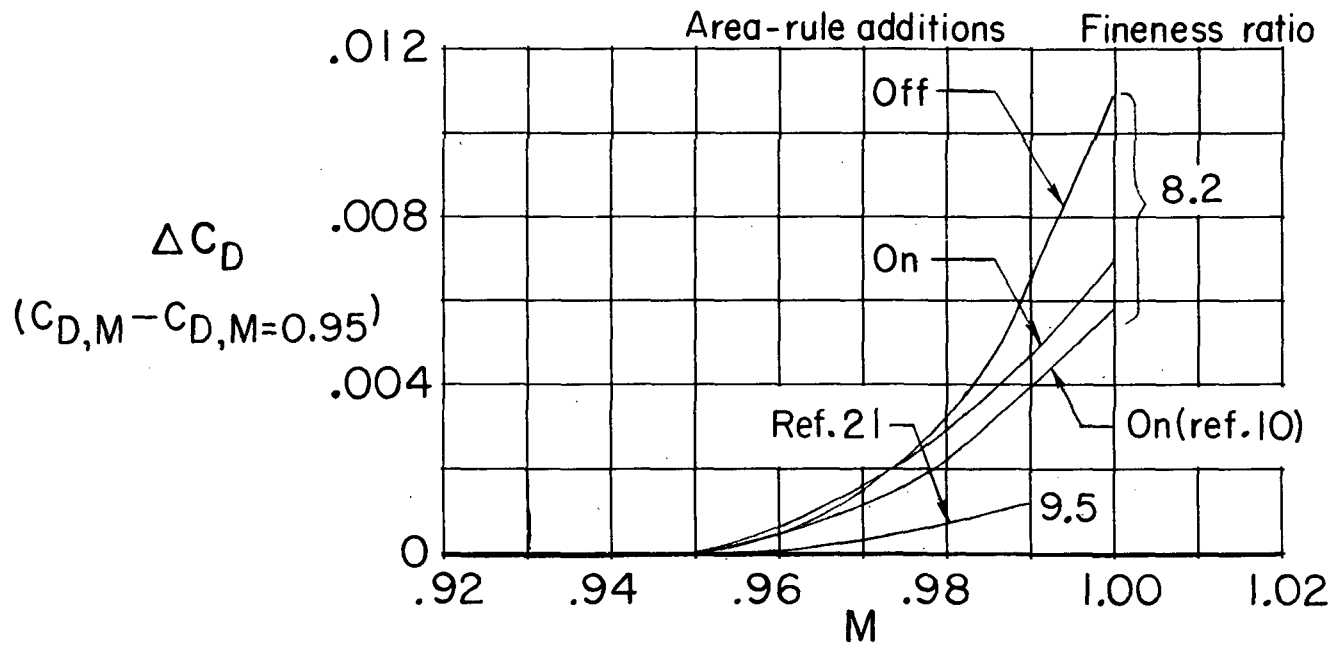
(f) $M = 0.99$. Concluded.

Figure 7.- Concluded.



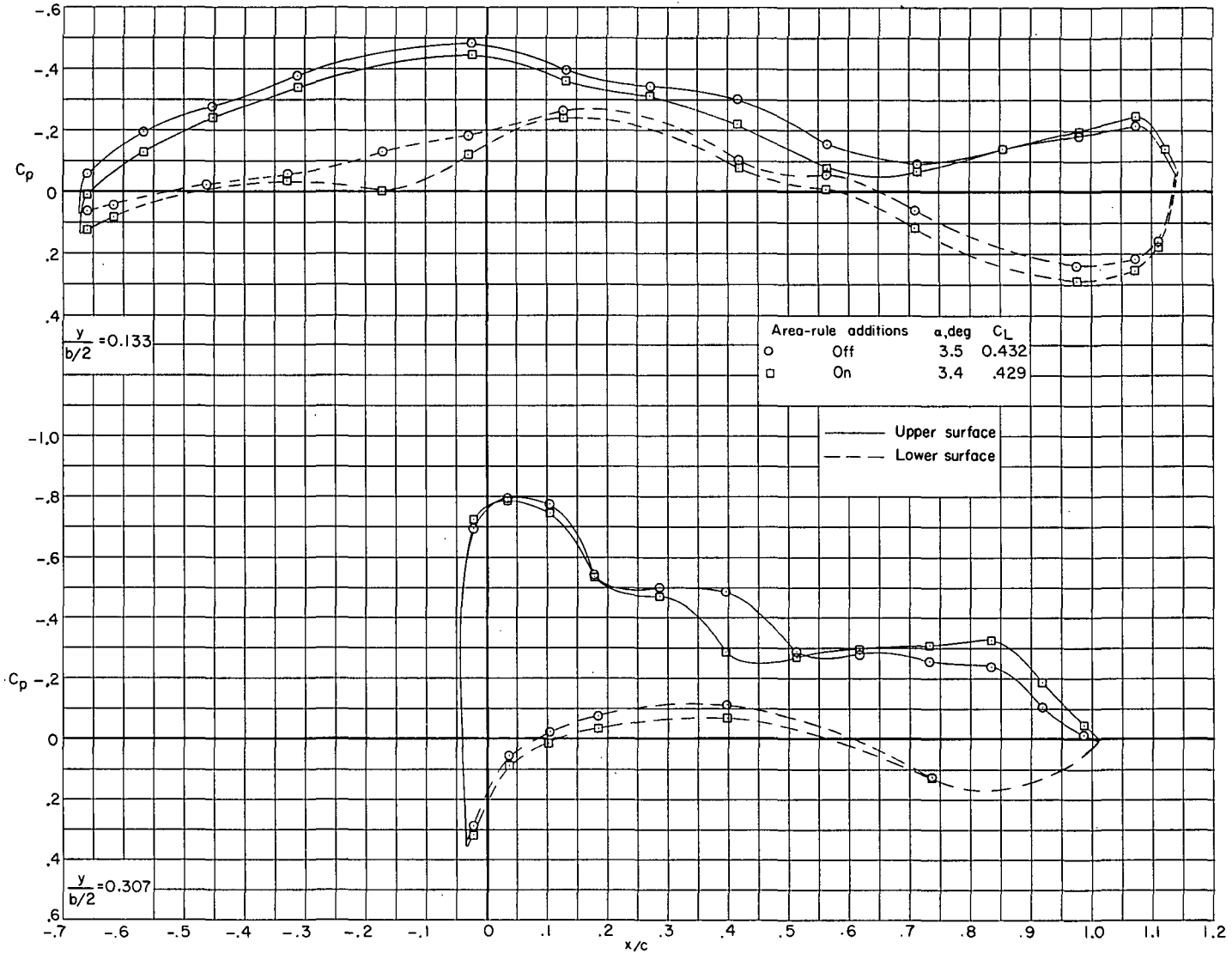
(a) Variation with Mach number of drag coefficient at lift coefficients from 0.20 to 0.50. $\delta_h = -2.5^\circ$.

Figure 8.- Variation of drag characteristics with Mach number. $\beta = 0^\circ$.



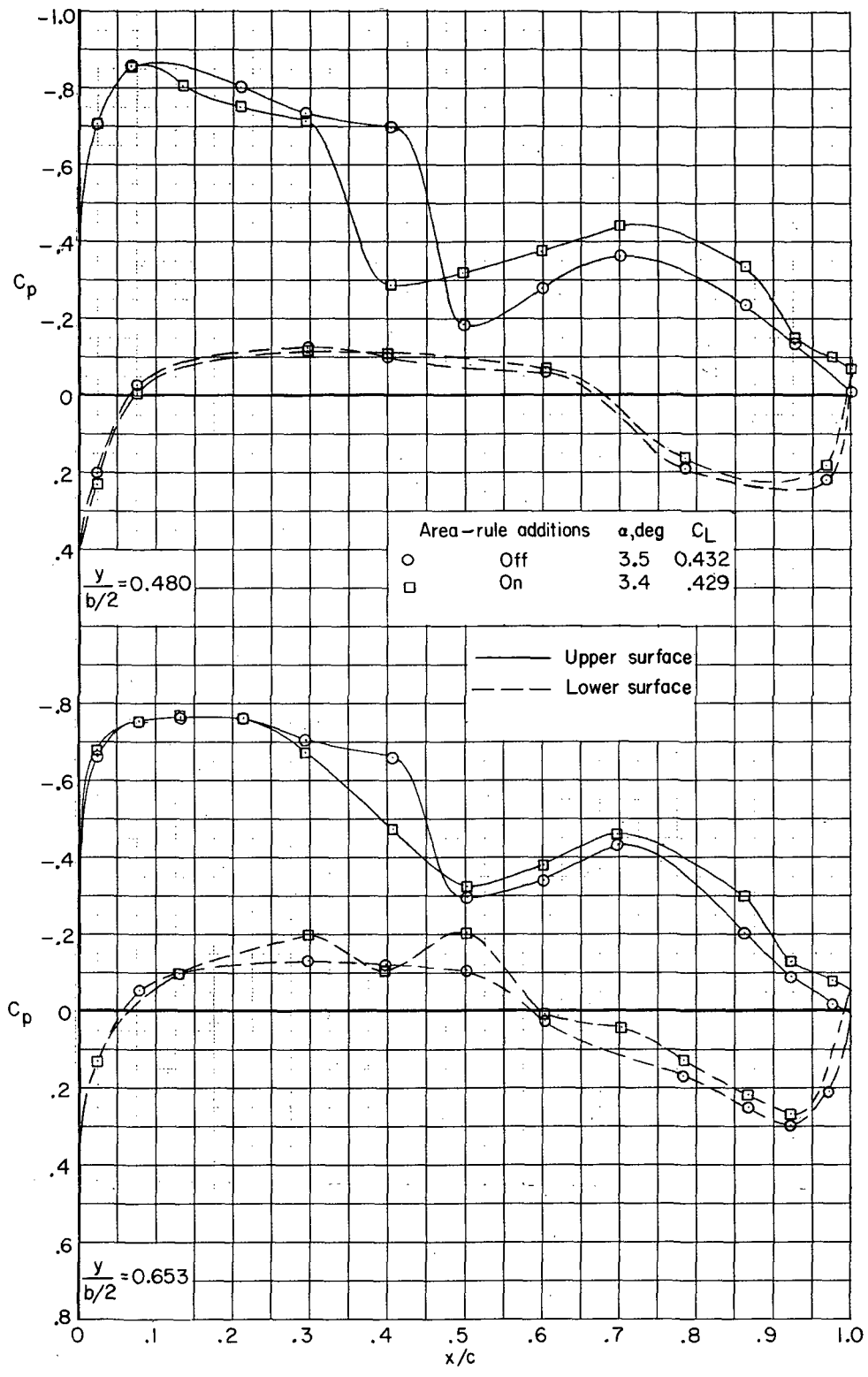
(b) Comparison of incremental drag-rise characteristics of present configuration ($\delta_h = -2.5^\circ$) with and without area-rule additions with those of the configurations in references 10 and 21. $C_L = 0.4$.

Figure 8. - Concluded.



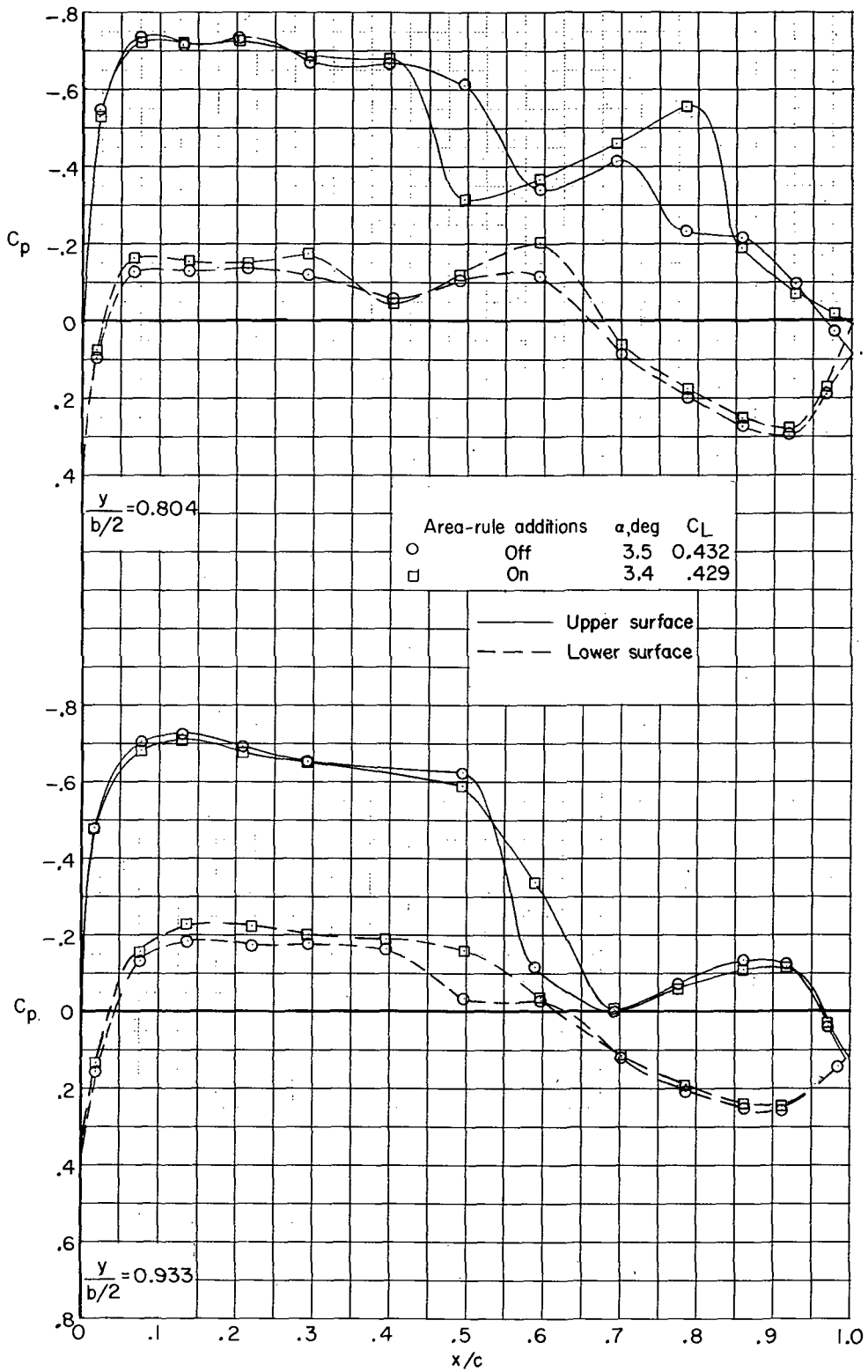
(a) $M = 0.97$.

Figure 9.- Effect of fuselage area-rule additions on wing streamwise pressure distributions near cruise lift coefficient. $\beta = 0^\circ$; $\delta_h = -2.5^\circ$.



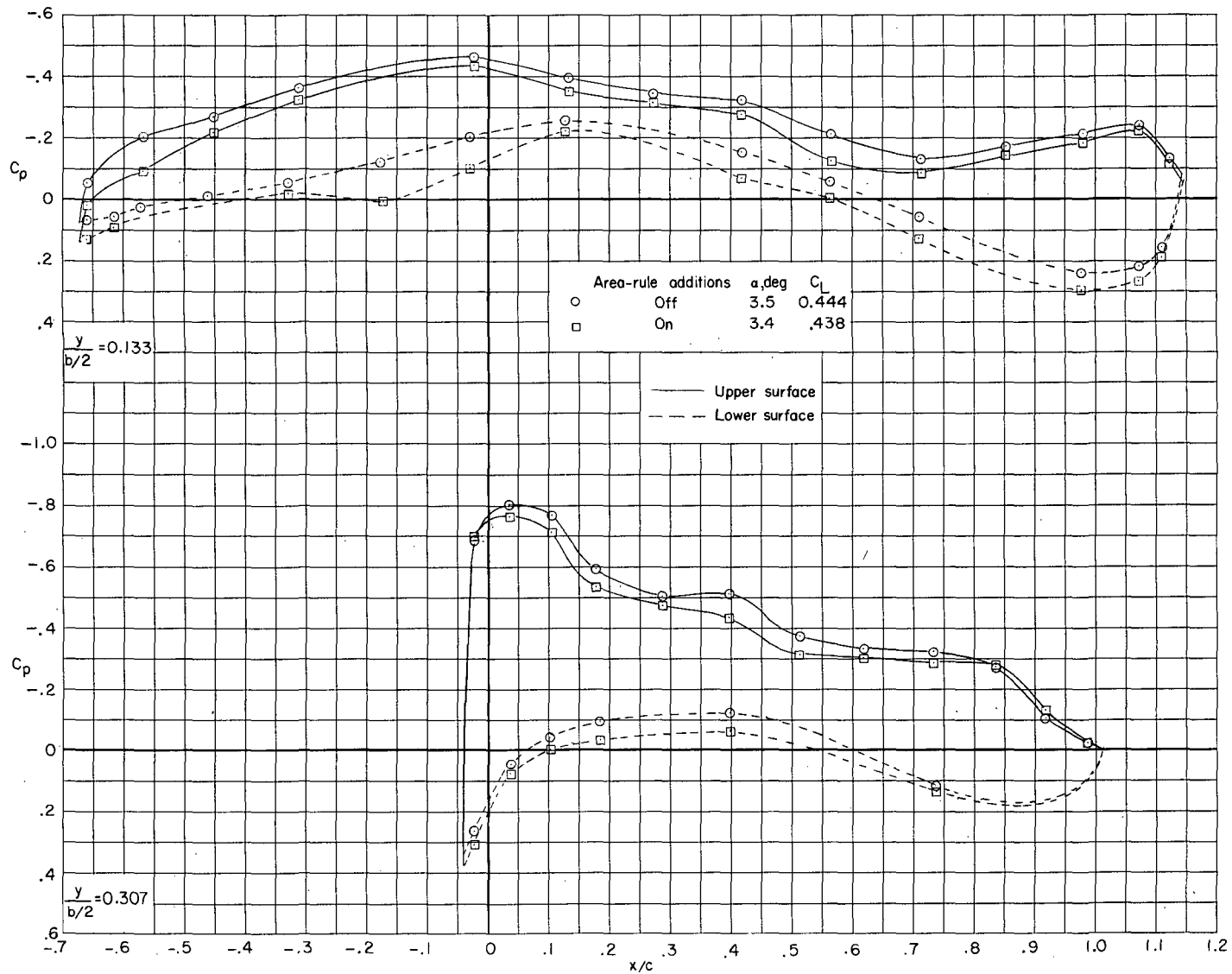
(a) $M = 0.97$. Continued.

Figure 9.- Continued.



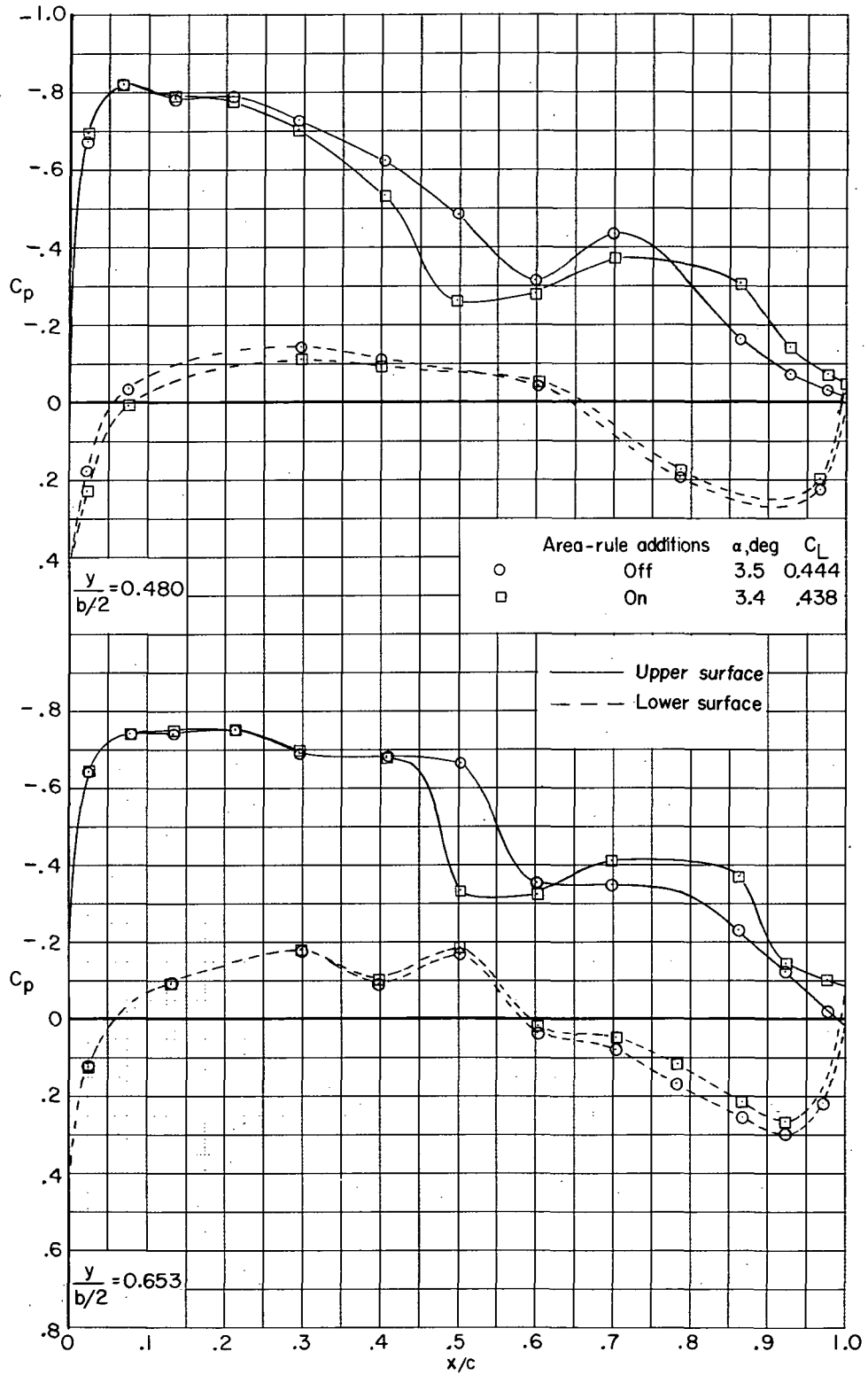
(a) $M = 0.97$. Concluded.

Figure 9. - Continued.



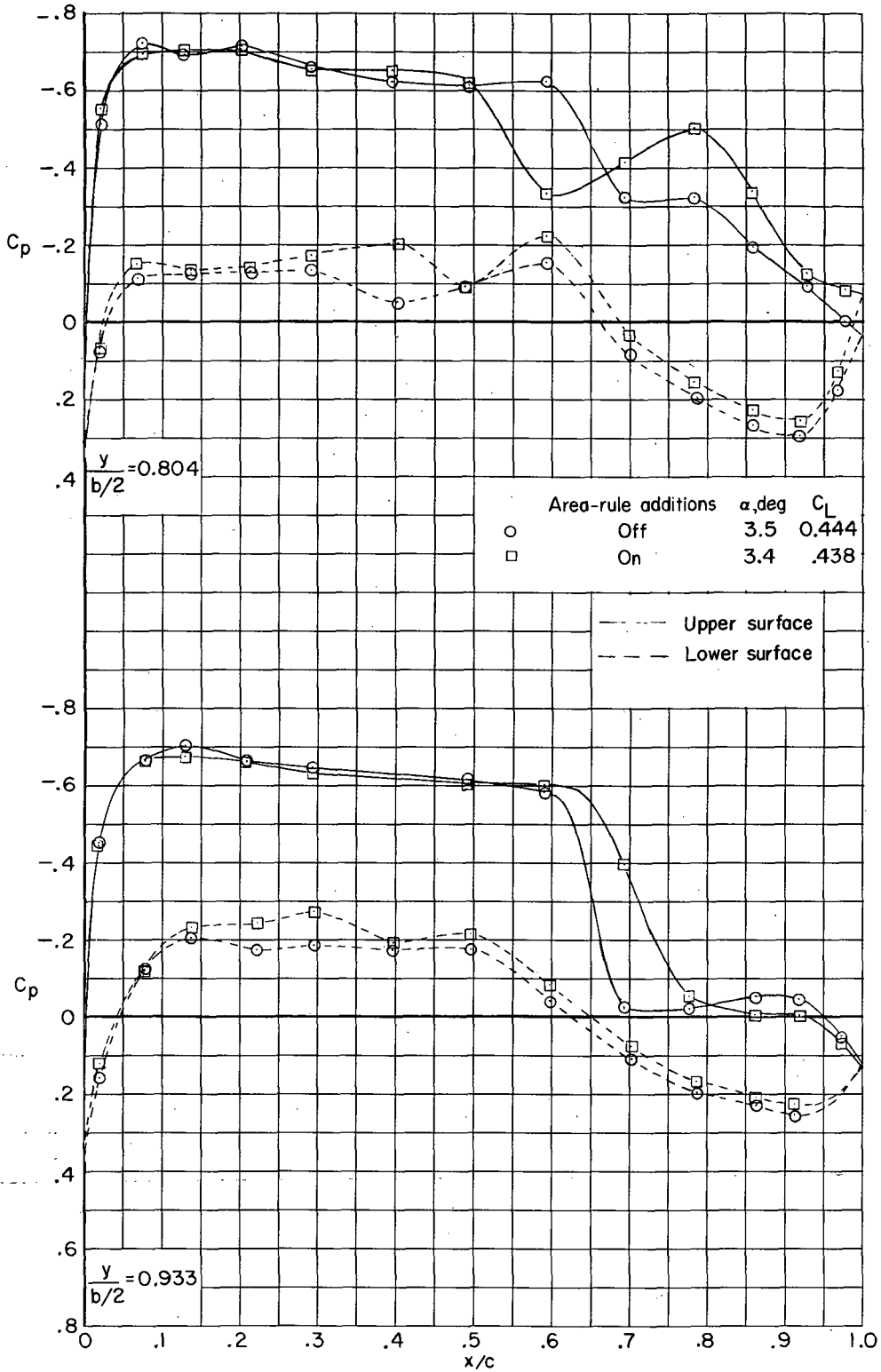
(b) $M = 0.98.$

Figure 9.- Continued.



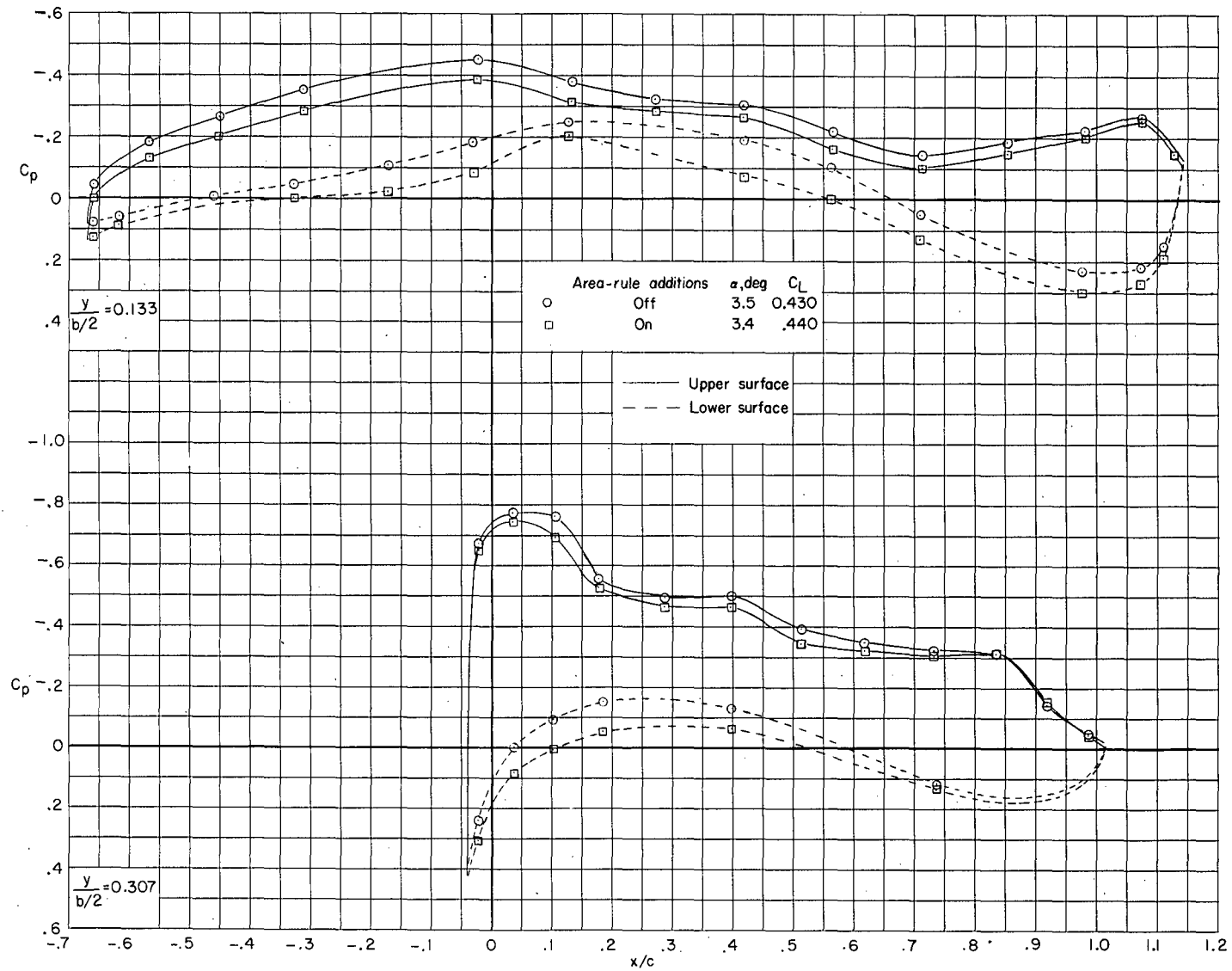
(b) $M = 0.98$. Continued.

Figure 9.- Continued.



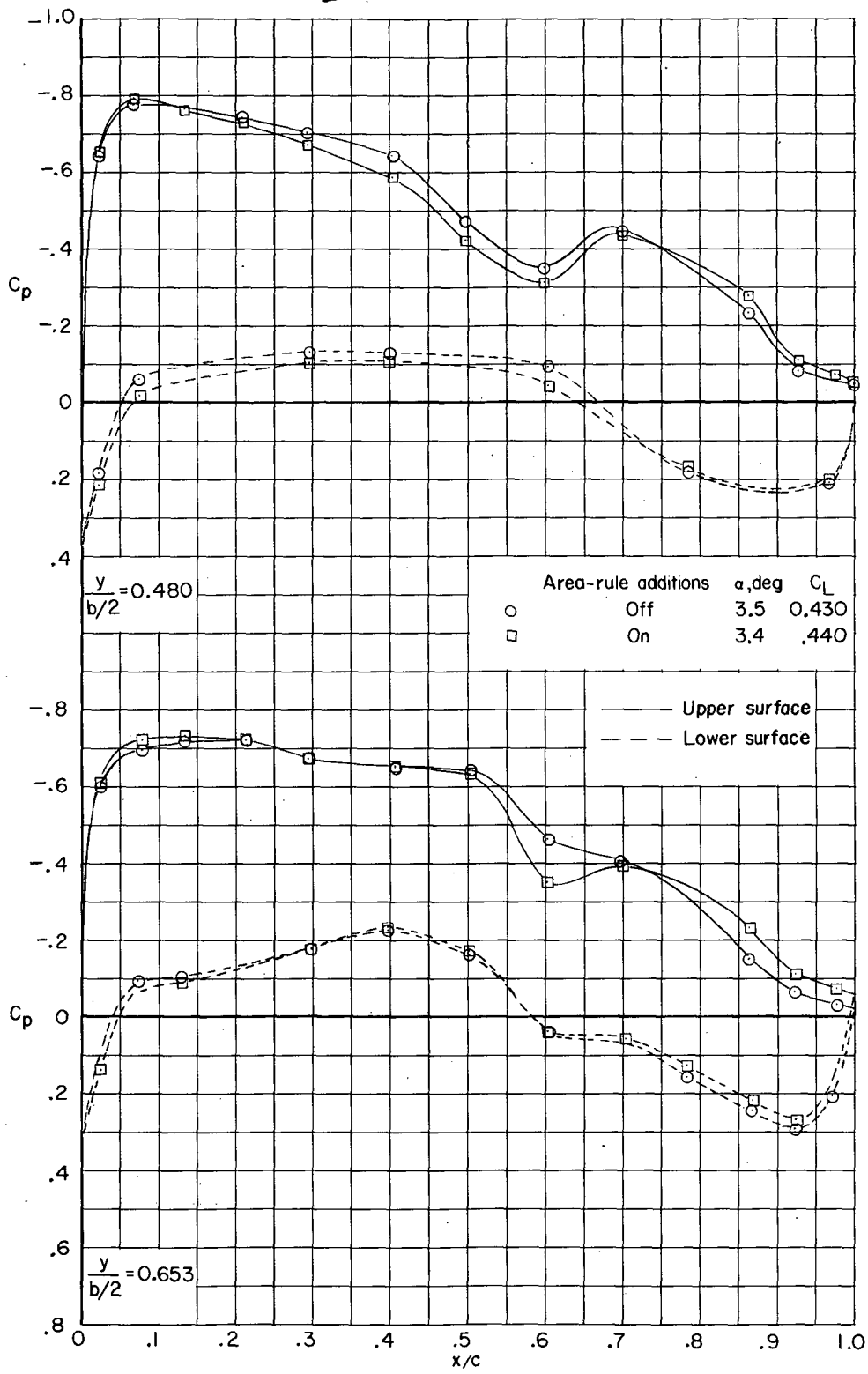
(b) $M = 0.98$. Concluded.

Figure 9.- Continued.



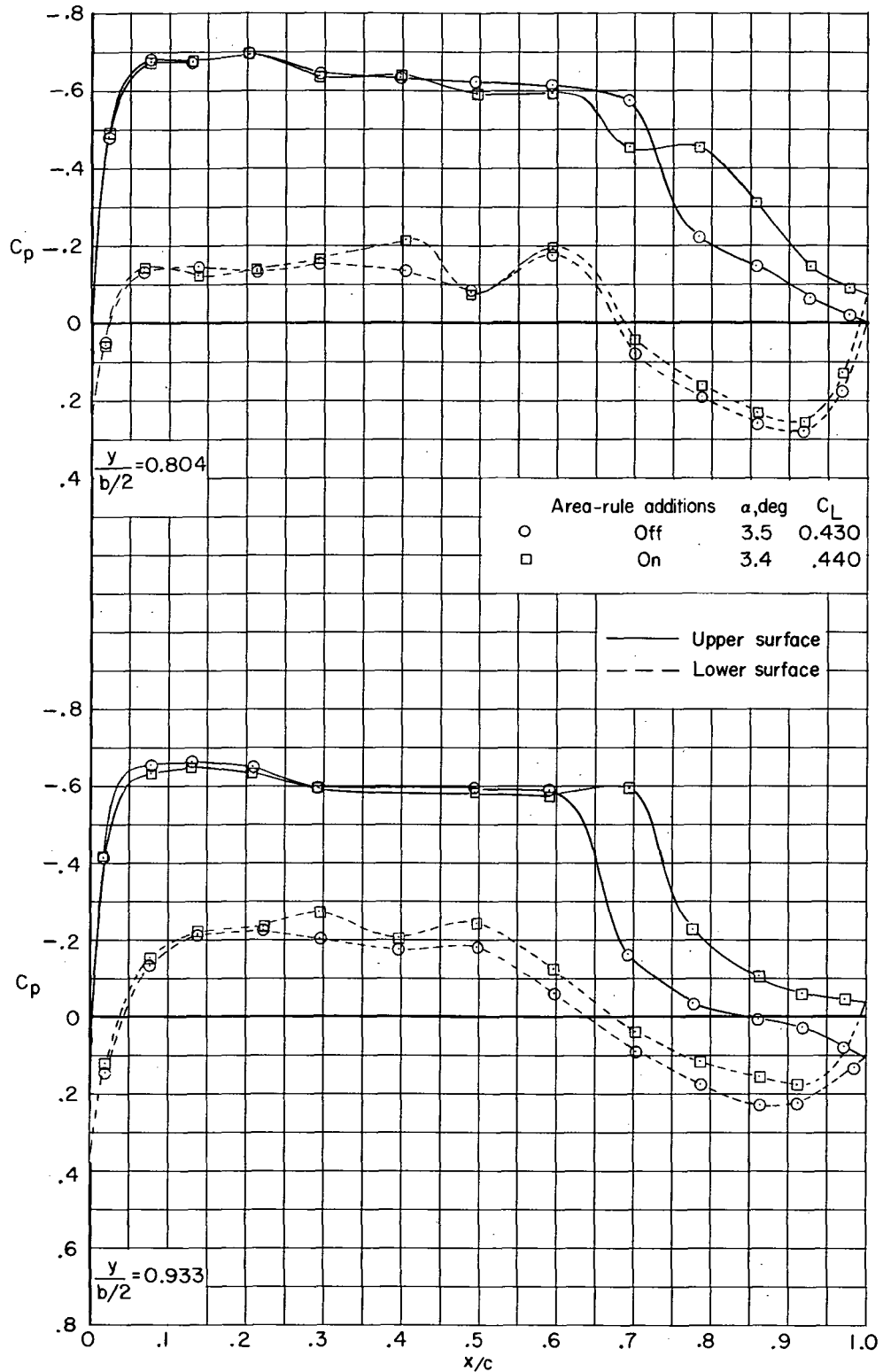
(c) $M = 0.99.$

Figure 9.- Continued.



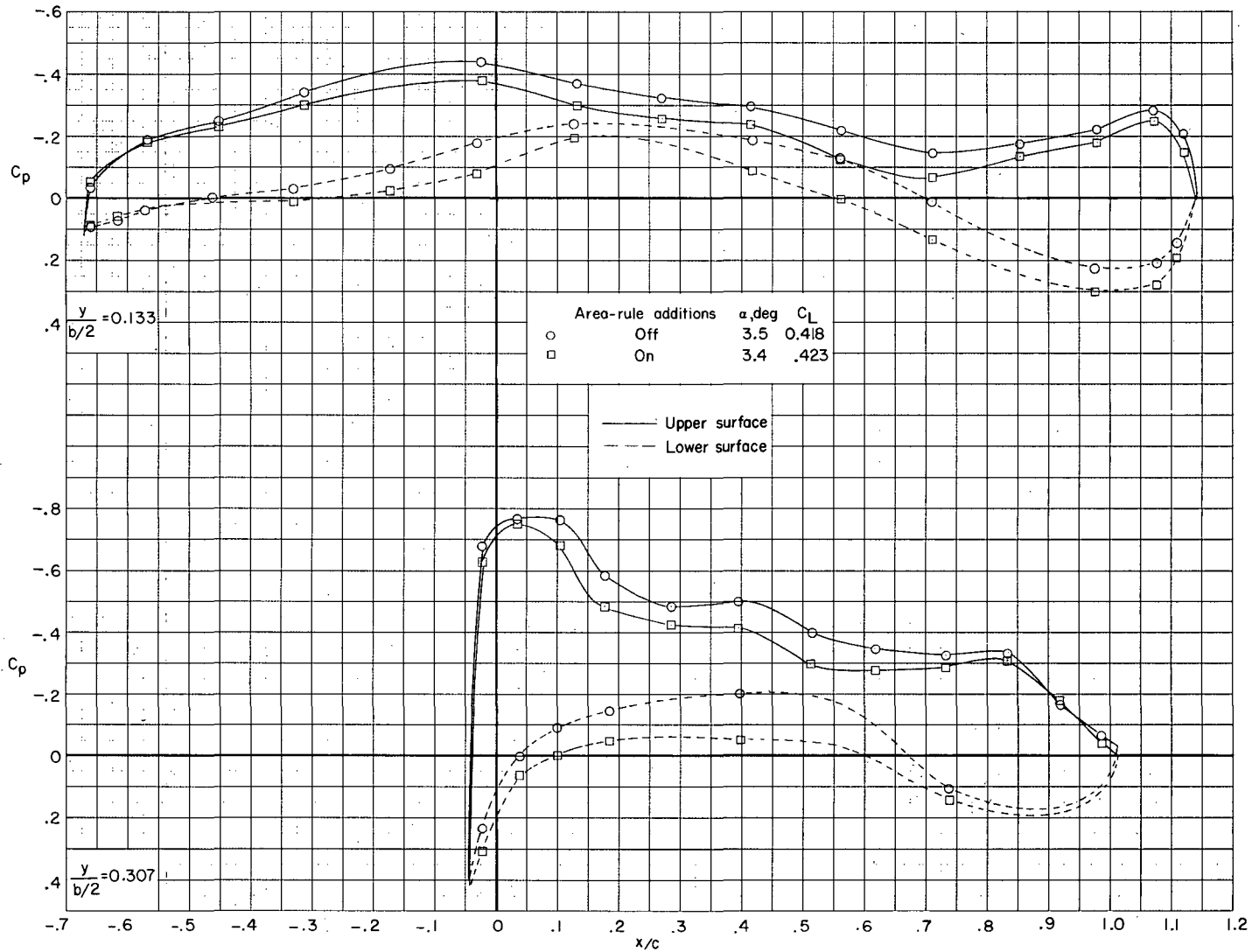
(c) $M = 0.99$. Continued.

Figure 9.- Continued.



(c) $M = 0.99$. Concluded.

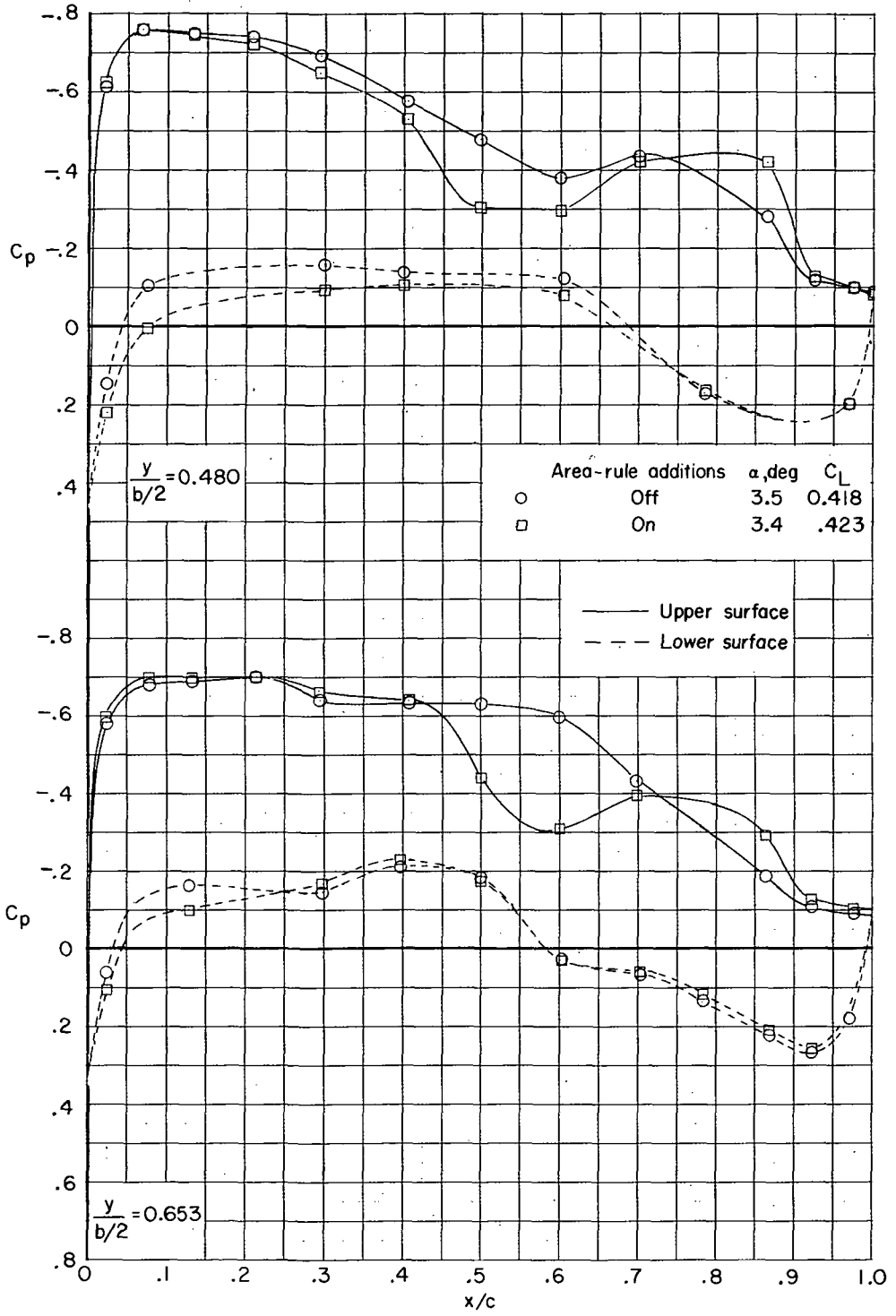
Figure 9. - Continued.



(d) $M = 1.00$.

Figure 9. - Continued.

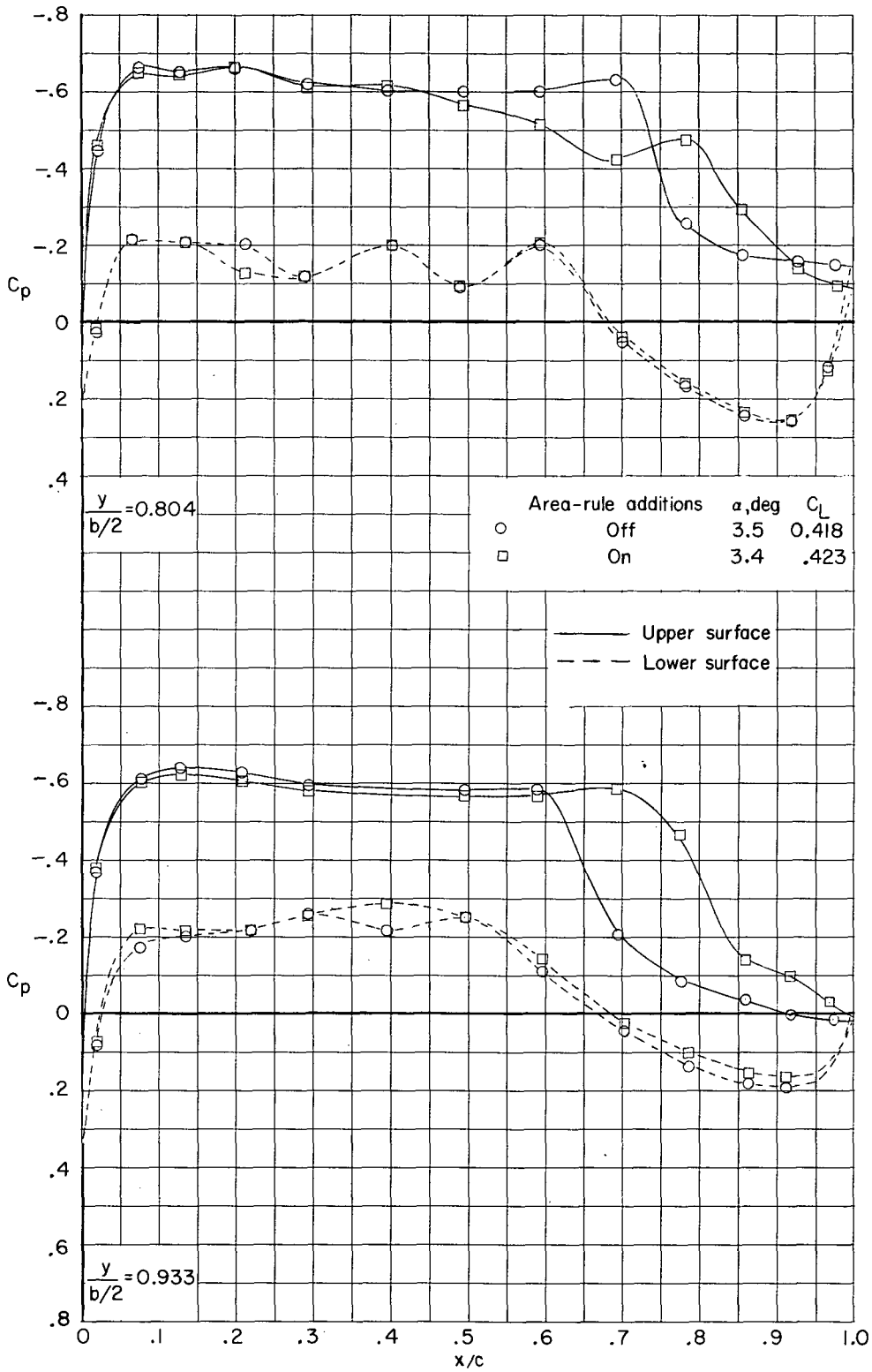
~~CONFIDENTIAL~~



(d) $M = 1.00$. Continued.

Figure 9. - Continued.

~~CONFIDENTIAL~~



(d) $M = 1.00$. Concluded.

Figure 9. - Concluded.

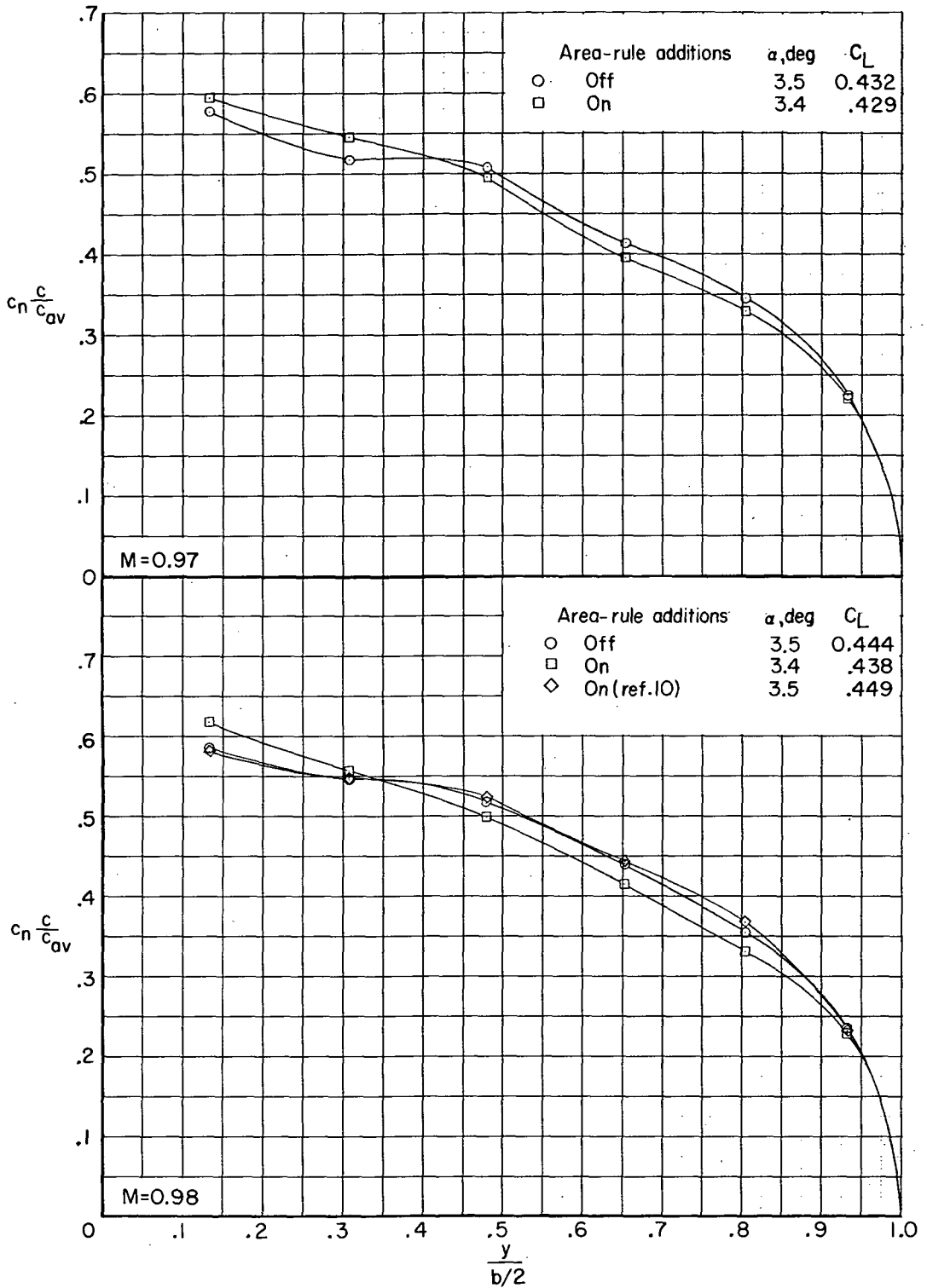


Figure 10.- Effect of fuselage area-rule additions on span-load distributions near cruise lift coefficient. $\beta = 0^\circ$; $\delta_h = -2.5^\circ$.

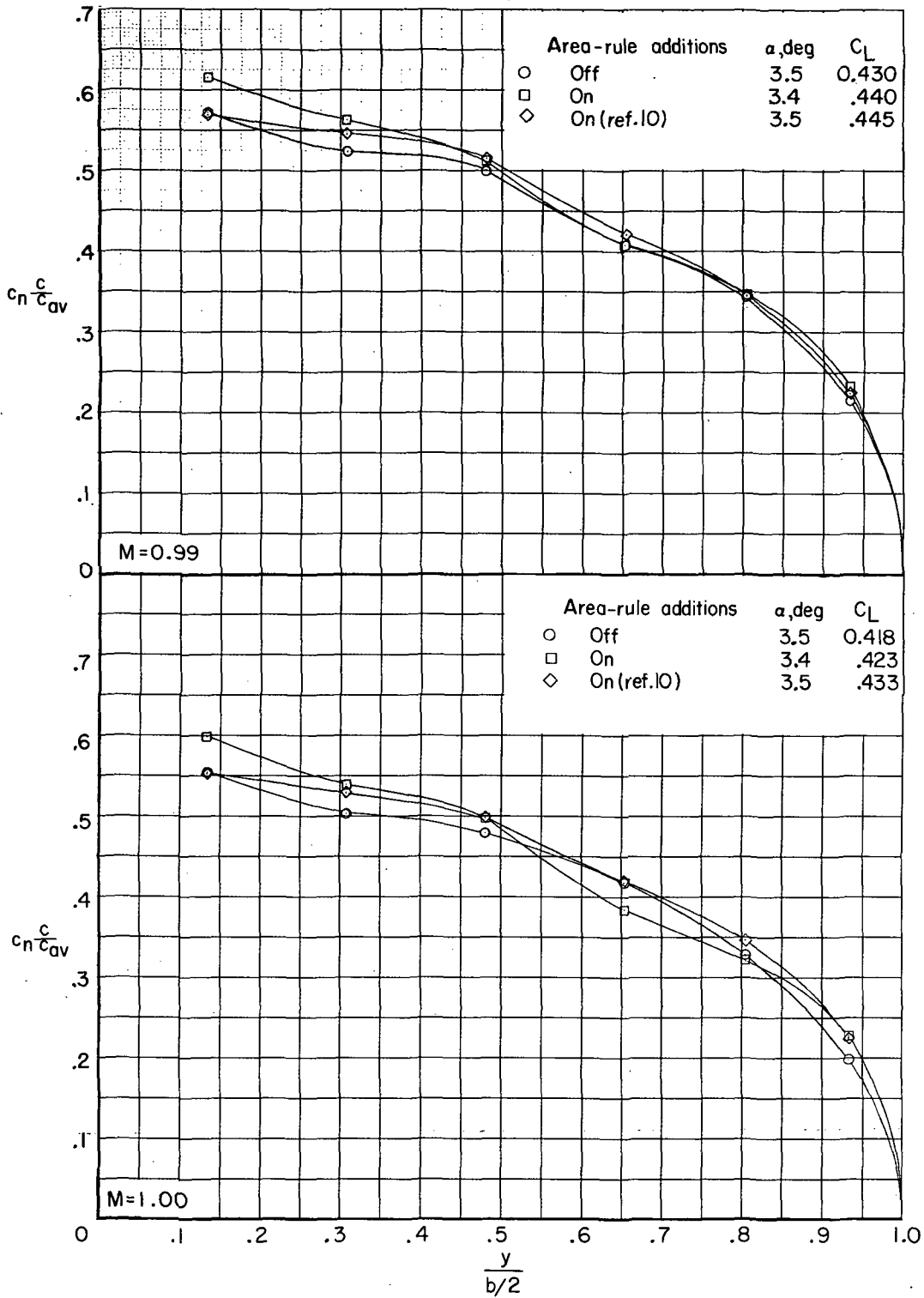
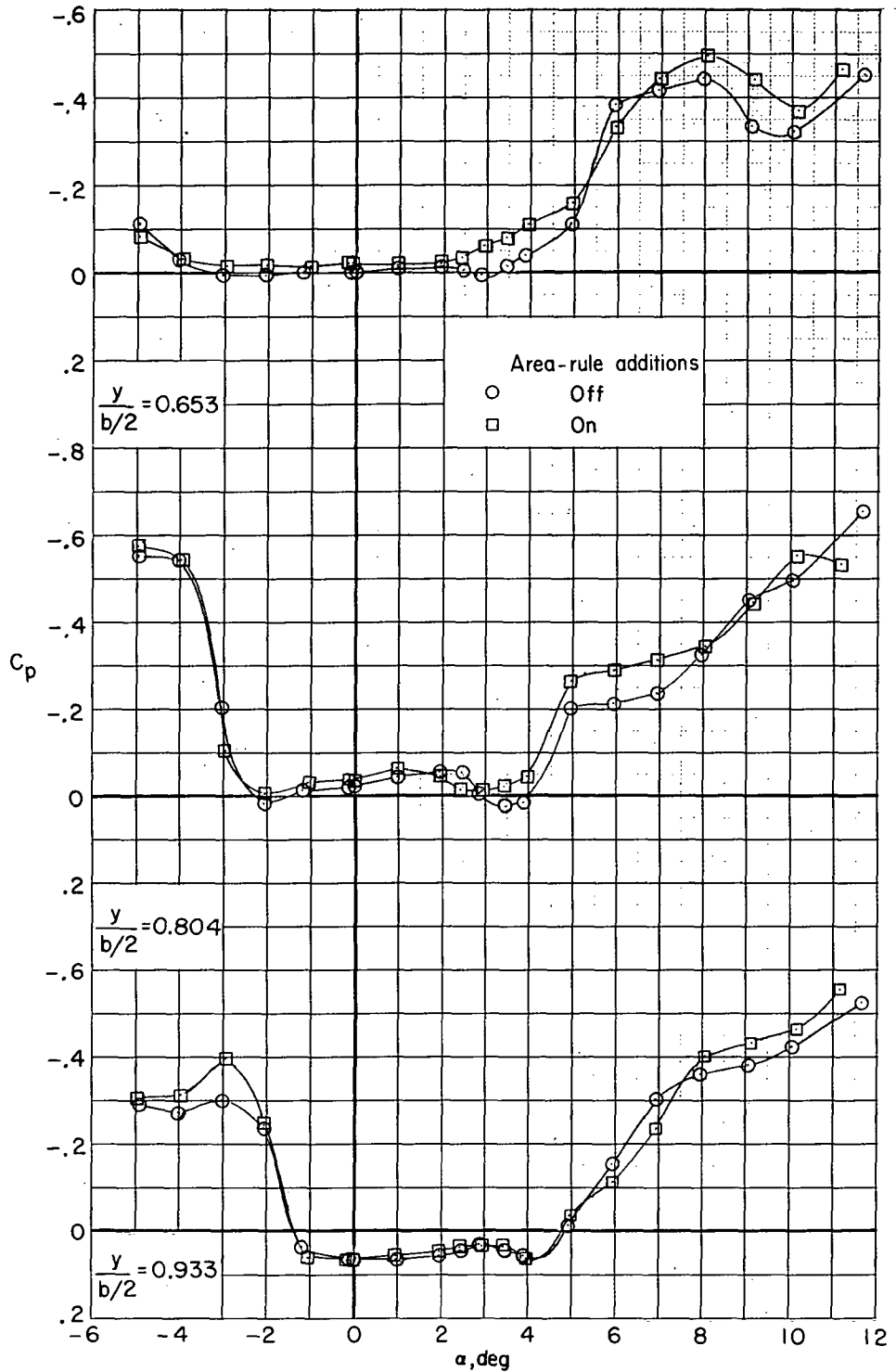
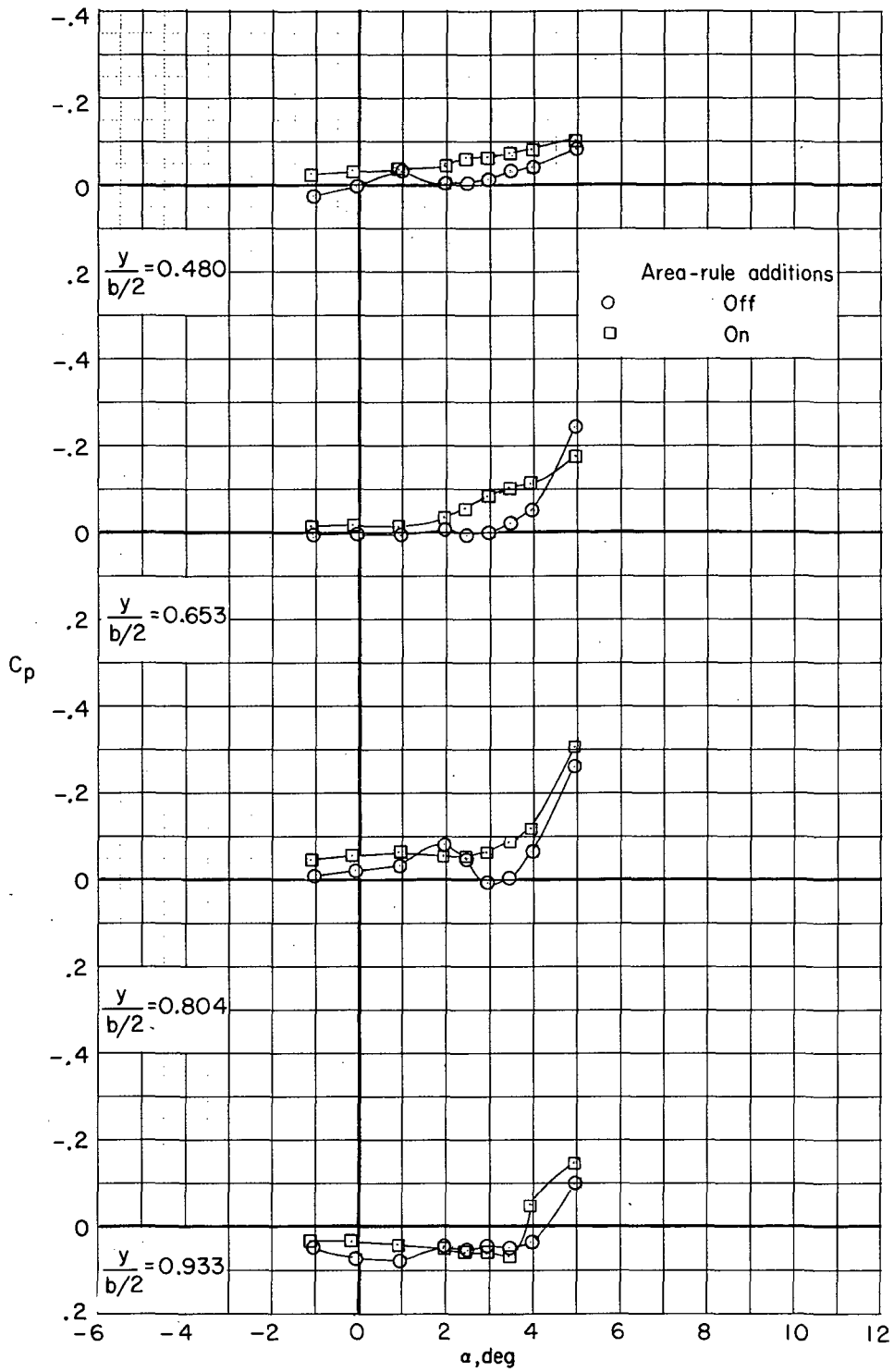


Figure 10.- Concluded.



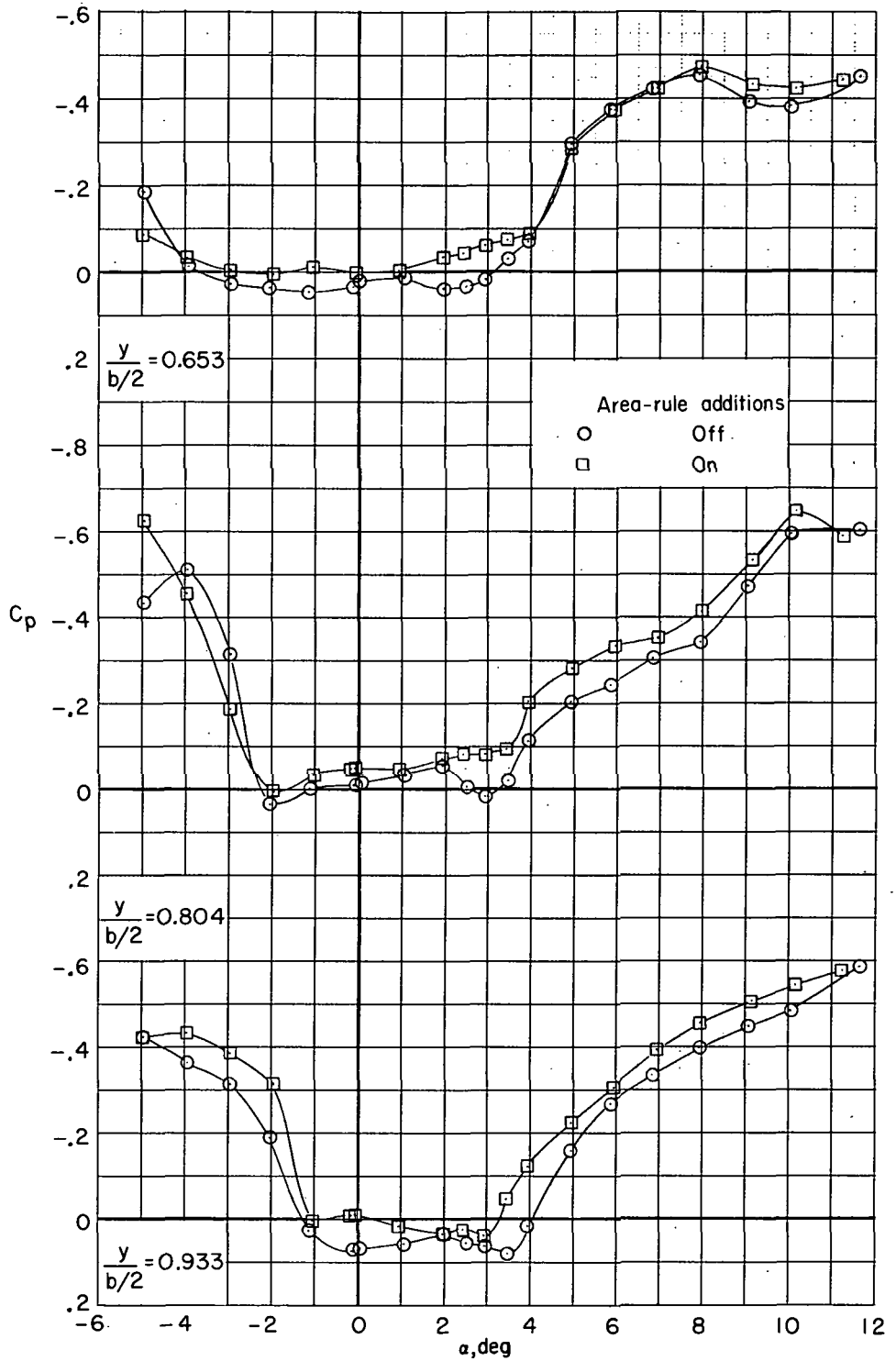
(a) $M = 0.97$.

Figure 11. - Effect of fuselage area-rule additions on wing upper-surface pressure coefficients near trailing edge. $\beta = 0^\circ$; $x/c = 0.98$; $\delta_h = -2.5^\circ$.



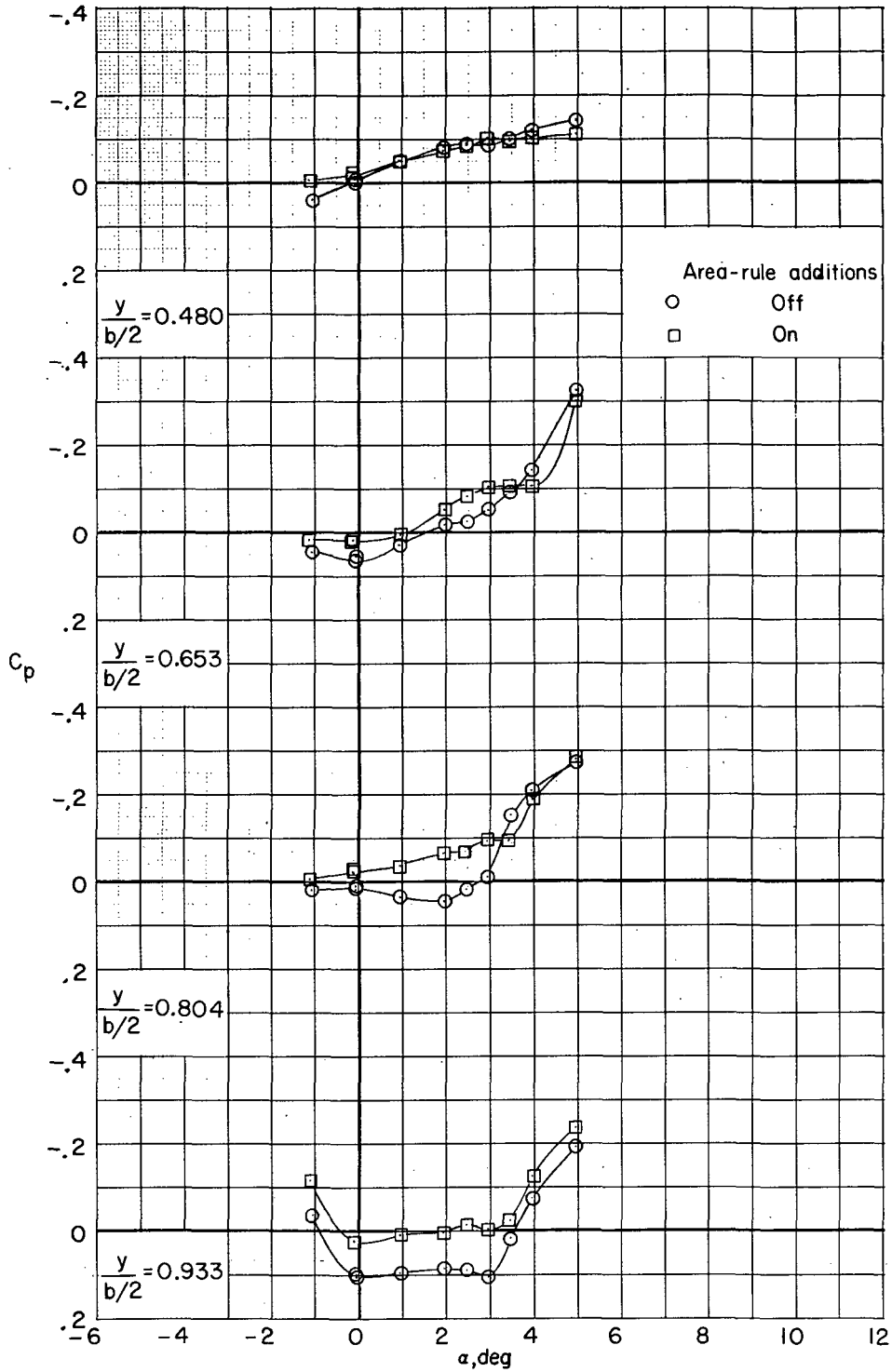
(b) $M = 0.98$.

Figure 11.- Continued.



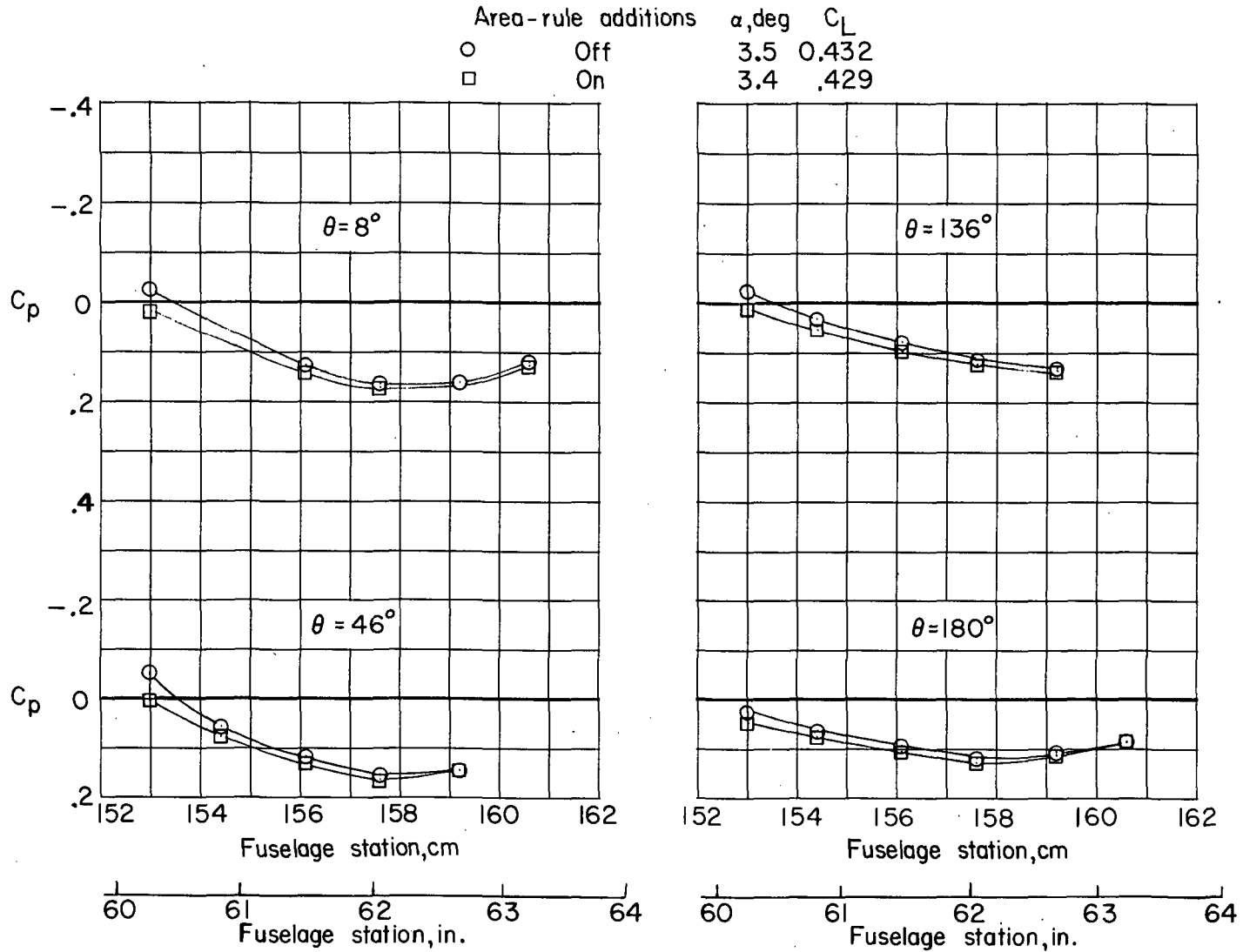
(c) $M = 0.99$.

Figure 11. - Continued.



(d) $M = 1.00$.

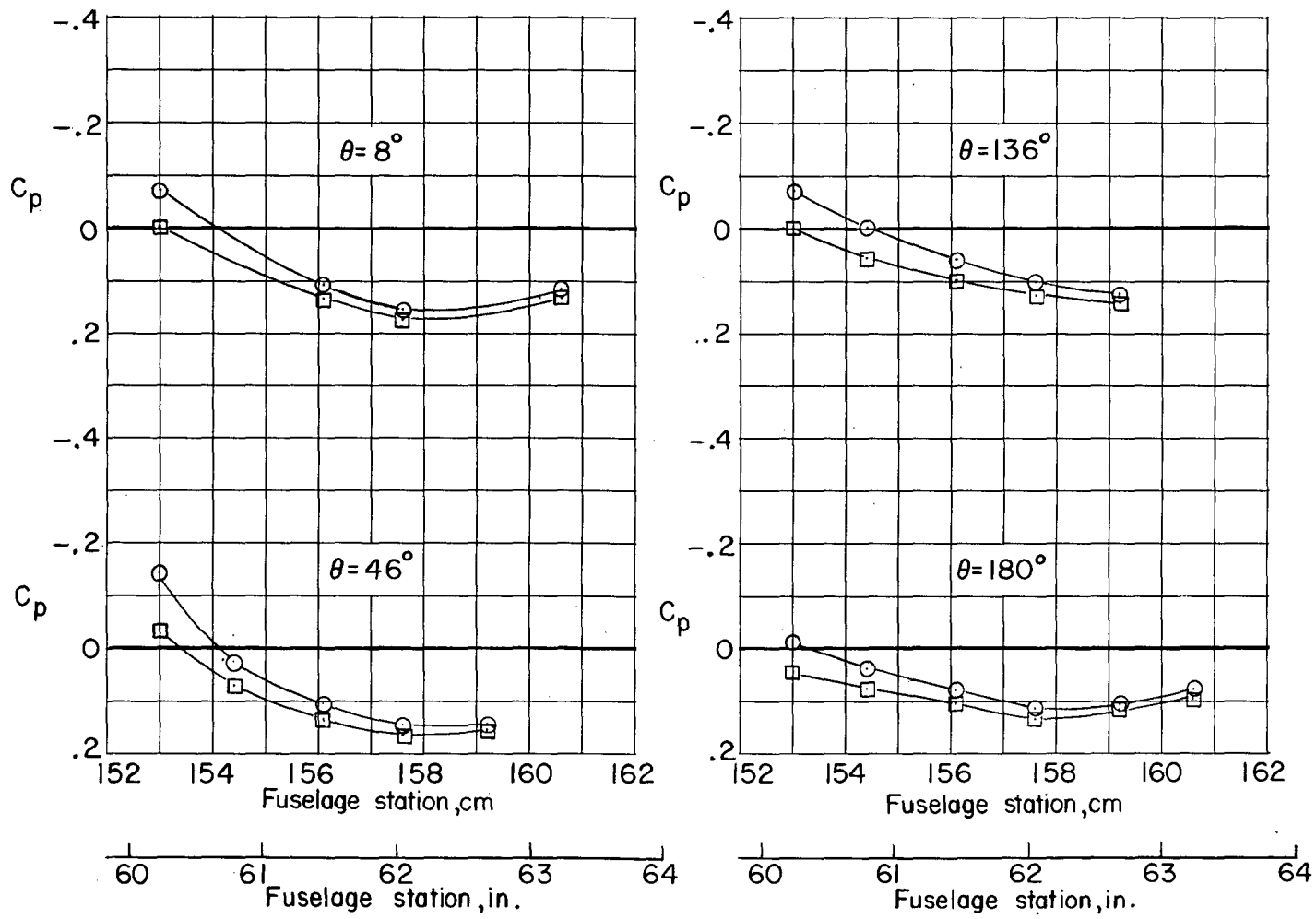
Figure 11.- Concluded.



(a) $M = 0.97$.

Figure 12.- Effect of fuselage area-rule additions on pressure distributions over rear of fuselage near cruise lift coefficient. $\beta = 0^\circ$; $\delta_h = -2.5^\circ$.

Area-rule additions		α, deg	C_L
○	Off	3.5	0.444
□	On	3.4	.438



(b) $M = 0.98$.

Figure 12. - Continued.

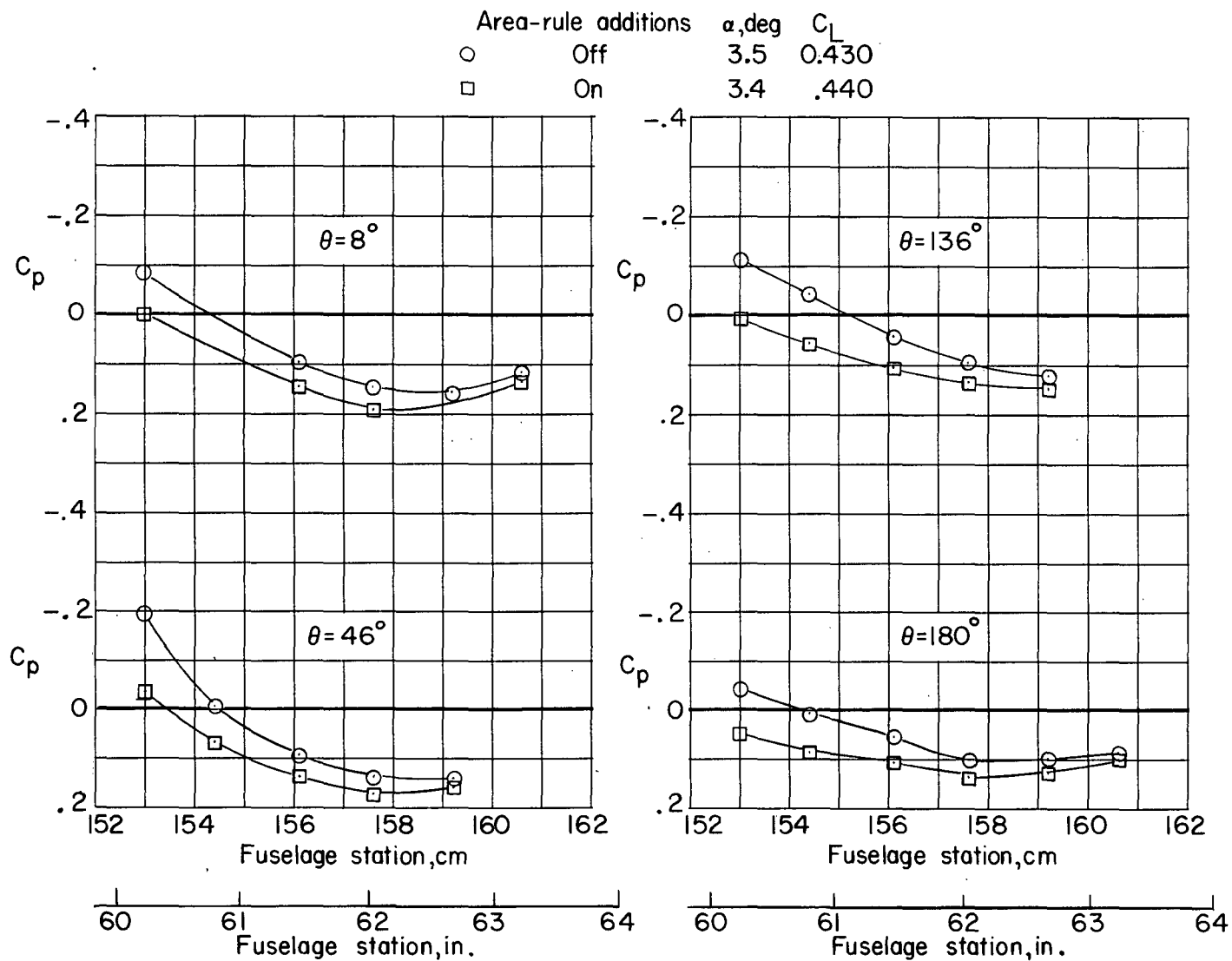
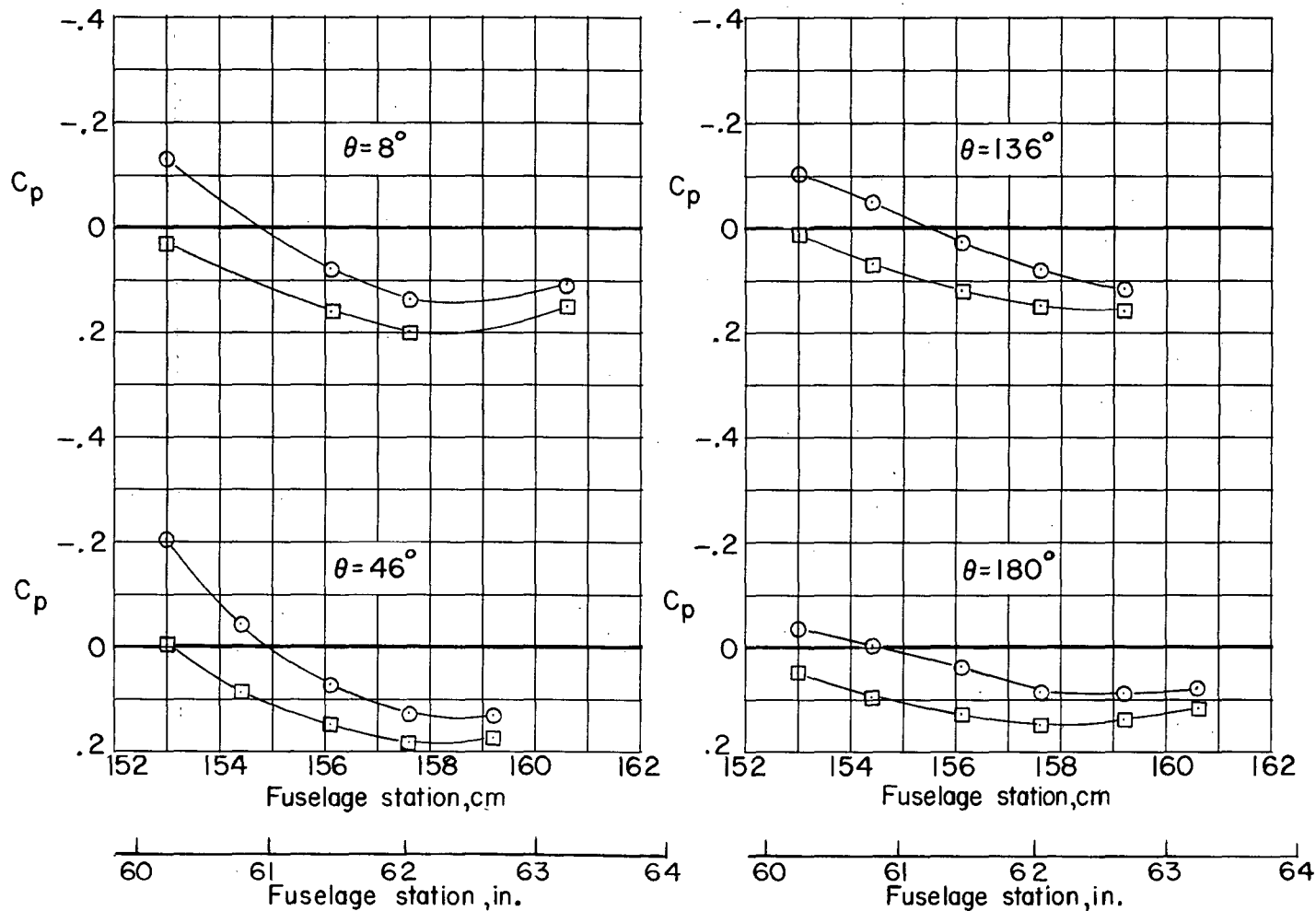
(c) $M = 0.99$.

Figure 12. - Continued.

Area-rule additions		α , deg	C_L
○	Off	3.5	0.418
□	On	3.4	.423



(d) $M = 1.00$.

Figure 12. - Concluded.

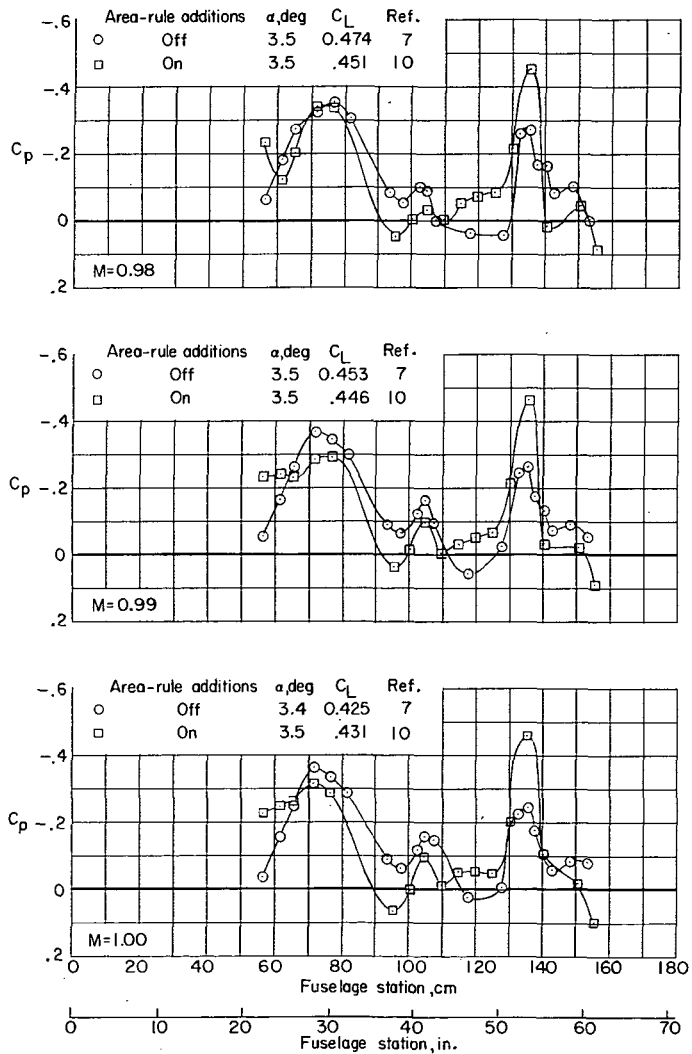
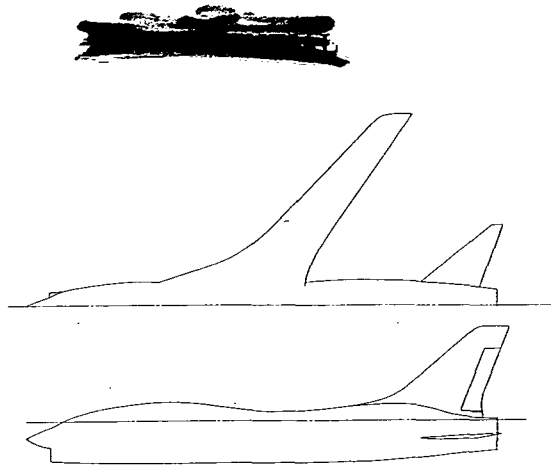


Figure 13.- Effect of fuselage area-rule additions on pressure distributions along top of fuselage near cruise lift coefficient. $\beta = 0^\circ$; $\delta_h = -2.5^\circ$.

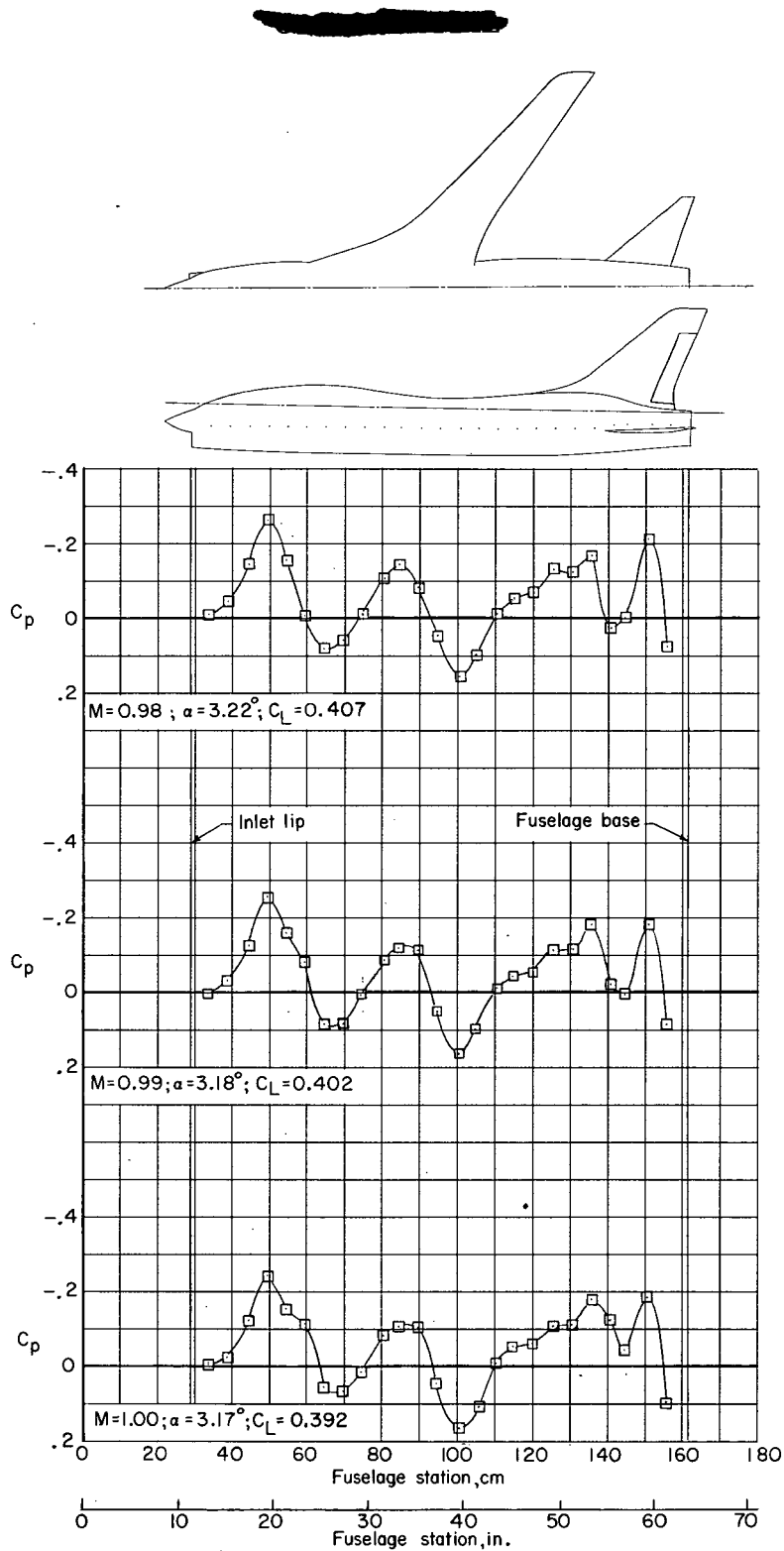


Figure 14.- Typical pressure distributions along side of fuselage near cruise lift coefficient with area-rule additions on model. $\beta = 0^\circ$; $\delta_h = -2.5^\circ$; data from reference 10.

~~CONFIDENTIAL~~

1. Report No. NASA TM X-2633	2. Government Accession No.	3. Recipient's Catalog No.	
4. Title and Subtitle AERODYNAMIC CHARACTERISTICS OF AN NASA SUPERCRITICAL-WING RESEARCH AIRPLANE MODEL WITH AND WITHOUT FUSELAGE AREA-RULE ADDITIONS AT MACH 0.25 TO 1.00 (U)		5. Report Date December 1972	6. Performing Organization Code
		8. Performing Organization Report No. L-8422	10. Work Unit No. 742-73-01-14
7. Author(s) Dennis W. Bartlett and Charles D. Harris		11. Contract or Grant No.	13. Type of Report and Period Covered Technical Memorandum
9. Performing Organization Name and Address NASA Langley Research Center Hampton, Va. 23365		14. Sponsoring Agency Code	
		12. Sponsoring Agency Name and Address National Aeronautics and Space Administration Washington, D.C. 20546	
15. Supplementary Notes			
16. Abstract <p>An investigation has been conducted in the Langley 8-foot transonic pressure tunnel at Mach numbers from 0.25 to 1.00 to determine the effects of area-rule additions to the sides of the fuselage on the aerodynamic characteristics of a 0.087-scale model of an NASA supercritical-wing research airplane. Presented are the longitudinal aerodynamic force and moment characteristics for horizontal-tail deflection angles of -2.5° and -5° with the side fuselage area-rule additions on and off the model. The effects of the side fuselage area-rule additions on selected wing and fuselage pressure distributions at near-cruise conditions are also presented.</p> <p style="text-align: center;">CLASSIFICATION CHANGE To UNCLASSIFIED By authority of <u>NASA HDQ. T.D. 77-163</u> Changed by <u>L. Shirley</u> Date <u>6-15-76</u> Classified Document Master Control Station, NASA Scientific and Technical Information Facility</p>			
17. Key Words (Suggested by Author(s)) Area-rule application Supercritical-airfoil application Transonic aerodynamics		18. Distribution Statement CONFIDENTIAL Available to U.S. Government Agencies and Their Contractors Only	
19. Security Classif. (of this report) CONFIDENTIAL	20. Security Classif. (of this page) Unclassified	21. No. of Pages 131	22. Price
"NATIONAL SECURITY INFORMATION" Unauthorized Disclosure Subject to Criminal Sanctions.		CONFIDENTIAL BY Henry Fedzick SUBJECT TO FEDERAL DECLASSIFICATION SCHEDULE OF EXECUTIVE ORDER 11652 AUTOMATICALLY DOWNGRADED AT TWO YEAR INTERVALS AND DECLASSIFIED ON DEC 31, 1978	

~~CONFIDENTIAL~~

"The aeronautical and space activities of the United States shall be conducted so as to contribute . . . to the expansion of human knowledge of phenomena in the atmosphere and space. The Administration shall provide for the widest practicable and appropriate dissemination of information concerning its activities and the results thereof."

— NATIONAL AERONAUTICS AND SPACE ACT OF 1958

NASA SCIENTIFIC AND TECHNICAL PUBLICATIONS

TECHNICAL REPORTS: Scientific and technical information considered important, complete, and a lasting contribution to existing knowledge.

TECHNICAL NOTES: Information less broad in scope but nevertheless of importance as a contribution to existing knowledge.

TECHNICAL MEMORANDUMS: Information receiving limited distribution because of preliminary data, security classification, or other reasons.

CONTRACTOR REPORTS: Scientific and technical information generated under a NASA contract or grant and considered an important contribution to existing knowledge.

TECHNICAL TRANSLATIONS: Information published in a foreign language considered to merit NASA distribution in English.

SPECIAL PUBLICATIONS: Information derived from or of value to NASA activities. Publications include conference proceedings, monographs, data compilations, handbooks, sourcebooks, and special bibliographies.

TECHNOLOGY UTILIZATION PUBLICATIONS: Information on technology used by NASA that may be of particular interest in commercial and other non-aerospace applications. Publications include Tech Briefs, Technology Utilization Reports and Notes, and Technology Surveys.

Details on the availability of these publications may be obtained from:

**SCIENTIFIC AND TECHNICAL INFORMATION OFFICE
NATIONAL AERONAUTICS AND SPACE ADMINISTRATION
Washington, D.C. 20546**

~~CONFIDENTIAL~~